Supporting Information

Construction of bright color-tunable chemiluminescent nanodots and their applications for in vivo bioimaging

Shijie Li,† Linyi Shi,† Xiaobo Zhou, Ke Zhang, Lingfeng Zhao, Zhonghao Chen, Guo Li, Yuling Qin,* Li Wu**

Jiangsu Key Laboratory of Advanced Medical Analysis and Public Health, Nantong Key Laboratory of Public Health and Medical Analysis, School of Public Health, Nantong University, No. 9, Seyuan Road, Nantong 226019, Jiangsu, P. R. China.

E-mail: xbzhou@ntu.edu.cn; ylqin@ntu.edu.cn; wuli8686@ntu.edu.cn

Contents

Instruments and methods

^{1}H and ^{13}C NMR spectra were recorded at room temperature using a Bruker UltraShield Plus 400 MHz NMR instrument. UV-Vis absorption spectra were measured on UV1900 (Shimadzu, Japan). Photoluminescence and chemiluminescence spectra were collected using an FS5 Photoluminescence Spectrometer (Edinburgh, England) with or without the input xenon lamp as the excitation source, respectively. Transmission electron microscopy (TEM) was conducted on a FEI Talos F200X TEM at an acceleration voltage of 100 kV. Dynamic light scattering (DLS) measurements were taken using a Malvern nanoparticle size zeta potential analyzer. HR-MS analyses were conducted on a 5800 proteomic analyzer (Applied Biosystems, Framingham, MA, USA). Chemiluminescence signals *in vitro* and *in vivo* were recorded using a luminescence imaging system (Tanon X6 imaging system, which is equipped with EMCCD (PIXIS-1024B_eXcelon, Princeton) as luminescence signal detector).

Materials

All chemicals were purchased from commercial sources and used without further purification unless otherwise stated. All solvents were purified before the experiment. Phosphate-buffered Saline (10X PBS, pH=7.4) was obtained from Beyotimes Inc. Some fluorophores with different structures for preparing POCL nanoparticles were obtained through a commercial approach. The fluorophores DPA, DPEA, Rubrene, RhB, Coumarin153, Courmarin102, BDP and Rh101 were purchased from J&K Scientific. The fluorophores BDP-590, BDP-650, and SQ640 were purchased from Lumiprobe. The cyanine dyes Cy3, Cy5, Cy7, and ICG were purchased from Sigma Aldrich. The fluorophores PFBDP, tDPA-BT, TPA-BT, TPE-BT, OTPA-BT, and SQ680 were developed in our previous works[1,2]. The fluorescent conjugated polymers PFO, PFOPV, F8BT, PFODPB, PFOHTBT, MEH-PPV, CN-PPV, PBQx-TF, and PFN-DOF were purchased from Polymer Source. F-127 and CPPO were purchased from General-Reagent.

Synthesis of different fluorophores[1-4]

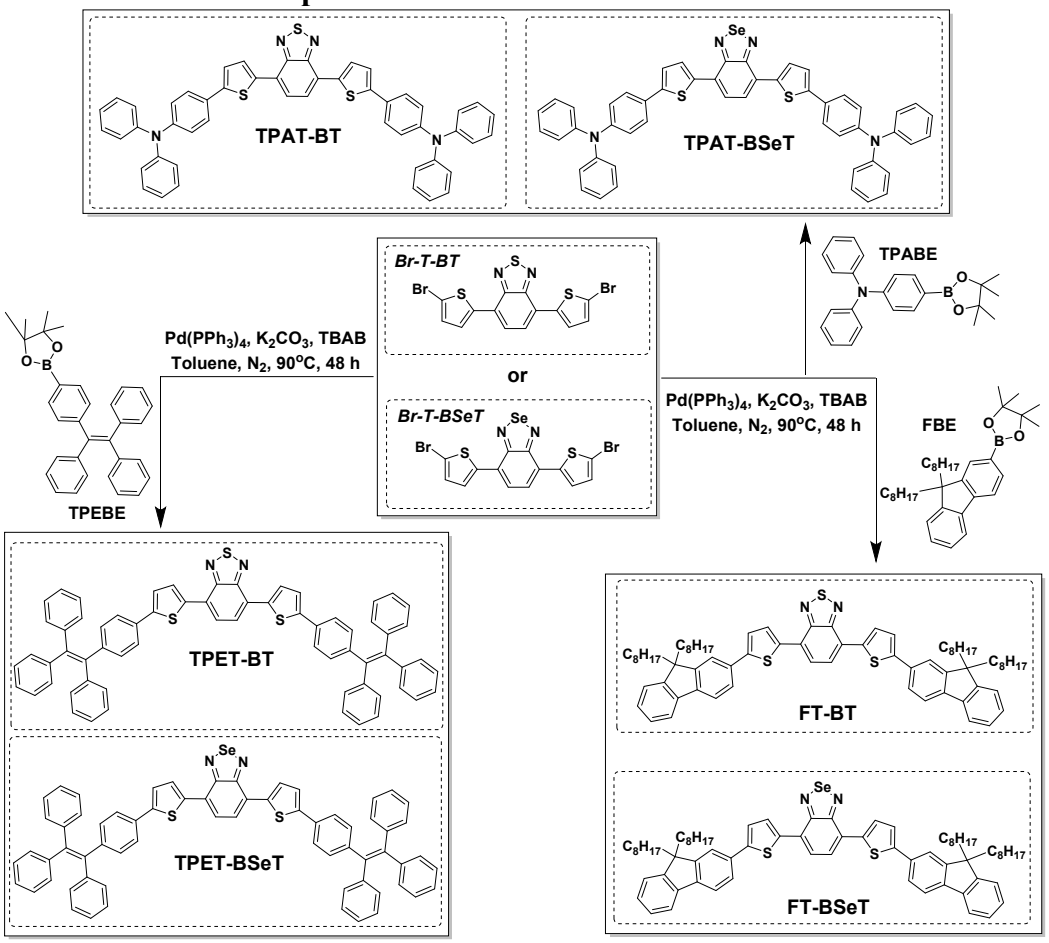

Scheme S1. Synthetic routes of **XT-BT** and **XT-BSeT (X =** Triphenylamine**-TPA,** Tetraphenyl ethylene**-TPE, or** Fluorene**-F)**.

TPAT-BT

A mixture of N,N-Diphenyl-4-(4,4,5,5-tetramethyl-1,3,2-dioxaborolan-2-yl)aniline (**TPABE**, 372 mg, 1.0 mmol), 4,7-Bis(2-bromo-5-thienyl)-2,1,3-benzothiadiazole (**Br-T-BT**, 183 mg, 0.4 mmol) and $Pd(PPh_3)_4$ (6 mg, 0.025 mmol), tetrabutylammonium bromide (3 mg), 2 M K_2CO_3 (2.5 mL) and toluene (5 mL) was heated to 90 °C and stirred in dark for 48 h. After cooling, the mixture was washed with brine and dried with anhydrous Na_2SO_4. Then the residue was purified by column chromatography (eluent: CH_2Cl_2/Petroleum ether) to give red solids. Yield: 245 mg, 78 %.

^{1}H NMR (400 MHz, Chloroform-*d*) δ 8.02 (d, *J* = 3.9 Hz, 2H), 7.76 (s, 2H), 7.49 (d, *J* = 8.3 Hz, 4H), 7.25-7.19 (m, 10H), 7.08-6.95 (m, 16H).

^{13}C NMR (101 MHz, Chloroform-*d*) δ 152.60, 147.61, 147.43, 129.39, 128.71, 128.06, 126.63, 125.64, 125.19, 124.68, 123.50, 123.27.

HR-MS (ESI) *m/z*: calcd for $[C_{50}H_{34}N_4S_3]^+$ 786.195, found 785.727.

TPAT-BSeT

A mixture of **TPABE** (372 mg, 1.0 mmol), 4,7-Bis(5-bromothiophen-2-yl)benzo[c][1,2,5]selenadiazole (**Br-T-BSeT**, 202 mg, 0.4 mmol) and $Pd(PPh_3)_4$ (6 mg, 0.025 mmol), tetrabutylammonium bromide (3 mg), 2 M K_2CO_3 (2.5 mL) and toluene (5 mL) was heated to 90 °C and stirred in dark for 48 h. After cooling, the mixture was washed with brine and dried with anhydrous Na_2SO_4. Then the residue was purified by column chromatography (eluent: CH_2Cl_2/Petroleum ether) to give black solids. Yield: 250 mg, 75 %.

^{1}H NMR (400 MHz, Chloroform-*d*) δ 7.94 (d, *J* = 3.9 Hz, 2H), 7.72 (s, 2H), 7.52-7.48 (m, 4H), 7.25-7.19 (m, 10H), 7.08-6.98 (m, 16H).

^{13}C NMR (101 MHz, Chloroform-*d*) δ 147.55, 147.44, 145.79, 138.23, 129.38, 128.55, 128.20, 127.15, 126.62, 125.43, 124.64, 124.49, 124.02, 123.54, 123.23, 123.01.

HR-MS (ESI) *m/z*: calcd for $[C_{50}H_{34}N_4S_2Se]^+$ 834.139, found 833.647.

TPET-BT

A mixture of 1-(4-phenylboronic acid pinacol ester)-1,2,2-triphenylethene (**TPEBE**, 458 mg, 1.0 mmol), **Br-T-BT** (183 mg, 0.4 mmol) and $Pd(PPh_3)_4$ (6 mg, 0.025 mmol), tetrabutylammonium bromide (3 mg), 2 M K_2CO_3 (2.5 mL) and toluene (5 mL) was heated to 90 °C and stirred in dark for 48 h. After cooling, the mixture was washed with brine and dried with anhydrous Na_2SO_4. Then the residue was purified by column chromatography (eluent: CH_2Cl_2/Petroleum ether) to give red solids. Yield: 326 mg, 85 %.

^{1}H NMR (400 MHz, Chloroform-*d*) δ 8.08 (d, *J* = 4.0 Hz, 2H), 7.86 (s, 2H), 7.45 (d, *J* = 8.1 Hz, 4H), 7.36 (d, *J* = 3.8 Hz, 2H), 7.17-7.07 (m, 34H).

^{13}C NMR (101 MHz, Chloroform-*d*) δ 142.43, 133.83, 133.59, 133.36, 133.00, 132.94, 132.77, 132.70, 132.46, 130.05, 129.80, 129.57.

HR-MS (ESI) *m/z*: calcd for $[C_{66}H_{44}N_2S_3]^+$ 960.267, found 959.660.

TPET-BSeT

A mixture of **TPEBE** (458 mg, 1.0 mmol), **Br-T-BSeT** (202 mg, 0.4 mmol), and $Pd(PPh_3)_4$ (6 mg, 0.025 mmol), tetrabutylammonium bromide (3 mg), 2 M K_2CO_3 (2.5 mL), and toluene (5 mL) was heated to 90 °C and stirred in the dark for 48 h. After cooling, the mixture was washed with brine and dried with anhydrous Na_2SO_4. Then the residue was purified by column chromatography (eluent: CH_2Cl_2/Petroleum ether) to give dark purple solids. Yield: 318 mg, 79 %.

^{1}H NMR (400 MHz, Chloroform-*d*) δ 7.97 (d, *J* = 3.9 Hz, 2H), 7.78 (s, 2H), 7.45 (d, *J* = 8.2 Hz, 4H), 7.33 (d, *J* = 3.9 Hz, 2H), 7.10 (dddd, *J* = 22.6, 12.4, 5.8, 3.2 Hz, 34H).

^{13}C NMR (101 MHz, Chloroform-*d*) δ 158.12, 145.75, 143.68, 143.65, 143.55, 143.37, 141.33, 140.34, 138.78, 131.94, 131.45, 131.36, 128.38, 127.85, 127.75, 127.66, 127.18, 126.63, 126.57, 125.47, 124.90, 124.48, 124.00, 123.67.

HR-MS (ESI) *m/z*: calcd for $[C_{66}H_{44}N_2S_2Se]^+$ 1008.211, found 1007.621.

FT-BT

A mixture of 9,9-Di-n-octylfluorene-2-boronic acid pinacol ester (**FBE**, 516 mg, 1.0 mmol), **Br-T-BT** (183 mg, 0.4 mmol) and $Pd(PPh_3)_4$ (6 mg, 0.025 mmol), tetrabutylammonium bromide (3 mg), 2 M K_2CO_3 (2.5 mL) and toluene (5 mL) was heated to 90 °C and stirred in dark for 48 h. After cooling, the mixture was washed with brine and dried with anhydrous Na_2SO_4. Then the residue was purified by column chromatography (eluent: CH_2Cl_2/Petroleum ether) to give magenta solids. Yield: 362 mg, 84 %.

^{1}H NMR (400 MHz, Chloroform-*d*) δ 8.20-8.09 (m, 2H), 7.93 (s, 2H), 7.75-7.65 (m, 8H), 7.49 (d, *J* = 3.9 Hz, 2H), 7.35 (t, *J* = 6.9 Hz, 6H), 2.07-1.98 (m, 8H), 1.23-1.02 (m, 48H), 0.80 (td, *J* = 7.0, 1.7 Hz, 12H).

^{13}C NMR (101 MHz, Chloroform-*d*) δ 152.65, 151.62, 150.96, 146.49, 141.15, 140.58, 138.30, 132.88, 128.66, 127.24, 126.86, 125.78, 125.28, 124.76, 123.91, 122.90, 120.13, 120.03, 119.78, 55.22, 40.42, 31.79, 30.03, 29.71, 29.22, 23.77, 22.70, 22.59, 14.13, 14.07.

HR-MS (ESI) *m/z*: calcd for $[C_{72}H_{88}N_2S_3]^+$ 1076.611, found 1075.975.

FT-BSeT

A mixture of **FBE** (516 mg, 1.0 mmol), **Br-T-BSeT** (202 mg, 0.4 mmol), and $Pd(PPh_3)_4$ (6 mg, 0.025 mmol), tetrabutylammonium bromide (3 mg), 2 M K_2CO_3 (2.5 mL), and toluene (5 mL) was heated to 90 °C and stirred in the dark for 48 h. After cooling, the mixture was washed with brine and dried with anhydrous Na_2SO_4. Then the residue was purified by column chromatography (eluent: CH_2Cl_2/Petroleum ether) to give violet solids. Yield: 355 mg, 79 %.

^{1}H NMR (400 MHz, Chloroform-*d*) δ 7.97 (d, *J* = 3.9 Hz, 2H), 7.78 (s, 2H), 7.69-7.56 (m, 8H), 7.40 (d, *J* = 3.9 Hz, 2H), 7.27 (t, *J* = 6.5 Hz, 6H), 1.95 (p, *J* = 7.4 Hz, 8H), 1.22-0.92 (m, 48H), 0.73 (t, *J* = 7.0 Hz, 12H).

^{13}C NMR (101 MHz, Chloroform-*d*) δ 158.24, 151.61, 150.96, 146.85, 141.09, 140.63, 138.67, 133.01, 128.46, 127.30, 127.24, 126.87, 125.54, 124.73, 123.68, 122.92, 120.13, 120.04, 119.78, 58.51, 55.24, 40.45, 31.82, 30.06, 29.26, 23.79, 22.62, 18.46, 14.11.

HR-MS (ESI) *m/z*: calcd for $[C_{72}H_{88}N_2S_2Se]^+$ 1124.555, found 1123.874.

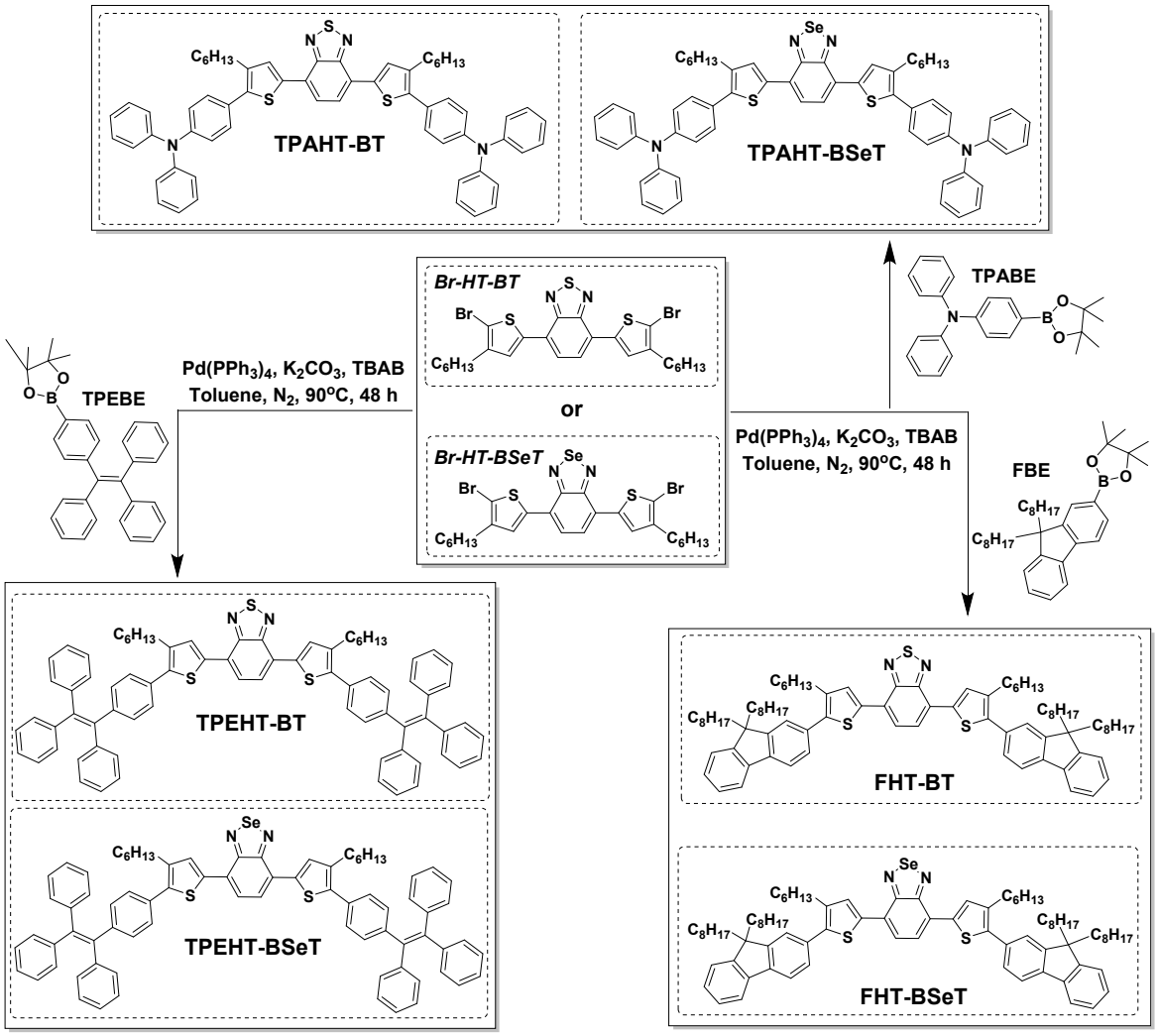

Scheme S2. Synthetic routes of **XHT-BT** and **XHT-BSeT (X** = Triphenylamine**-TPA,** Tetraphenyl ethylene**-TPE, or** Fluorene**-F)**.

TPAHT-BT

A mixture of **TPABE** (372 mg, 1.0 mmol), 4,7-Bis(5-broMo-4-hexylthiophen-2-yl)benzo[c][1,2,5]thiadiazole (**Br-HT-BT**, 250 mg, 0.4 mmol) and $Pd(PPh_3)_4$ (6 mg, 0.025 mmol), tetrabutylammonium bromide (3 mg), 2 M K_2CO_3 (2.5 mL) and toluene (5 mL) was heated to 90 °C and stirred in dark for 48 h. After cooling, the mixture was washed with brine and dried with anhydrous Na_2SO_4. Then the residue was purified by column chromatography (eluent: CH_2Cl_2/Petroleum ether) to give magenta solids. Yield: 317 mg, 83 %.

^{1}H NMR (400 MHz, Chloroform-*d*) δ 8.02 (s, 2H), 7.83 (s, 2H), 7.41-7.36 (m, 4H), 7.31-7.26 (m, 8H), 7.18-7.10 (m, 12H), 7.08-7.03 (m, 4H), 2.75 (t, *J* = 7.9 Hz, 4H), 1.72 (dt, *J* = 15.4, 7.5 Hz, 4H), 1.37-1.21 (m, 12H), 0.89 (td, *J* = 6.9, 5.7, 3.1 Hz, 6H).

^{13}C NMR (101 MHz, Chloroform-*d*) δ 152.66, 147.54, 147.24, 139.39, 130.28, 129.85, 129.34, 128.15, 125.16, 124.70, 123.18, 123.04, 58.48, 31.67, 29.26, 22.64, 18.42, 14.13.

HR-MS (ESI) *m/z*: calcd for $[C_{62}H_{58}N_4S_3]^+$ 954.382, found 953.805.

TPAHT-BSeT

A mixture of **TPABE** (372 mg, 1.0 mmol), 4,7-Bis(5-bromo-4-hexylthiophen-2-yl)benzo[c][1,2,5]selenadiazole (**Br-HT-BSeT**, 269 mg, 0.4 mmol) and $Pd(PPh_3)_4$ (6 mg, 0.025 mmol), tetrabutylammonium bromide (3 mg), 2 M K_2CO_3 (2.5 mL) and toluene (5 mL) was heated to 90 °C and stirred in dark for 48 h. After cooling, the mixture was washed with brine and dried with anhydrous Na_2SO_4. Then the residue was purified by column chromatography (eluent: CH_2Cl_2/Petroleum ether) to give dark purple solids. Yield: 250 mg, 75 %.

^{1}H NMR (400 MHz, Chloroform-*d*) δ 7.91 (s, 2H), 7.75 (s, 2H), 7.38 (d, *J* = 8.3 Hz, 4H), 7.31-7.26 (m, 8H), 7.17-7.09 (m, 12H), 7.08-7.02 (m, 4H), 2.74 (t, *J* = 8.0 Hz, 4H), 1.75-1.66 (m, 4H), 1.38-1.26 (m, 12H), 0.91-0.86 (m, 6H).

^{13}C NMR (101 MHz, Chloroform-*d*) δ 147.51, 147.17, 139.08, 130.15, 129.86, 129.33, 128.31, 125.38, 124.68, 123.16, 123.09, 58.47, 31.68, 29.26, 22.64, 18.43, 14.14.

HR-MS (ESI) *m/z*: calcd for $[C_{62}H_{58}N_4S_2Se]^+$ 1002.327, found 1001.693.

TPEHT-BT

A mixture of **TPEBE** (458 mg, 1.0 mmol), **Br-HT-BT** (250 mg, 0.4 mmol), and $Pd(PPh_3)_4$ (6 mg, 0.025 mmol), tetrabutylammonium bromide (3 mg), 2 M K_2CO_3 (2.5 mL), and toluene (5 mL) was heated to 90 °C and stirred in the dark for 48 h. After cooling, the mixture was washed

with brine and dried with anhydrous Na_2SO_4. Then the residue was purified by column chromatography (eluent: CH_2Cl_2/Petroleum ether) to give crimson solids. Yield: 361 mg, 80 %.

^{1}H NMR (400 MHz, Chloroform-*d*) δ 7.98 (s, 2H), 7.82 (s, 2H), 7.27 (s, 4H), 7.14-7.04 (m, 34H), 2.72-2.64 (m, 4H), 1.66 (p, *J* = 7.6 Hz, 4H), 1.35-1.26 (m, 12H), 0.89 (t, *J* = 6.8 Hz, 6H).

^{13}C NMR (101 MHz, Chloroform-*d*) δ 152.66, 143.69, 143.65, 143.56, 143.00, 141.41, 140.47, 139.88, 139.52, 137.03, 132.50, 131.52, 131.45, 131.39, 131.36, 130.30, 128.30, 127.74, 127.67, 126.59, 126.55, 126.49, 125.65, 125.19, 31.61, 30.87, 29.21, 29.01, 22.64, 14.11.

HR-MS (ESI) *m/z*: calcd for $[C_{78}H_{68}N_2S_3]^+$ 1128.454, found 1127.748.

TPEHT-BSeT

A mixture of **TPEBE** (458 mg, 1.0 mmol), **Br-HT-BSeT** (269 mg, 0.4 mmol) and $Pd(PPh_3)_4$ (6 mg, 0.025 mmol), tetrabutylammonium bromide (3 mg), 2 M K_2CO_3 (2.5 mL) and toluene (5 mL) was heated to 90 °C and stirred in the dark for 48 h. After cooling, the mixture was washed with brine and dried with anhydrous Na_2SO_4. Then the residue was purified by column chromatography (eluent: CH_2Cl_2/Petroleum ether) to give dark purple solids. Yield: 351 mg, 75 %.

^{1}H NMR (400 MHz, Chloroform-*d*) δ 7.79 (s, 2H), 7.65 (s, 2H), 7.18 (d, *J* = 8.1 Hz, 4H), 7.07-6.96 (m, 34H), 2.64-2.55 (m, 4H), 1.57 (t, *J* = 7.8 Hz, 4H), 1.21 (td, *J* = 10.9, 10.1, 6.4 Hz, 12H), 0.81 (t, *J* = 6.7 Hz, 6H).

^{13}C NMR (101 MHz, Chloroform-*d*) δ 158.27, 143.73, 143.69, 143.61, 142.95, 141.40, 140.52, 139.92, 139.57, 137.38, 132.65, 131.54, 131.49, 131.43, 131.40, 130.15, 128.32, 127.79, 127.77, 127.70, 127.13, 126.62, 126.58, 126.52, 125.39, 31.65, 30.91, 29.26, 29.02, 22.69, 14.16.

HR-MS (ESI) *m/z*: calcd for $[C_{78}H_{68}N_2S_2Se]^+$ 1176.399, found 1175.668.

FHT-BT

A mixture of **FBE** (516 mg, 1.0 mmol), **Br-HT-BT** (250 mg, 0.4 mmol), and $Pd(PPh_3)_4$ (6 mg, 0.025 mmol), tetrabutylammonium bromide (3 mg), 2 M K_2CO_3 (2.5 mL), and toluene (5 mL) was heated to 90 °C and stirred in the dark for 48 h. After cooling, the mixture was washed with brine and dried with anhydrous Na_2SO_4. Then the residue was purified by column chromatography (eluent: CH_2Cl_2/Petroleum ether) to give magenta solids. Yield: 423 mg, 85 %.

^{1}H NMR (400 MHz, Chloroform-*d*) δ 8.06 (s, 2H), 7.89 (s, 2H), 7.78-7.71 (m, 4H), 7.53-7.47 (m, 4H), 7.39-7.31 (m, 6H), 2.79 (t, *J* = 7.9 Hz, 4H), 2.00 (t, *J* = 8.2 Hz, 8H), 1.74 (p, *J* = 7.6 Hz, 4H), 1.41-1.03 (m, 60H), 0.89-0.85 (m, 6H), 0.81 (t, *J* = 7.0 Hz, 12H).

^{13}C NMR (101 MHz, Chloroform-*d*) δ 152.67, 151.64, 150.98, 146.52, 141.17, 140.60, 138.32, 132.89, 128.67, 127.27, 126.89, 125.81, 125.33, 124.77, 123.94, 122.93, 120.16, 120.05, 119.81, 55.25, 40.45, 31.82, 30.06, 29.74, 29.26, 23.79, 22.63, 14.11.

HR-MS (ESI) *m/z*: calcd for $[C_{84}H_{112}N_2S_3]^+$ 1244.799, found 1244.0026.

FHT-BSeT

A mixture of **FBE** (516 mg, 1.0 mmol), **Br-HT-BSeT** (269 mg, 0.4 mmol), and $Pd(PPh_3)_4$ (6 mg, 0.025 mmol), tetrabutylammonium bromide (3 mg), 2 M K_2CO_3 (2.5 mL), and toluene (5 mL) was heated to 90 °C and stirred in the dark for 48 h. After cooling, the mixture was washed with brine and dried with anhydrous Na_2SO_4. Then the residue was purified by column chromatography (eluent: CH_2Cl_2/Petroleum ether) to give dull purple solids. Yield: 355 mg, 79 %.

^{1}H NMR (400 MHz, Chloroform-*d*) δ 7.97 (d, *J* = 3.9 Hz, 2H), 7.78 (s, 2H), 7.69-7.56 (m, 8H), 7.40 (d, *J* = 3.9 Hz, 2H), 7.27 (t, *J* = 6.5 Hz, 6H), 1.95 (p, *J* = 7.4 Hz, 8H), 1.22-0.92 (m, 48H), 0.73 (t, *J* = 7.0 Hz, 12H).

^{13}C NMR (101 MHz, Chloroform-*d*) δ 158.24, 151.61, 150.96, 146.85, 141.09, 140.63, 138.67, 133.01, 128.46, 127.30, 127.24, 126.87, 125.54, 124.73, 123.68, 122.92, 120.13, 120.04, 119.78, 58.51, 55.24, 40.45, 31.82, 30.06, 29.26, 23.79, 22.62, 18.46, 14.11.

HR-MS (ESI) *m/z*: calcd for $[C_{72}H_{88}N_2S_2Se]^+$ 1124.555, found 1123.874.

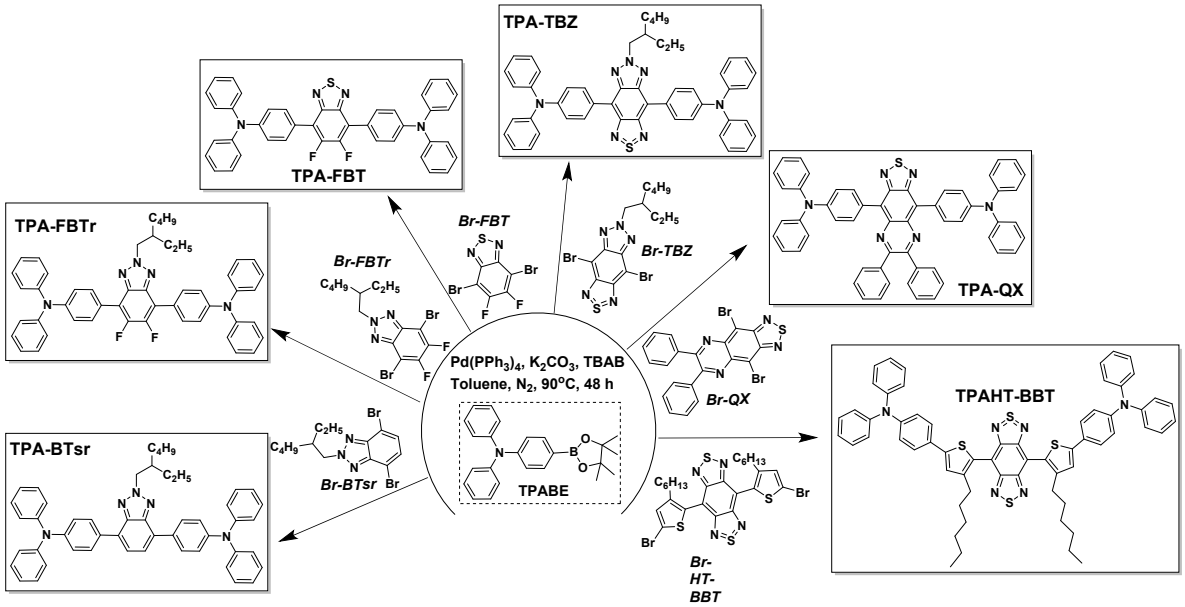

Scheme S3. Synthetic routes of **TPA-X** (**X= BTr, FBTr, FBT, TBZ, QX or HT-BBT**).

TPA-BTsr

A mixture of **TPABE** (372 mg, 1.0 mmol), 4,7-dibromo-2-(2-ethylhexyl)-2H-benzo[d][1,2,3]triazole (**Br-BTsr**, 155 mg, 0.4 mmol) and $Pd(PPh_3)_4$ (6 mg, 0.025 mmol), tetrabutylammonium bromide (3 mg), 2 M K_2CO_3 (2.5 mL) and toluene (5 mL) was heated to 90 °C and stirred in dark for 48 h. After cooling, the mixture was washed with brine and dried with anhydrous Na_2SO_4. The residue was purified by column chromatography (eluent: CH2Cl2/Petroleum ether) to give light-green solids. Yield: 232 mg, 81 %.

^{1}H NMR (400 MHz, Chloroform-*d*) δ 7.93 (d, *J* = 8.2 Hz, 4H), 7.52 (s, 2H), 7.22 (t, *J* = 7.7 Hz, 8H), 7.11 (d, *J* = 8.0 Hz, 12H), 6.98 (d, *J* = 7.5 Hz, 4H), 4.62 (d, *J* = 6.9 Hz, 2H), 2.22 (q, *J* = 6.3 Hz, 1H), 1.34-1.21 (m, 8H), 0.87 (t, *J* = 7.4 Hz, 3H), 0.78 (t, *J* = 7.1 Hz, 3H).

^{13}C NMR (101 MHz, Chloroform-*d*) δ 147.65, 147.54, 143.38, 131.20, 129.32, 129.19, 124.72, 123.76, 123.39, 123.09, 59.83, 40.39, 30.54, 28.43, 23.95, 22.99, 14.06, 10.55.

HR-MS (ESI) *m/z*: calcd for $[C_{50}H_{47}N_5]^+$ 717.3831, found 717.3830.

TPA-FBTr

A mixture of **TPABE** (372 mg, 1.0 mmol), 4,7-Dibromo-2-(2-ethyl-hexyl)-5,6-difluoro-2H-benzotriazole (**Br-BTr**, 170 mg, 0.4 mmol) and $Pd(PPh_3)_4$ (6 mg, 0.025 mmol), tetrabutylammonium bromide (3 mg), 2 M K_2CO_3 (2.5 mL) and toluene (5 mL) was heated to 90 °C and stirred in dark for 48 h. After cooling, the mixture was washed with brine and dried with anhydrous Na_2SO_4. The residue was purified by column chromatography (eluent: CH2Cl2/Petroleum ether) to give light-green solids. Yield: 226 mg, 75 %.

^{1}H NMR (400 MHz, Chloroform-*d*) δ 7.89-7.84 (m, 4H), 7.30 (dd, *J* = 8.5, 7.2 Hz, 8H), 7.22-7.17 (m, 12H), 7.10-7.05 (m, 4H), 4.61 (d, *J* = 7.0 Hz, 2H), 2.21 (t, *J* = 6.3 Hz, 1H), 1.36-1.29 (m, 8H), 0.91 (t, *J* = 7.4 Hz, 3H), 0.85 (d, *J* = 6.9 Hz, 3H).

^{13}C NMR (101 MHz, Chloroform-*d*) δ 148.01, 147.42, 139.25, 131.05, 129.39, 125.14, 124.27, 123.46, 122.23, 58.49, 40.30, 28.35, 23.92, 22.96, 18.44, 14.02, 10.50.

HR-MS (ESI) *m/z*: calcd for $[C_{50}H_{45}F_2N_5]^+$ 753.3643, found 757.3704.

TPA-FBT

A mixture of **TPABE** (372 mg, 1.0 mmol), 4,7-dibroMo-5,6-difluorobenzo[c][1,2,5]thiadiazole (**Br-FBT**, 131 mg, 0.4 mmol) and $Pd(PPh_3)_4$ (6 mg, 0.025 mmol), tetrabutylammonium bromide (3 mg), 2 M K_2CO_3 (2.5 mL) and toluene (5 mL) was heated to 90 °C and stirred in dark for 48 h. After cooling, the mixture was washed with brine and dried with anhydrous Na_2SO_4. Then the residue was purified by column chromatography (eluent: CH_2Cl_2/Petroleum ether) to give orange solids. Yield: 208 mg, 79 %.

^{1}H NMR (400 MHz, Chloroform-*d*) δ 7.73 (d, *J* = 8.6 Hz, 4H), 7.33-7.28 (m, 8H), 7.23-7.17 (m, 12H), 7.11-7.07 (m, 4H).

^{13}C NMR (101 MHz, Chloroform-*d*) δ 148.48, 147.26, 131.35, 129.45, 125.30, 123.67, 123.26, 121.82.

HR-MS (ESI) *m/z*: calcd for $[C_{42}H_{28}F_2N_4S]^+$ 658.2003, found 658.1999.

TPA-TBZ

A mixture of **TPABE** (372 mg, 1.0 mmol), 4,8-dibromo-6-(2-ethylhexyl)-[1,2,5]thiadiazolo[3,4-f]benzotriazole (**Br-TBZ**, 179 mg, 0.4 mmol) and $Pd(PPh_3)_4$ (6 mg, 0.025 mmol), tetrabutylammonium bromide (3 mg), 2 M K_2CO_3 (2.5 mL) and toluene (5 mL) was heated to 90 °C and stirred in dark for 48 h. After cooling, the mixture was washed with brine and dried with anhydrous Na_2SO_4. Then the residue was purified by column chromatography (eluent: CH_2Cl_2/Petroleum ether) to give dark blue solids. Yield: 229 mg, 74 %.

^{1}H NMR (400 MHz, C_6D_6) δ 8.74 (d, *J* = 8.8 Hz, 4H), 7.40 (d, *J* = 8.4 Hz, 4H), 7.14-7.09 (m, 8H), 7.07-7.01 (m, 8H), 6.87 (dd, J_1, J_2 = 7.2 Hz, 4H), 4.41 (d, *J* = 6.8 Hz, 4H), 2.05-1.95 (m, 1H), 1.50-1.40 (m, 2H) , 1.25-1.15 (m, 6H), 0.78 (t, *J* = 6.2 Hz, 3H), 0.70 (t, *J* = 7.4 Hz, 3H) .

^{13}C NMR (101 MHz, C_6D_6) δ 153.40, 152.55, 148.17, 147.88, 139.15, 134.62, 130.15, 129.36, 125.15, 123.16, 121.82, 64.16, 36.47, 34.06, 32.01, 30.10, 25.96, 22.80, 14.06.

HR-MS (ESI) *m/z*: calcd for $[C_{50}H_{45}N_7S+H]^+$ 776.3491, found 776.3530.

TPA-QX

A mixture of **TPABE** (372 mg, 1.0 mmol), 4,9-Dibromo-6,7-diphenyl-[1,2,5]thiadiazolo[3,4-g]quinoxaline (**Br-QX**, 200 mg, 0.4 mmol) and $Pd(PPh_3)_4$ (6 mg, 0.025 mmol), tetrabutylammonium bromide (3 mg), 2 M K_2CO_3 (2.5 mL) and toluene (5 mL) was heated to 90 °C and stirred in dark for 48 h. After cooling, the mixture was washed with brine and dried

with anhydrous Na_2SO_4. Then the residue was purified by column chromatography (eluent: CH_2Cl_2/Petroleum ether) to give dark blue solids. Yield: 91 mg, 28 %.

^{1}H NMR (400 MHz, C_6D_6) δ 8.17 (d, J = 8.4 Hz, 4H), 7.77-7.68 (m, 4H), 7.42 (d, J = 8.4 Hz, 4H) 7.17-7.02 (m, 26H), 6.89 (m, 4H).

^{13}C NMR (101 MHz, C_6D_6) δ 153.39, 152.56, 148.17, 147.88, 139.14, 136.28, 134.61, 130.15, 129.36, 129.14, 129.06, 128.86, 128.06, 127.59, 125.15, 123.16, 121.82.

HR-MS (ESI) *m/z*: calcd for $[C_{56}H_{38}N_6S+H]^+$ 827.2879, found 827.2954.

TPAHT-BBT

A mixture of **TPABE** (372 mg, 1.0 mmol), 4,9-Dibromo-6,7-diphenyl-[1,2,5]thiadiazolo[3,4-g]quinoxaline (**Br-QX**, 200 mg, 0.4 mmol) and $Pd(PPh_3)_4$ (6 mg, 0.025 mmol), tetrabutylammonium bromide (3 mg), 2 M K_2CO_3 (2.5 mL) and toluene (5 mL) was heated to 90 °C and stirred in dark for 48 h. After cooling, the mixture was washed with brine and dried with anhydrous Na_2SO_4. Then the residue was purified by column chromatography (eluent: CH_2Cl_2/Petroleum ether) to give dark green solids. Yield: 157 mg, 39 %.

^{1}H NMR (400 MHz, C_6D_6) δ 7.55 (d, J = 8.4 Hz, 4H), 7.34 (s, 2H), 7.42 (d, J = 8.4 Hz, 4H) 7.13-7.03 (m, 20H), 6.87 (dd, J_1 = 7.2 Hz, J_2 = 6.8 Hz, 4H), 2.72 (t, J = 7.6 Hz, 4H), 1.72-1.60 (m, 4H), 1.15-0.97 (m, 12H), 0.73 (t, J = 6.8 Hz, 4H).

^{13}C NMR (101 MHz, C_6D_6) δ 153.21, 146.60, 145.46, 143.94, 143.78, 143.59, 141.50, 140.68, 132.72, 132.25, 131.58, 129.85, 125.54, 125.27, 116.20, 31.58, 30.66, 30.30, 29.15, 22.53, 13.92.

HR-MS (ESI) *m/z*: calcd for $[C_{62}H_{56}N_6S_4]$ 1012.3449, found 1012.3478.

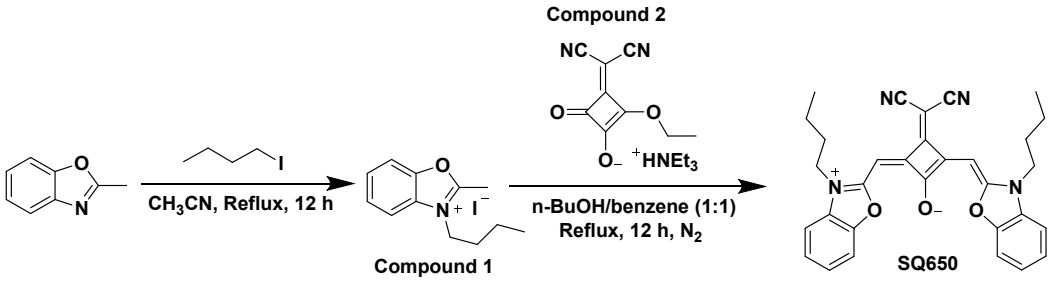

Scheme S4. Synthetic route of **SQ650**.

SQ650

A mixture of 2-methylbenzoxazole (1.33 g, 10 mmol) and 1-iodobutane (3.68 g, 20 mmol) was heated to reflux in acetonitrile for 12 h. After cooling to room temperature, the solvent was removed by filtration, and the solids were washed with cool acetonitrile three times to yield compound 1 (2.85 g, 90%) as a purple solid. The compound 1 was used in the next step without further purification.

A mixture of 189 mg (0.5 mmol) of compound 2, 380 mg (1.2 mmol) of compound 1, and the mixed solvent of n-butanol and benzene (1:1, 6 mL) was heated to reflux under N_2 using a Dean-Stark trap for 12 h. The solvent was then evaporated, and the residue was purified by column chromatography (eluent: DCM/MeOH). Subsequently, the residue was precipitated from DCM/hexane solutions to afford the pure purple solid. Yield: 102 mg, 20 %.

Preparation of chemiluminescent nanodots[5]

A mixture of organic luminophor with a different structure (0.1 mg), F-127 (4.4 mg), CPPO (0.5 mg), and THF (0.5 mL) was sonicated to obtain a clear solution. Then the mixture was swiftly injected into DI water (4 mL), stirred in a fume hood for 1h, and concentrated under vacuum to remove THF. Then, a membrane filter (Pore Size = 0.22 μm) was used to filter the solution, yielding water-dispersed nanoparticles. The prepared nanoparticles were stored at 4 ℃ for further usage.

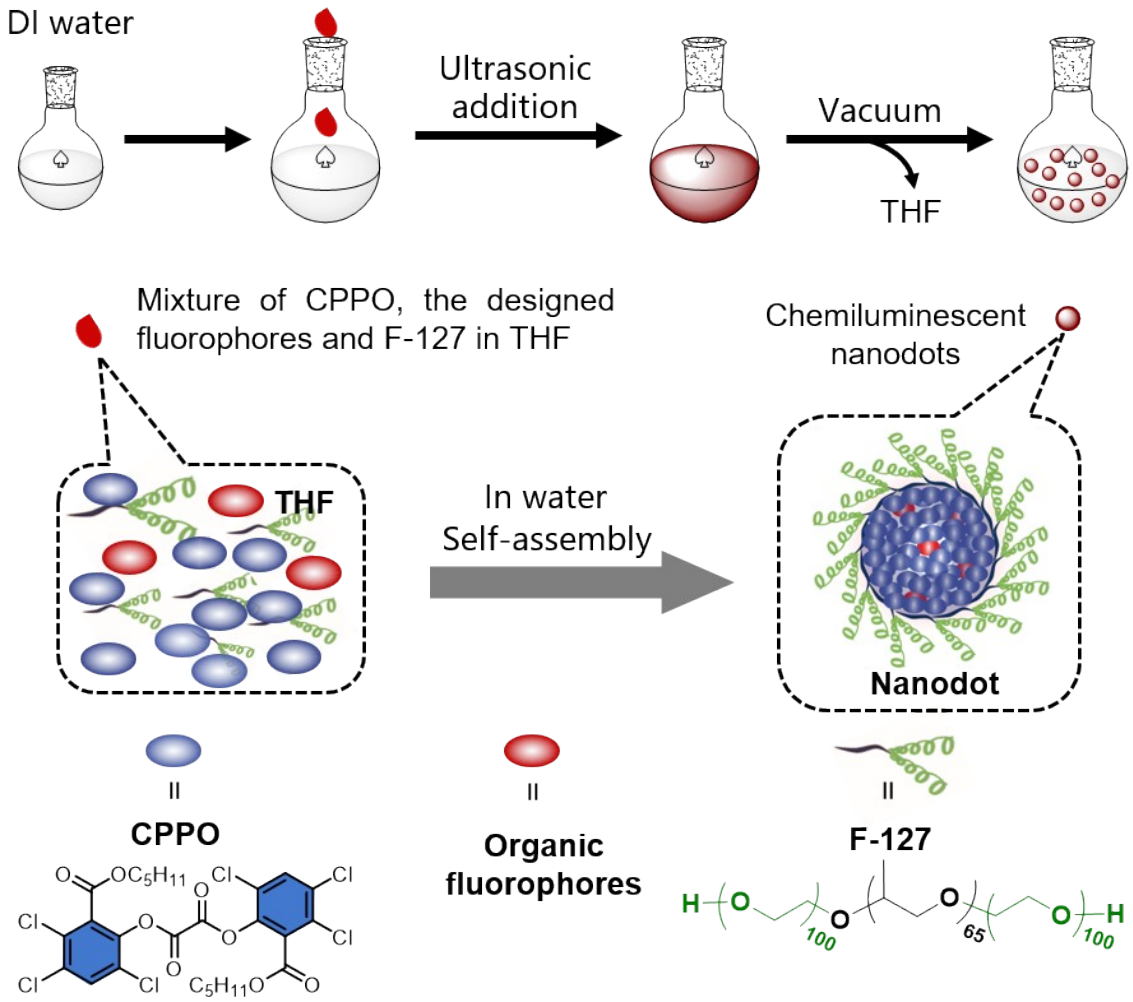

Scheme S5. Schematic illustration of the preparation with different fluorophores and CPPO co-doped nanoparticles (water-dispersible POCL system) using F-127 as a loading matrix.

Fluorescence quantum yield measurement[6]

Coumarin 102 in ethanol (QY = 78%) , FITC dissolved in pH 8 PBS (QY = 90%) , and Rh101 in ethanol (QY = 91%) were chosen as the reference fluorophores to measure the quantum yield of different fluorophores. The quantum yield was calculated as follows：

$$\phi = \phi_{ref} \times \left(\frac{n_{sample}^2}{n_{ref}^2}\right)\left(\frac{I_{sample}}{A_{sample}}\right)\left(\frac{A_{ref}}{I_{ref}}\right) \quad (1)$$

Different concentrations at or below OD 0.1 were measured, and the integrated fluorescence was plotted against absorbance for every fluorescent molecule. Comparison of the slopes yielded the quantum yield of the fluorophore.

Preparation of different reactive oxygen species (ROS)[5,7]

H_2O_2: Commercial H_2O_2 solution (30 % in H_2O_2) was diluted to 1 M H_2O_2, then 50 μL of the diluted solution was added to 1950 μL of the diluted solution; the final concentration is 25 mM.

ClO^-: Hypochlorite stock solution was prepared by dilution of commercial NaClO. 3.72 mg of solid NaClO was added to 5 mL of water to form a 10 mM NaClO solution. Then, 50 μL of the solution was added to 1950 μL of the solution, yielding a final concentration of 250 μM.

O_2^-: 3.5 mg of Solid KO_2 was added to 5 mL of water to form a 10 mM solution directly; then 50 μL of the solution was added to 1950 μL of the solution, yielding a final concentration of 250 μM.

$ONOO^-$: Peroxynitrite stock was prepared following the literature procedure and assayed using a spectrophotometer using $\varepsilon_{302\ nm} = 1670\ cm^{-1}M^{-1}$.

·OH: Hydroxy radical was generated in situ by the addition of 2 mL 50 mM $FeSO_4$ stock solution into a solution containing excess H_2O_2 through Fenton chemistry, then 50 μL of the solution was added to 1950 μL solution, the final concentration is 250 μM.

Theoretical calculations

All theoretical calculations were conducted using the Gaussian 09 suite.[8] Geometry optimizations of all organic dyes and DOD were performed using density functional theory (DFT) with B3LYP/6-31G (d) basis set. Then Multiwfn and VMD[9,10] were used to observe orbitals and map orbital distributions.

Cytotoxicity test

In vitro cytotoxicity was measured using a standard methyl thiazolyl tetrazolium (MTT, Sigma Aldrich) assay in HeLa cell lines. Cells growing in log phase were seeded into a 96-well cell culture plate at 1×10^4/well. Then, TPAHT-BT CLdot were added to the wells of the treatment group at concentrations of 0, 25, 50, 100, 200, 400, 600, and 1000 μg/mL. For the negative control group, 1 μL/well of solvent was diluted in DMEM with a final concentration of 1 %.

The cells were incubated for 24 h at 37 °C under 5 % CO_2. The combined MTT/PBS solution was added to each well of the 96-well assay plate and incubated for an additional 4 h. After removal of the culture solution, 200 μL DMSO was added to each well, and the plate was shaken for 10 min at the shaking table. An enzyme-linked immunosorbent assay (ELISA) reader was used to measure the OD_{570} (absorbance) of each well, with 490 nm as the reference wavelength. The following formula was used to calculate the viability of cell growth:

Viability (%) = (mean of absorbance value of treatment group/mean of absorbance value of control) × 100

In vivo FL and CL imaging of the mouse arthrosis inflammation model

Animal experiments were conducted according to the guidelines of the Institutional Animal Care and Use Committee, Laboratory Animal Center, Nantong University (P20250226-024). The arthrosis inflammation model in mice was established by intra-articular injection of 20 mM hydrogen peroxide (5 μL). Then, 20 μL of TPAHT-BT CLdot (3 mg/mL) were injected into the arthritic joints of mice after 1 minute. Then the mice were transferred into the homemade CL imaging system we fabricated for CL imaging without a light source. At least 3 mice were used as parallel controls in each imaging experiment. A red LED light was used as the excitation light, and a 792 band-pass filter was adopted for FL imaging.

Histological analysis

After intravenous injection of TPAHT-BT CLdot, the organs were harvested and fixed in 4% paraformaldehyde for H&E staining analysis, embedded in paraffin, sectioned, and stained with hematoxylin and eosin. The sections were observed under an optical microscope.

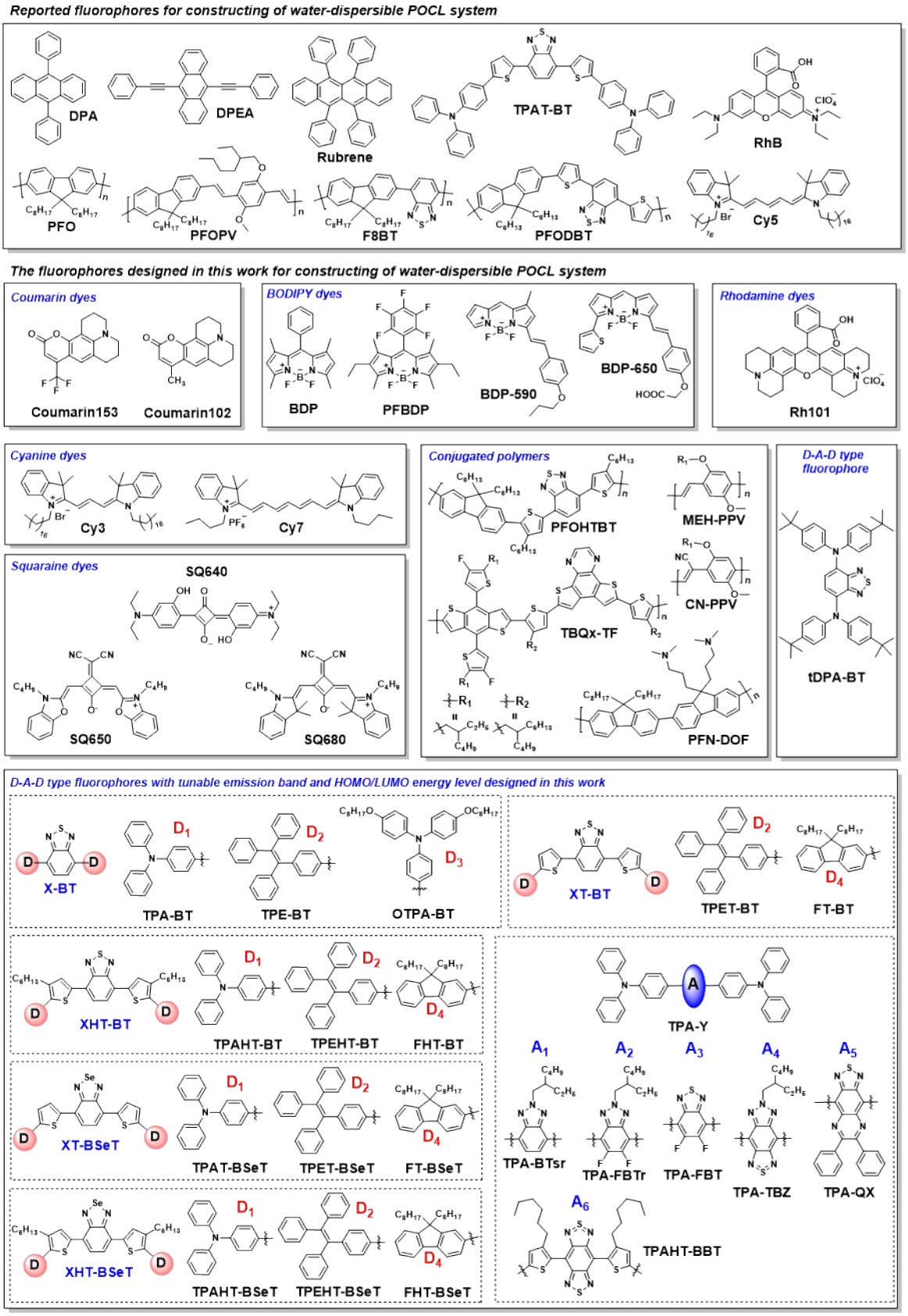

Figure S1. Chemical structures of the dyes used for constructing water-dispersible POCL nanoparticles

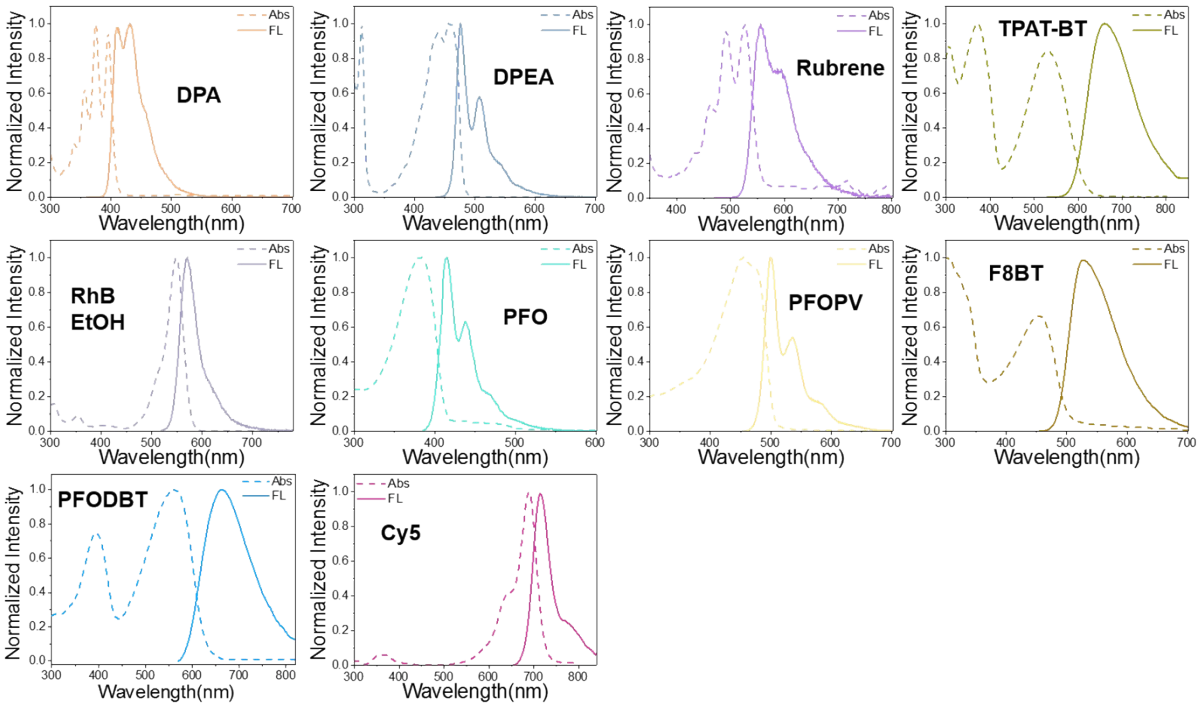

Figure S2. Absorption and emission spectra (in organic solvent, the spectra without indicating solvent were measured in toluene) of the reported emitters for constructing a water-dispersible POCL system.

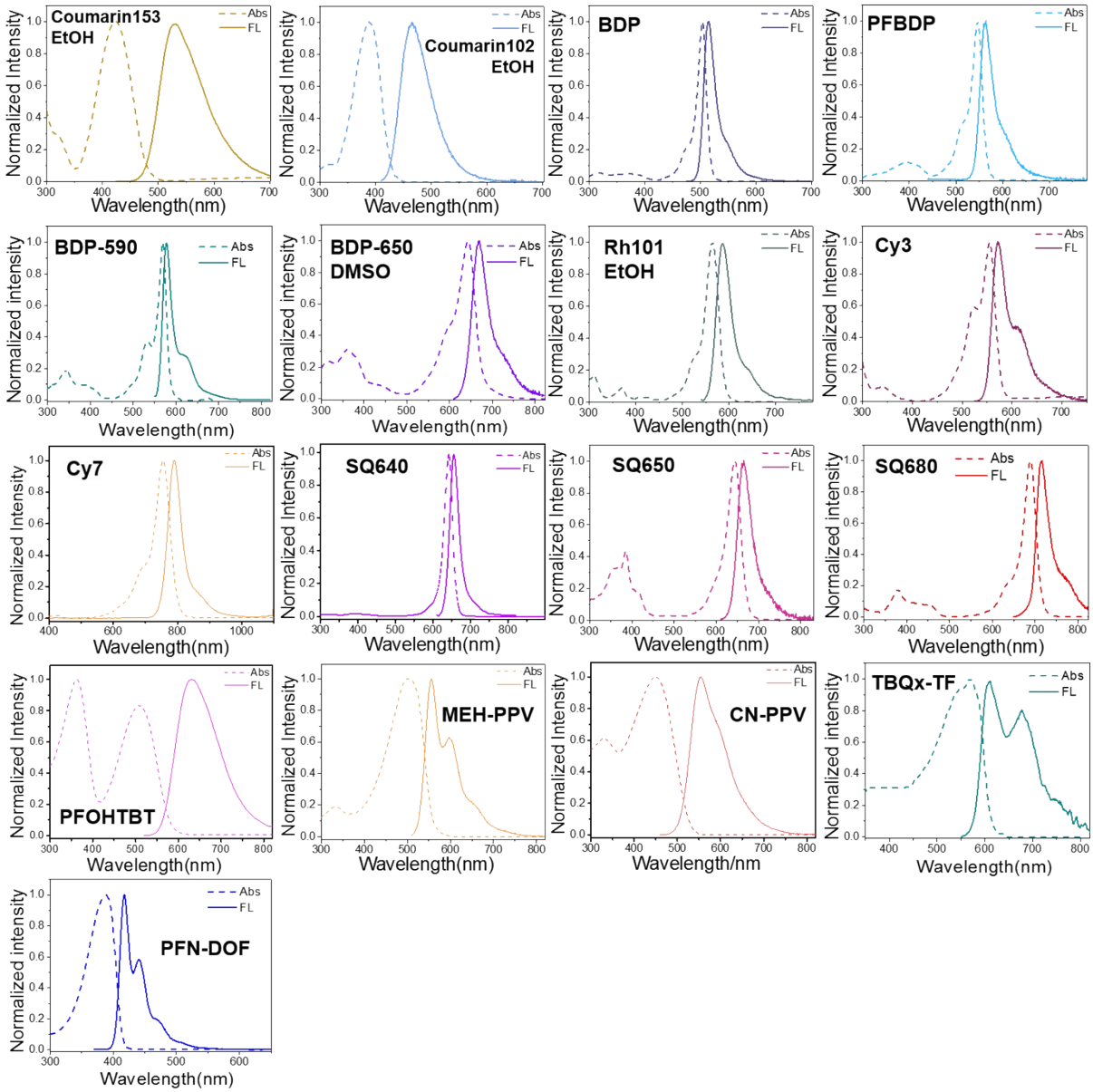

Figure S3. Absorption and emission spectra of the designed traditional organic dyes and conjugated polymers for constructing a water-dispersible POCL system in this work. The fluorophores are generally dissolved in toluene for optical determination. The spectra of several fluorophores determined in other organic solvents were labeled.

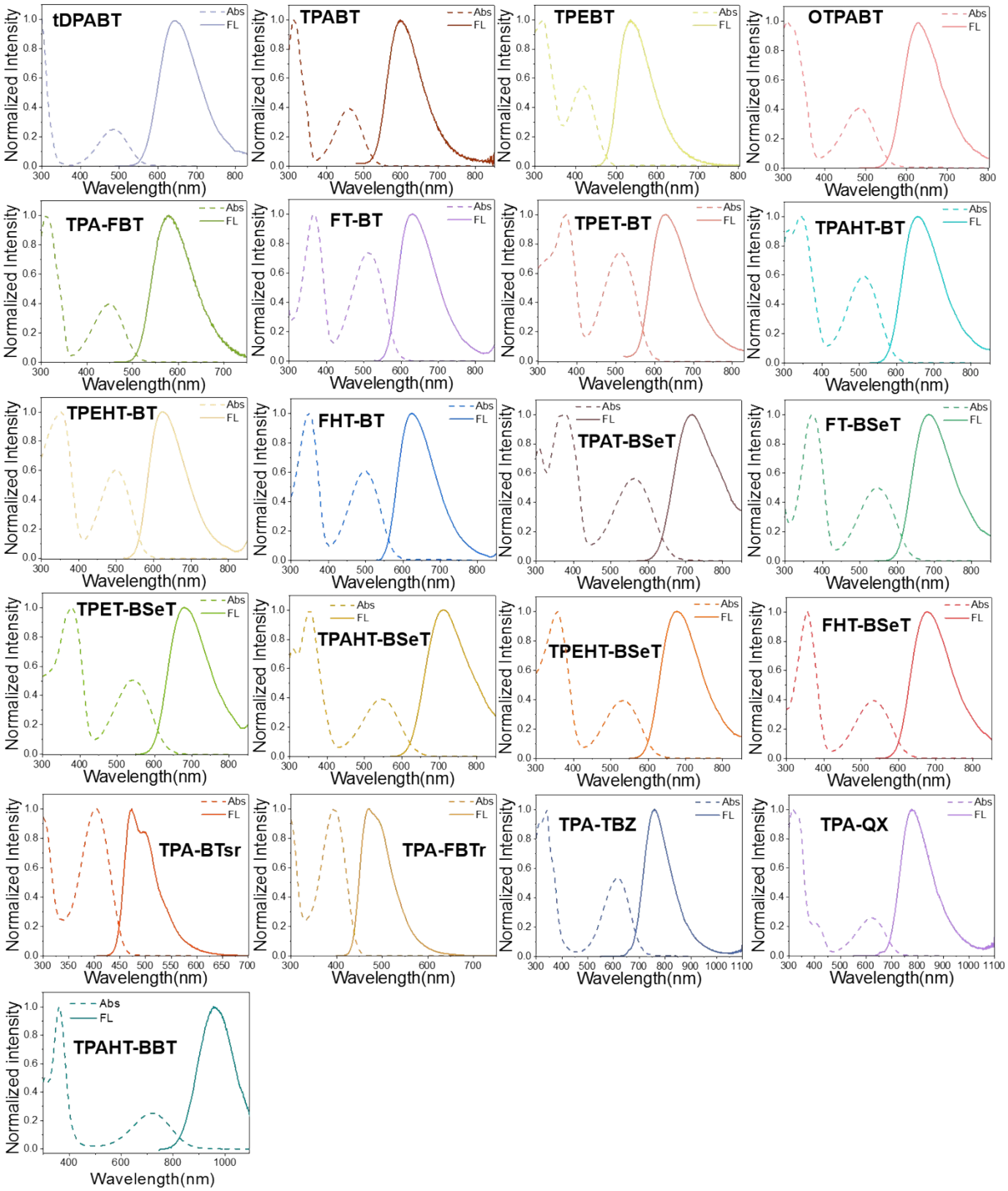

Figure S4. Absorption and emission spectra (in toluene) of the designed D-A-D type fluorophores for constructing a water-dispersible POCL system in this work.

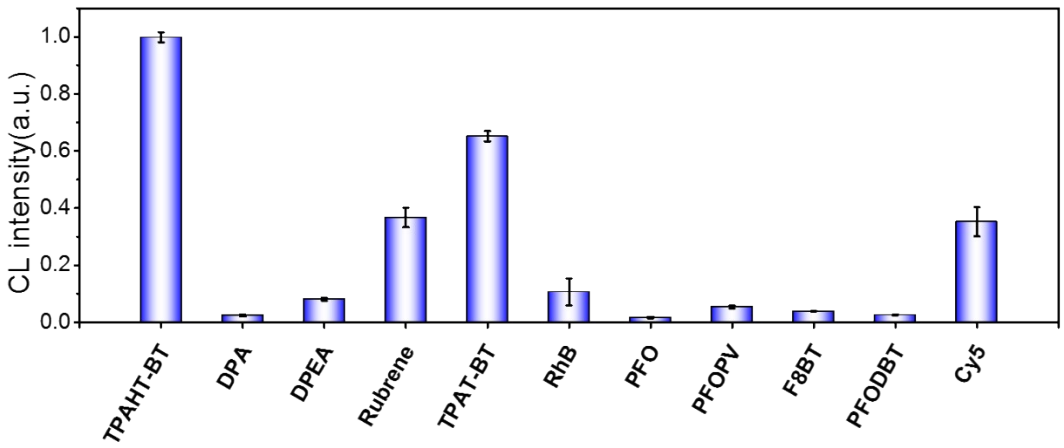

Figure S5. Comparison of the chemiluminescence intensity of POCL nanoparticles, which use TPAHT-BT and the reported fluorophores as the emitters in aqueous solution, respectively (TPAHT-BT is used as reference).

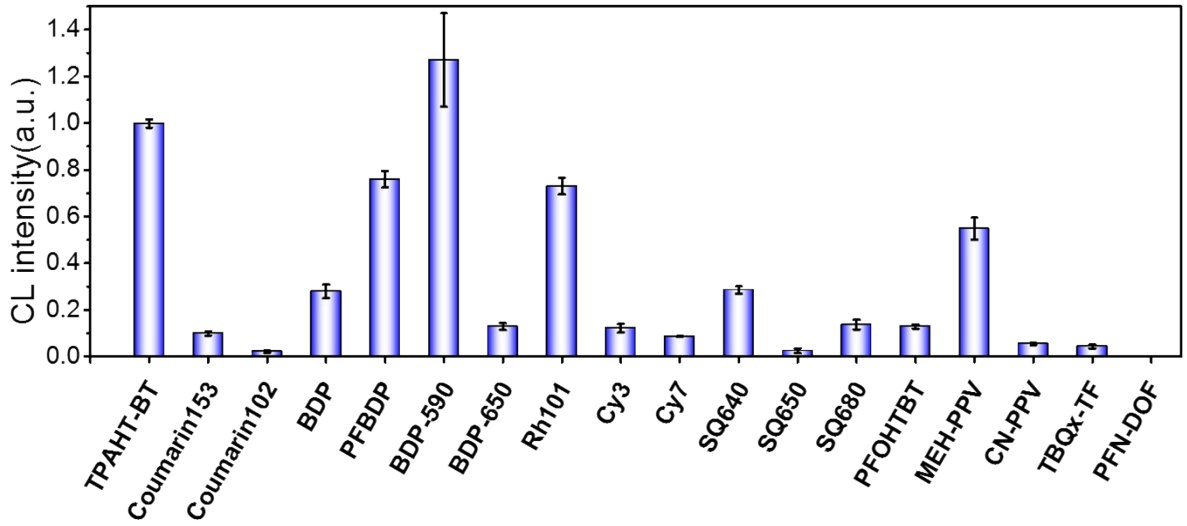

Figure S6. Comparison of the chemiluminescence intensity of POCL nanoparticles that use TPAHT-BT and other traditional fluorophores as the emitters in aqueous solution, respectively.

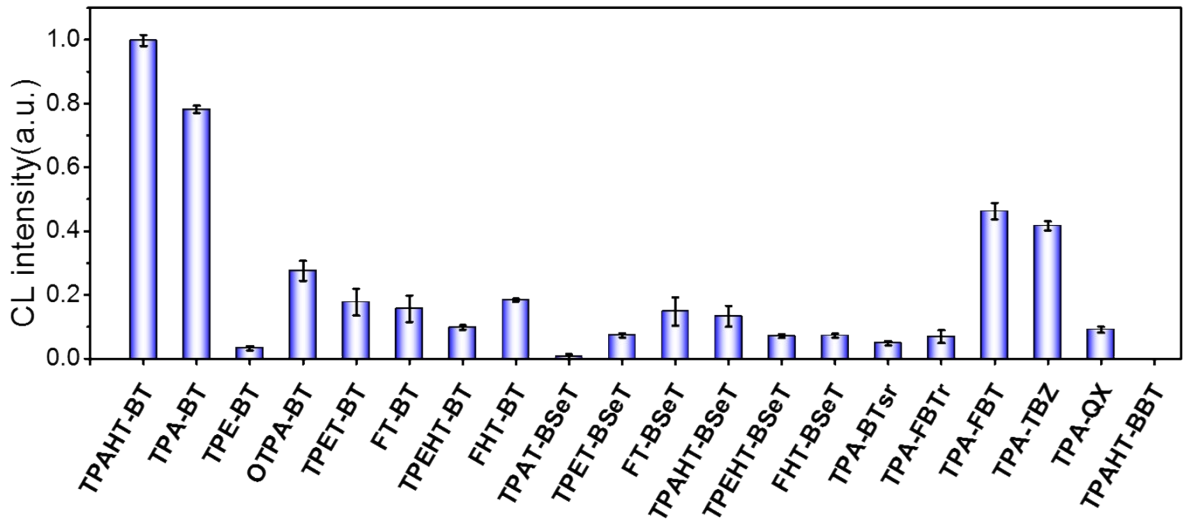

Figure S7. Comparison of the chemiluminescence intensity of POCL nanoparticles that use TPAHT-BT and other D-A-D-type fluorophores as the emitters in aqueous solution, respectively.

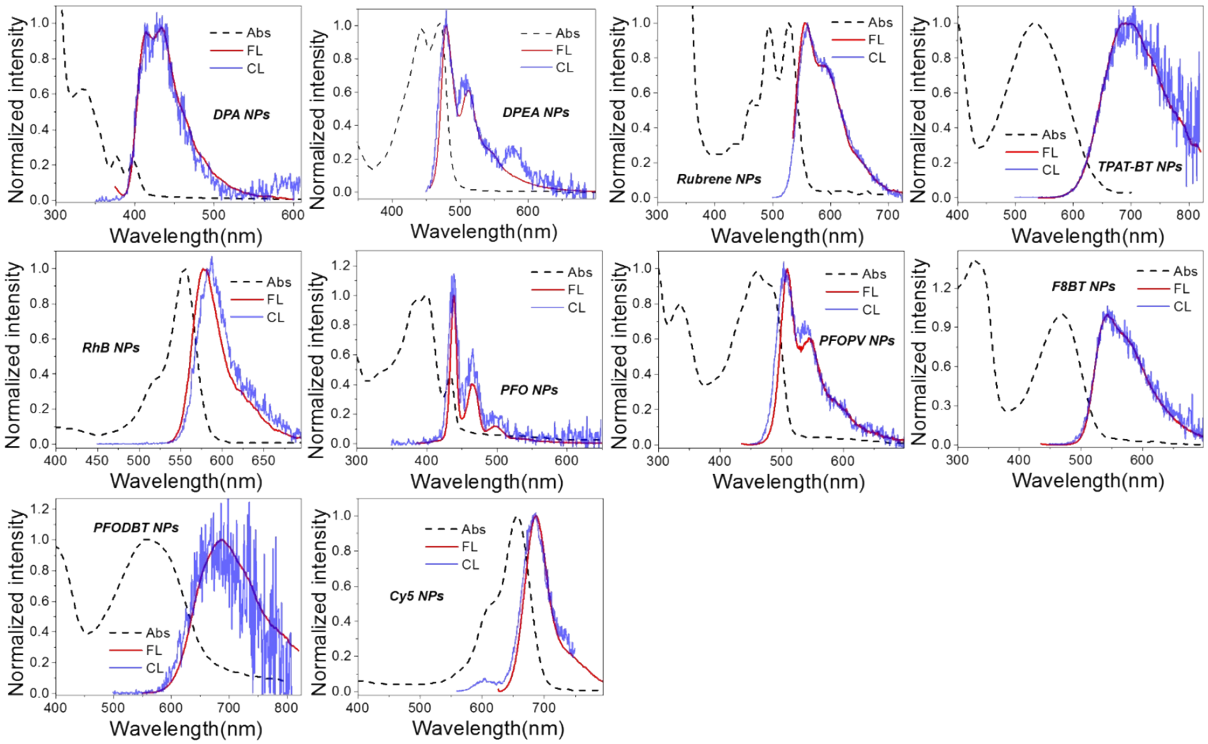

Figure S8. Normalized absorption, emission, and chemiluminescence spectra of the water-dispersible POCL system (nanoparticles, NPs), which uses different reported fluorophores as the emitters, respectively.

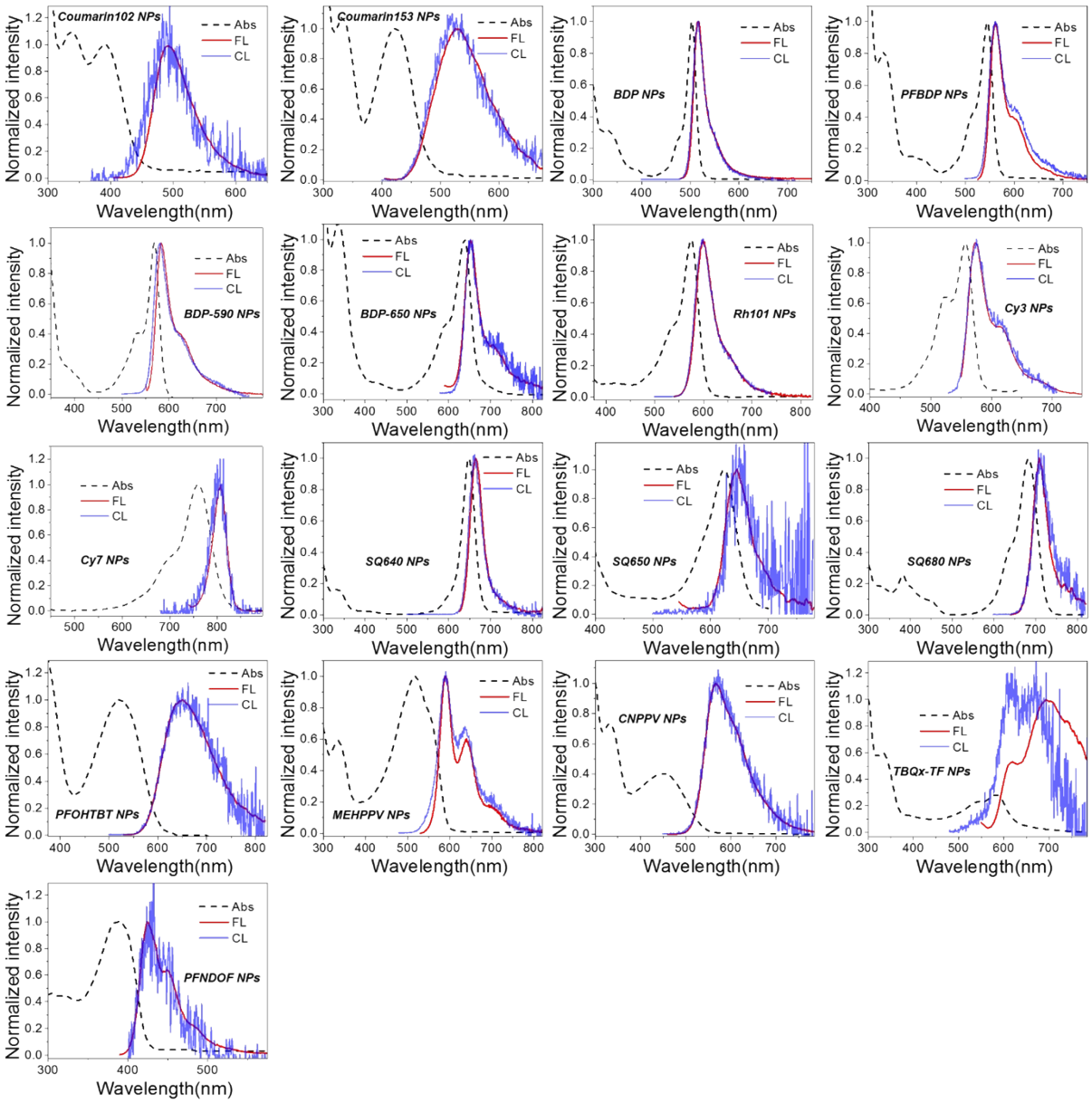

Figure S9. Normalized absorption, emission, and chemiluminescence spectra of the water-dispersible POCL system (nanoparticles, NPs), which uses different traditional fluorophores (including coumarin, BODIPY, cyanine, squaraine, and fluorescent conjugated polymers) as the emitters, respectively.

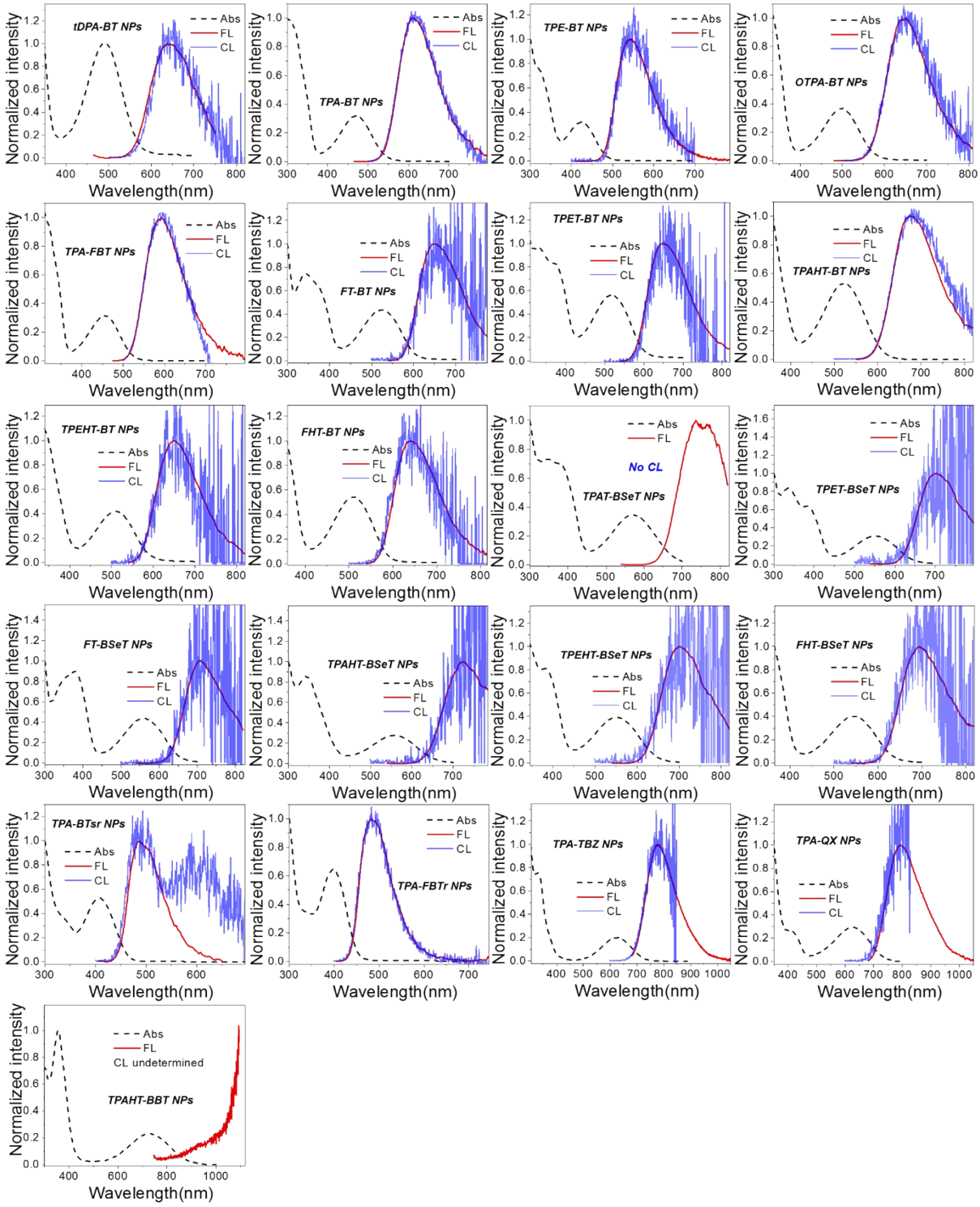

Figure S10. Normalized absorption, emission, and chemiluminescence spectra of the water-dispersible POCL system (nanoparticles, NPs), which uses D-A-D-type fluorophores as the emitters, respectively.

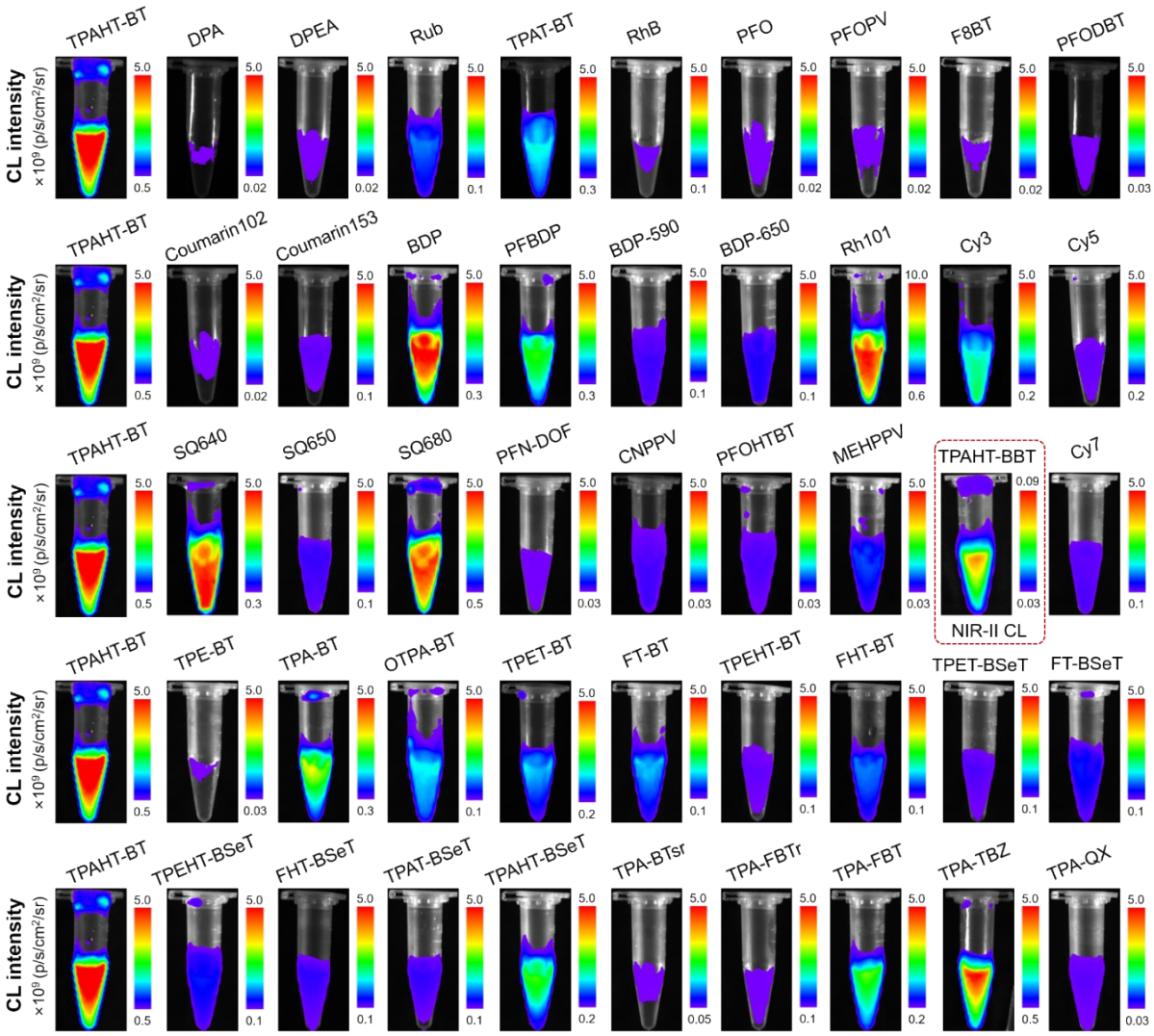

Figure S11. Comparison of the CL of the POCL NPs separately composed of different fluorophores. The chemiluminescence images were collected (at 3 min post the mixing of POCL NPs and H_2O_2) by a highly sensitive chemiluminescence imaging system (Biolight biotechnology Co., Ltd., Aniview 100) at identical conditions (H2O2: 50 mM, POCL NPs:0.1 mg/mL, 37 ºC).

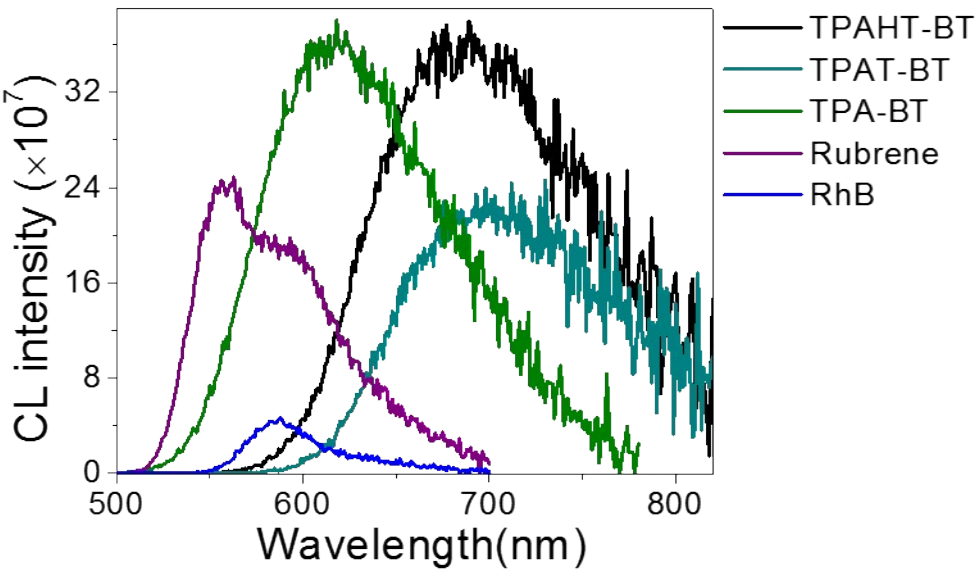

Figure S12. Comparison of the CL of the POCL NPs separately composed by TPAHT-BT, TPAT-BT, and TPA-BT, and the reported fluorophores (Rubrene and Rhodamine B)

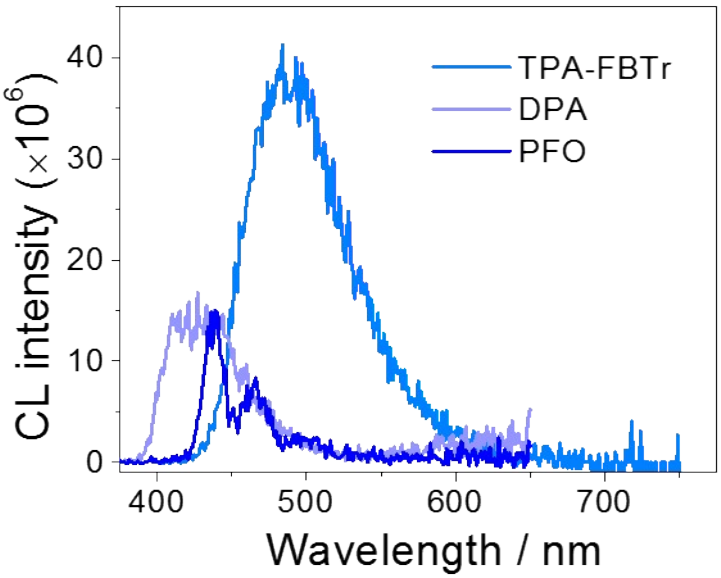

Figure S13. Comparison of the CL of the POCL NPs composed by TPA-FBTr, and the reported blue POCL emitters (PFO and DPA)

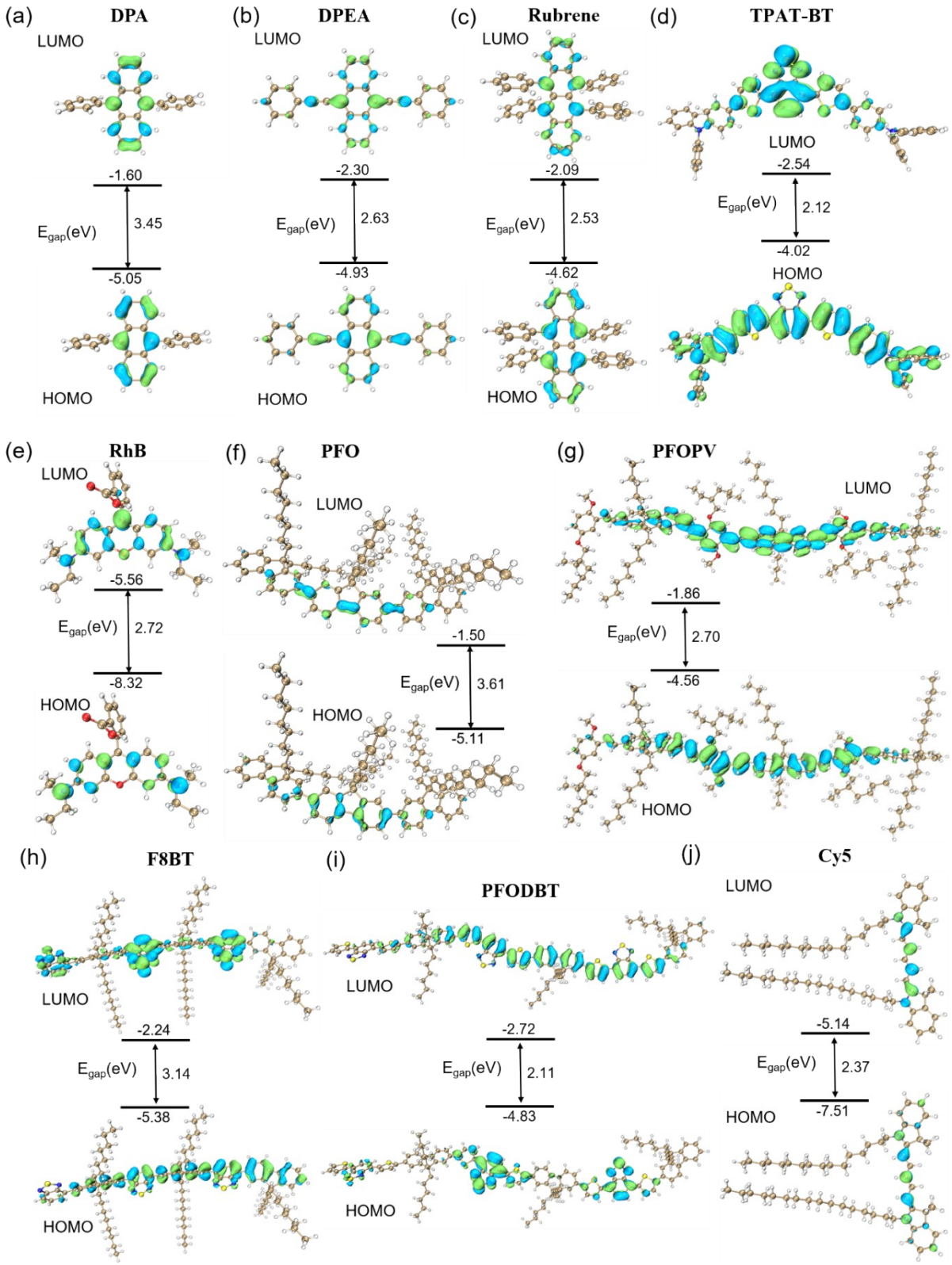

Figure S14. Calculated orbital distribution of the reported fluorophores.

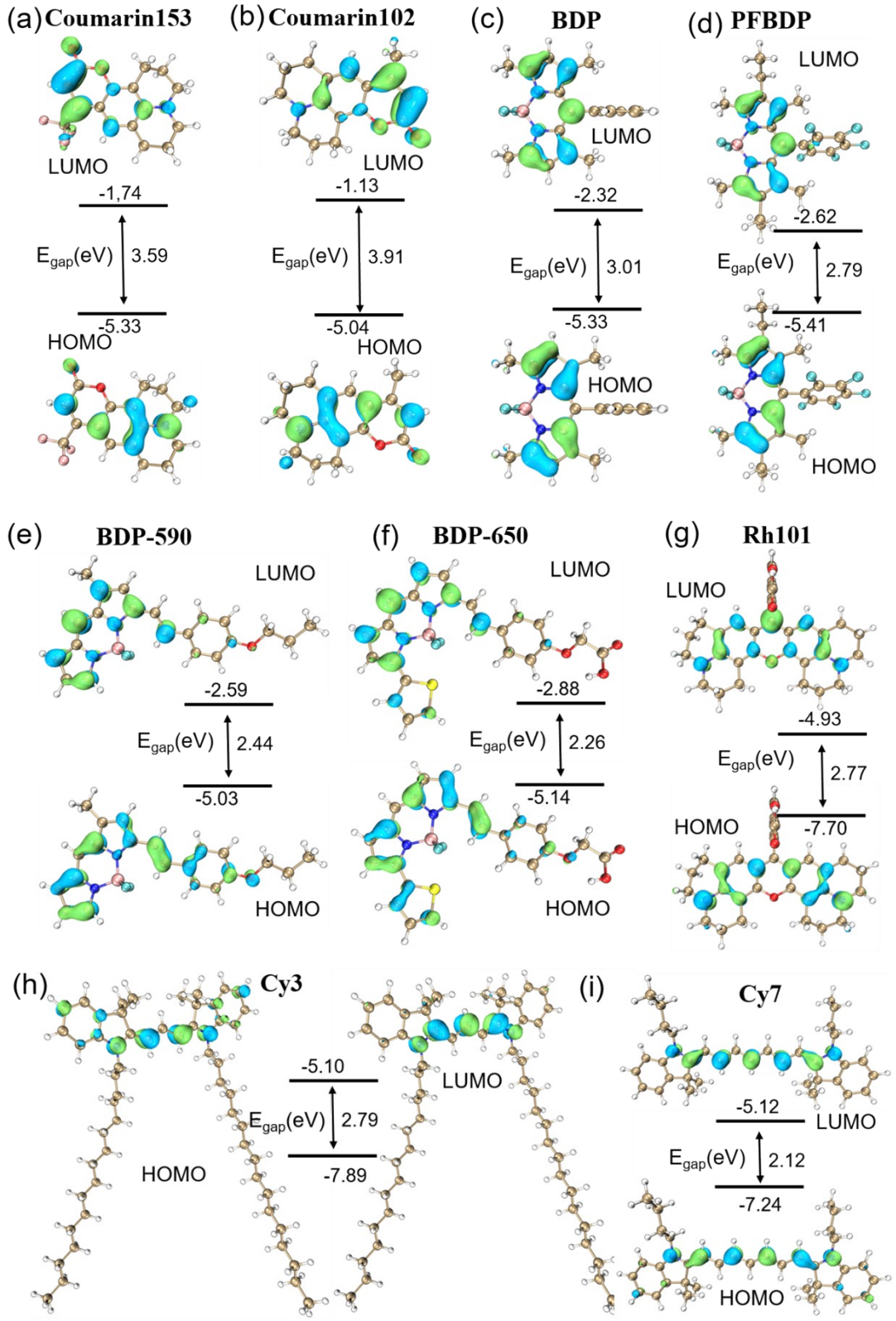

Figure S15. Calculated orbital distribution of traditional fluorophores, including a) coumarin 153, b) coumarin 102, c) BDP, d) PFBDP, e) BDP-590, f) BDP-650, g) Rh101, h) Cy3 and i) Cy7.

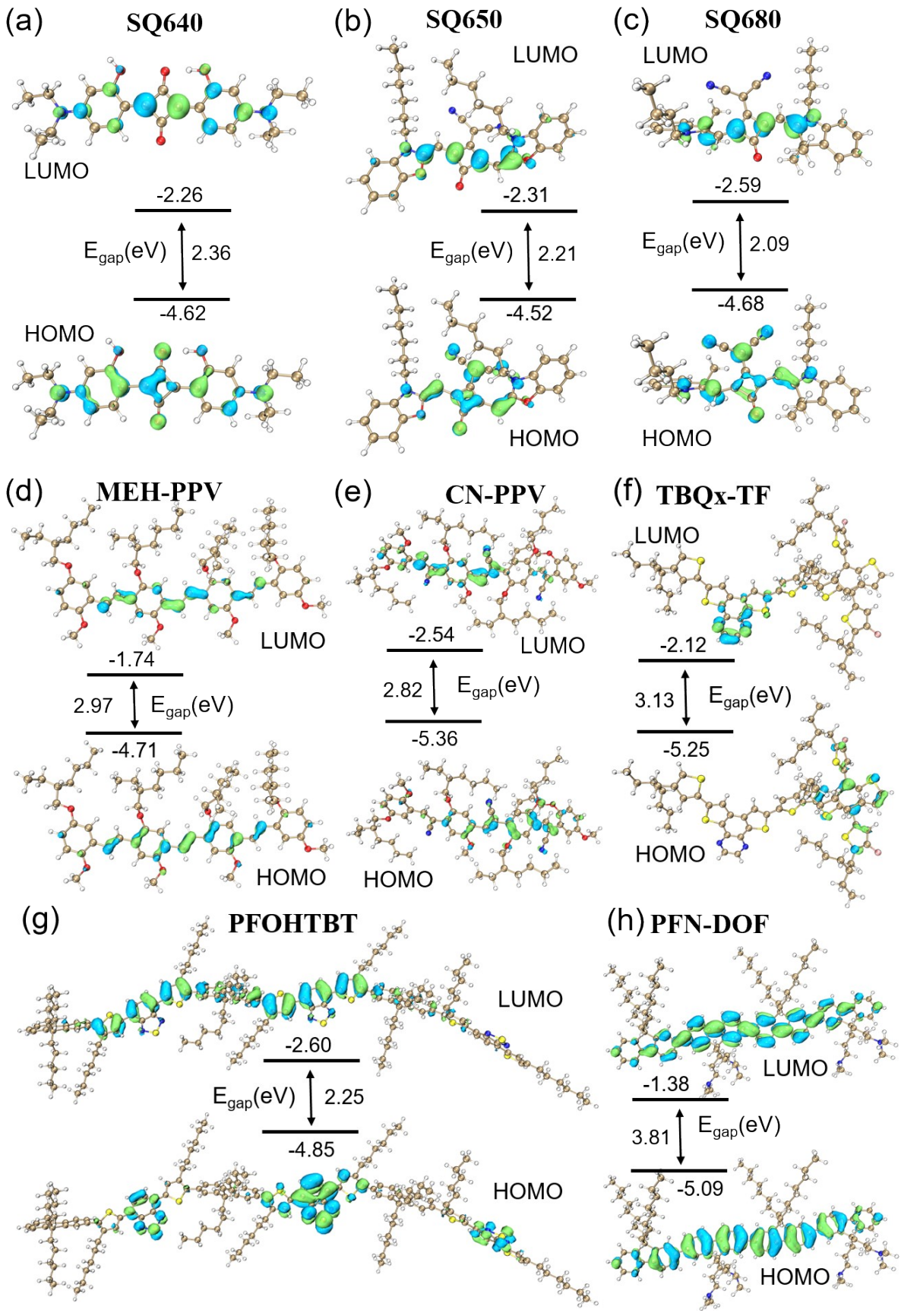

Figure S16. Calculated orbital distribution of traditional fluorophores, including a) SQ640, b) SQ650, c) SQ680, d) MEHPPV, e) CN-PPV, f) TBQx-TF, g) PFOHTBT, and h) PFN-DOF.

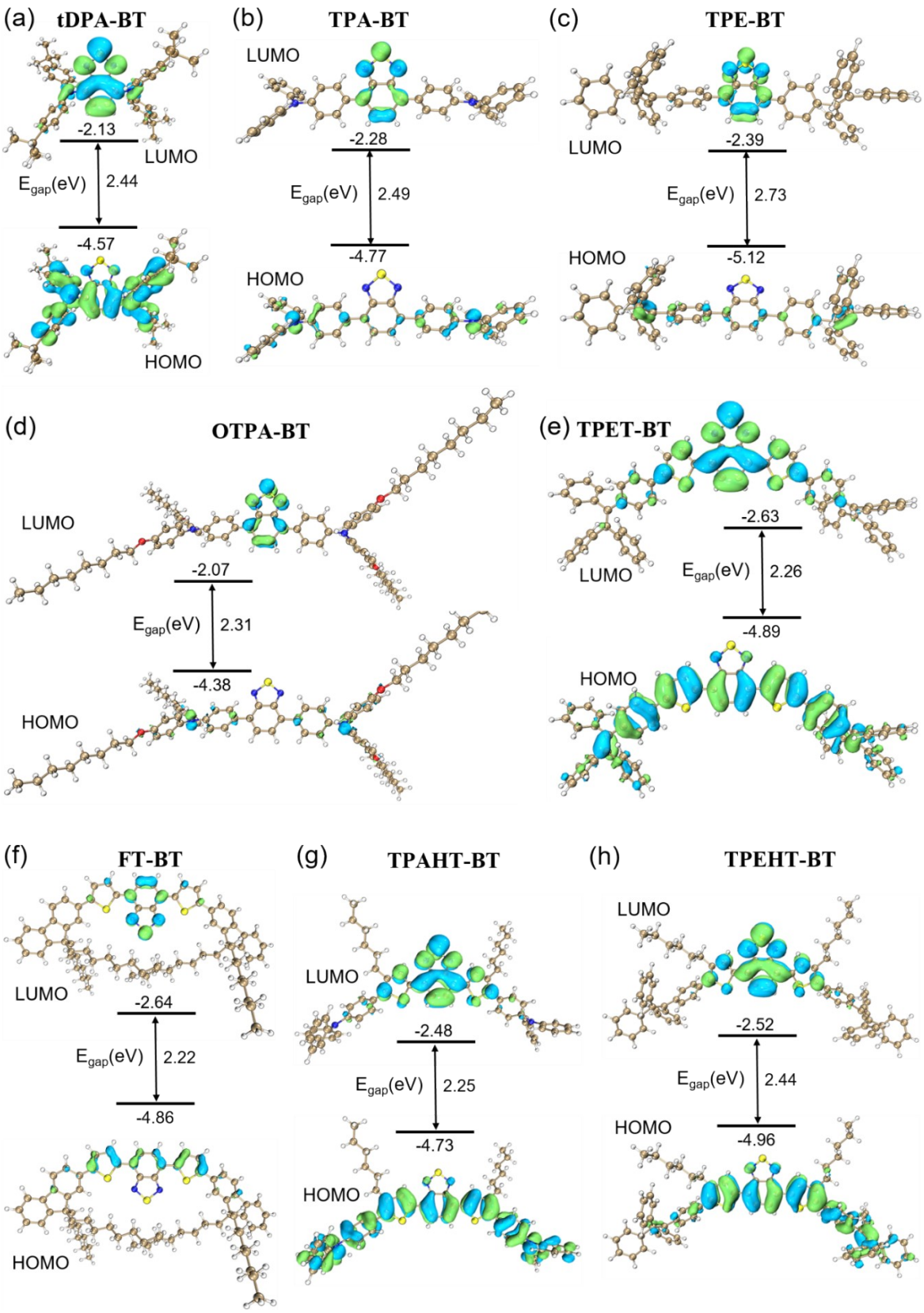

Figure S17. Calculated orbital distribution of the developed fluorophores, including a) tDPA-BT, b) TPA-BT, c) TPE-BT, d) OTPA-BT, e) TPET-BT, f) FT-BT, g) TPAHT-BT, and h) TPEHT-BT.

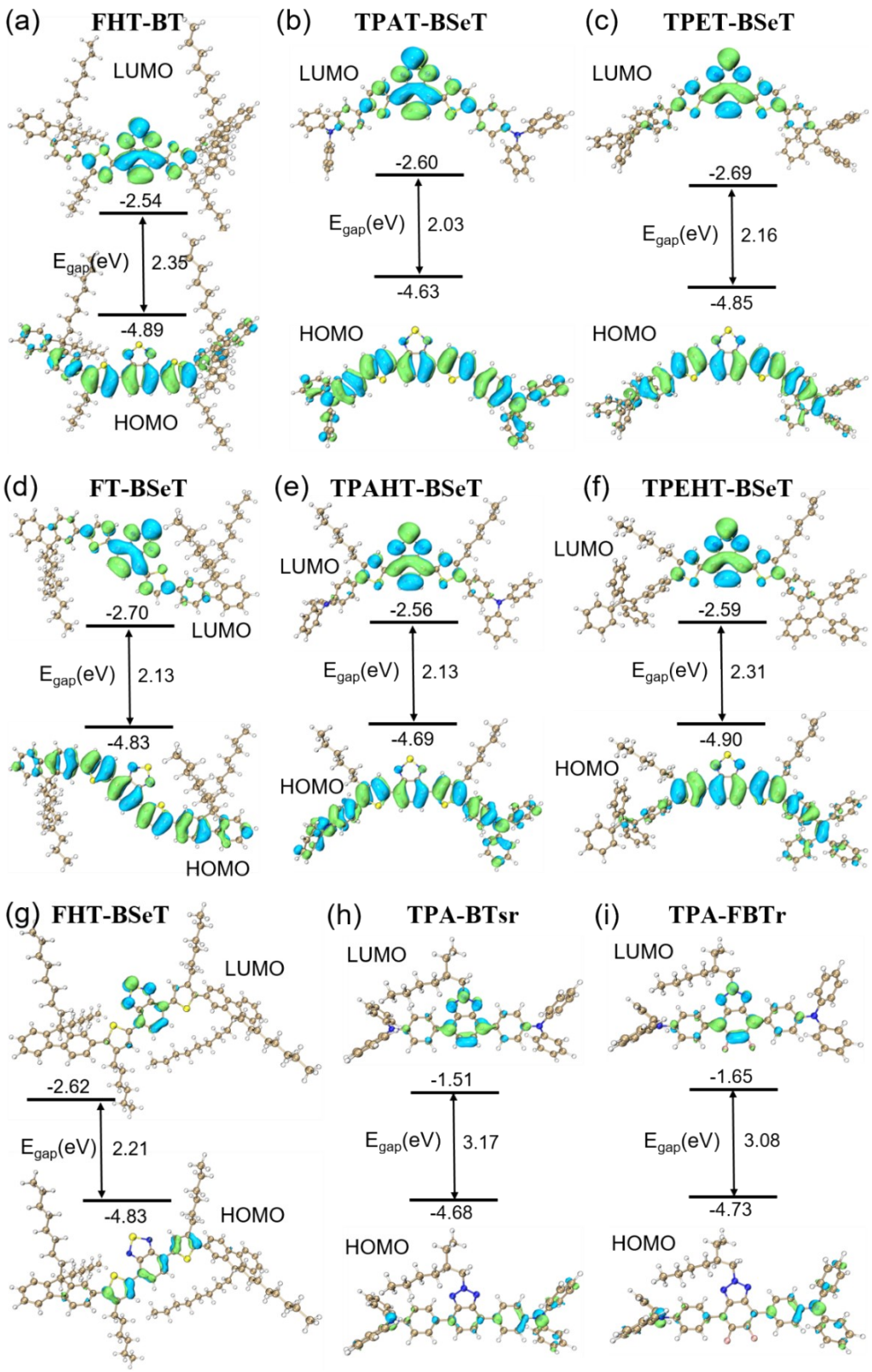

Figure S18. Calculated orbital distribution of traditional fluorophores including a) FHT-BT, b) TPAT-BSeT, c) TPET-BSeT, d) FT-BSeT, e) TPAHT-BSeT, f) TPEHT-BSeT, g) FHT-BSeT, h) TPA-BTsr and i) TPA-FBTr.

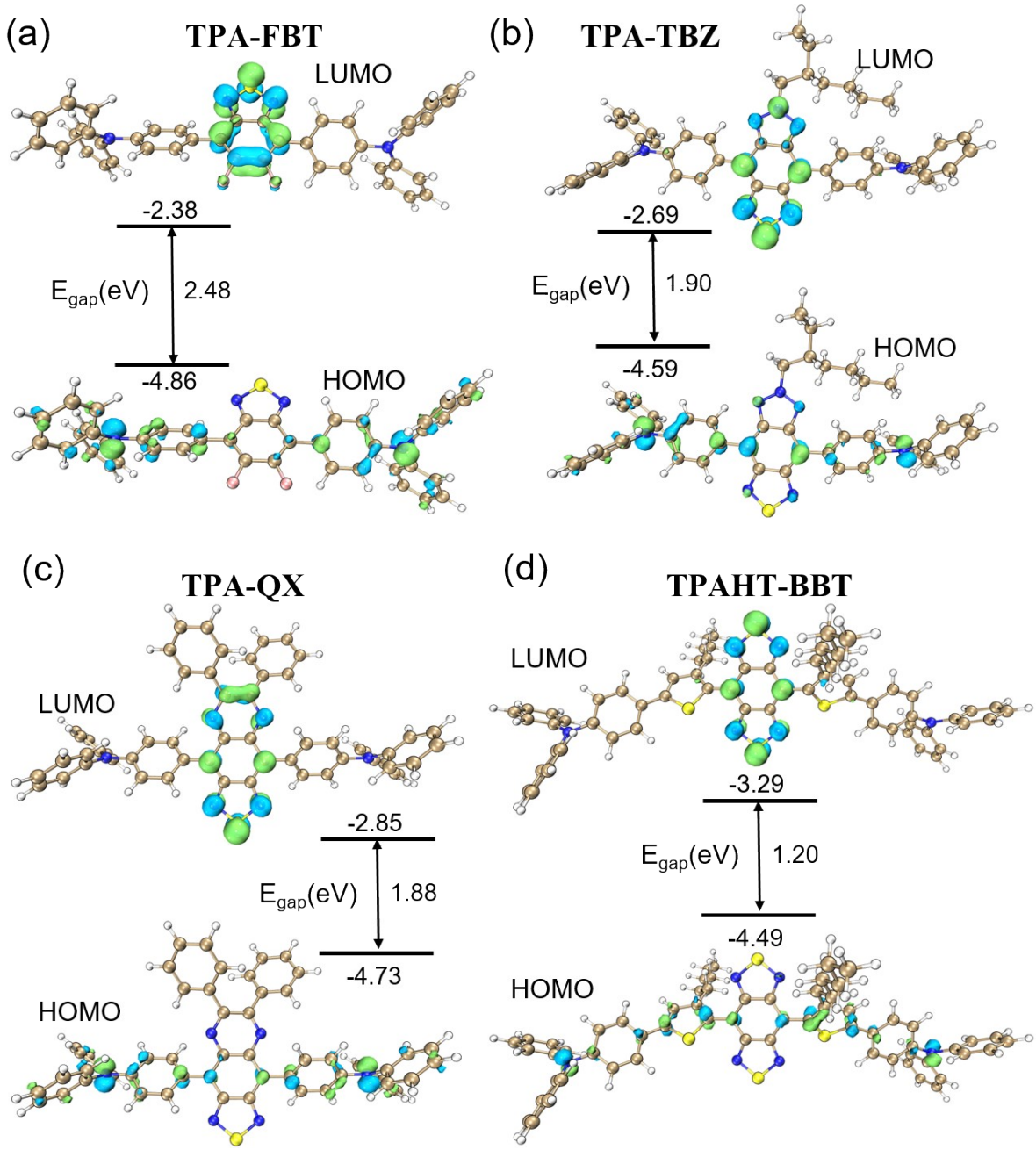

Figure S19. Calculated orbital distribution of traditional fluorophores, including a) TPA-FBT b) TPA-TBZ c) TPA-QX and d) TPAHT-BBT.

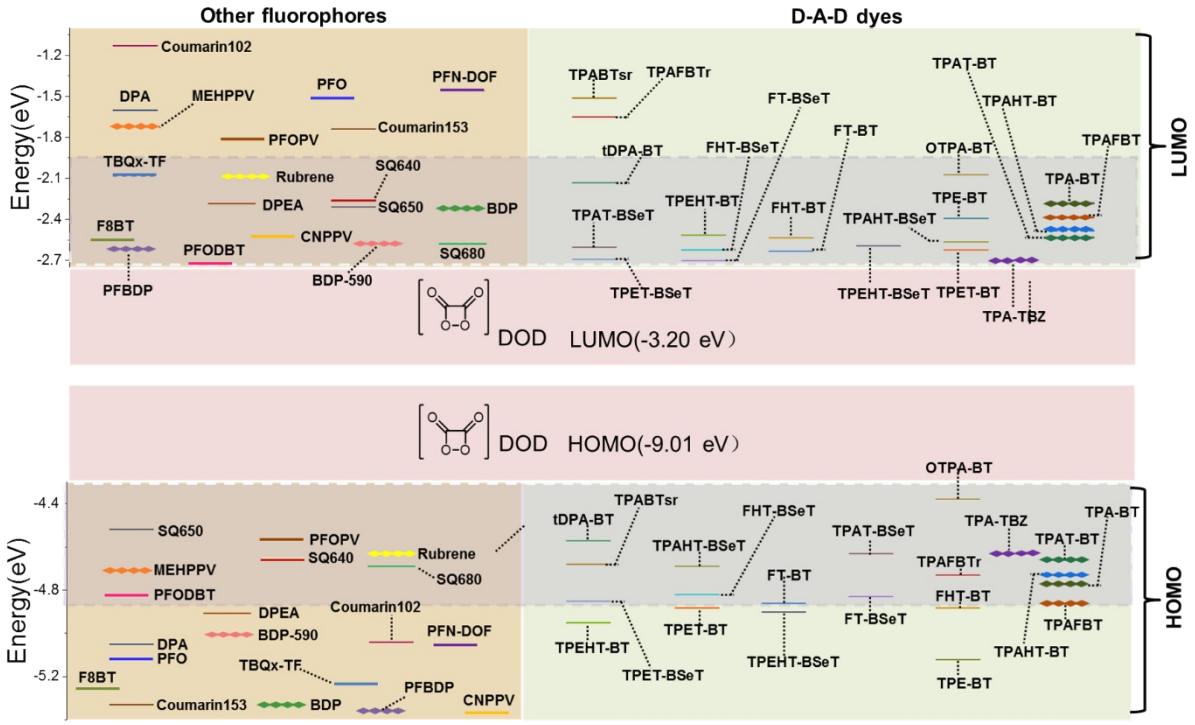

Figure S20. HOMO and LUMO energy levels of DOD and different lumoniphors (as the chemiluminescent emitter of CLNPs).

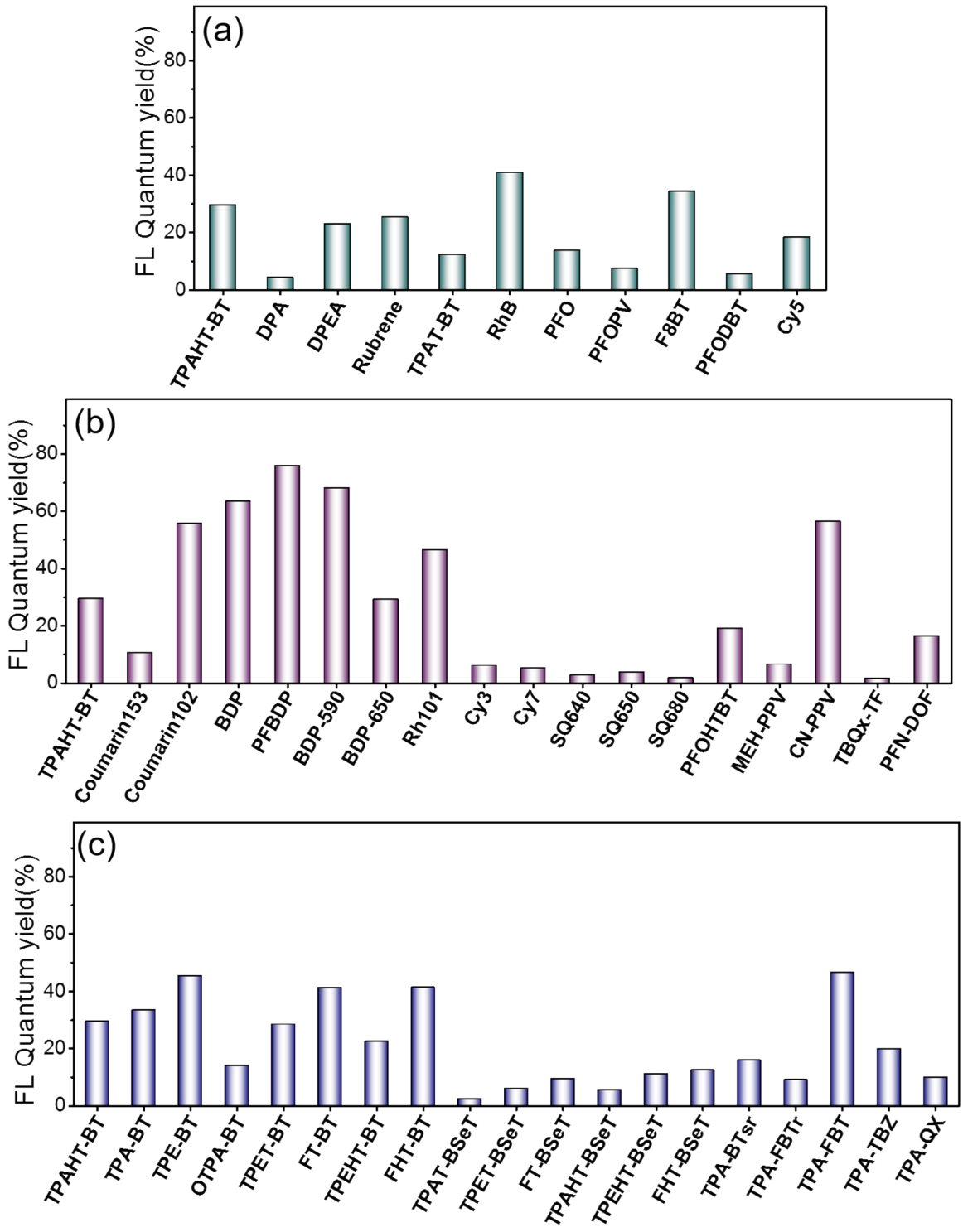

Figure S21. Fluorescence quantum yield of the POCL NPs composed of different kinds of fluorophores in aqueous solution. a) Reported fluorophores, b) traditional fluorophores, and c) the D-A-D type fluorophores developed in this work.

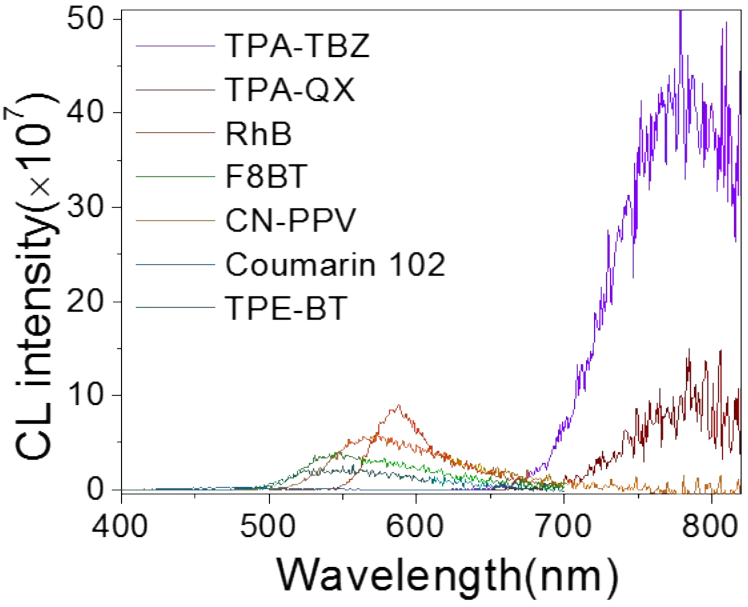

Figure S22. Comparison of the CL intensity of the POCL NPs, which were composed by using TPA-TPZ, TPA-QX, RhB, F8BT, CN-PPV, Coumarin 102, and TPE-BT as the emitter, respectively. The deep NIR emissive fluorophores (TPA-TPZ: QY~19.8% and TPA-QX: 9.9%) exhibited superior chemiluminescence in aqueous solution compared to various visible emissive fluorophores, including RhB (40.8%), TPE-BT (45.3%), coumarin102 (55.7%), FHT-BT (41.2%), CN-PPV (56.4%), and F8BT (34.3%), despite their relatively lower QY. This phenomenon can be attributed to the enhanced intramolecular charge-transfer (ICT) effect and the energy-gap law. It is noteworthy that the ΔE_{LUMO} and ΔE_{HOMO} values of these two dyes also fall within the optimal region, specifically the fourth quadrant. These results confirmed the universality of the proposed design principle for achieving a bright, water-dispersible POCL system, as demonstrated in this study. Furthermore, since the red-shifting emission of organic fluorophores is typically achieved by extending their conjugated scaffolds or enhancing the push-pull electron effect, it can be predicted that the energy levels of the organic POCL emitters with red-shifted emission will tend to fall within the optimal energy level region. Therefore, it is suggested that the bright deep-NIR-I/NIR-II POCL system could be achieved when the QY of the deep-NIR-I/NIR-II emissive fluorophores was significantly enhanced.

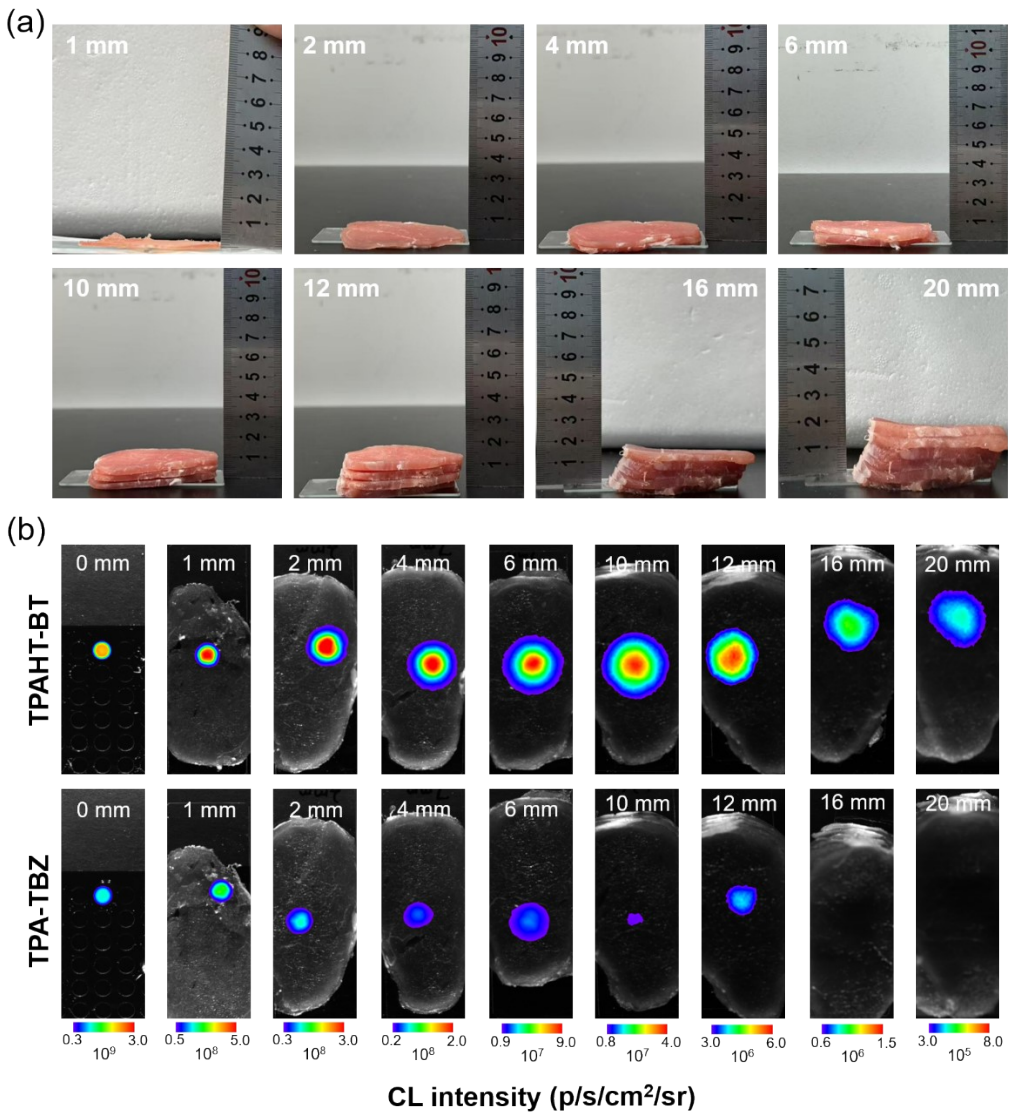

Figure S23. (a) The experimental setup of the CL imaging under the cover of tissues with different thicknesses. (b) Tissue penetration depth determination of TPAHT-BT and TPA-TBZ CLdot (1 mg/mL) at 37 °C.

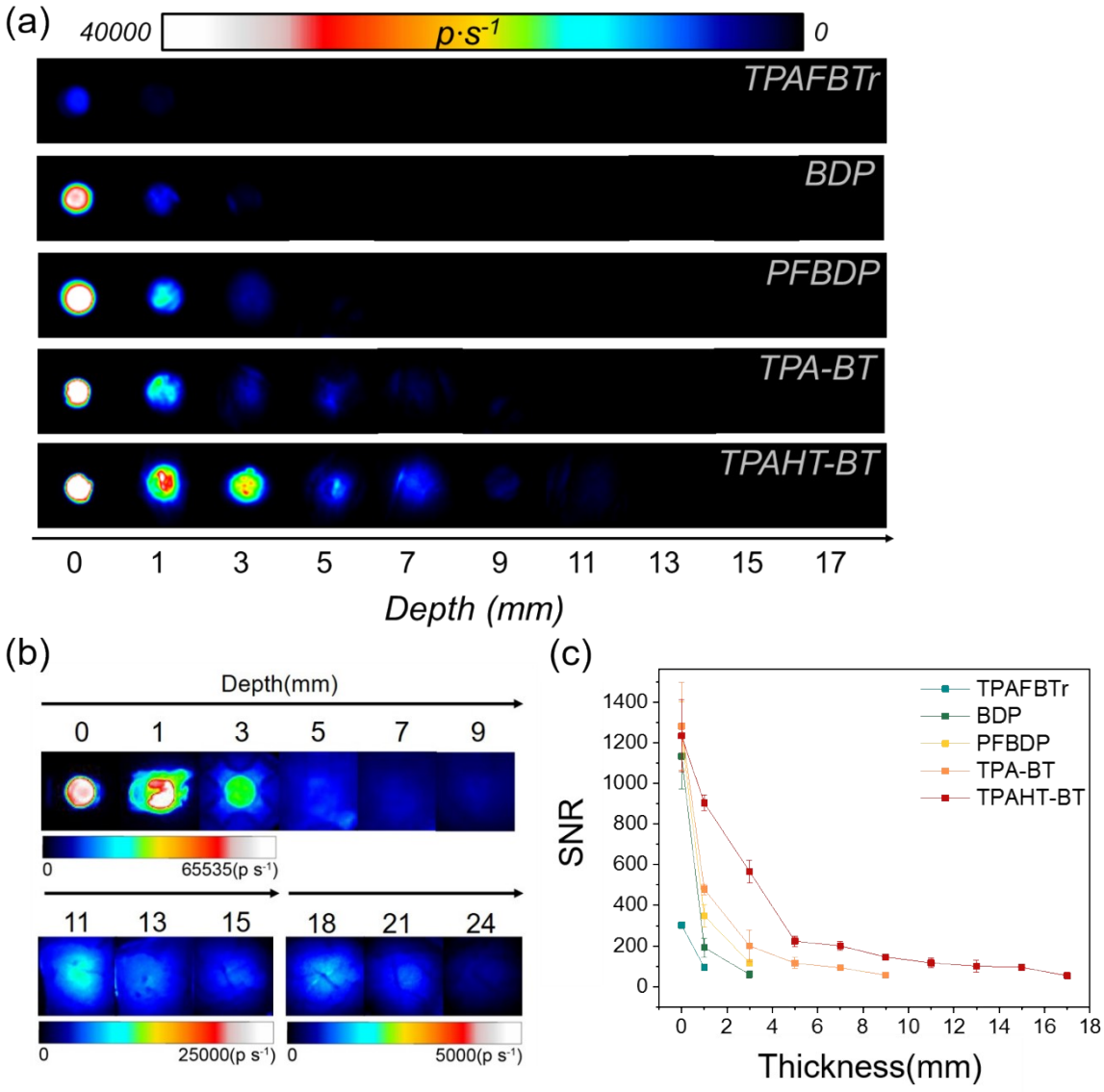

Figure S24. (a) Tissue penetration depth determinations of the water-dispersible POCL system separately using TPAFBTr, BDP, PFBDP, TPABT and TPAHT-BT as the emitters in chemiluminescence imaging. (b) Tissue penetration depth determination of TPAHT-BT CLdot (1 mg/mL) at 37 ºC. (c) Signal-to-noise ratio (SNR) of the chemiluminescent nanoparticles composed of different emitters (including TPA-FBTr, BDP, PFBDP, TPA-BT, and TPAHT-BT) for CL imaging under the cover of tissues with different thickness.

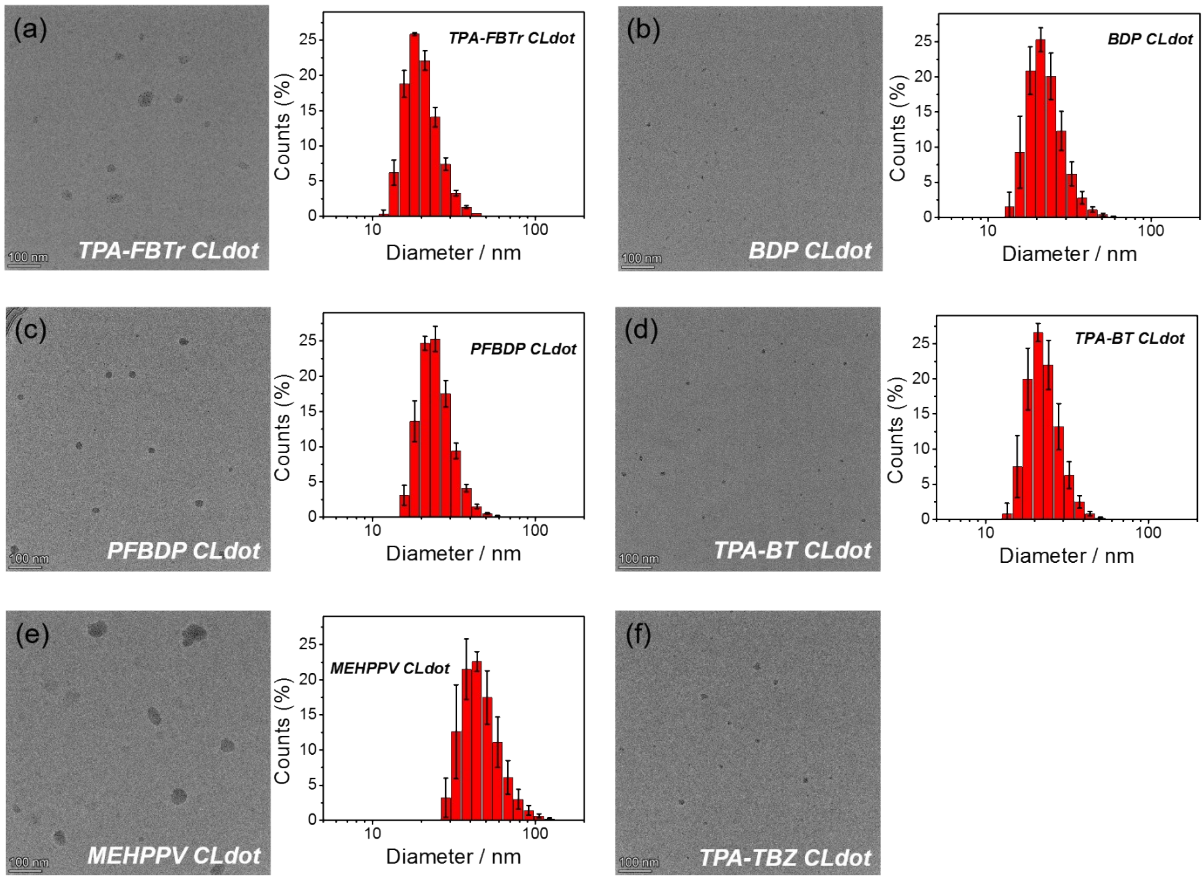

Figure S25. TEM image and DLS of (a) TPA-FBTr Cldot, (b) BDP Cldot, (c) PFBDP Cldot, (d) TPA-BT Cldot, (e) MEHPPV Cldot and (f) TPA-TBZ Cldot (DLS can not determined).

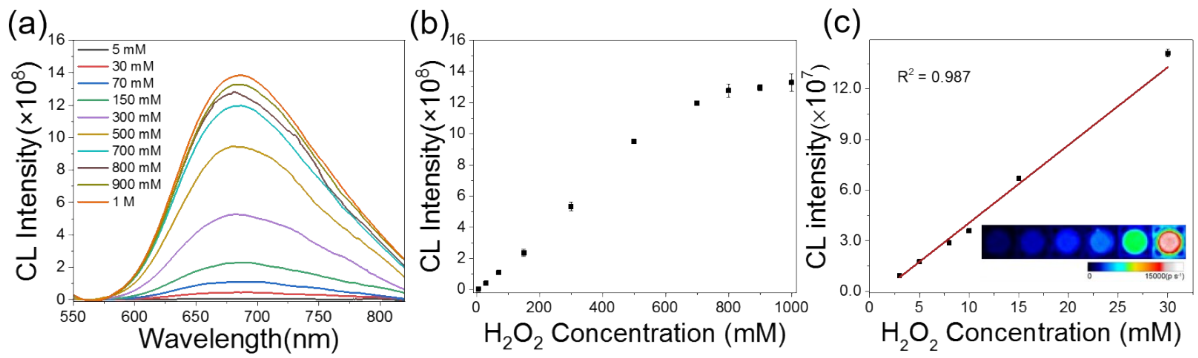

Figure S26. (a) CL spectra (smoothed) of TPAHT-BT CLdot upon addition of different concentrations of H_2O_2 in aqueous solutions at room temperature. (b) Plots of CL intensities with the concentrations of H_2O_2. (c) Function of the chemiluminescence intensity of TPAHT-BT CLdot (0.1 mg/mL) with the concentrations of H_2O_2 (2.5-30 mM) in aqueous solution.

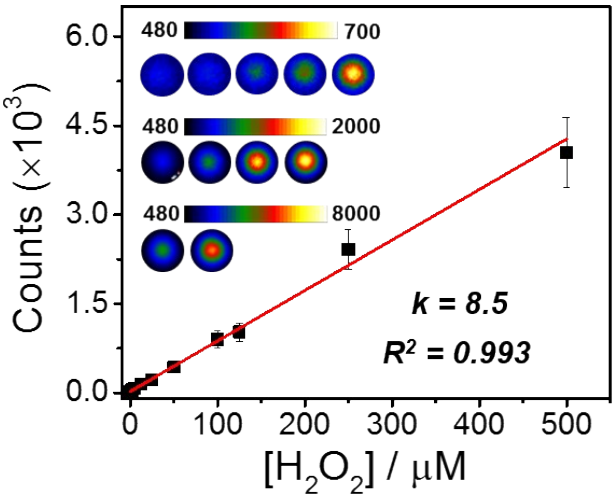

Figure S27. Function of the chemiluminescence intensity of TPAHT-BT CLdot (0.1 mg/mL) with the concentrations of H_2O_2 in aqueous solution (0-0.5 mM) determined by IVIS spectrum (PerkinElmer).

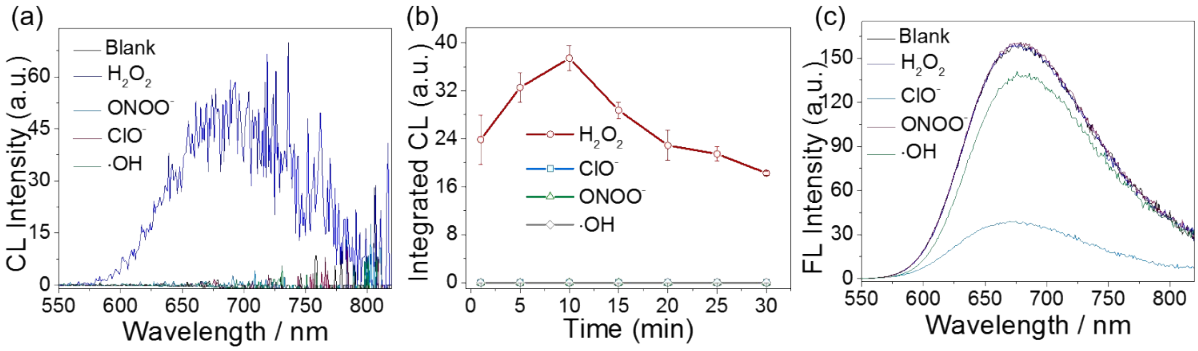

Figure S28. (a) Chemiluminescence spectra of TPAHT-BT CLdot aqueous solution (1mg/mL) in the presence of different ROS (H_2O_2~20 mM, $ONOO^-$~20 mM, ClO^-~20 mM, and ·OH~20 mM) and in the absence of ROS (Blank). (b) Time-dependent CL intensity of TPAHT-BT CLNPs in the presence of 50 mM H_2O_2, $ONOO^-$, ClO^- or ·OH at 37 °C. (c) Fluorescence spectra of TPAHT-BT CLdot aqueous solution (1mg/mL) in the presence of different ROS (H_2O_2~300 mM, $ONOO^-$~20 mM, ClO^-~20 mM, and ·OH~20 mM) and in the absence of ROS (Blank).

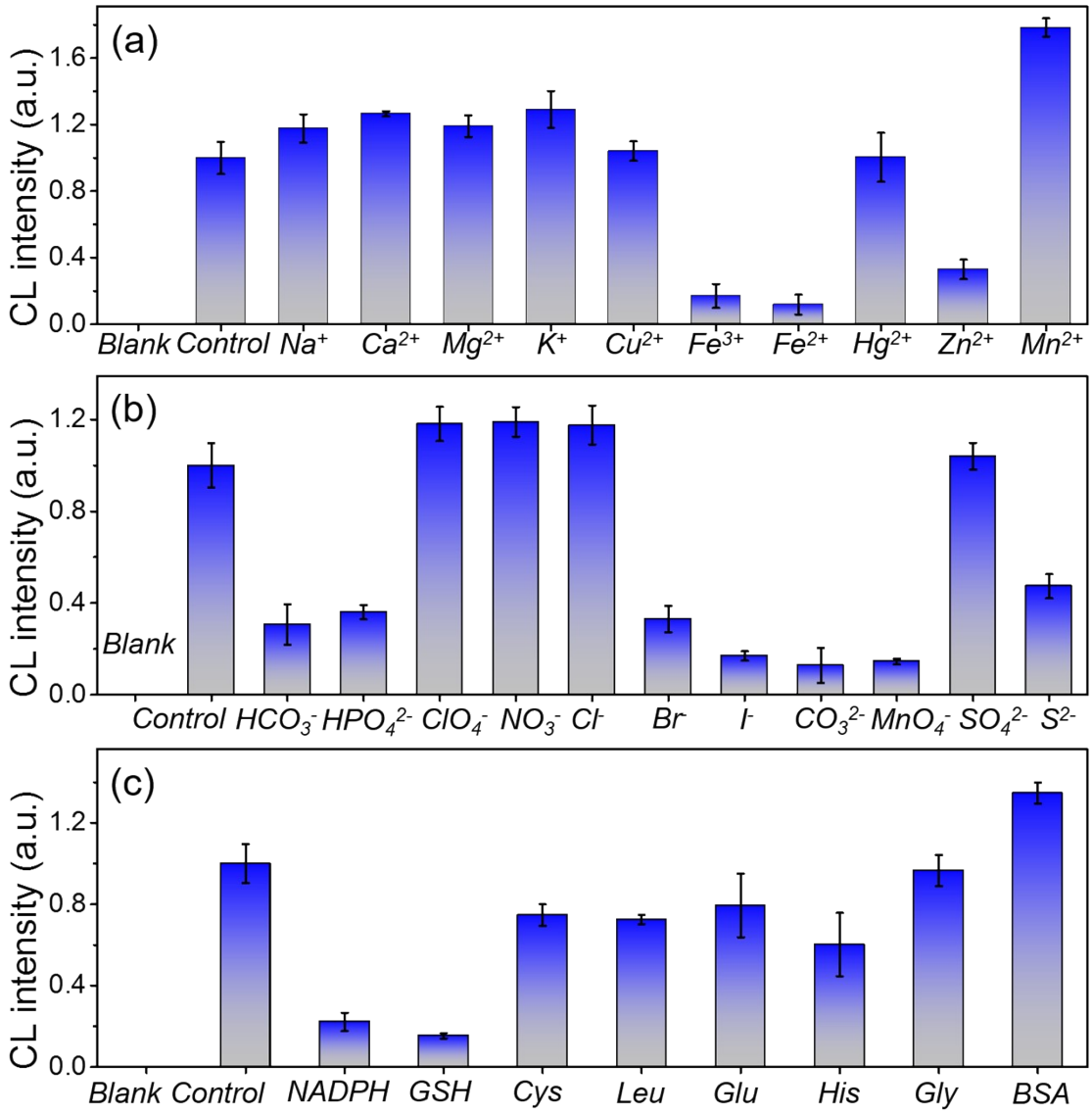

Figure S29. (a) Integrated CL intensity of the mixture of TPAHT-BT CLdot, H_2O_2 (25 mM), and different metal ions (1 mM). (b) Integrated CL intensity of the mixture of TPAHT-BT CLdot, H_2O_2 (25 mM), and different negative ions (1 mM). (c) Integrated CL intensity of the mixture of TPAHT-BT CLdot, H_2O_2 (25 mM), and different biomolecules (the concentration of NADPH, glutathione-GSH, cysteine-Cys, leuciene-Leu, glutamic acid-Glu, histidine-His or glycine-Gly is 1 mM, respectively, the concentration of Bovine Serum Albumin-BSA is 5 mg/mL). Blank group: TPAHT-BT CLdot solution without H_2O_2 and other ions or biomolecules. Control group: mixture of TPAHT-BT CLdot and H_2O_2 (25 mM). n=3

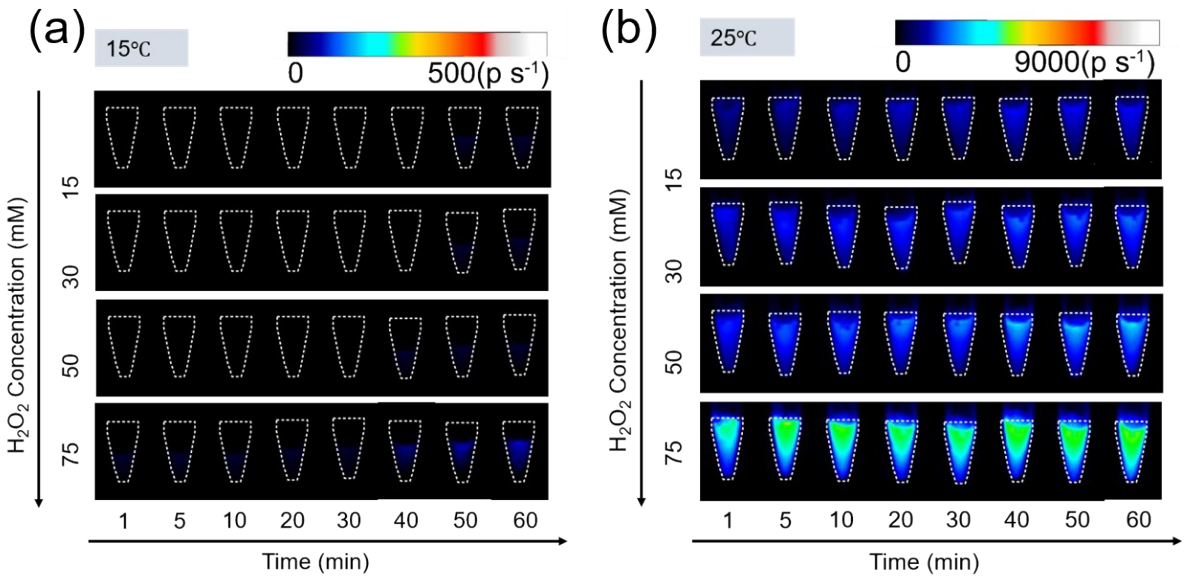

Figure S30. Chemiluminescence images of the TPAHT-BT CLdot upon the addition of different concentration of H_2O_2 over time under 15 °C and 25 °C. Exposure time: 1 s.

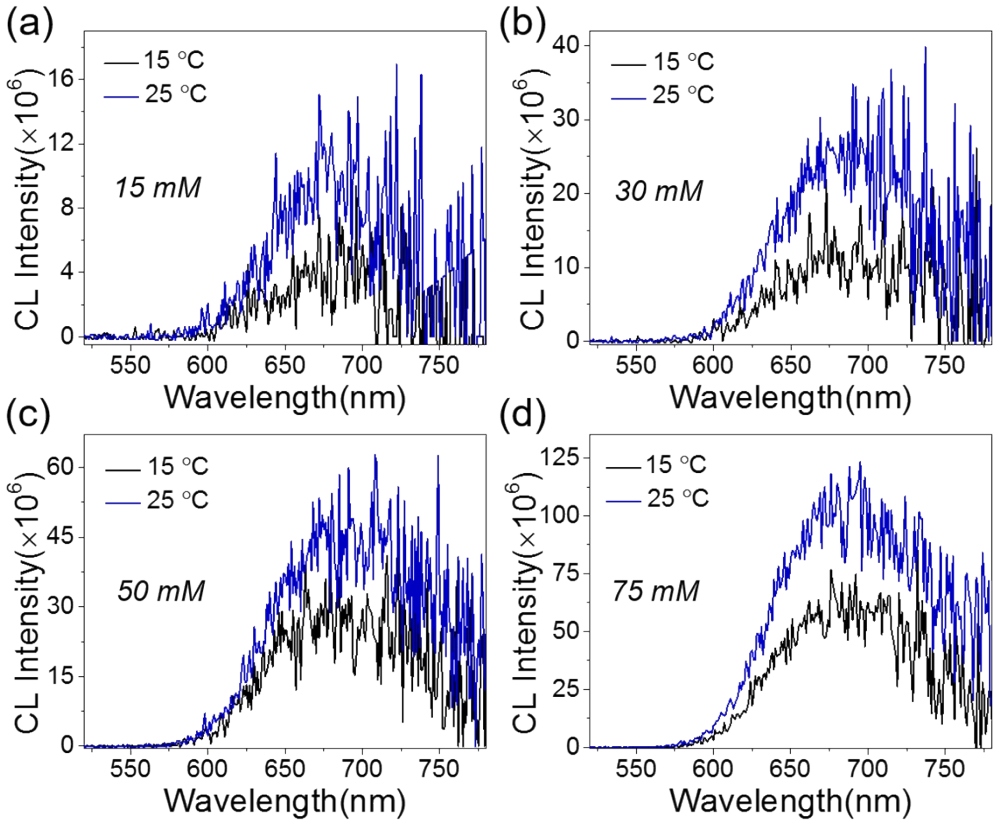

Figure S31. Chemiluminescence spectra of the mixtures of TPAHT-BT CLdot and different concentrations of H_2O_2 (a-15 mM, b-30 mM, c-50 mM, and d-75 mM) at 15 °C and 25 °C. The spectra were collected 10 minutes after the addition of H_2O_2 in TPAHT-BT CLdot solutions.

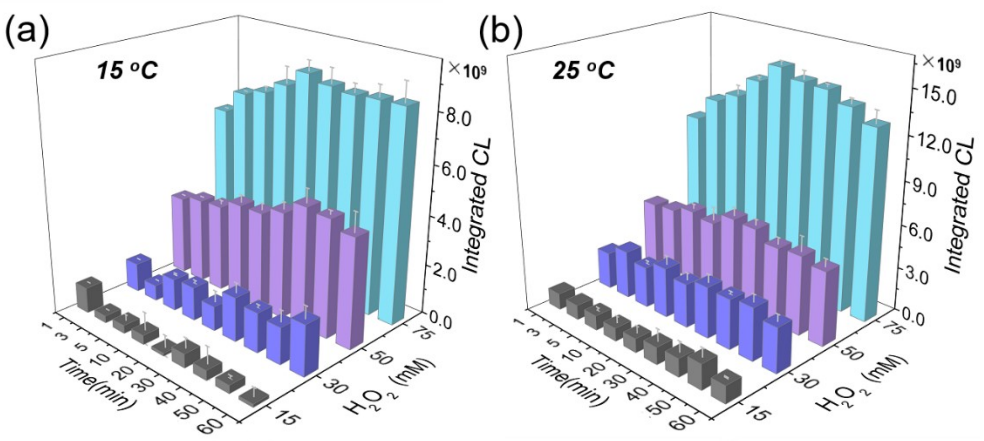

Figure S32. Chemiluminescence intensity variations of the TPAHT-BT CLNPs determined by fluorescence spectrometer (determined without light source) upon the addition of different concentration of H_2O_2 over time under 15 °C (a) and 25 °C (b).

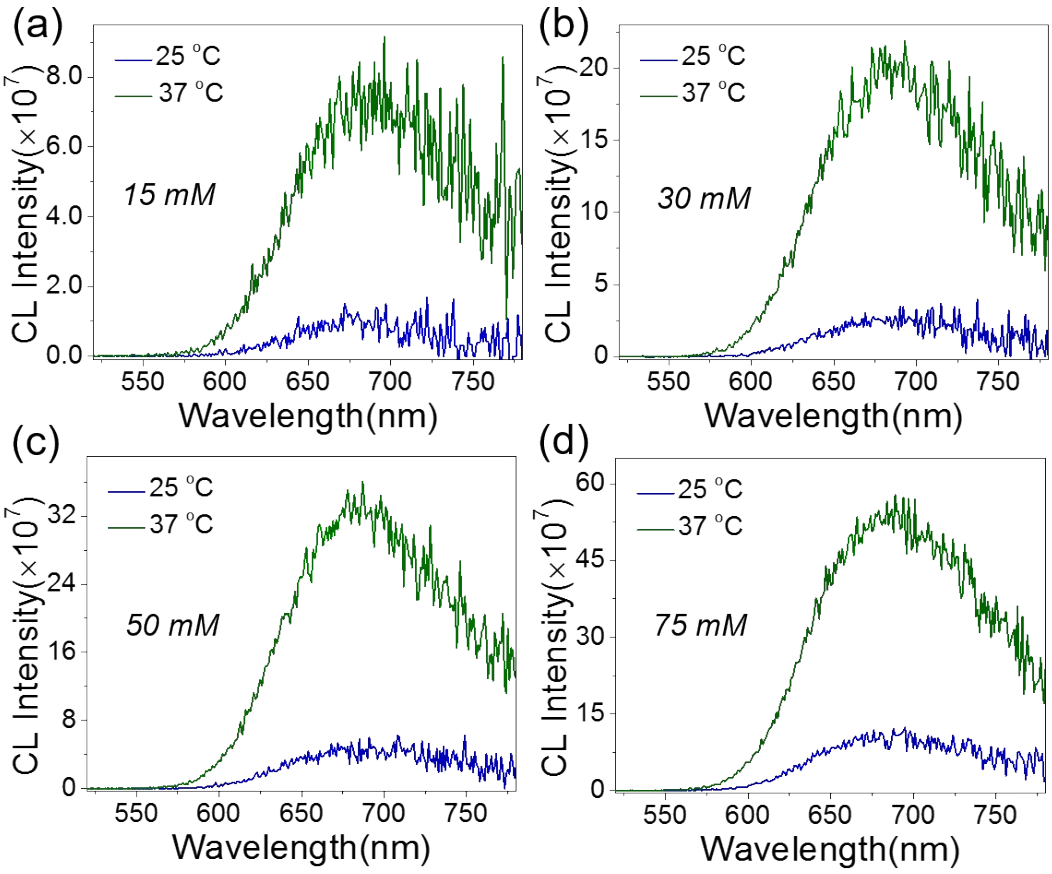

Figure S33. Chemiluminescence spectra of the mixtures of TPAHT-BT CLdot and different concentrations of H_2O_2 (a-15 mM, b-30 mM, c-50 mM, and d-75 mM) at 25 °C and 37 °C. The spectra were collected 10 minutes after the addition of H_2O_2 in TPAHT-BT CLdot solutions.

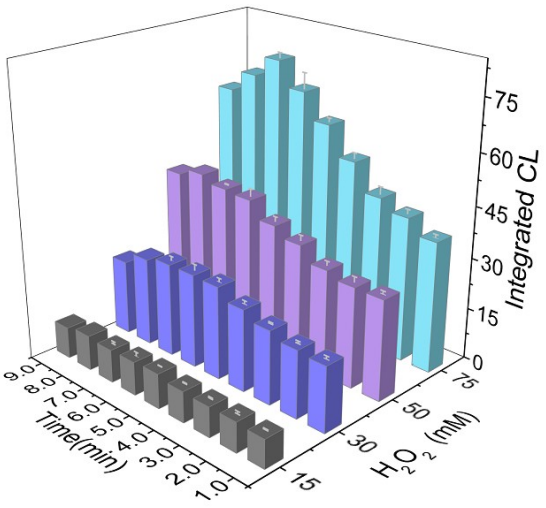

Figure S34. Chemiluminescence intensity variations of the TPAHT-BT CLNPs determined by fluorescence spectrometer (determined without light source) upon the addition of different concentration of H_2O_2 over time under 37 °C.

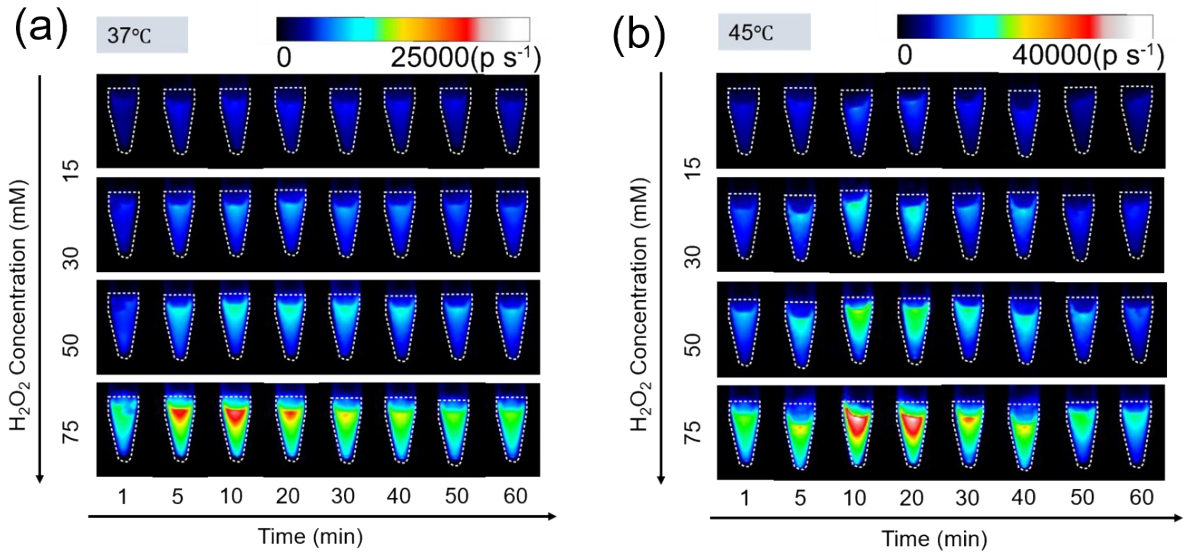

Figure S35. Chemiluminescence images of the TPAHT-BT CLdot upon the addition of different concentration of H_2O_2 over time under 37 °C and 45 °C. Exposure time: 1 s.

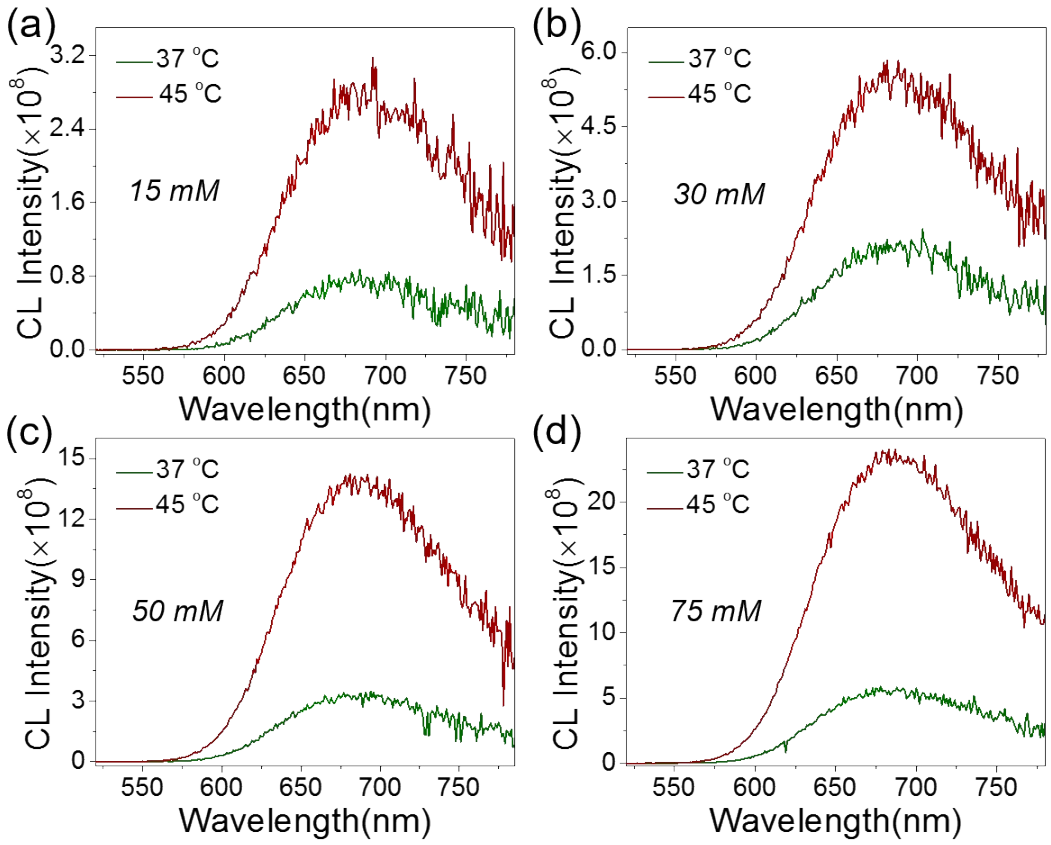

Figure S36. Chemiluminescence spectra of the mixtures of TPAHT-BT CLdot and different concentrations of H_2O_2 (a-15 mM, b-30 mM, c-50 mM, and d-75 mM) at 45 °C and 37 °C. The spectra were collected 5 min after the addition of H_2O_2 in TPAHT-BT CLdot solutions.

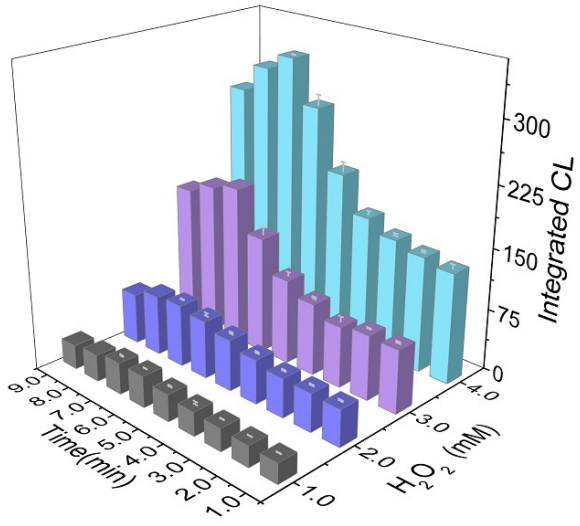

Figure S37. Chemiluminescence intensity variations of the TPAHT-BT CLNPs determined by fluorescence spectrometer (determined without light source) upon the addition of different concentration of H_2O_2 over time under 37 °C.

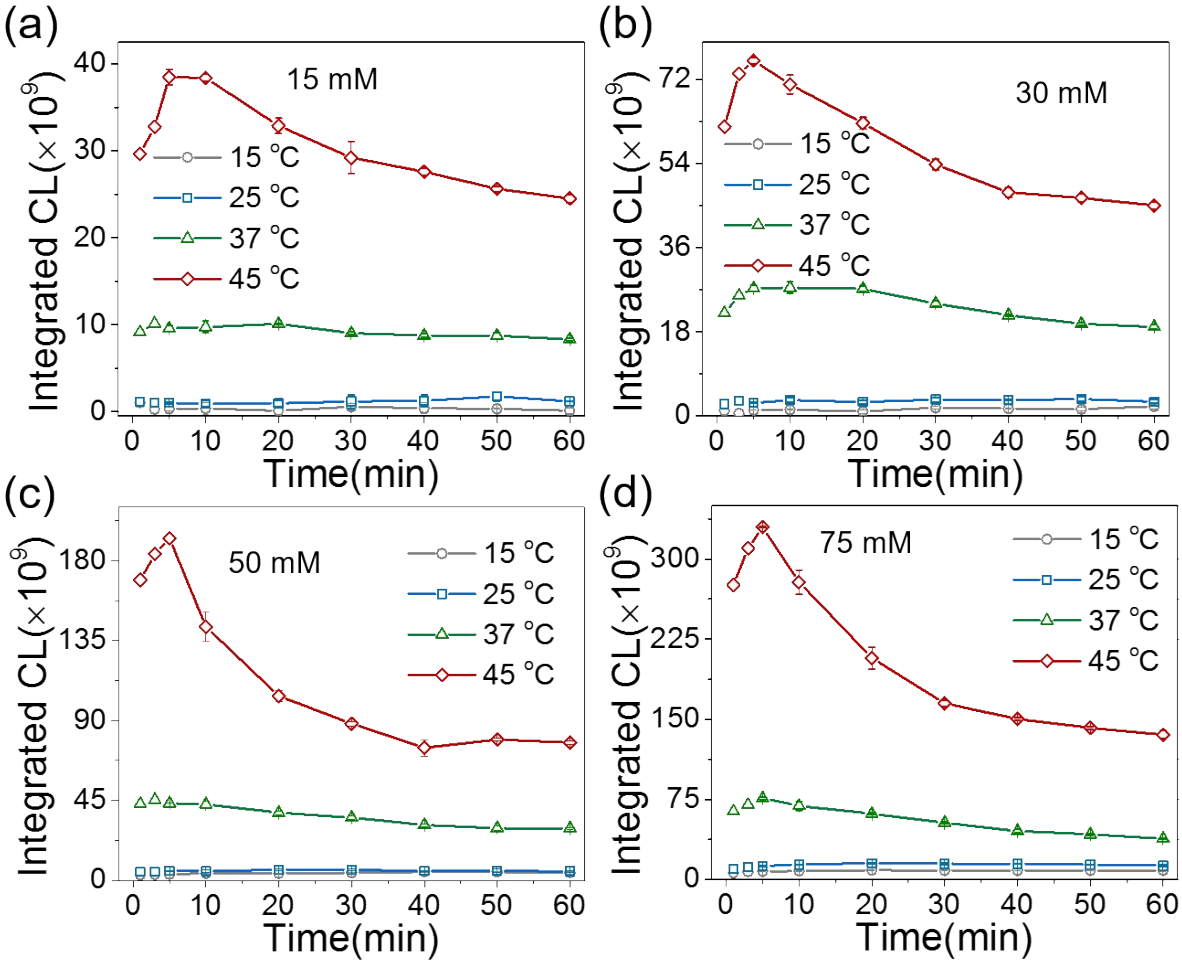

Figure S38. Time-dependent CL intensity of TPAHT-BT CLdot in the presence of 15 mM (a), 30 mM (b), 50 mM (c) and 75 mM (d) H_2O_2 at different environmental temperatures. n=3

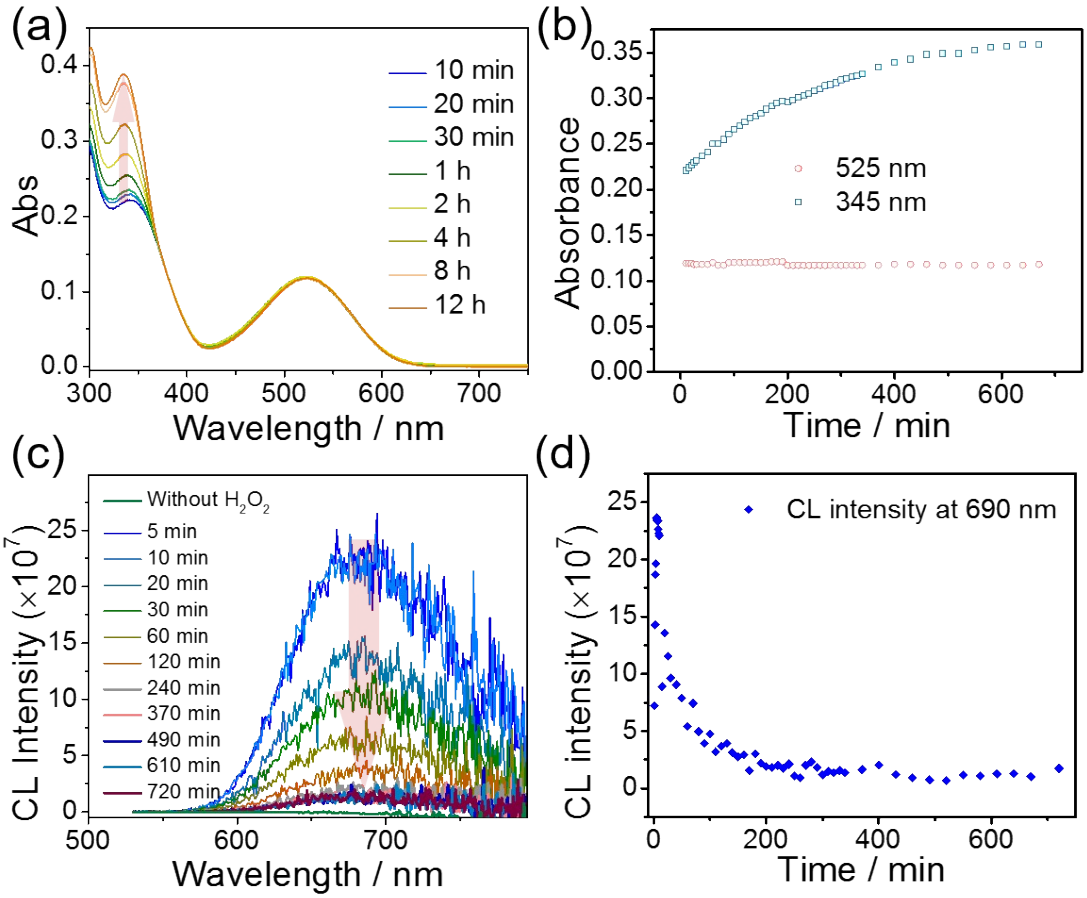

Figure S39. (a) Long-term time-dependent absorption spectra of TPAHT-BT CLdot upon addition of 25 mM H_2O_2 at 37 °C. (b) Long-term time-dependent absorbance variation (separately monitored at 345 nm and 525 nm) of the TPAHT-BT CLdot after addition of H_2O_2. (c) Long-term time-dependent chemiluminescence spectra of TPAHT-BT CLdot upon addition of 25 mM H_2O_2 at 37 °C. (d) Long-term time-dependent absorbance variation (monitored at 690 nm) of the TPAHT-BT CLdot after addition of H_2O_2.

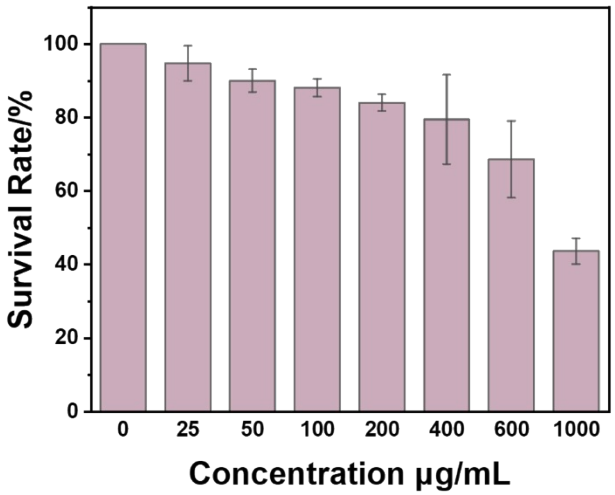

Figure S40. Cytotoxicity of TPAHT-BT CLdot over HeLa cell lines.

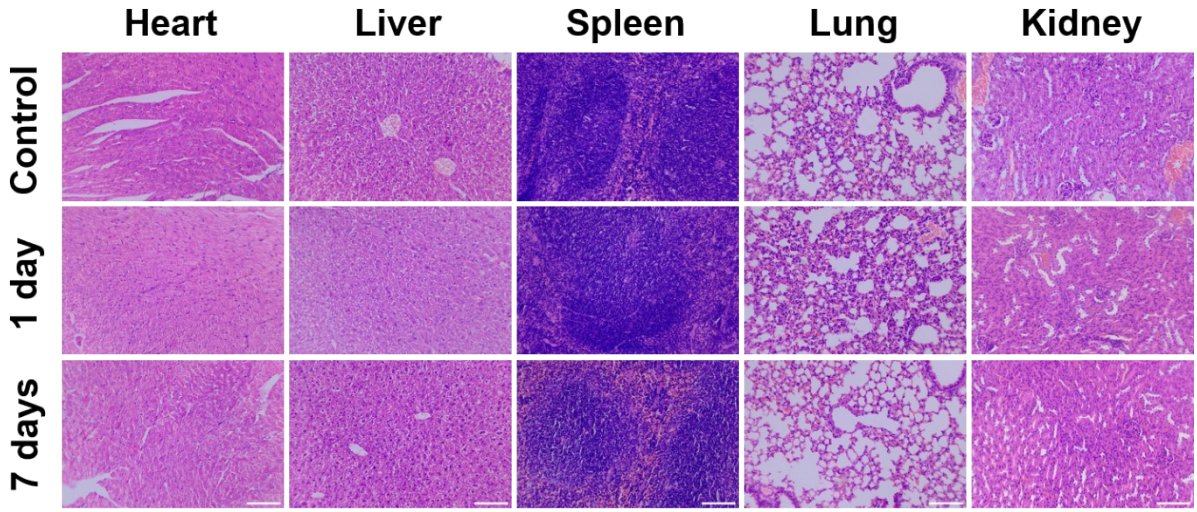

Figure S41. H&E-stained tissue sections of the heart, liver, spleen, lung, and kidney harvested from mice after intravenous injection without (control) or with TPAHT-BT CLdot (2.5 mg/mL, 200 μL). Scale bar: 100 μm.

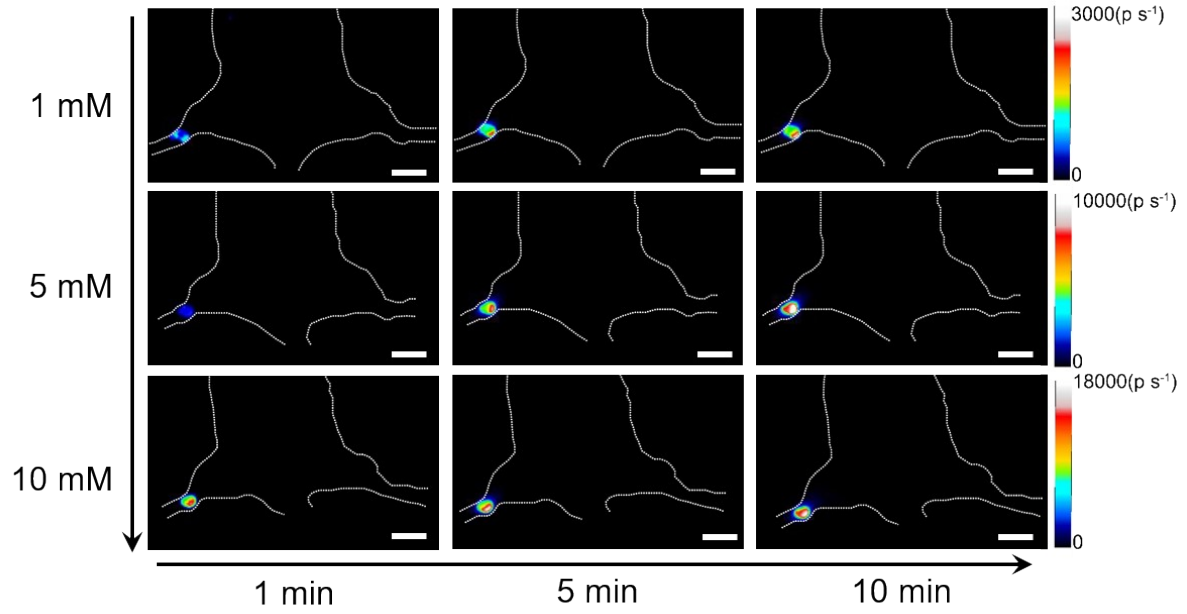

Figure S42. *In vivo* CL imaging of articulation injected with different concentrations of H_2O_2 at different times.

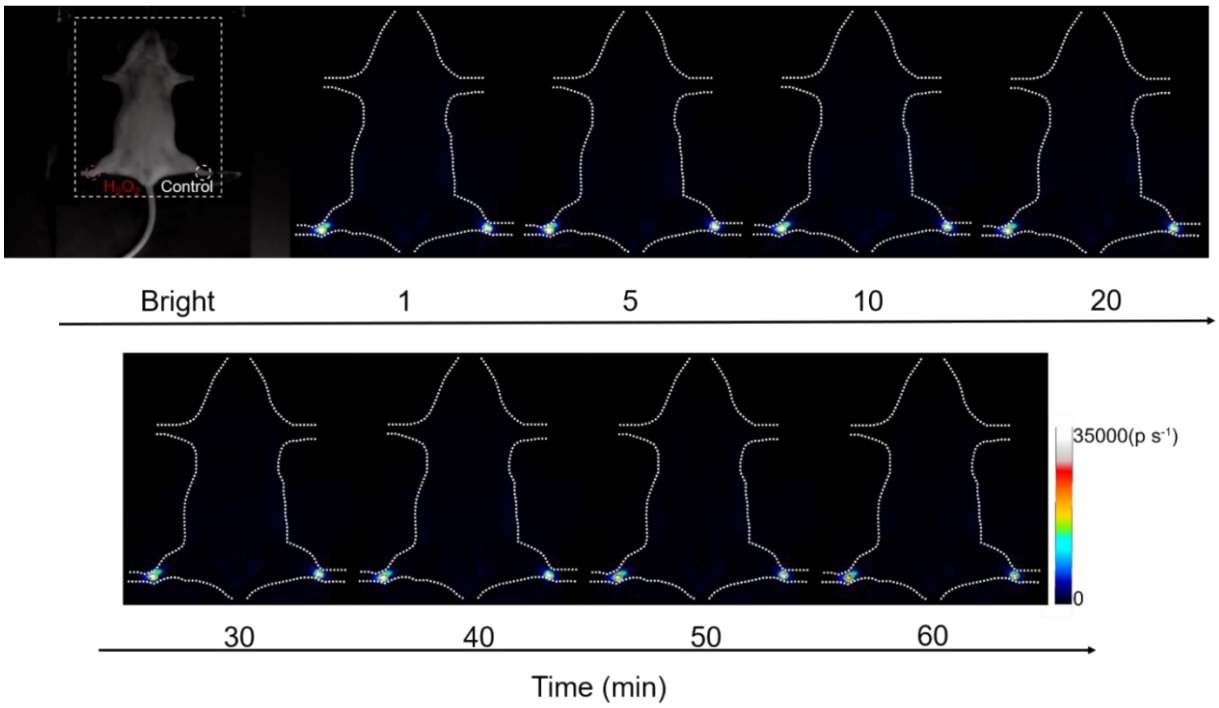

Figure S43. *In vivo* FL imaging of TPAHT-BT CLdot injected into lateral articulations (Left: inflammation, Right: control). Excitation: 532 nm, Collect: 700 LP.

Table S1. Photophysical properties of different organic luminophors in toluene and other organic solvents (labelled with *).

Name	$\lambda_{max,abs}$ [nm]	ε ($\lambda_{max,abs}$) [$M^{-1}cm^{-1}$]	$\lambda_{max,em}$ [nm]	Brightness (ε×Φ)	Stokes shift [nm]	Quantum yield Φ [%]
FT-BT	512	31200	631	24000	119	77.9
FT-BSeT	546	30600	685	12500	139	40.9
FHT-BT	498	39400	624	30000	126	76.3
FHT-BSeT	534	28000	678	13600	144	48.8
TPAT-BT	530	31200	660	19200	130	61.6
TPAT-BSeT	562	21600	719	5500	157	25.4
TPAHT-BT	512	25600	656	17000	144	65.8
TPAHT-BSeT	545	25200	709	7000	164	28.0
TPET-BT	510	22400	628	14200	118	63.3
TPET-BSeT	543	19000	679	7700	136	40.5
TPEHT-BT	499	24800	626	18700	127	75.5
TPEHT-BSeT	532	20000	677	9000	145	45.0
TPA-BT	310	22300	558	19800	140	91.7*
OTPA-BT	482	20800	585	13936	103	67* (Hexane)
TPE-BT	416	26500	516	17100	122	71.0*
tDPA-BT	481	7936	595	952	114	12.0*
TPABTsr	403	21600	473	14400	70	66.6
TPAFBT	449	26000	576	21400	127	82.4
TPAFBTr	394	17000	470	17300	76	~100
TPA-TBZ	613	24832	759	11147	146	46.2
TPA-QX	622	10696	778	2246	156	21.0
TPAHT-BBT	720	27000	957	297	237	11*
SQ650	644	99000	663	94700	19	91*
SQ640	642	364700	655	308500	13	84.6*
SQ680	700	239100	715	155400	15	65*
RhB	544	101000	569	65600	25	65* (EtOH)
Rh101	565	118600	588	108300	23	91.3* (EtOH)
Rubrene	521	49000	553	13200	32	27*
BDP	503	80000	513	70320	10	92* (Chloroform)
PFBDP	545	28600	562	26900	17	93.7*

BDP-590	567	138800	579	133250	12	96
BDP-650	643	243200	670	126500	27	52.0 (DMSO)
Cy3	552	255900	570	96470	18	37.7
Cy5	647	234000	669	77900	22	33.3(EtOH)
Cy7	755	127300	790	32840	35	25.8(DMSO)
Coumarin102	390	22000	465	17100	75	78* (EtOH)
Coumarin153	423	20000	530	10800	107	54.4* (EtOH)
DPA	373	13600	405	12200	32	90* (Cyclohexane)
DPEA	454	/	476	/	22	85*
PFO	380	/	415	/	45	82.8
PFOPV	452	/	500	/	48	79.5
F8BT	458	/	525	/	67	82.4
PFODBT	563	/	665	/	102	32.5
PFOHTBT	509	/	632	/	123	86.7
MEH-PPV	505	/	555	/	50	26.9
CN-PPV	450	/	555	/	105	42.5
TBQx-TF	570	/	610	/	40	21.4
PFN-DOF	390	/	418	/	28	78.7

Table S2. Electron energy levels of different organic luminophors and their maximum absorption and emission wavelengths. The fluorescence quantum yield of the chemiluminescent nanoparticles composed by different luminophors in aqueous solution.

Name	HOMO	LUMO	ΔE_{LUMO} $LUMO_{Dye}$-$LUMO_{DOD}$	ΔE_{HOMO} $HOMO_{\mathbf{Dye}}$-$HOMO_{\mathbf{DOD}}$	$\lambda_{max,abs}$ [nm]	$\lambda_{max,em}$ [nm]	Φ_{NP} [%]
DOD	-9.01	-3.2	-	-			-
FT-BT	-4.86	-2.63	0.57	4.15	522	651	41.2
FT-BSeT	-4.83	-2.7	0.5	4.18	557	709	9.4
FHT-BT	-4.88	-2.53	0.67	4.13	510	642	41.3
FHT-BSeT	-4.82	-2.62	0.58	4.19	543	694	12.4
TPAT-BT	-4.66	-2.53	0.67	4.35	537	695	12.3
TPAT-BSeT	-4.63	-2.6	0.6	4.38	569	742	2.3
TPAHT-BT	-4.73	-2.48	0.72	4.28	520	678	29.5
TPAHT-BSeT	-4.69	-2.56	0.64	4.32	556	723	5.3
TPET-BT	-4.88	-2.62	0.58	4.13	516	651	28.4
TPET-BSeT	-4.85	-2.69	0.51	4.16	550	702	6.0
TPEHT-BT	-4.95	-2.51	0.69	4.06	508	650	22.4
TPEHT-BSeT	-4.9	-2.59	0.61	4.11	540	692	11.1
TPA-BT	-4.77	-2.28	0.92	4.24	470	610	33.3
OTPA-BT	-4.38	-2.07	1.13	4.63	502	648	14.0
TPE-BT	-5.12	-2.39	0.81	3.89	425	520	45.3
tDPA-BT	-4.57	-2.13	1.07	4.44	485	643	6.1
TPABTsr	-4.68	-1.51	1.69	4.33	405	490	15.8
TPAFBT	-4.86	-2.38	0.82	4.15	455	588	46.5
TPAFBTr	-4.73	-1.65	1.55	4.28	395	480	9.0
TPA-TBZ	-4.59	-2.69	0.51	4.42	625	780	19.8
TPA-QX	-4.73	-2.85	0.35	4.28	626	795	9.9
TPAHT-BBT	-4.49	-3.29	-0.09	4.52	728	/	/
SQ650	-4.52	-2.31	0.89	4.49	625	645	3.7
SQ640	-4.62	-2.26	0.94	4.39	645	665	2.7
SQ680	-4.68	-2.59	0.61	4.33	680	710	1.7
RhB	-8.32	-5.56	-2.36	0.79	553	580	40.8
Rh101	-7.70	-4.93	-1.71	1.31	575	597	46.5
Rubrene	-4.62	-2.09	1.11	4.38	530	562	25.3
BDP	-5.33	-2.32	0.88	3.68	503	516	63.5

PFBDP	-5.41	-2.62	0.58	3.60	548	560	75.8
BDP-590	-5.03	-2.59	0.61	3.98	569	580	68.1
BDP-650	-5.14	-2.88	0.32	3.87	635	650	29.2
Cy3	-7.90	-5.11	-1.91	1.11	558	574	6.0
Cy5	-7.52	-5.15	-1.95	1.49	656	686	18.3
Cy7	-7.24	-5.12	-1.92	1.77	760	798	5.2
Coumarin102	-5.04	-1.13	2.07	3.97	395	488	55.7
Coumarin153	-5.33	-1.74	1.46	3.68	419	526	10.6
DPA	-5.05	-1.60	1.60	3.96	400	423	4.3
DPEA	-4.93	-2.30	0.90	4.08	468	478	23.0
PFO	-5.11	-1.50	1.70	3.90	401	440	13.7
PFOPV	-4.56	-1.86	1.34	4.45	455	503	7.3
F8BT	-5.22	-2.50	0.96	3.63	472	545	34.3
PFODBT	-4.83	-2.72	0.48	4.18	555	685	5.5
PFOHTBT	-4.85	-2.60	0.60	4.27	525	649	19.1
MEH-PPV	-4.71	-1.74	1.46	4.30	515	592	6.5
CN-PPV	-5.36	-2.54	0.66	3.65	450	570	56.4
TBQx-TF	-5.25	-2.12	1.08	3.76	589	700	1.6
PFN-DOF	-5.09	-1.38	1.82	4.92	390	425	16.2

Fluorescence quantum yield determination

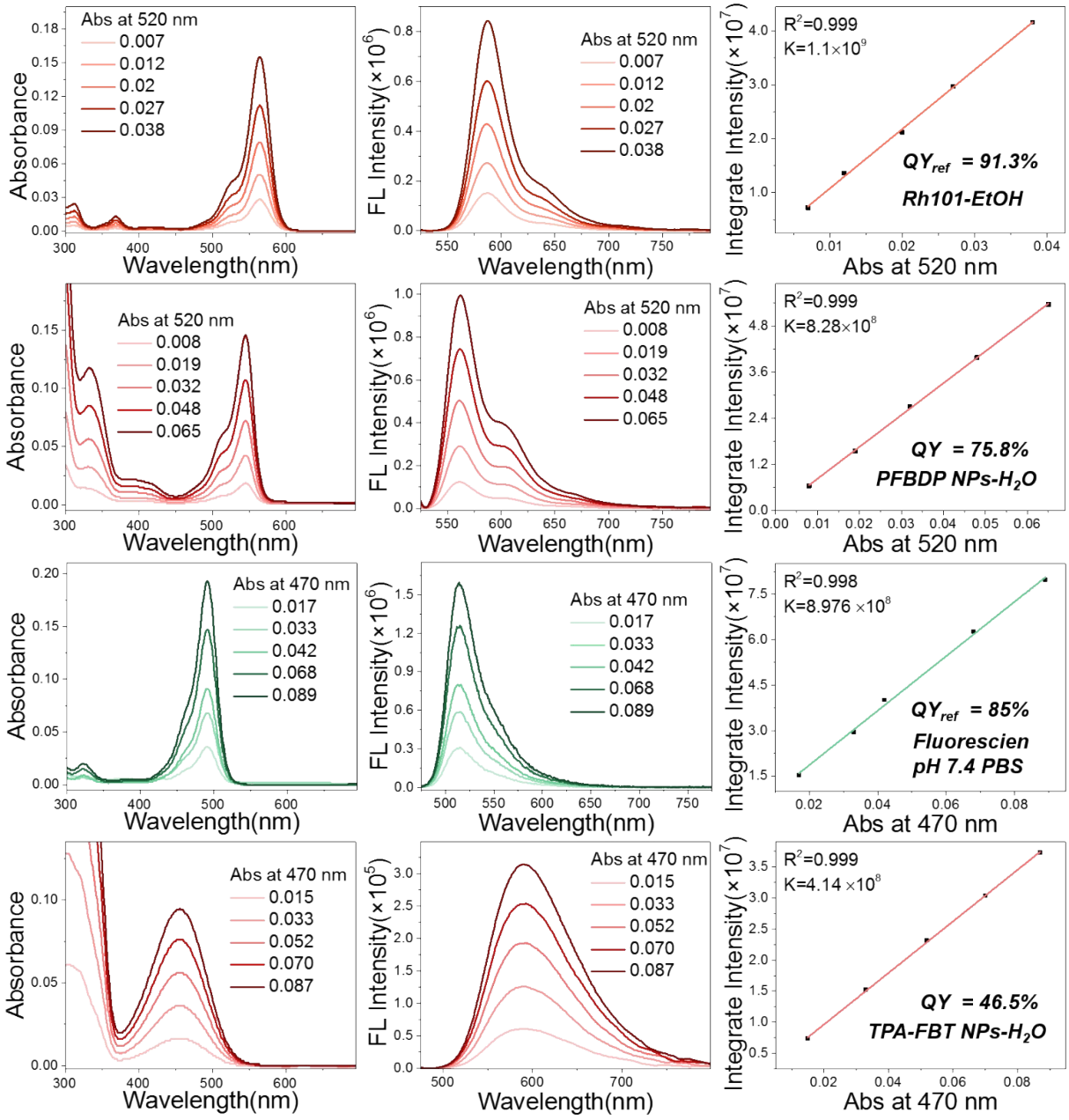

PFBDP NPs and TPA-FBT NPs

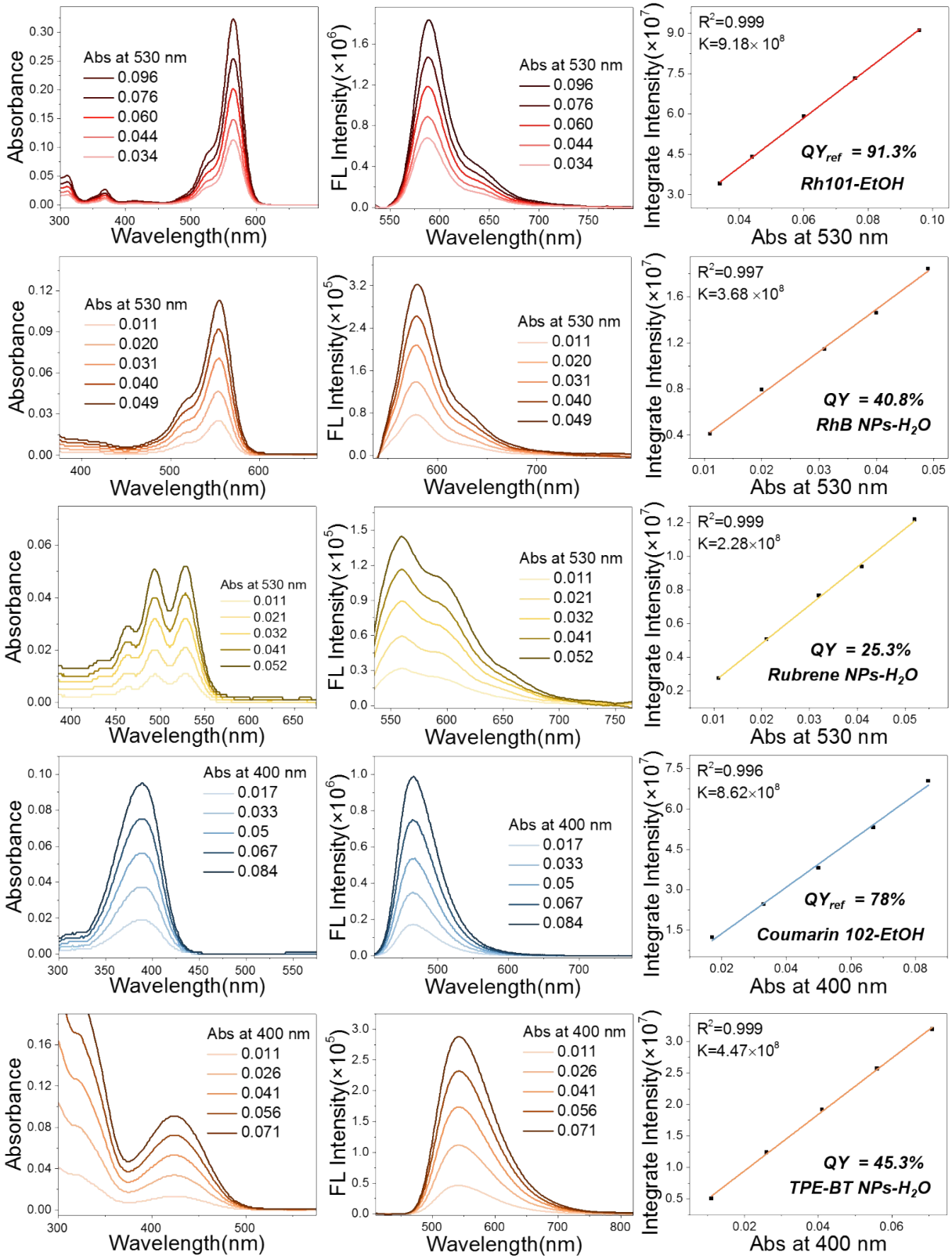

RhB NPs, Rubrene NPs, and TPEBT NPs

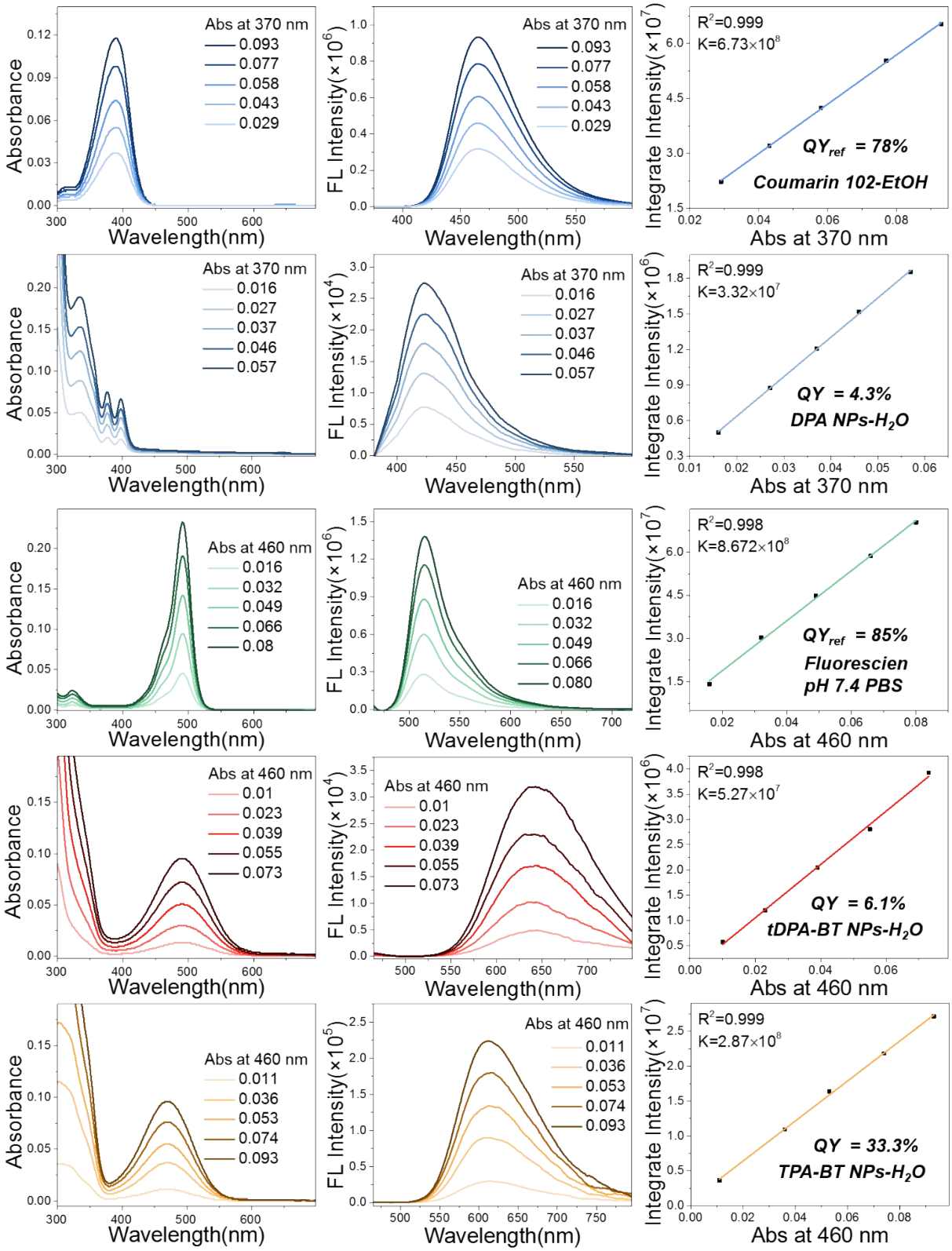

DPA NPs, tDPA-BT NPs, and TPA-BT NPs

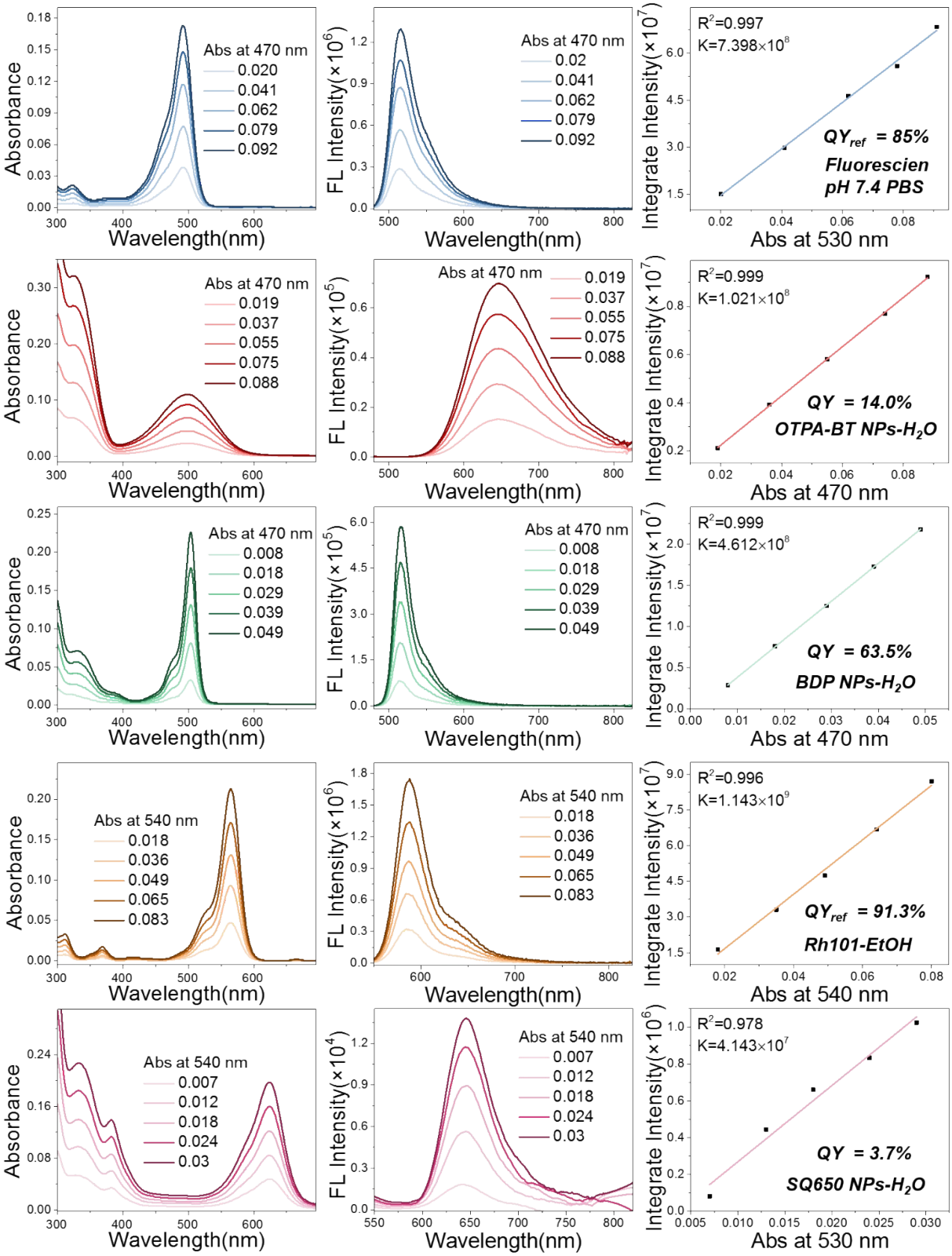

OTPA-BT NPs, BDP NPs, and SQ650 NPs

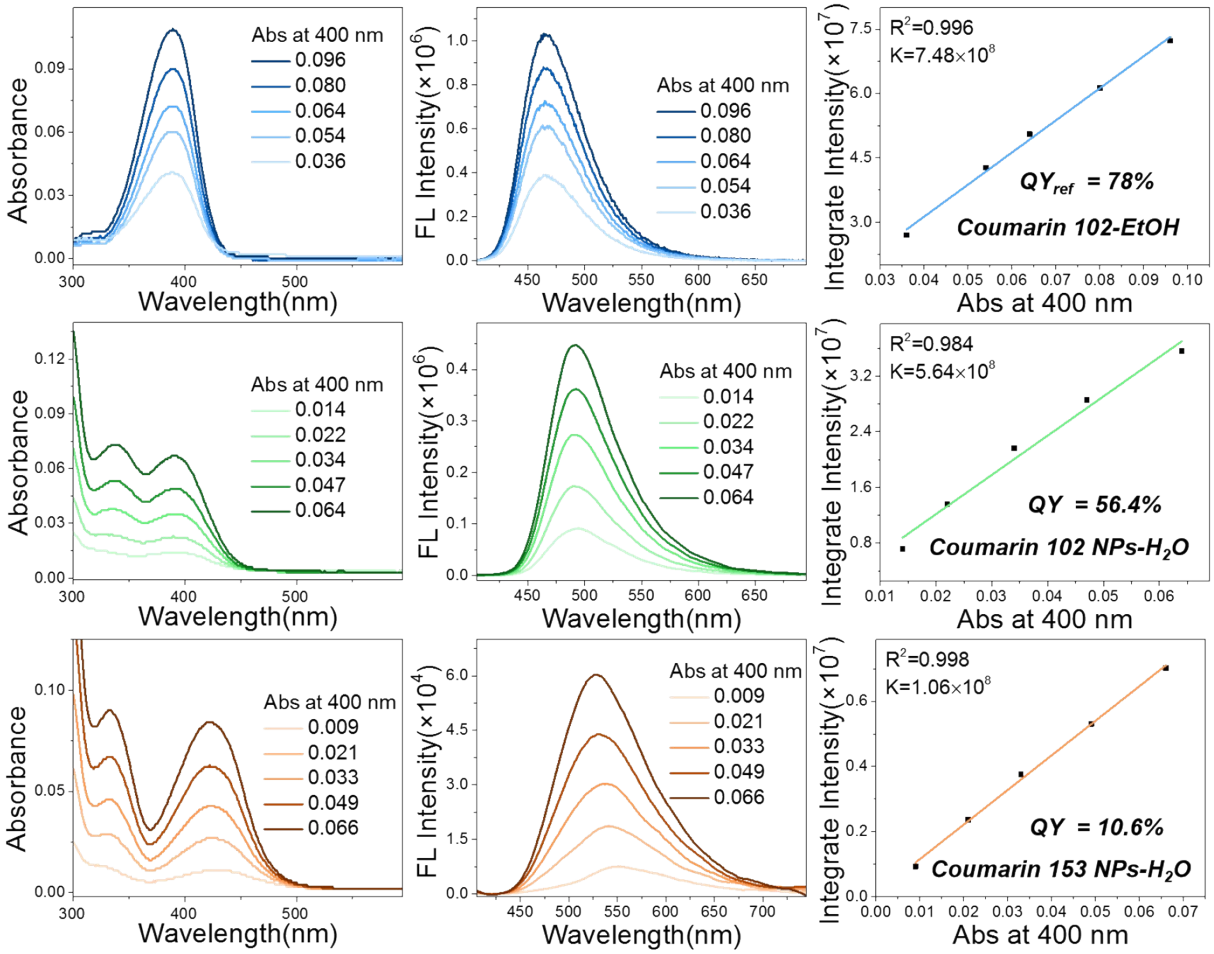

Coumarin 102 NPs and Coumarin 153 NPs

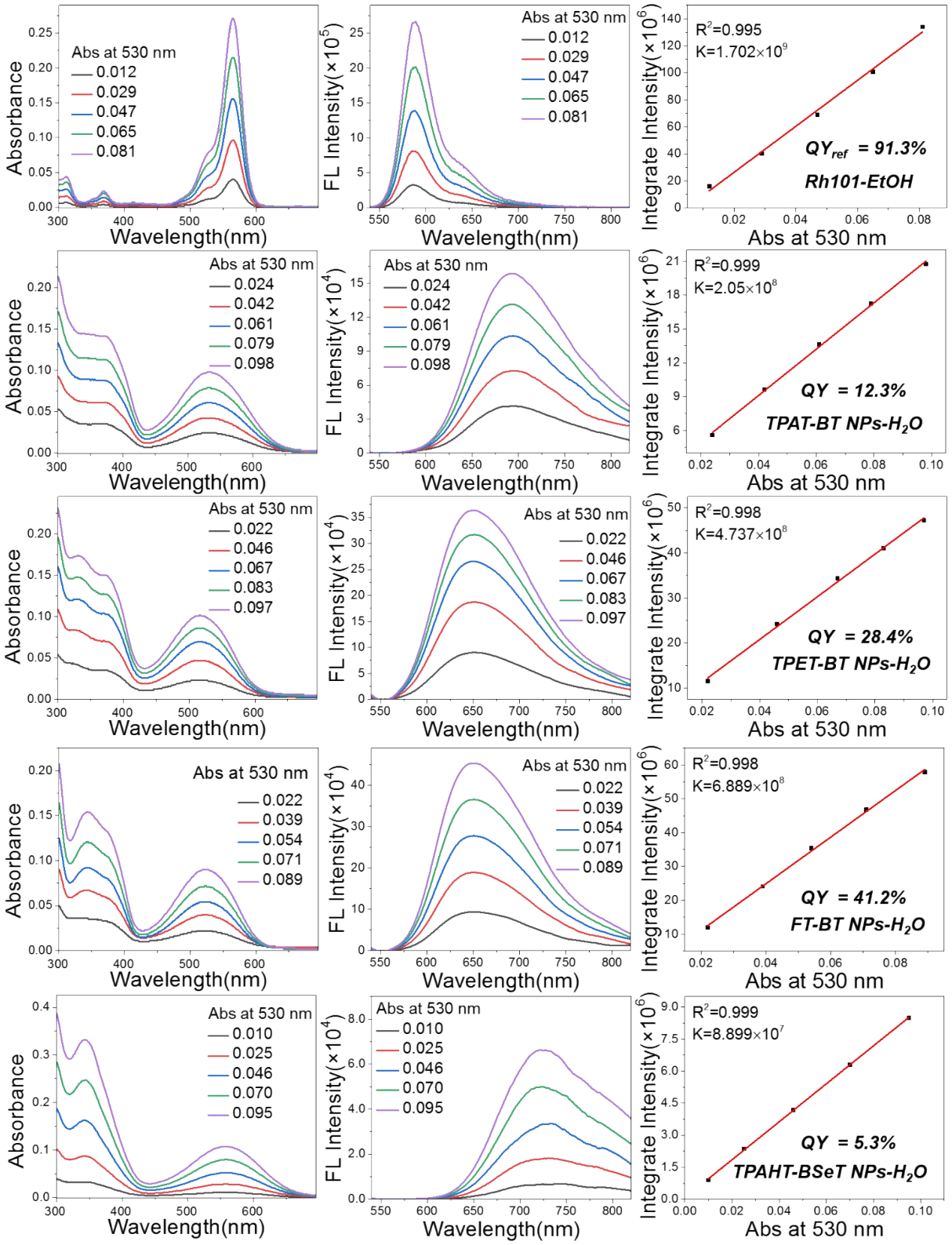

TPAT-BT NPs, TPET-BT NPs, FT-BT NPs, and TPAHT-BSeT NPs

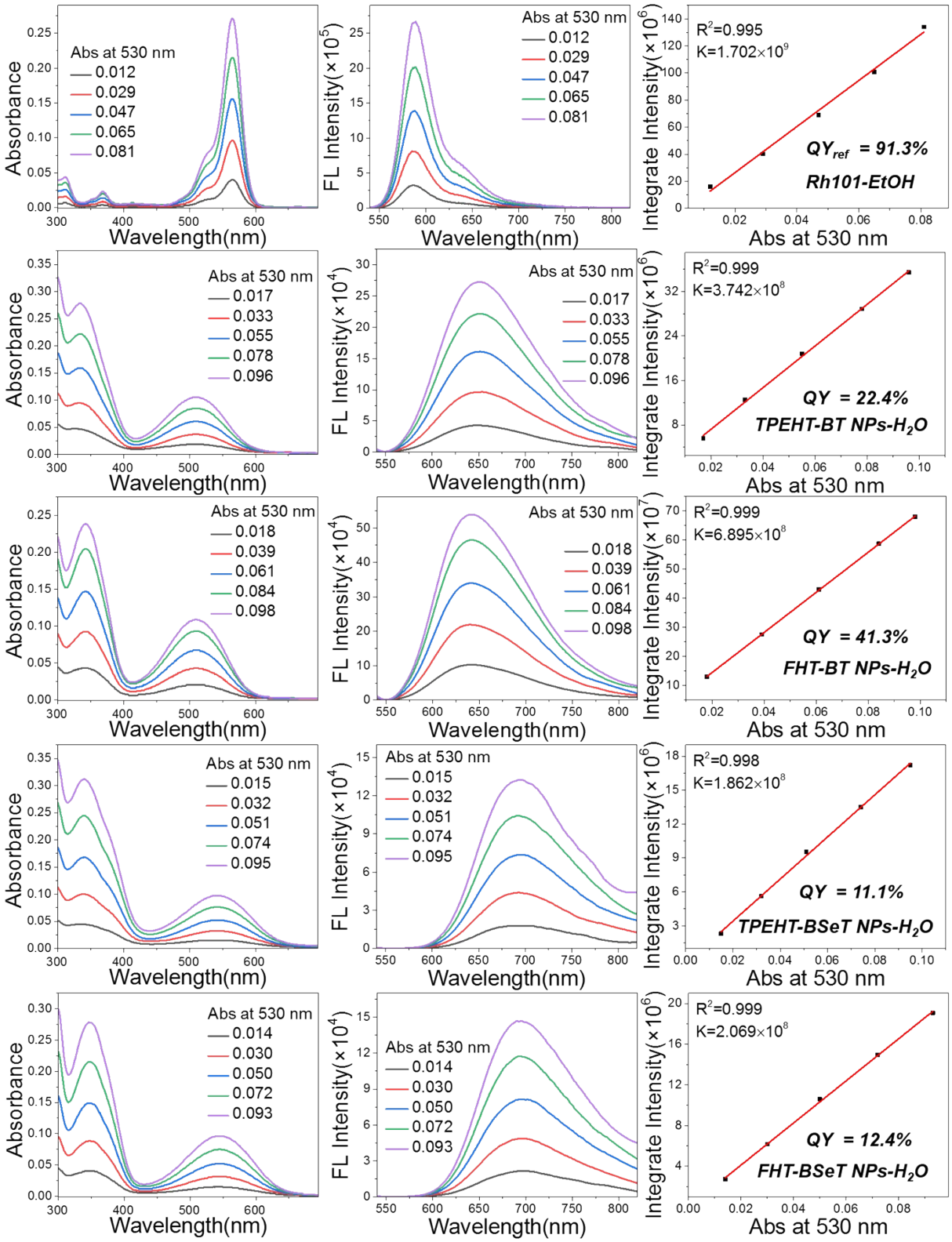

TPEHT-BT NPs, FHT-BT NPs, TPEHT-BSeT NPs, and FHT-BSeT NPs

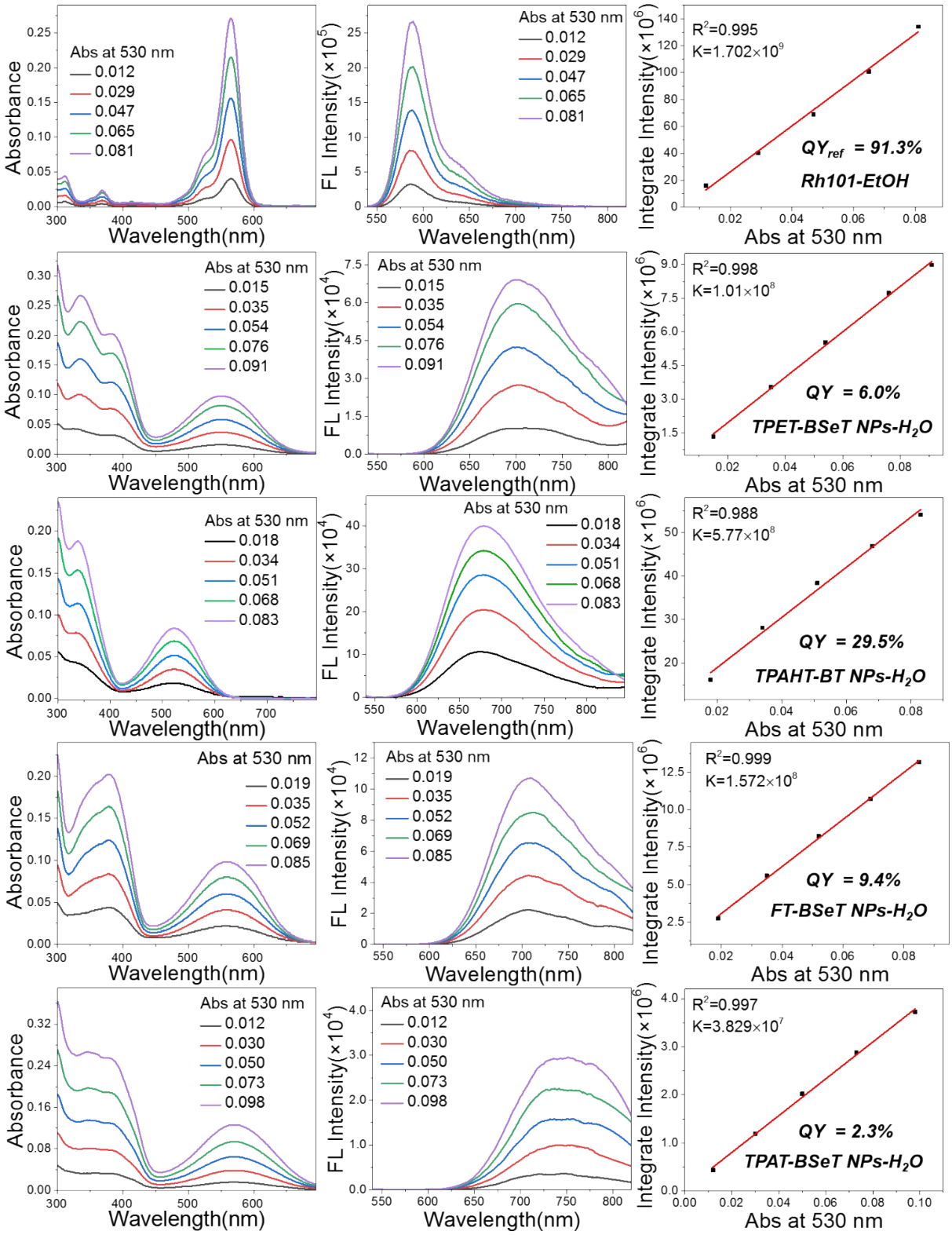

TPET-BSeT NPs, TPAHT-BT NPs, FT-BSeT NPs, and TPAT-BSeT NPs

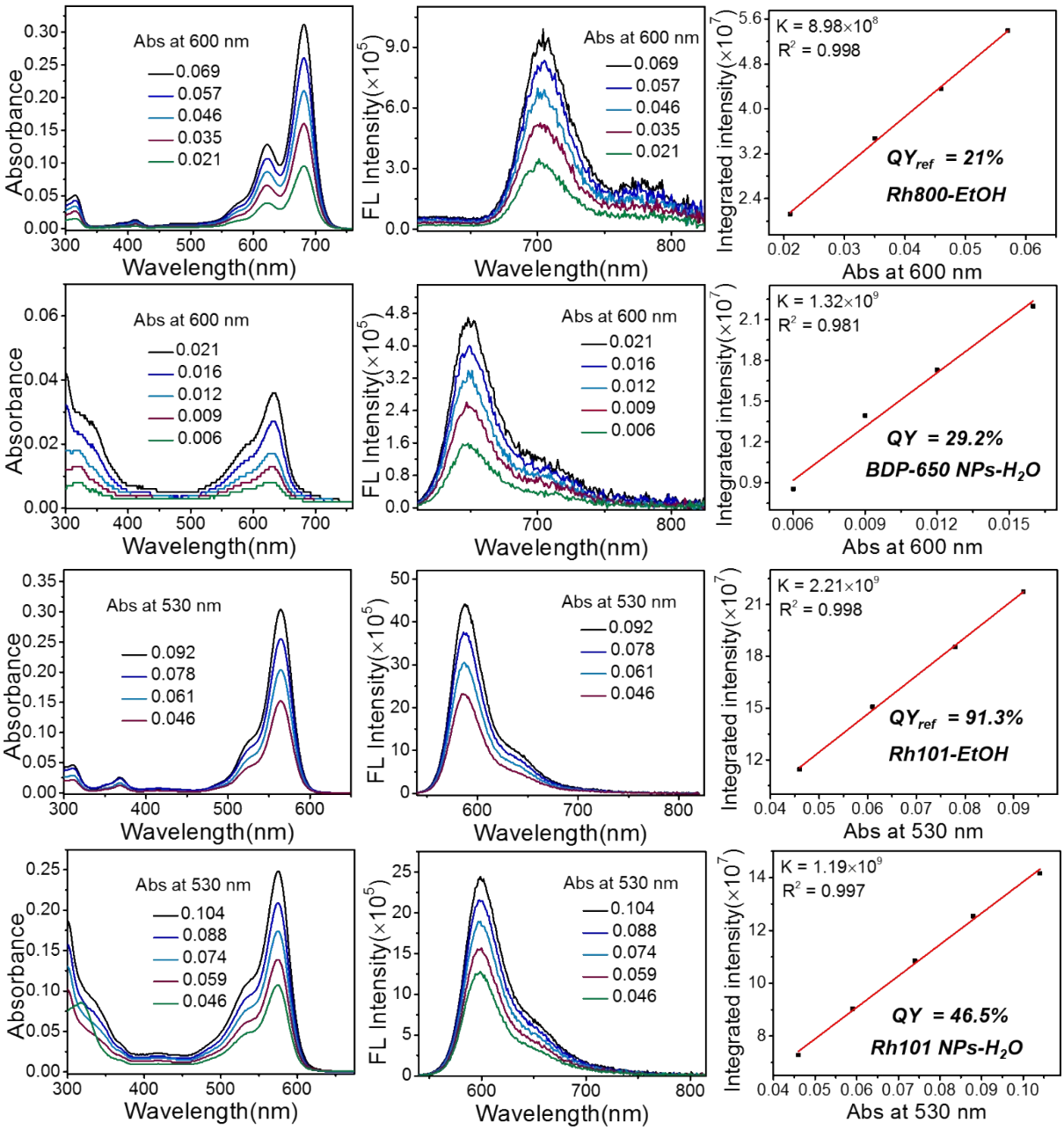

BDP-650 NPs and Rh101 NPs

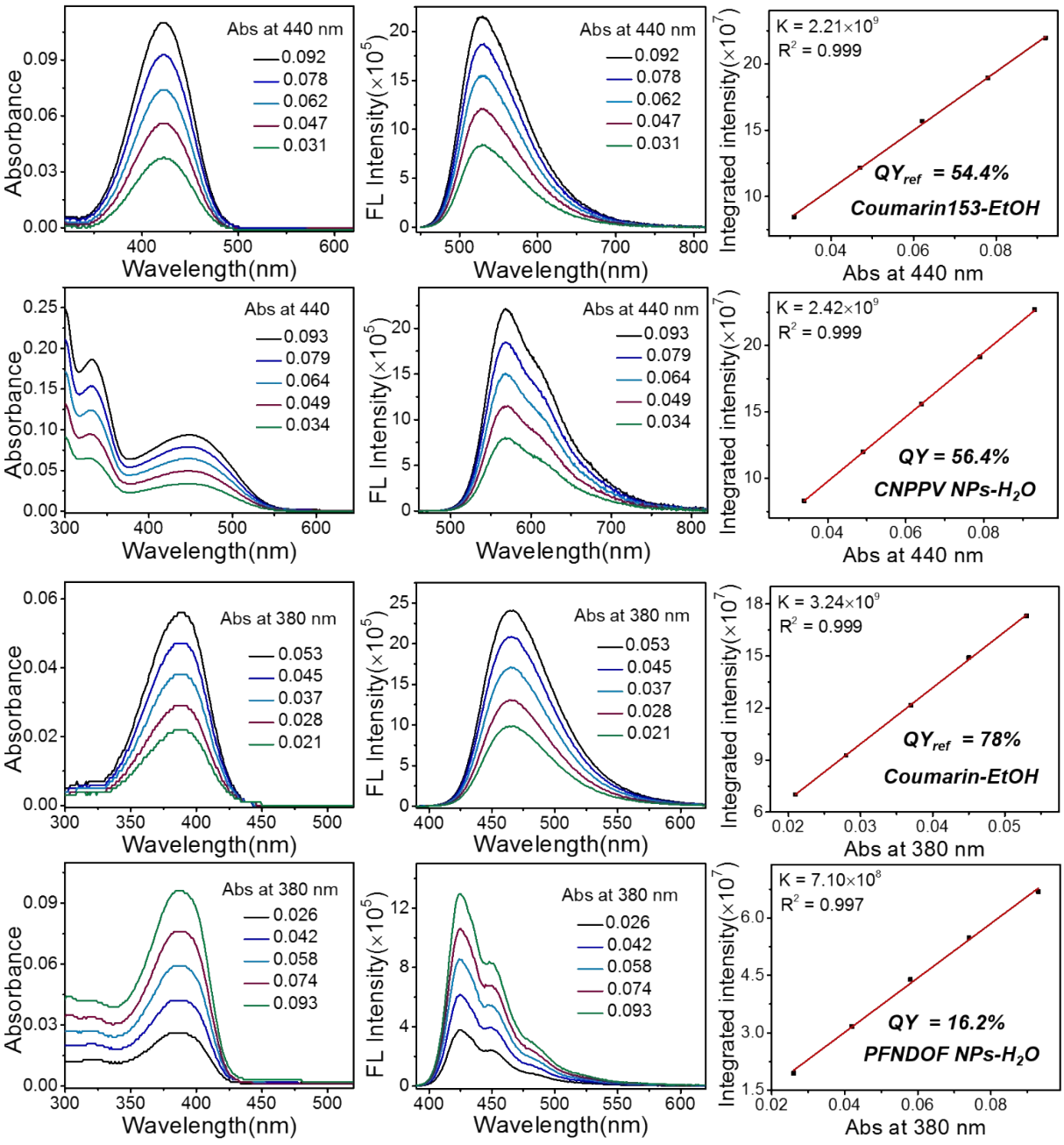

CNPPV NPs and PFN-DOF NPs

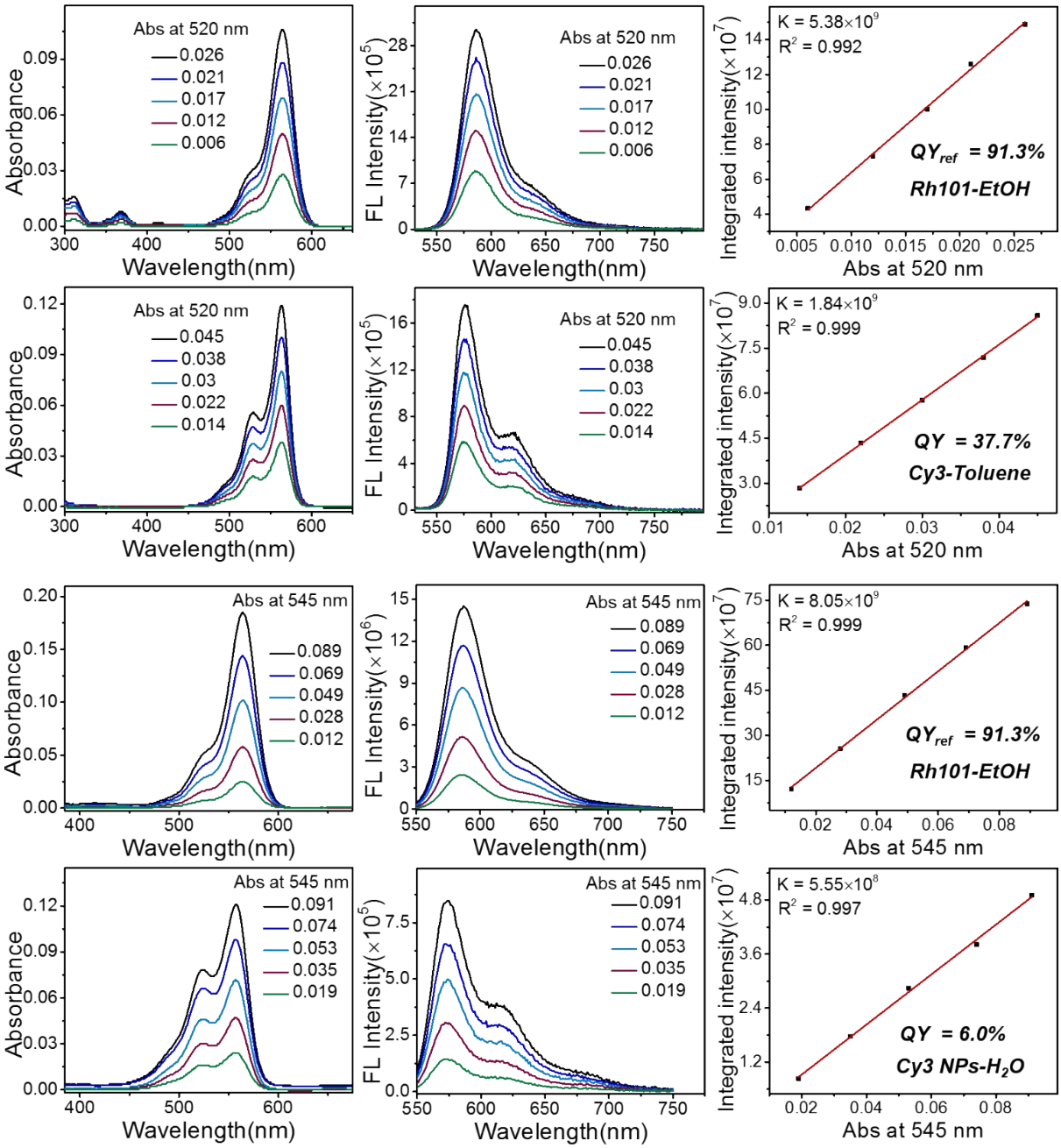

Cy3 (in toluene) and Cy3 NPs

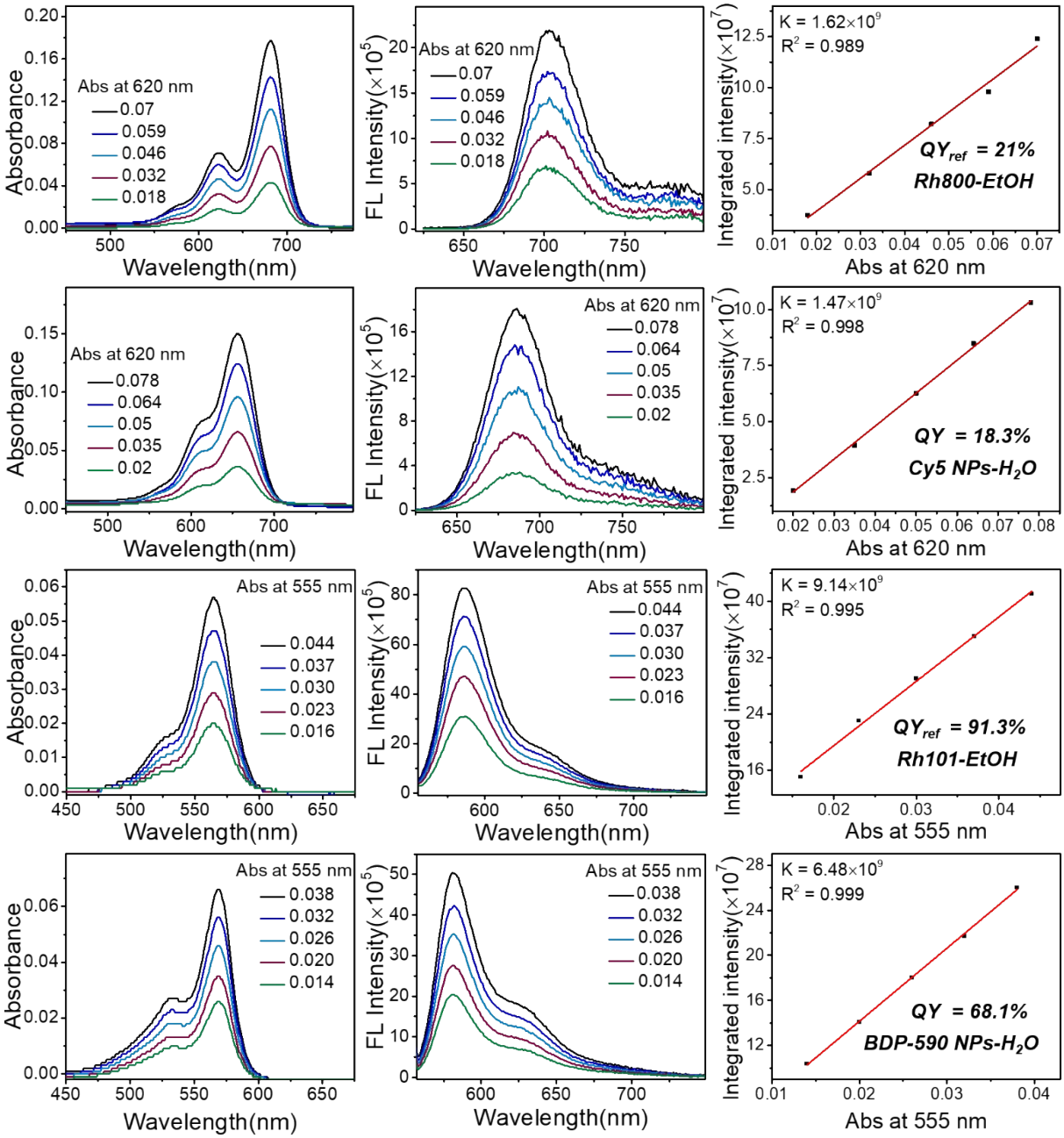

Cy5 NPs and BDP-590 NPs

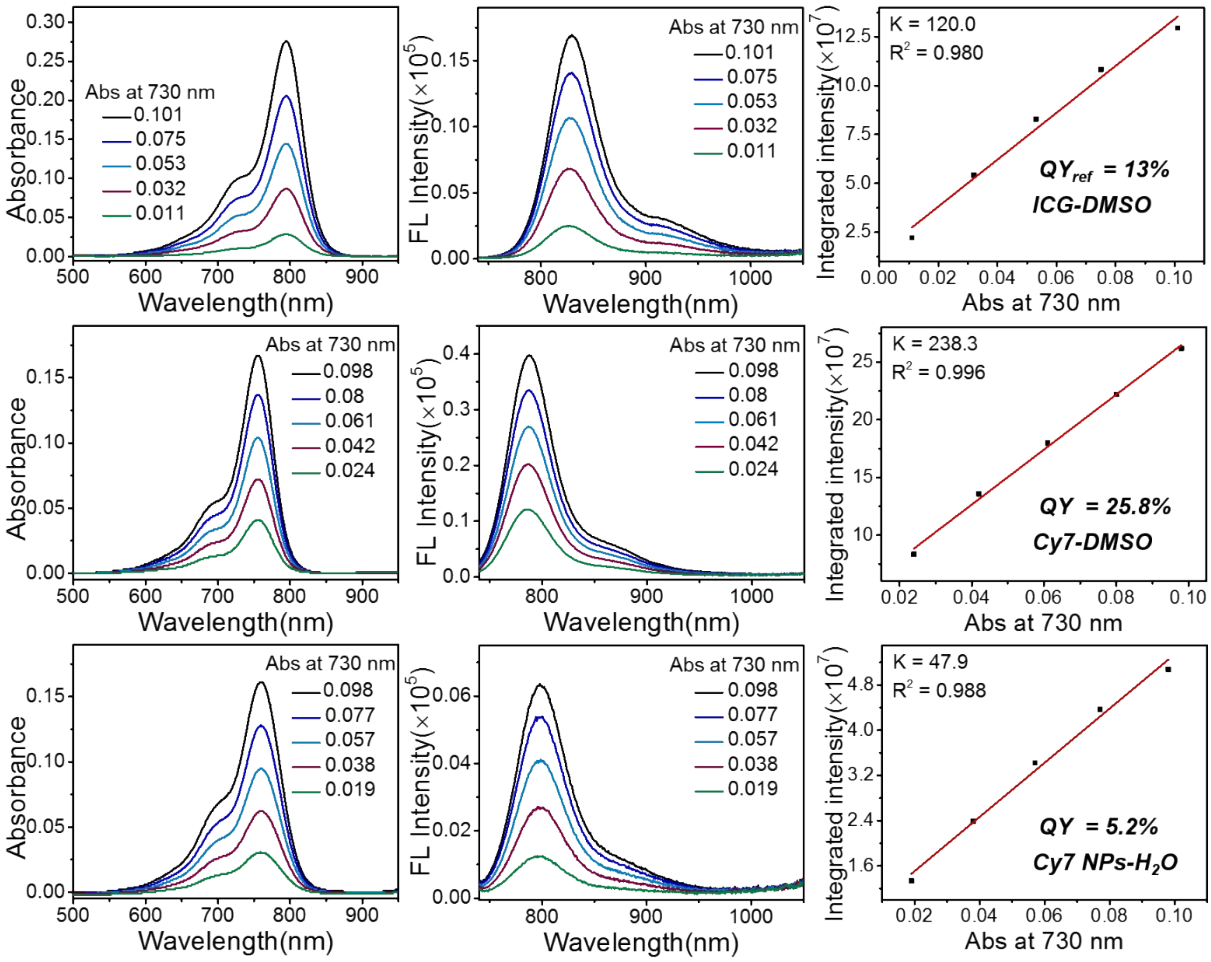

Cy7 (in DMSO) and Cy7 NPs

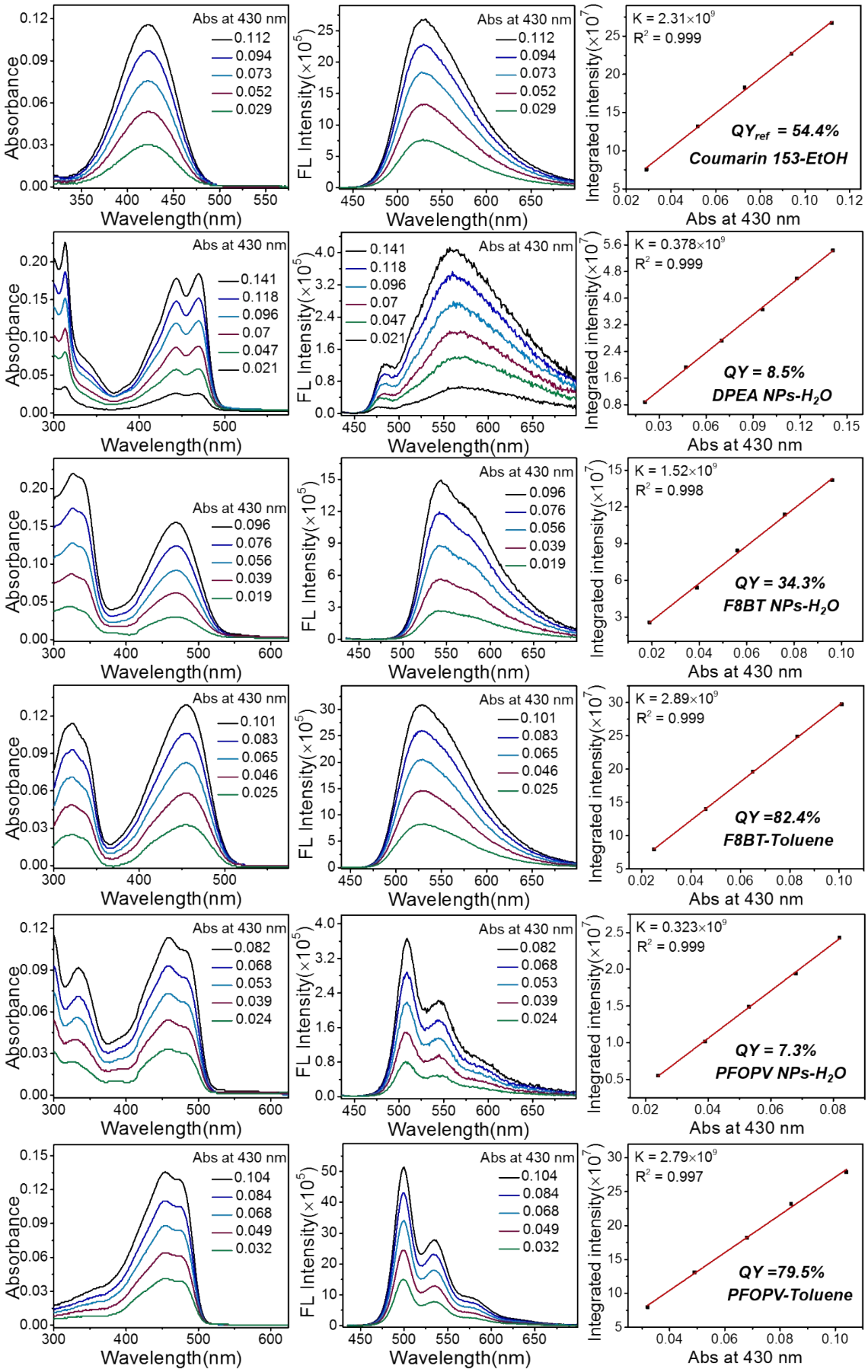

DPEA NPs, F8BT (in toluene), F8BT NPs, PFOPV (in toluene), and PFOPV NPs

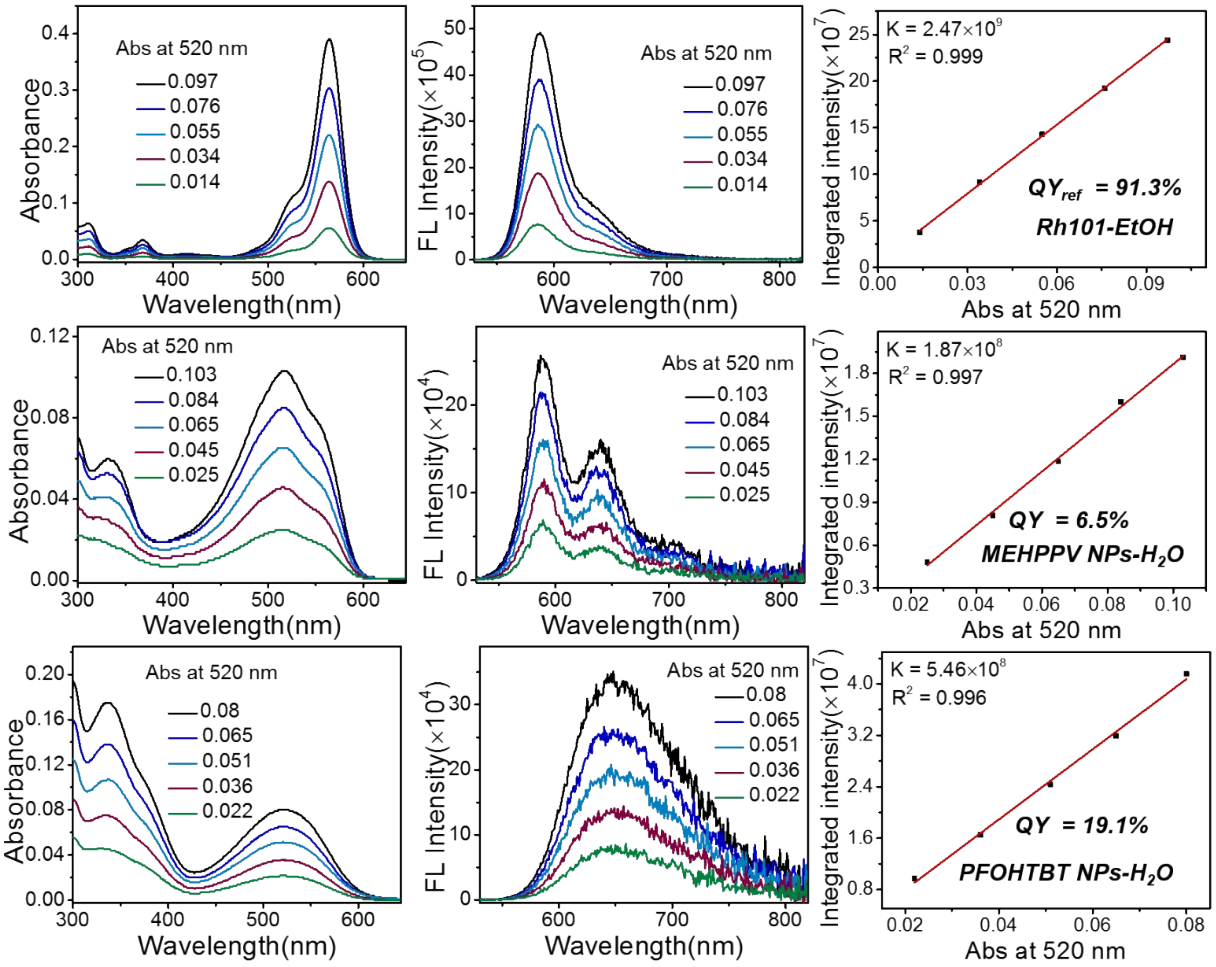

MEHPPV NPs and PFOHTBT NPs

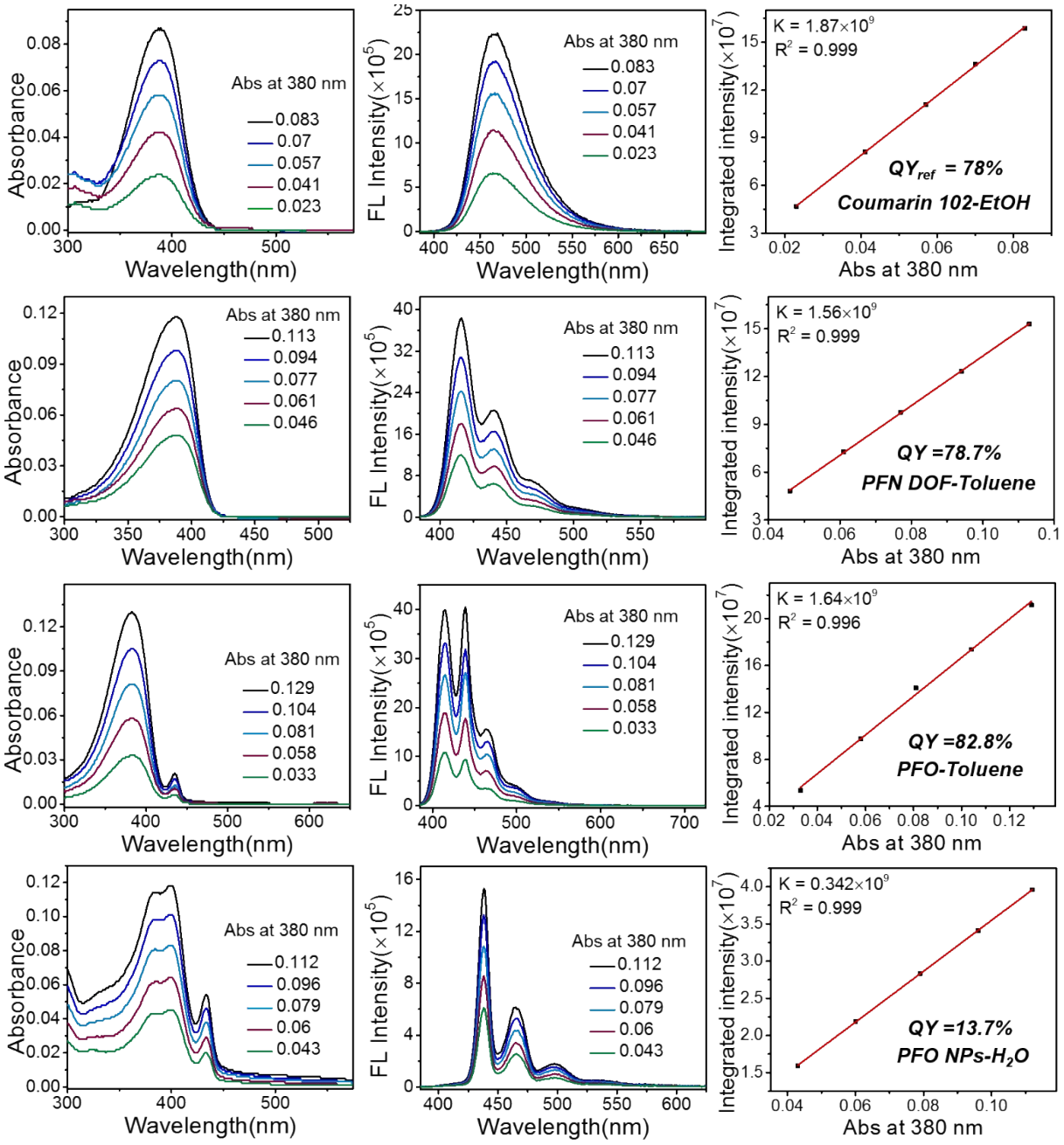

PFN-DOF (in toluene), PFO (in toluene), and PFO NPs

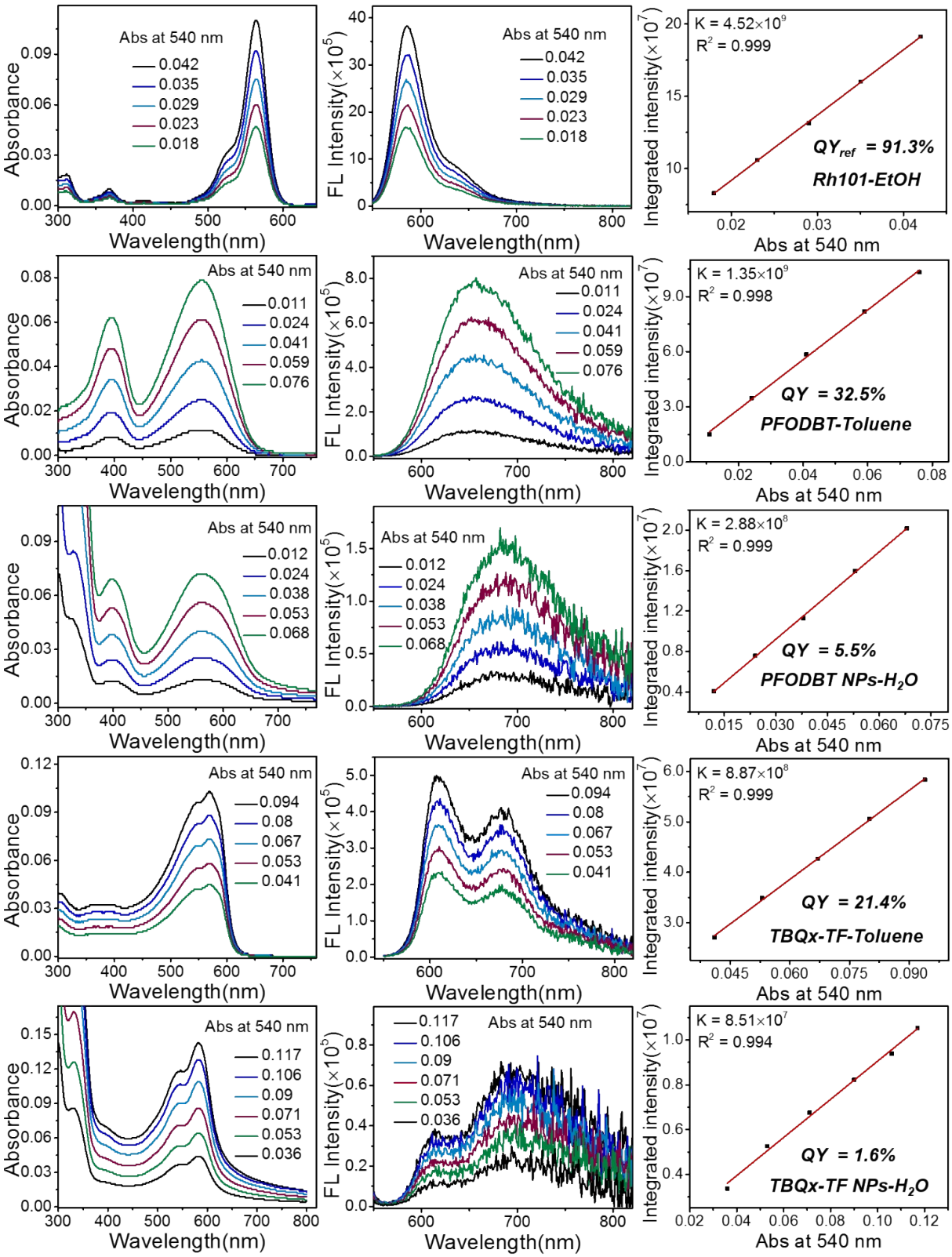

PFODBT (in toluene), PFODBT NPs, TBQx-TF (in toluene), and TBQx-TF NPs

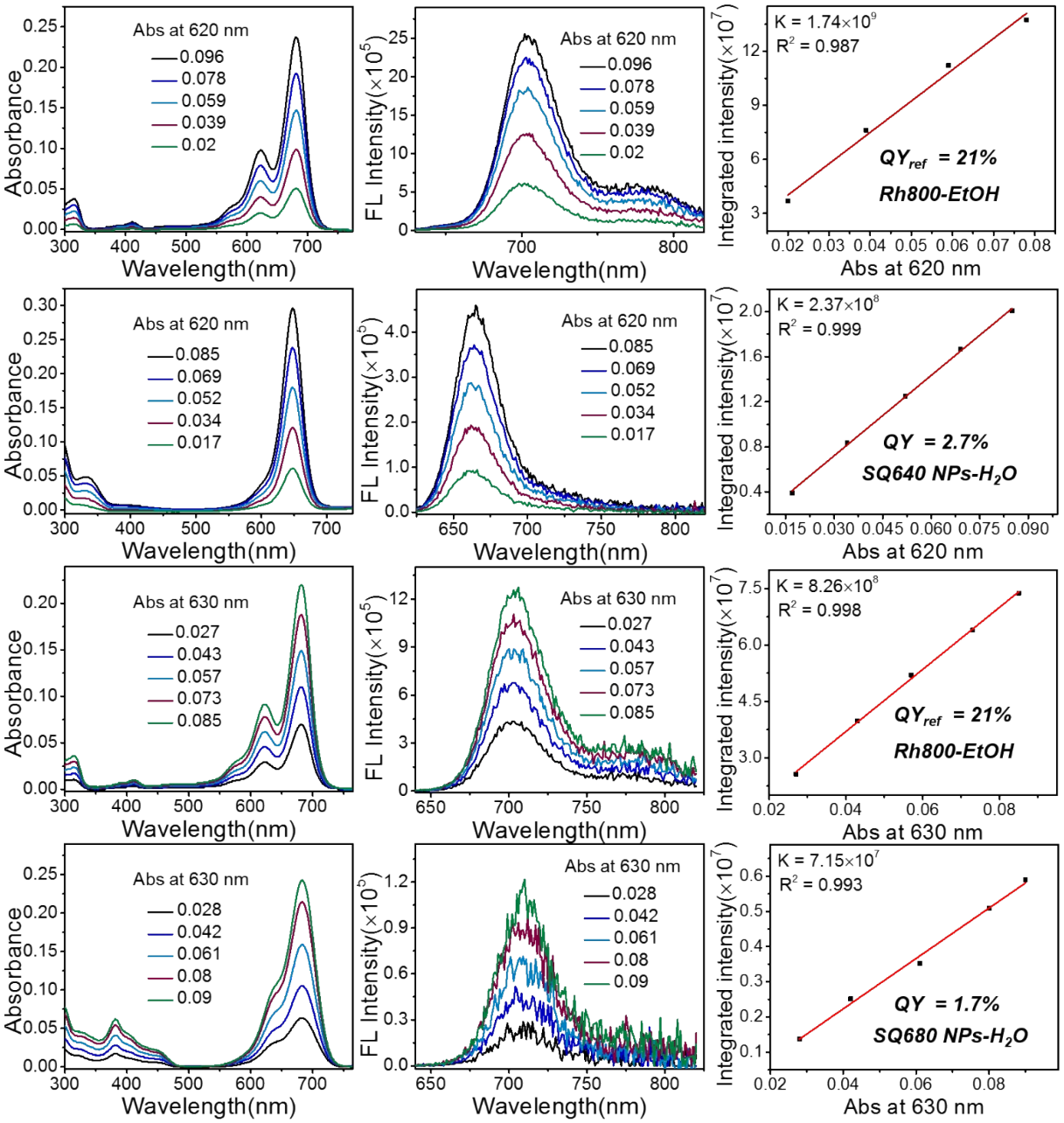

SQ640 NPs and SQ680 NPs

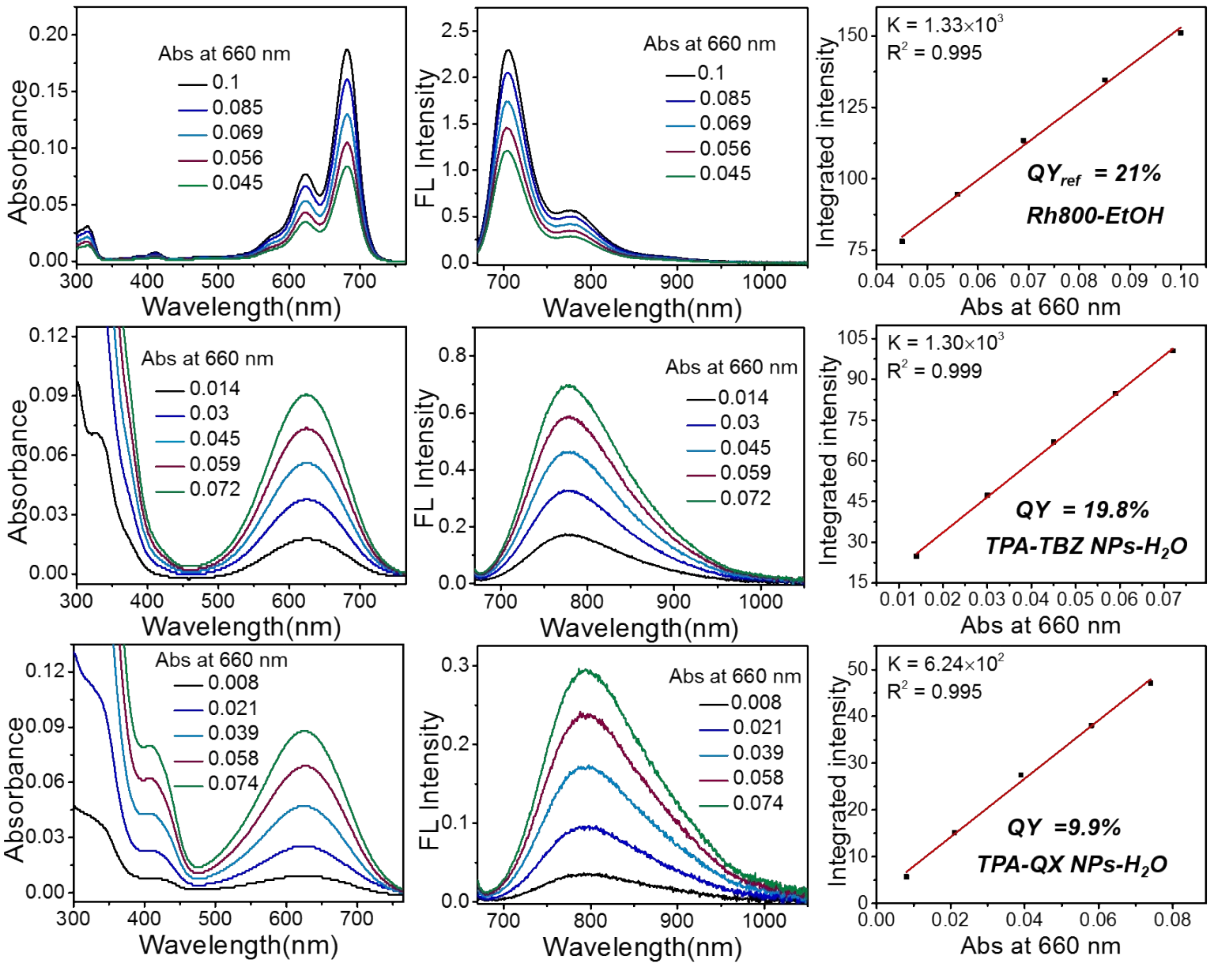

TPA-TBZ NPs and TPA-QX NPs

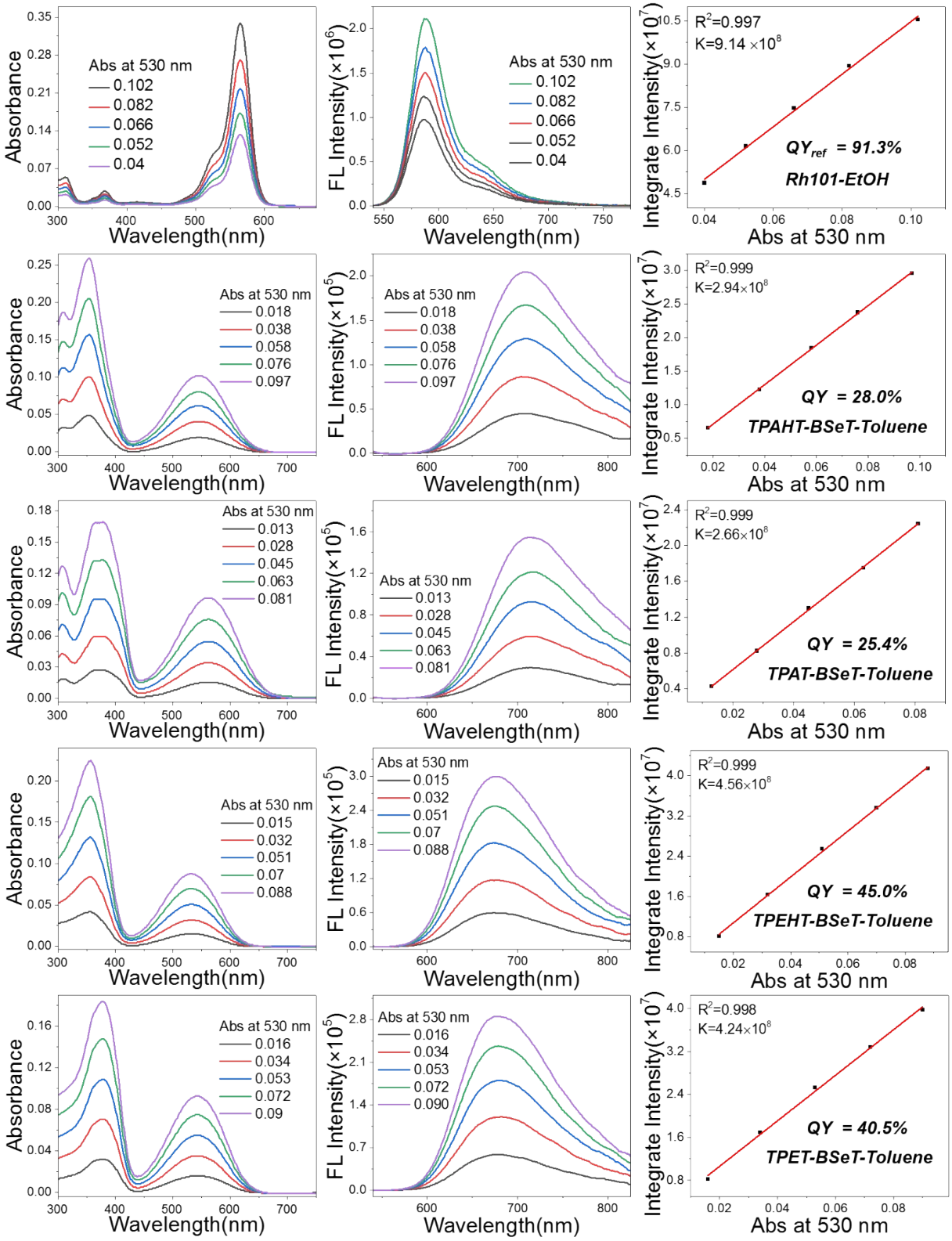

TPAHT-BseT, TPAT-BseT, TPEHT-BseT, and TPET-BseT, in toluene

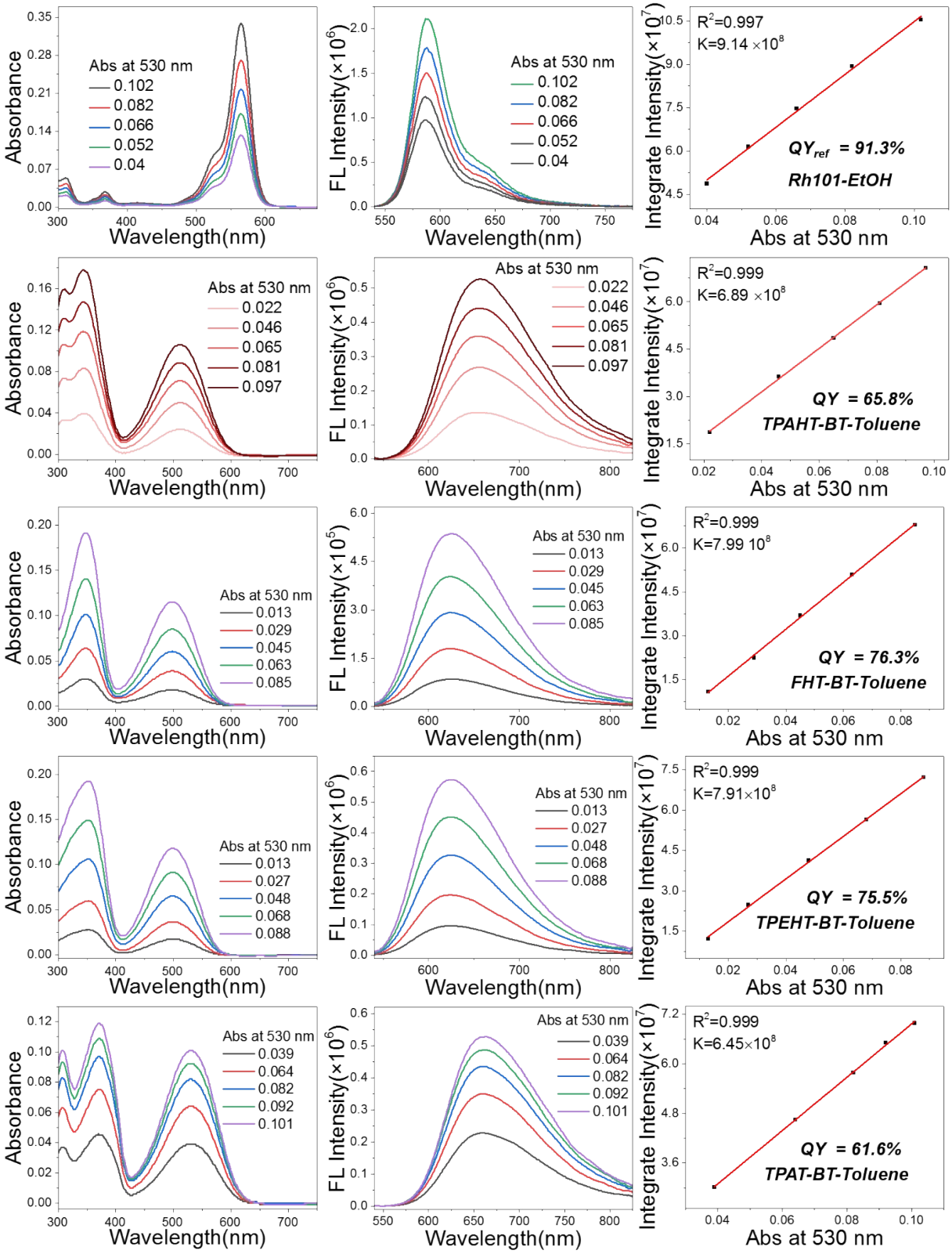

TPAHT-BT, FHT-BT, TPEHT-BT and TPAT-BT, in toluene

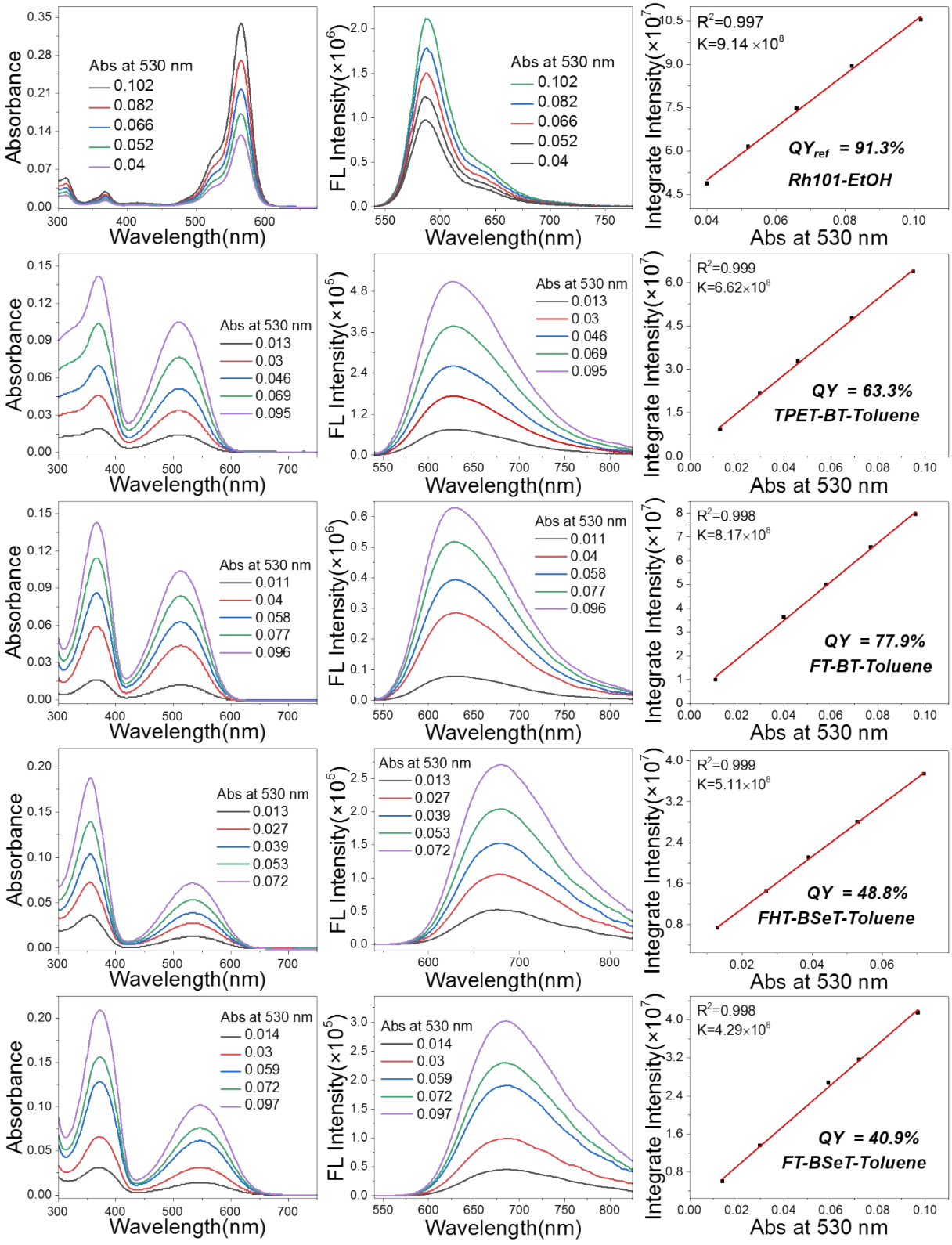

TPET-BT, FT-BT, FHT-BseT, and FT-BSeT, in toluene

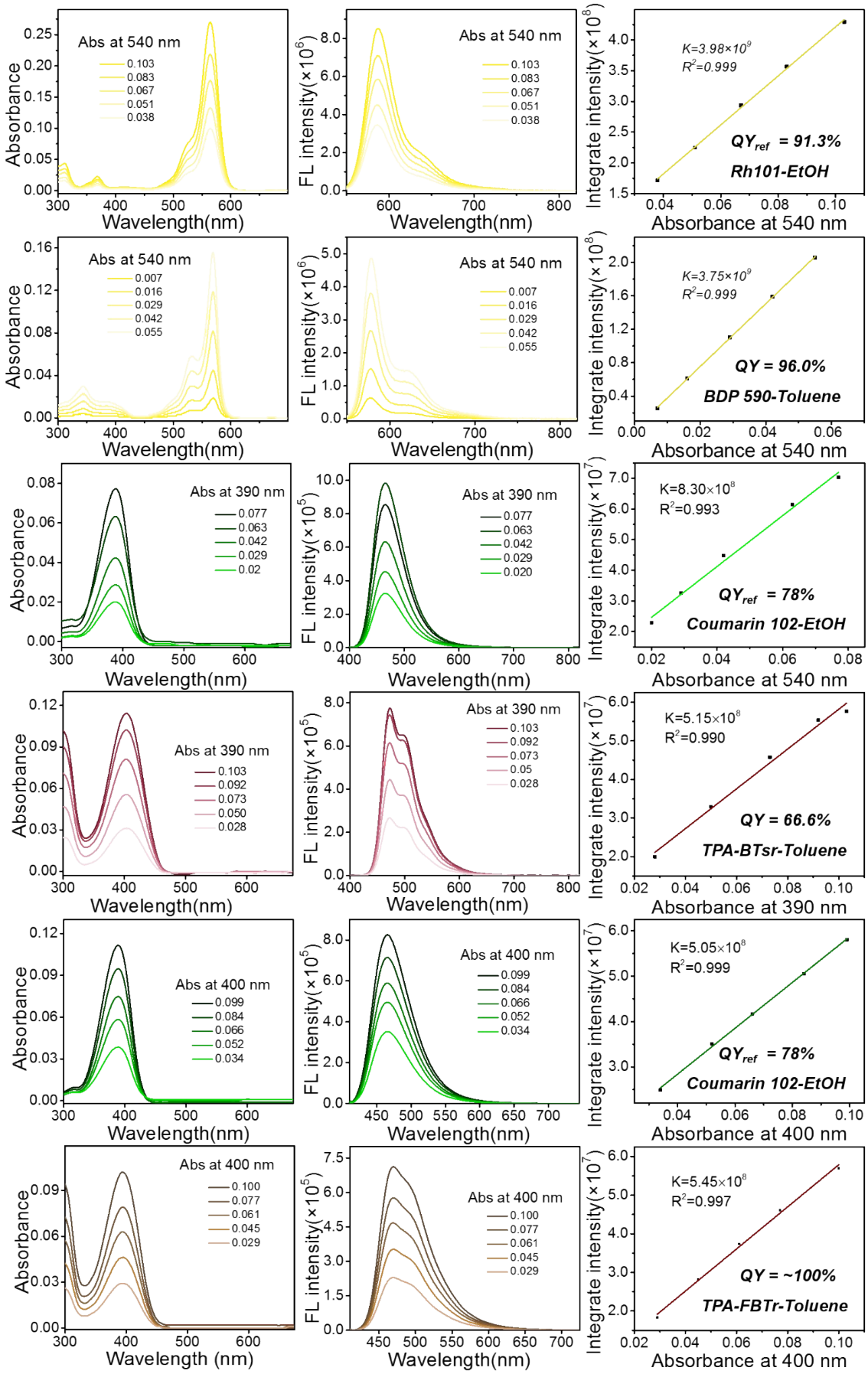

BDP-590, TPA-BTsr, and TPA-FBTr, in toluene

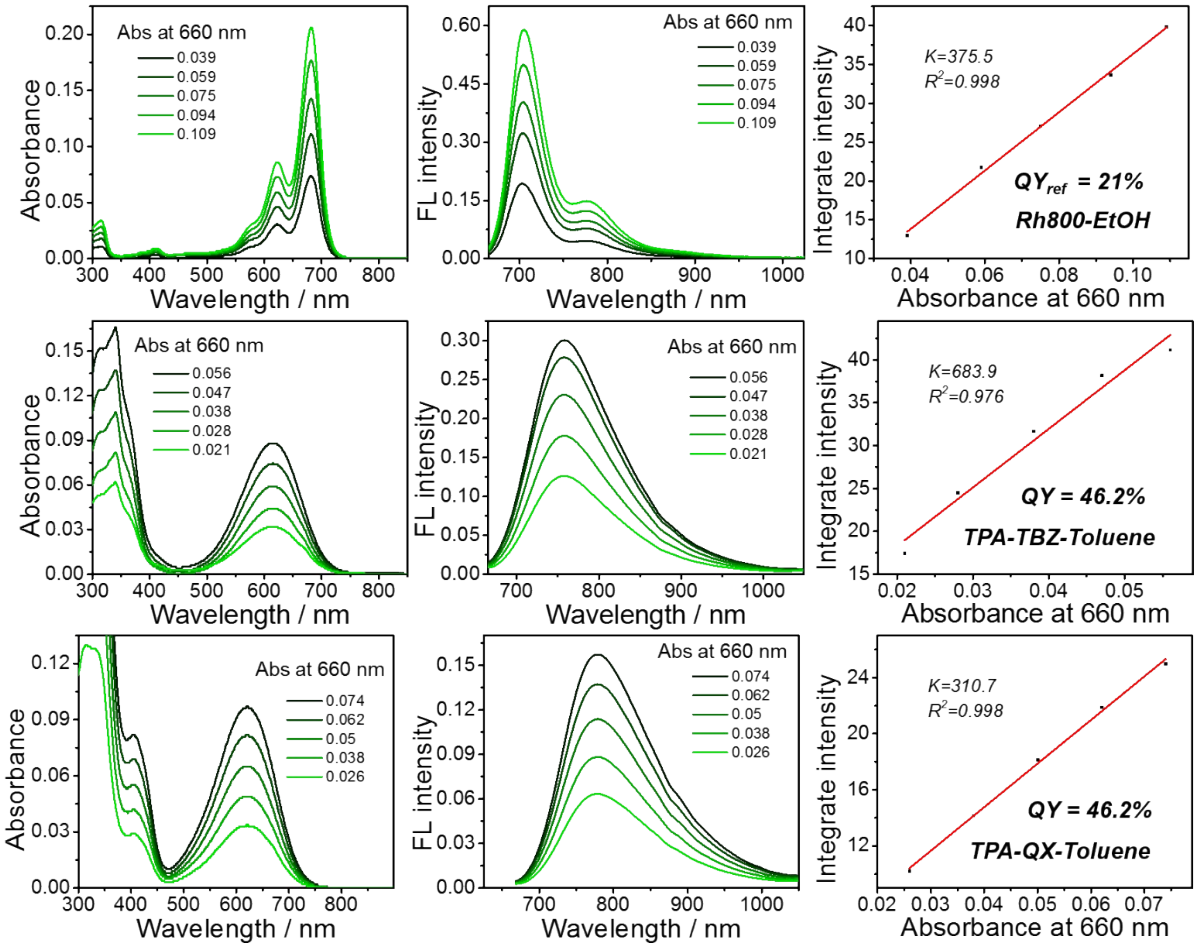

TPA-TBZ and TPA-QX, in toluene

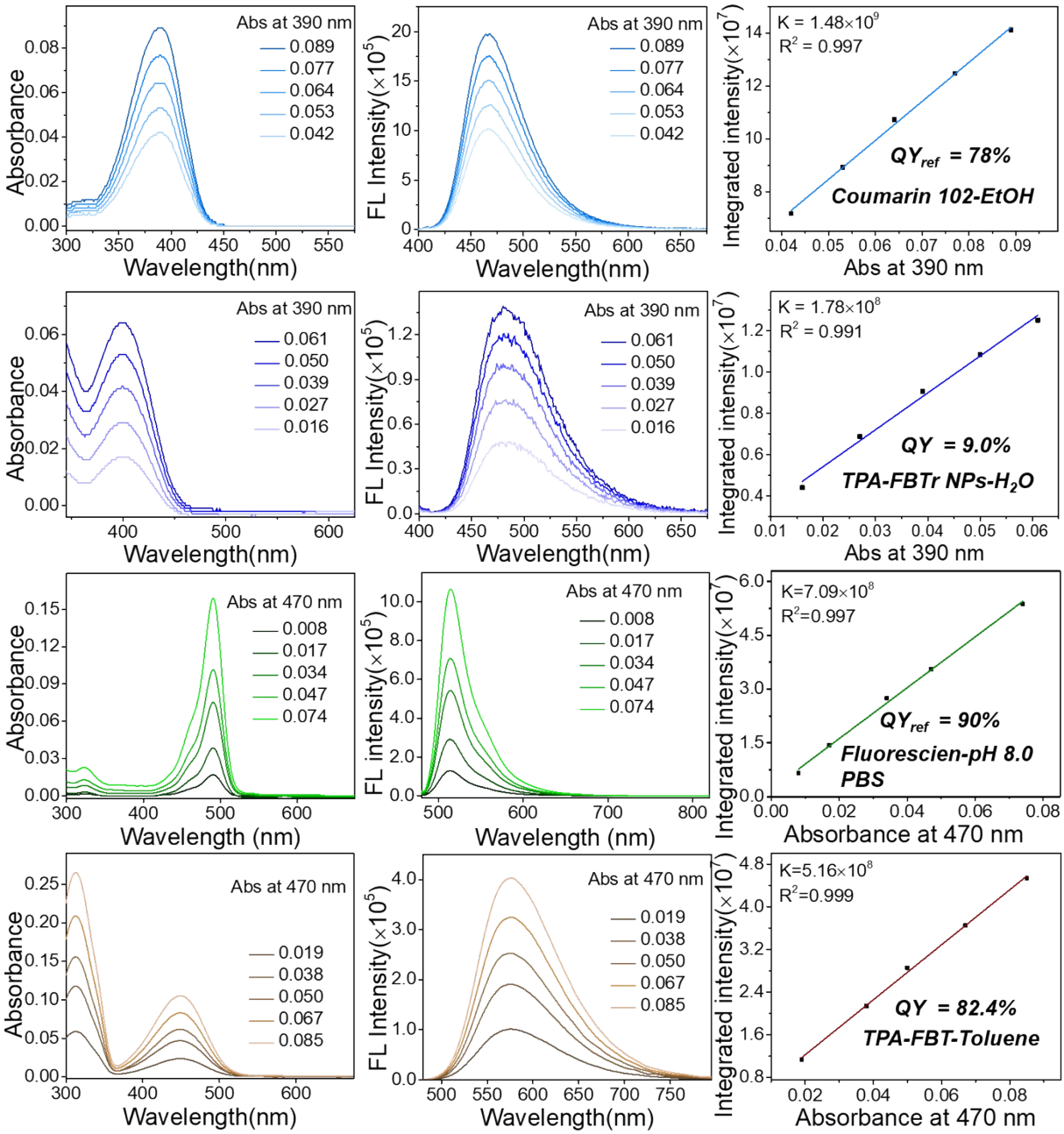

TPA-FBTr NPs (in H_2O) and TPA-FBT (in toluene)

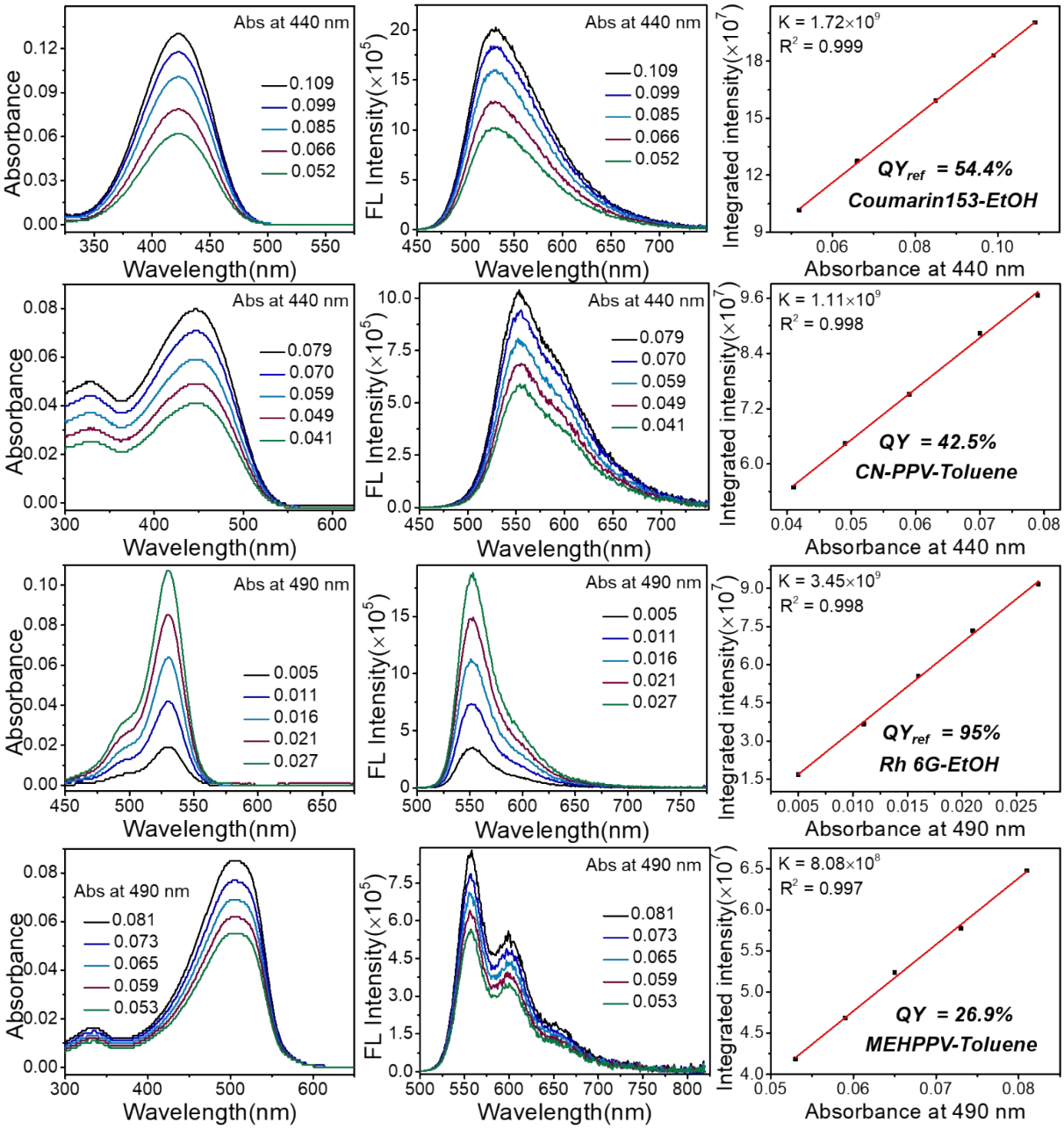

CNPPV and MENPPV, in toluene

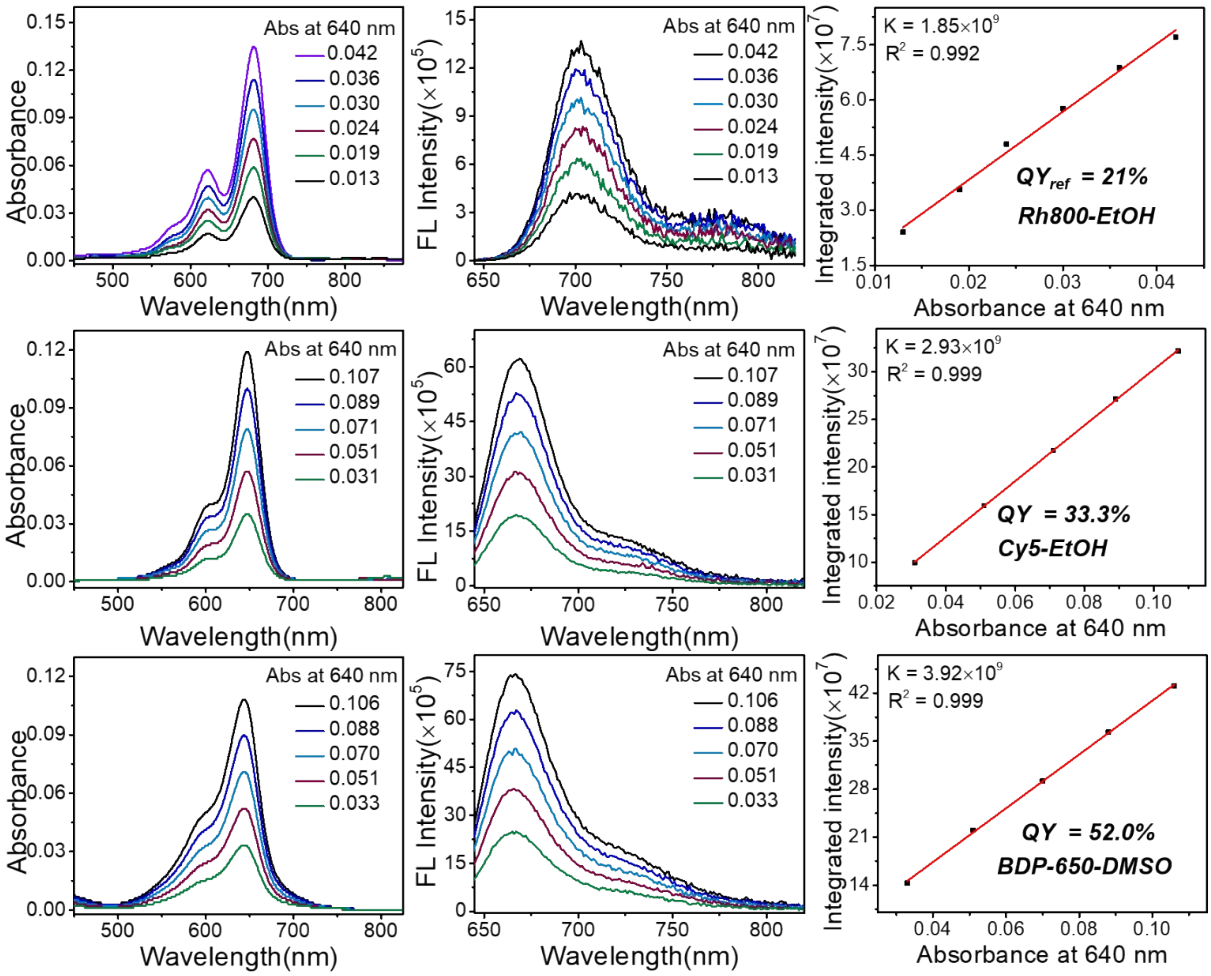

Cy5 (in EtOH) and BDP-650 (in DMSO)

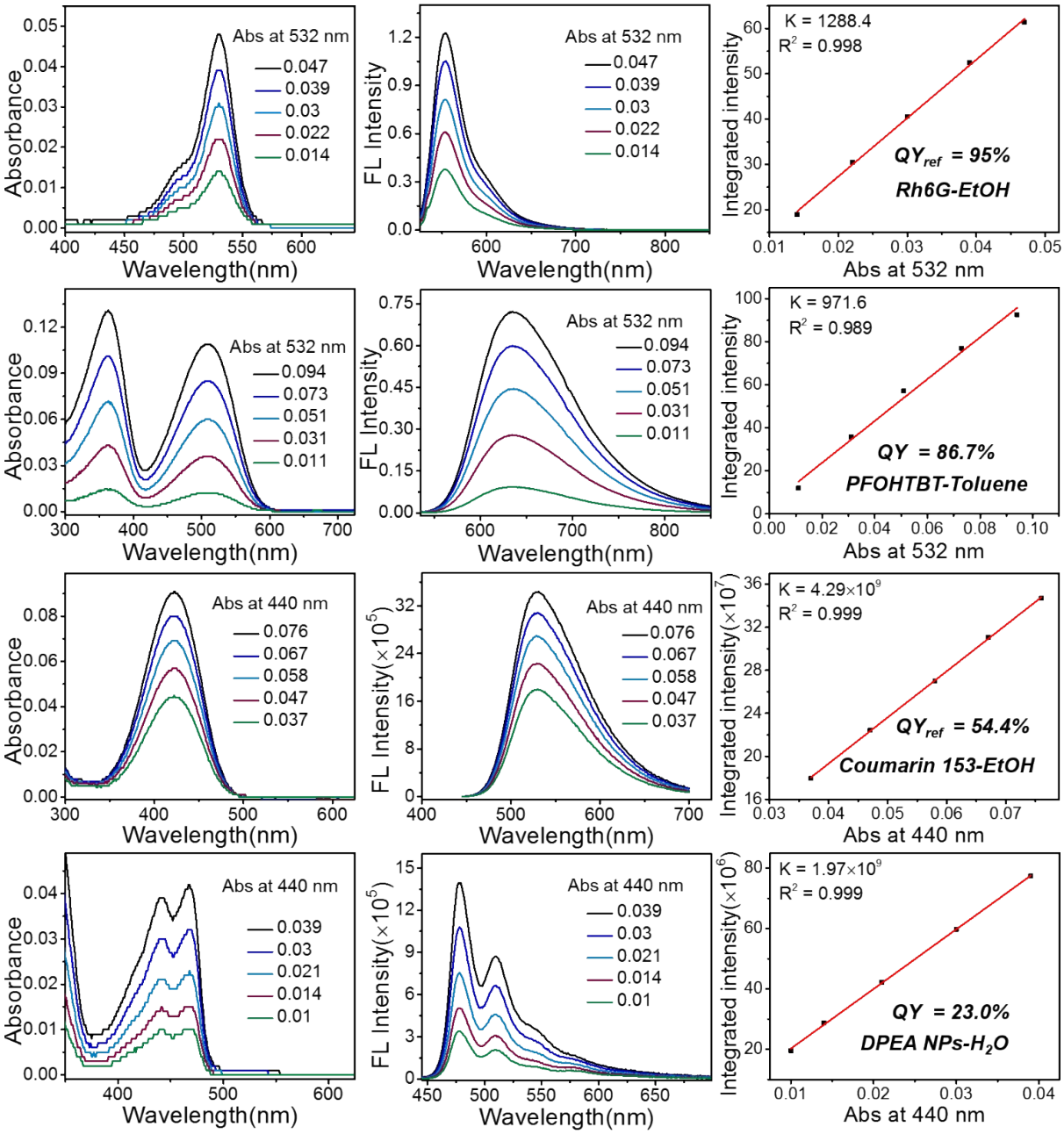

PFOHTBT (in toluene) and DPEA NPs (in H_2O)

^{1}H NMR, ^{13}C NMR and MS spectra characterizations

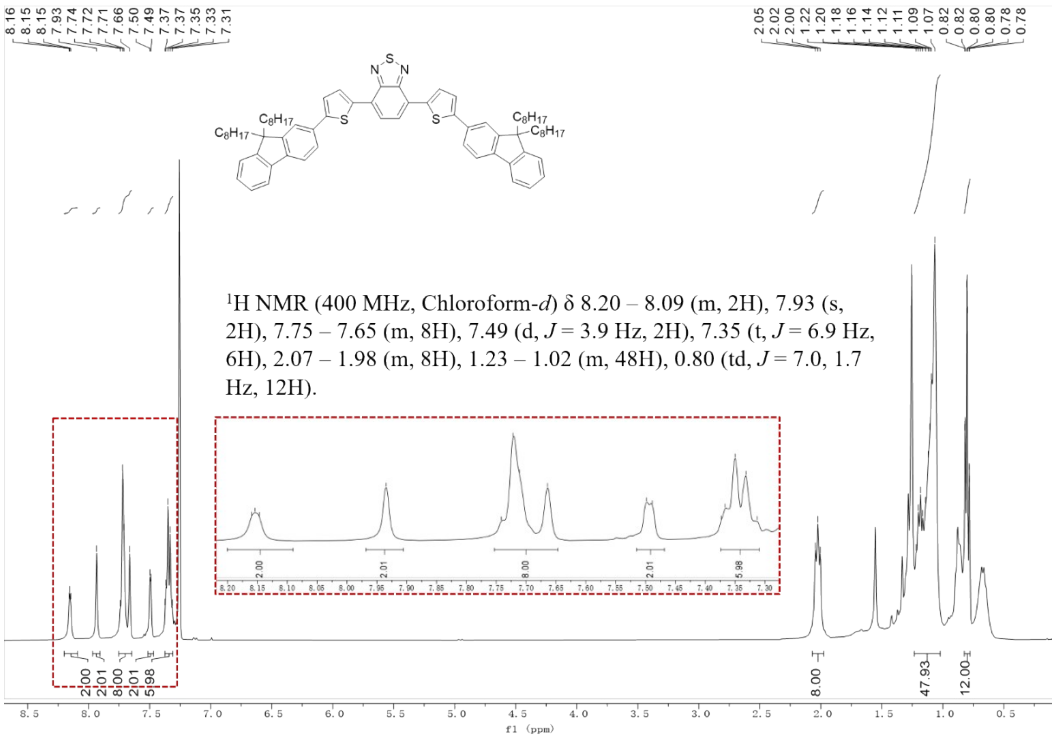

^{1}H NMR spectrum of FT-BT ($CDCl_3$)

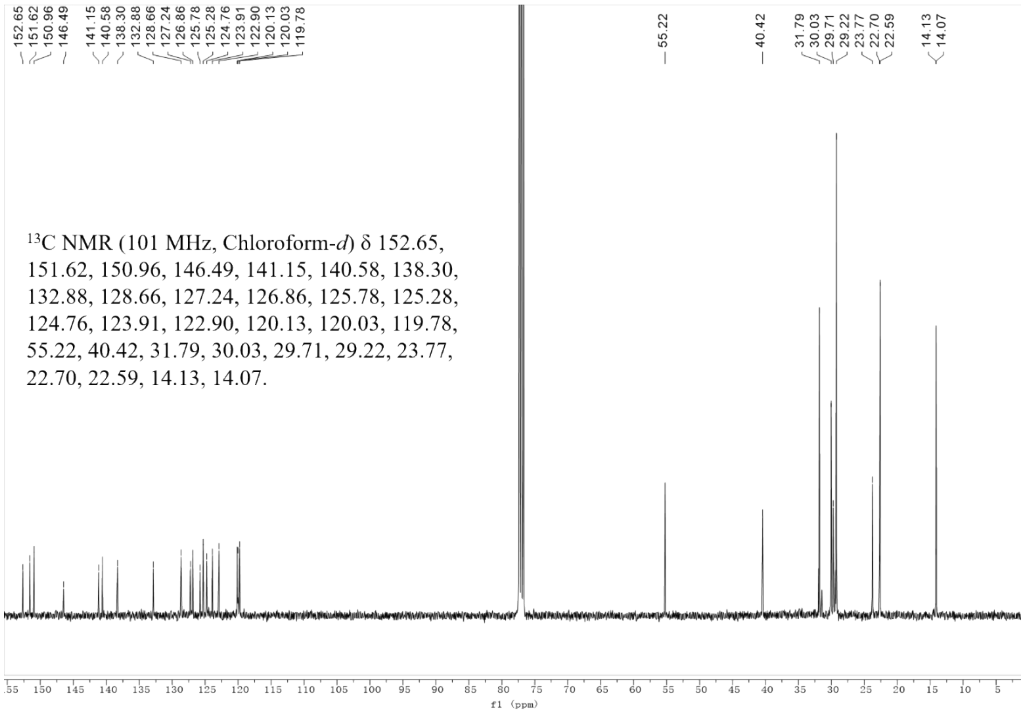

^{13}C NMR spectrum of FT-BT ($CDCl_3$)

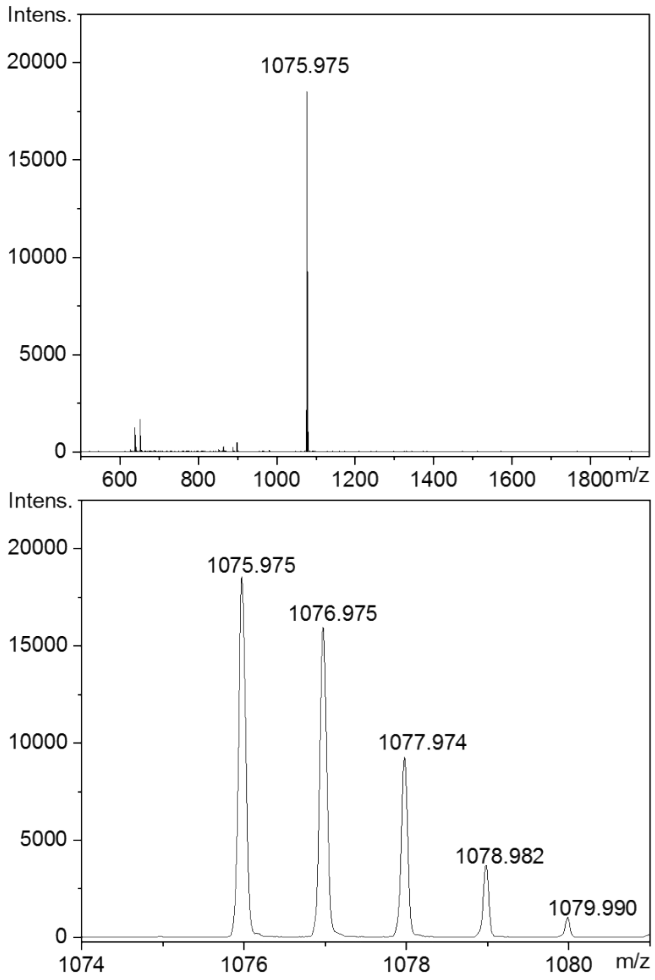

HR-MS spectrum of FT-BT

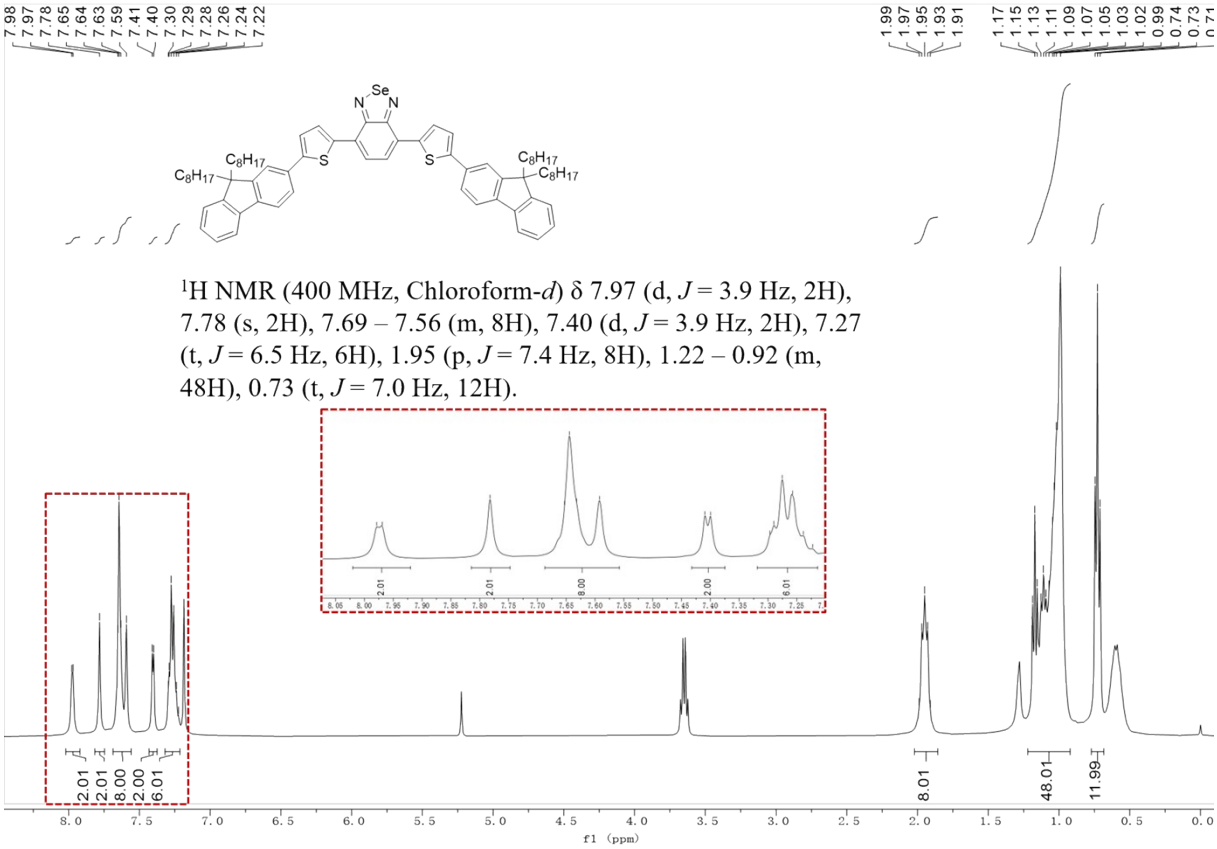

^{1}H NMR (400 MHz, Chloroform-*d*) δ 7.97 (d, *J* = 3.9 Hz, 2H), 7.78 (s, 2H), 7.69 – 7.56 (m, 8H), 7.40 (d, *J* = 3.9 Hz, 2H), 7.27 (t, *J* = 6.5 Hz, 6H), 1.95 (p, *J* = 7.4 Hz, 8H), 1.22 – 0.92 (m, 48H), 0.73 (t, *J* = 7.0 Hz, 12H).

^{1}H NMR spectrum of FT-BSeT ($CDCl_3$)

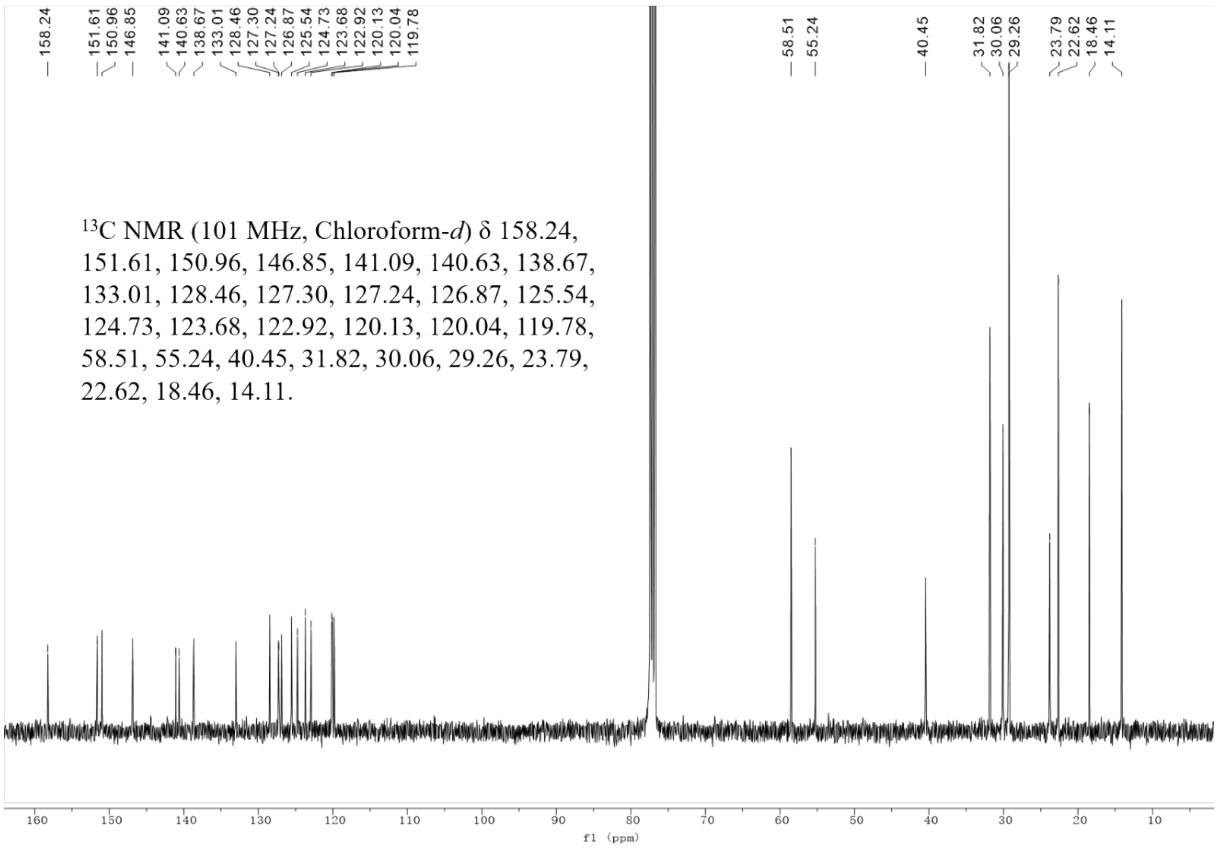

^{13}C NMR (101 MHz, Chloroform-*d*) δ 158.24, 151.61, 150.96, 146.85, 141.09, 140.63, 138.67, 133.01, 128.46, 127.30, 127.24, 126.87, 125.54, 124.73, 123.68, 122.92, 120.13, 120.04, 119.78, 58.51, 55.24, 40.45, 31.82, 30.06, 29.26, 23.79, 22.62, 18.46, 14.11.

^{13}C NMR spectrum of FT-BSeT ($CDCl_3$)

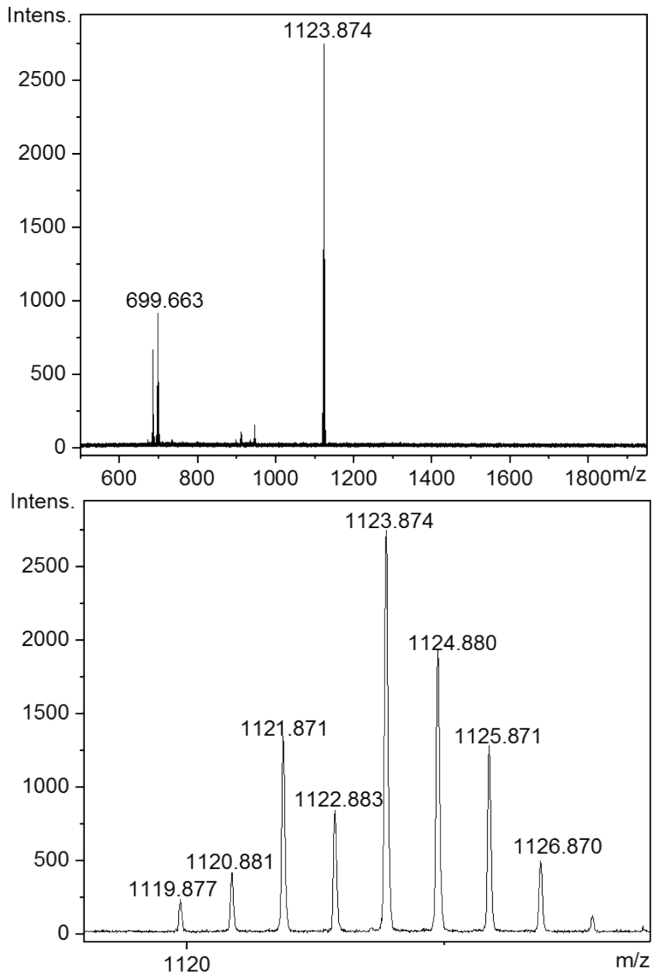

HR-MS spectrum of FT-BSeT

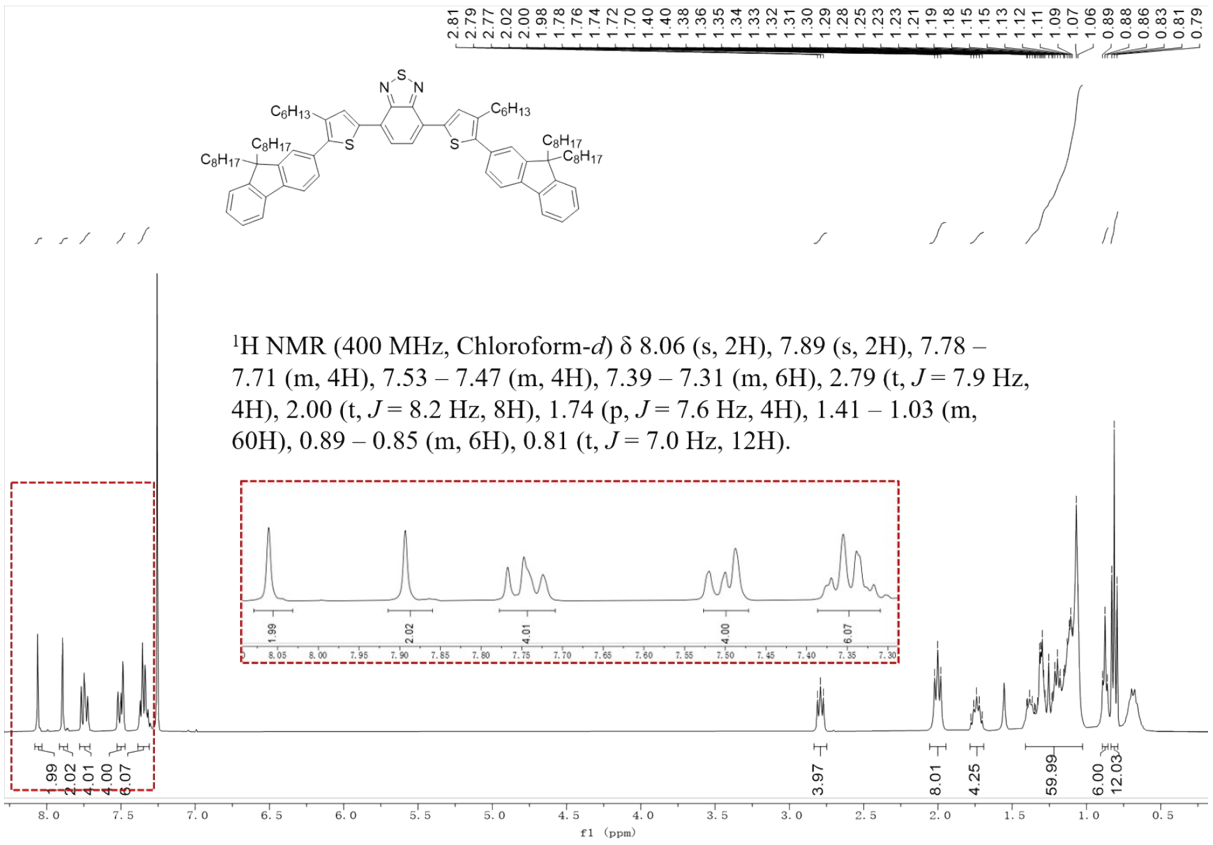

^{1}H NMR spectrum of FHT-BT ($CDCl_3$)

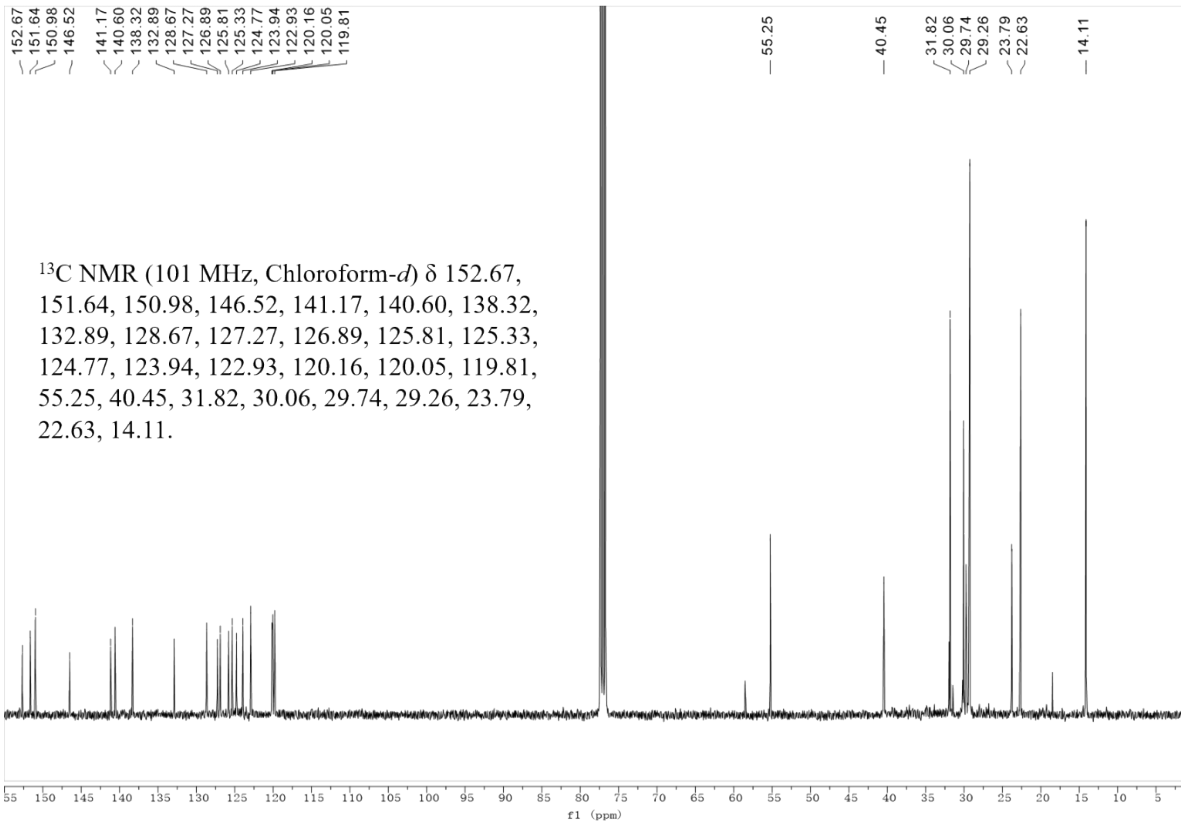

^{13}C NMR spectrum of FHT-BT ($CDCl_3$)

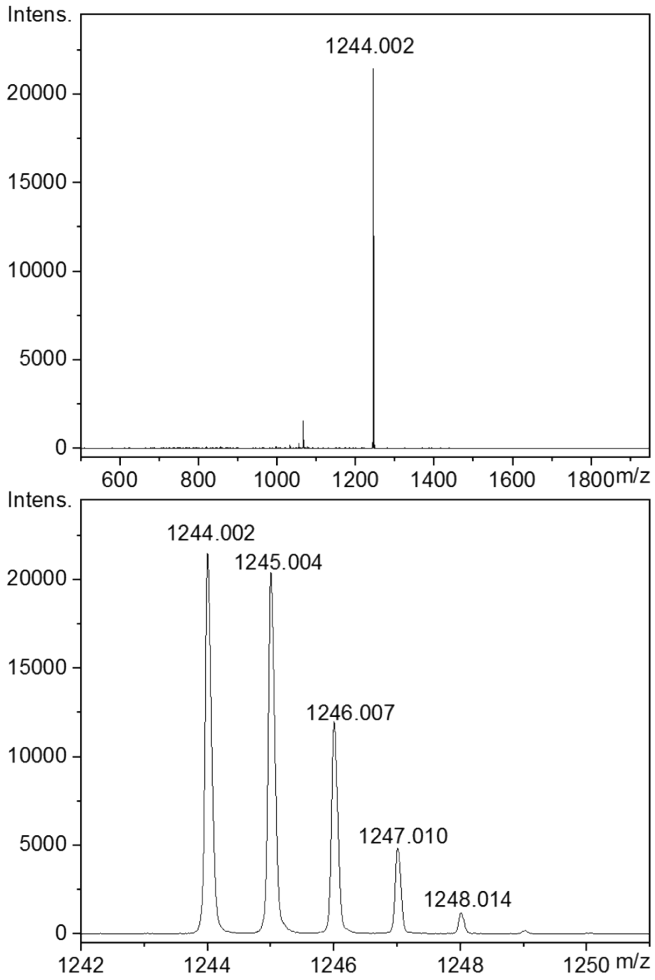

HR-MS spectrum of FHT-BT

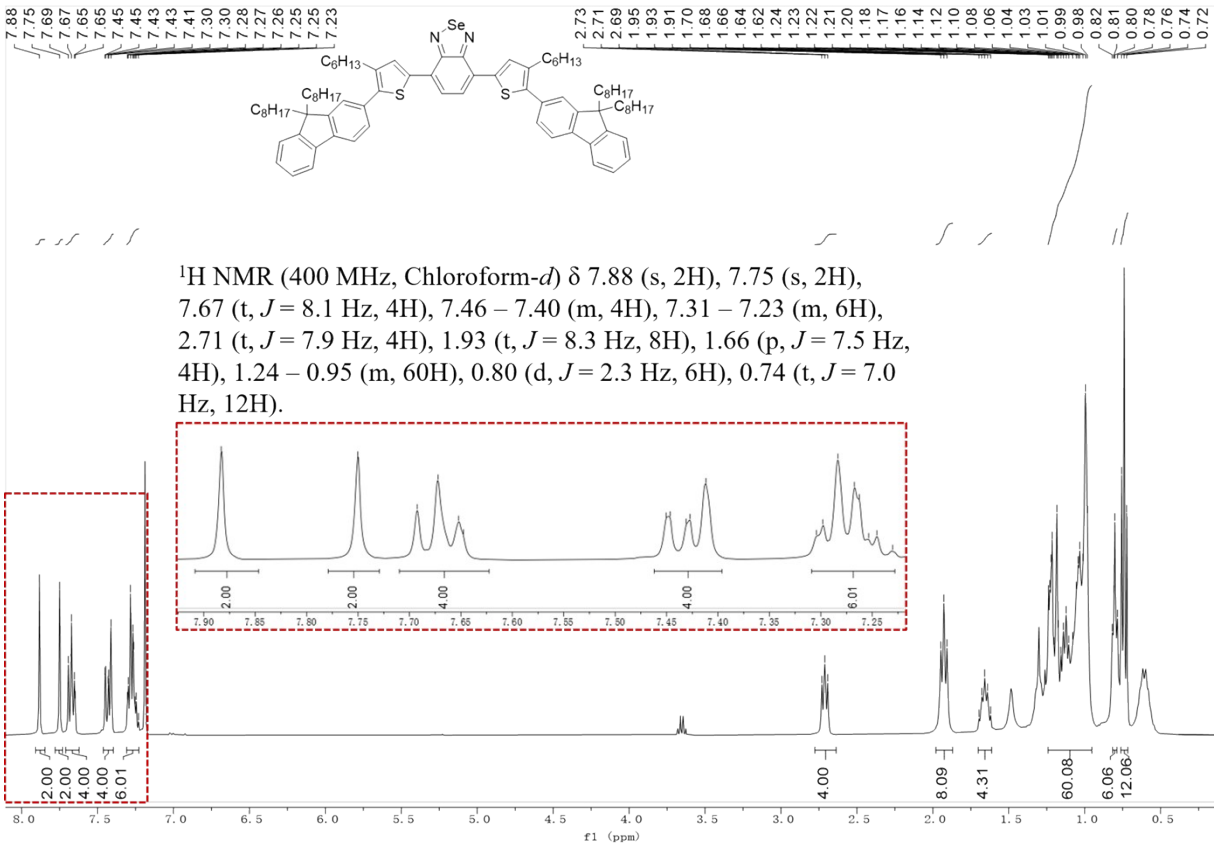

^{1}H NMR (400 MHz, Chloroform-*d*) δ 7.88 (s, 2H), 7.75 (s, 2H), 7.67 (t, *J* = 8.1 Hz, 4H), 7.46 – 7.40 (m, 4H), 7.31 – 7.23 (m, 6H), 2.71 (t, *J* = 7.9 Hz, 4H), 1.93 (t, *J* = 8.3 Hz, 8H), 1.66 (p, *J* = 7.5 Hz, 4H), 1.24 – 0.95 (m, 60H), 0.80 (d, *J* = 2.3 Hz, 6H), 0.74 (t, *J* = 7.0 Hz, 12H).

^{1}H NMR spectrum of FHT-BSeT ($CDCl_3$)

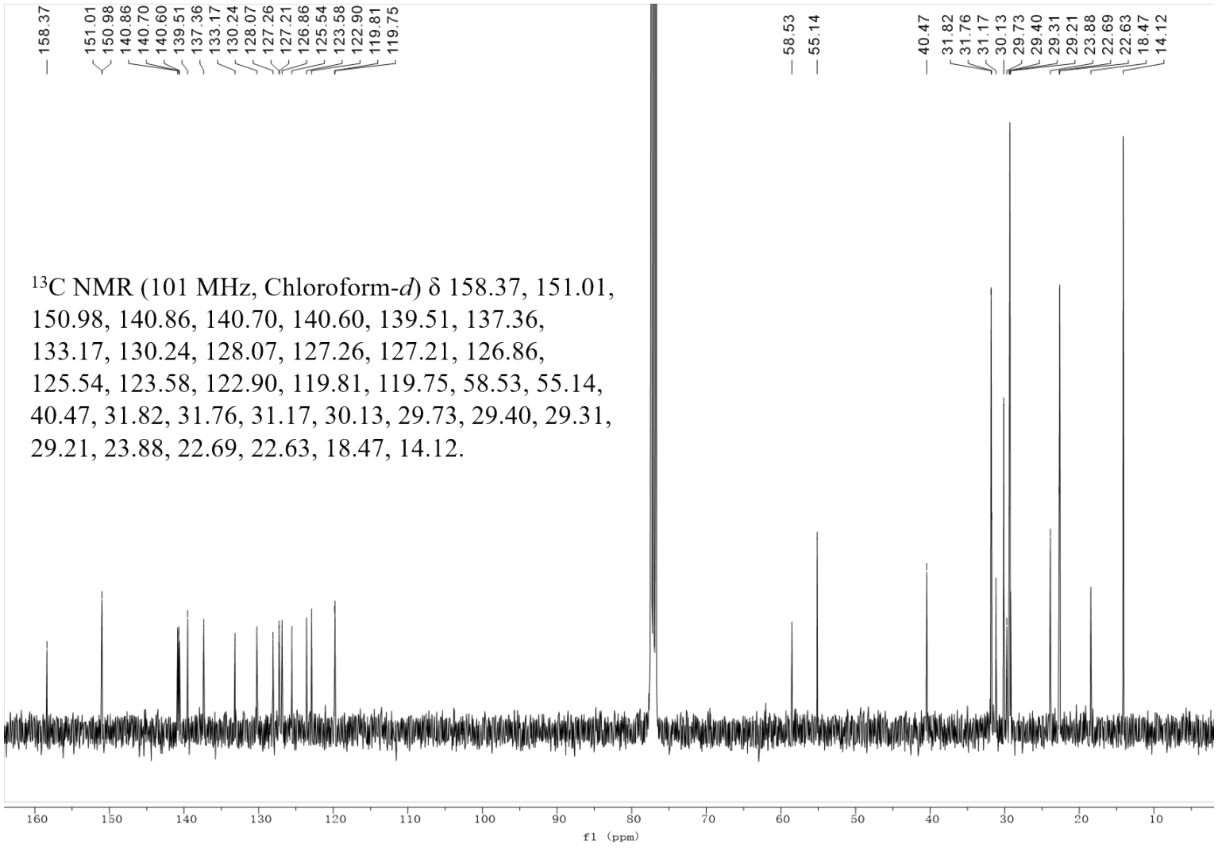

^{13}C NMR (101 MHz, Chloroform-*d*) δ 158.37, 151.01, 150.98, 140.86, 140.70, 140.60, 139.51, 137.36, 133.17, 130.24, 128.07, 127.26, 127.21, 126.86, 125.54, 123.58, 122.90, 119.81, 119.75, 58.53, 55.14, 40.47, 31.82, 31.76, 31.17, 30.13, 29.73, 29.40, 29.31, 29.21, 23.88, 22.69, 22.63, 18.47, 14.12.

^{13}C NMR spectrum of FHT-BSeT ($CDCl_3$)

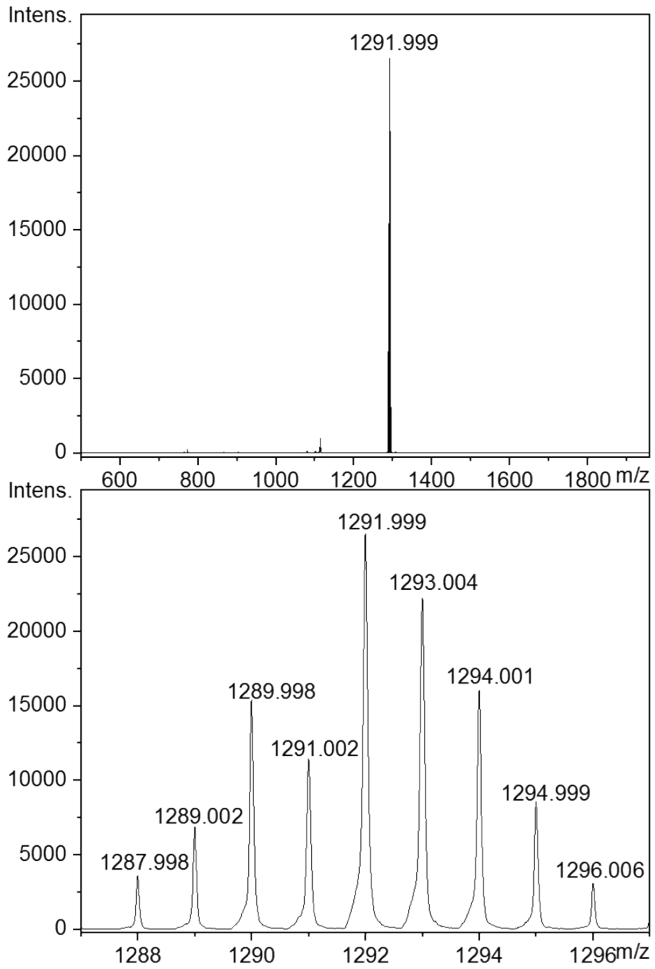

HR-MS spectrum of FHT-BSeT

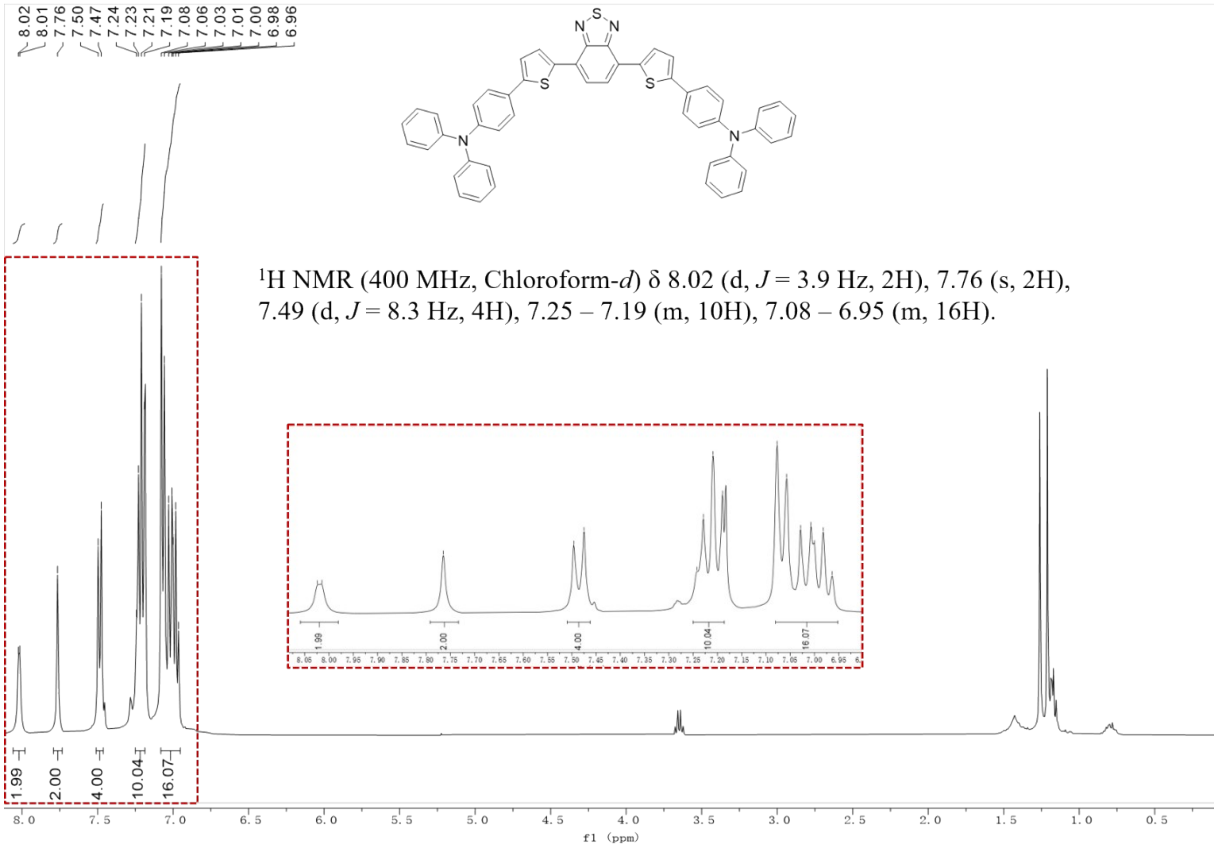

^{1}H NMR (400 MHz, Chloroform-*d*) δ 8.02 (d, *J* = 3.9 Hz, 2H), 7.76 (s, 2H), 7.49 (d, *J* = 8.3 Hz, 4H), 7.25 – 7.19 (m, 10H), 7.08 – 6.95 (m, 16H).

^{1}H NMR spectrum of TPAT-BT ($CDCl_3$)

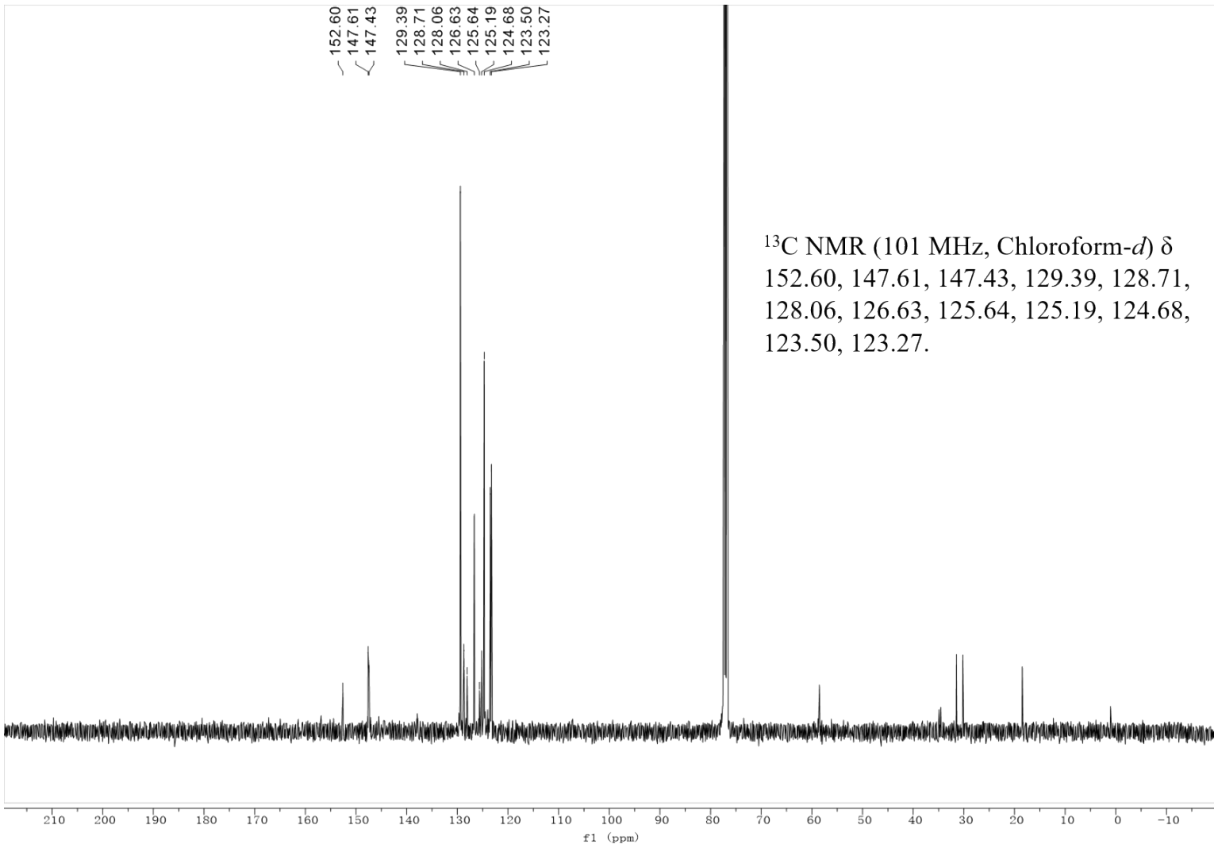

^{13}C NMR (101 MHz, Chloroform-*d*) δ 152.60, 147.61, 147.43, 129.39, 128.71, 128.06, 126.63, 125.64, 125.19, 124.68, 123.50, 123.27.

^{1}H NMR spectrum of TPAT-BT ($CDCl_3$)

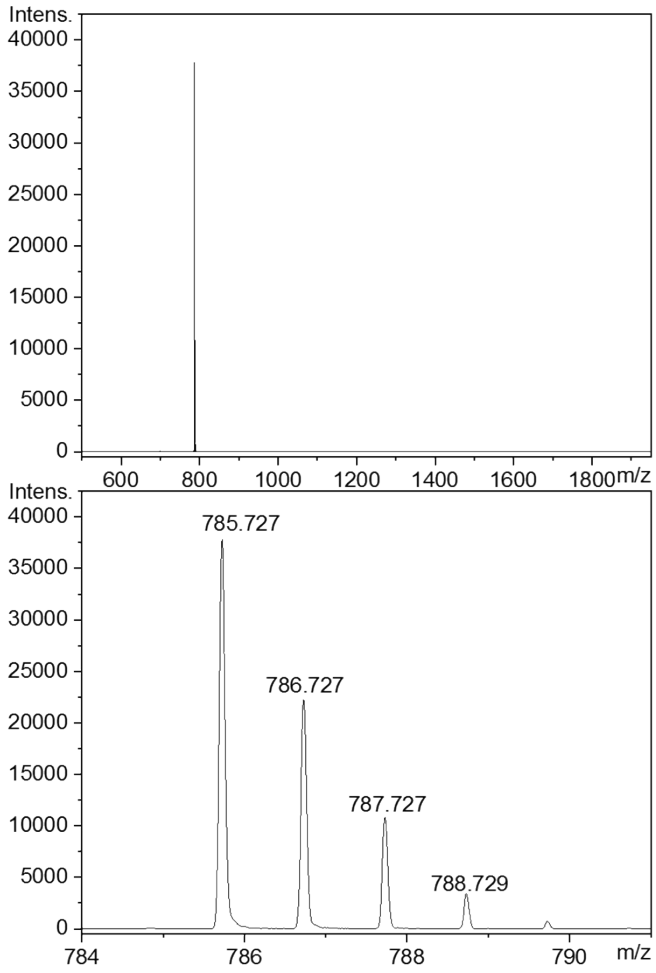

HR-MS spectrum of TPAT-BT

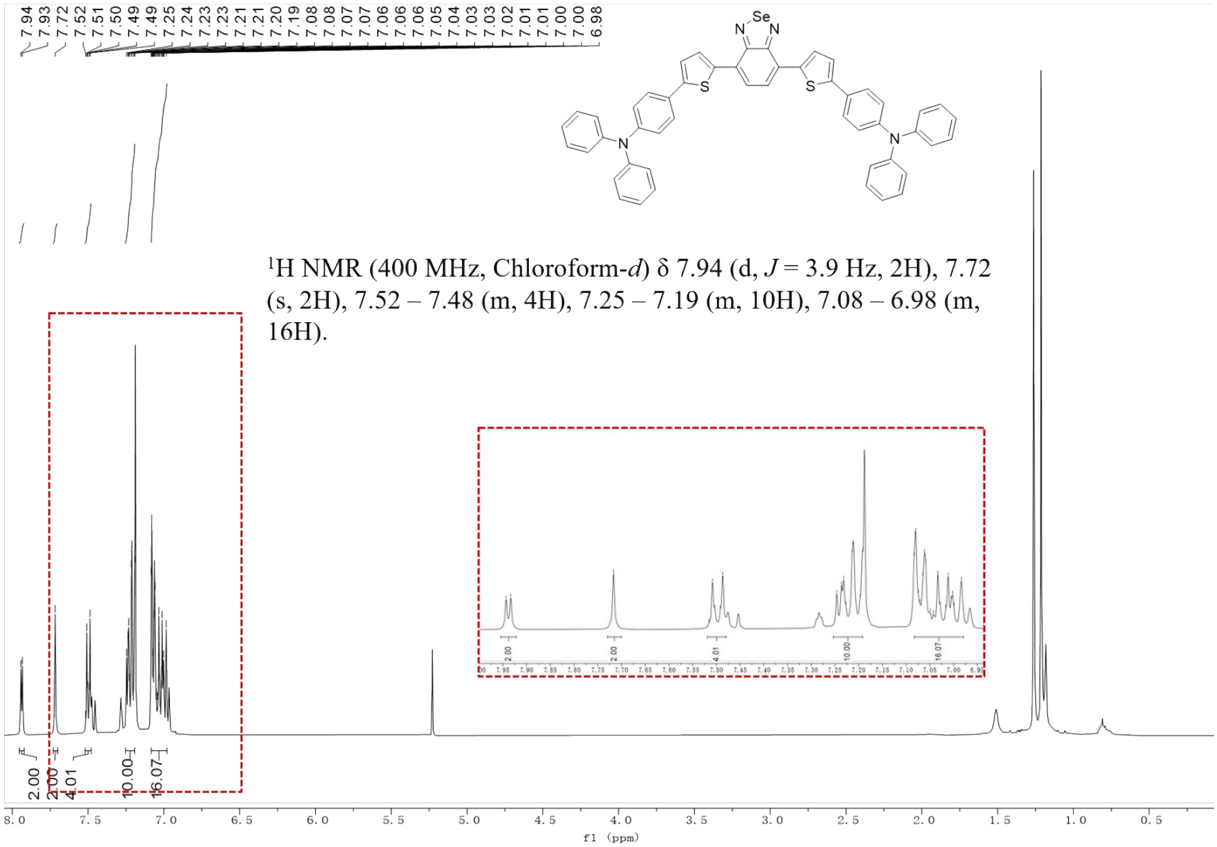

^{1}H NMR spectrum of TPAT-BSeT ($CDCl_3$)

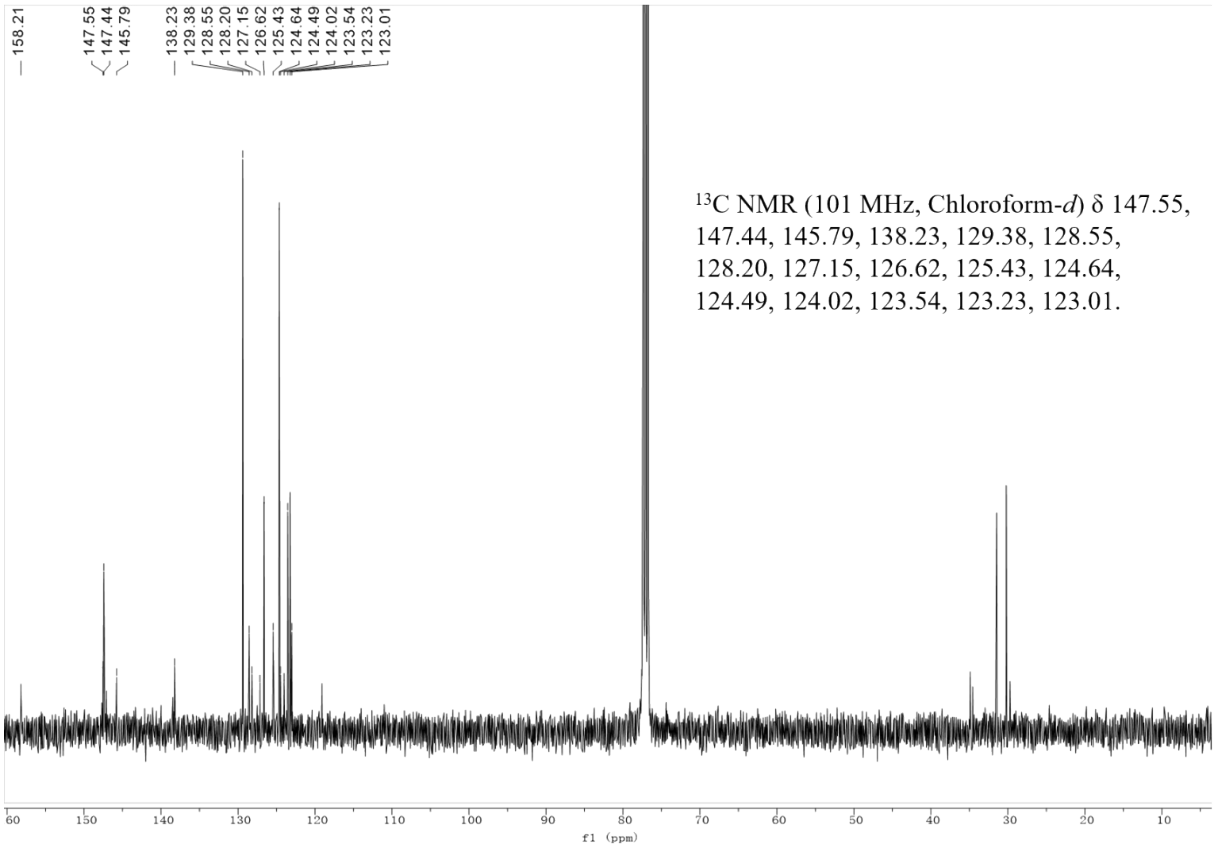

^{13}C NMR spectrum of TPAT-BSeT ($CDCl_3$)

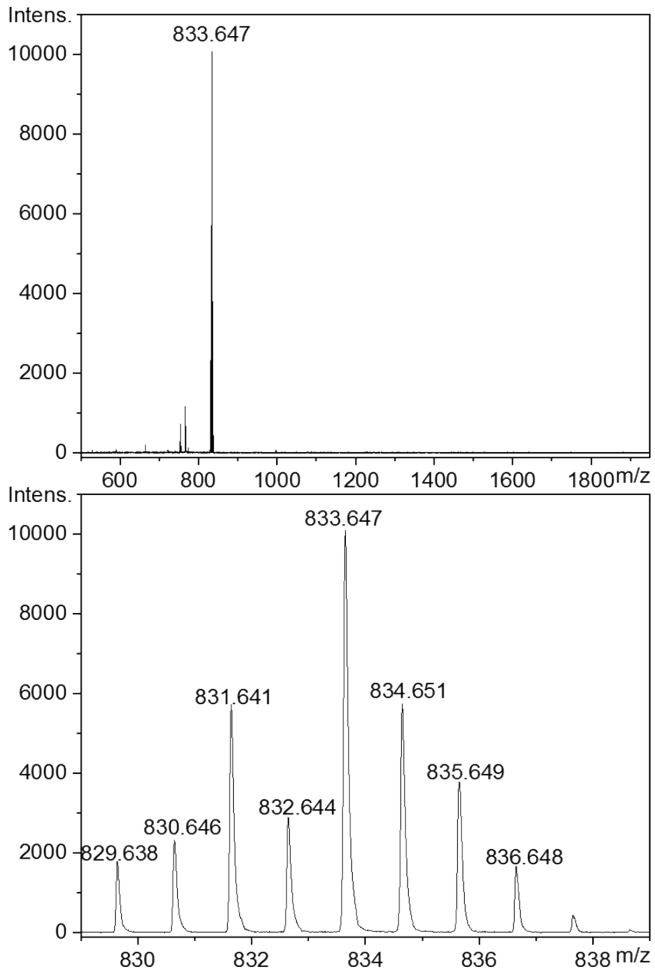

HR-MS spectrum of TPAT-BSeT

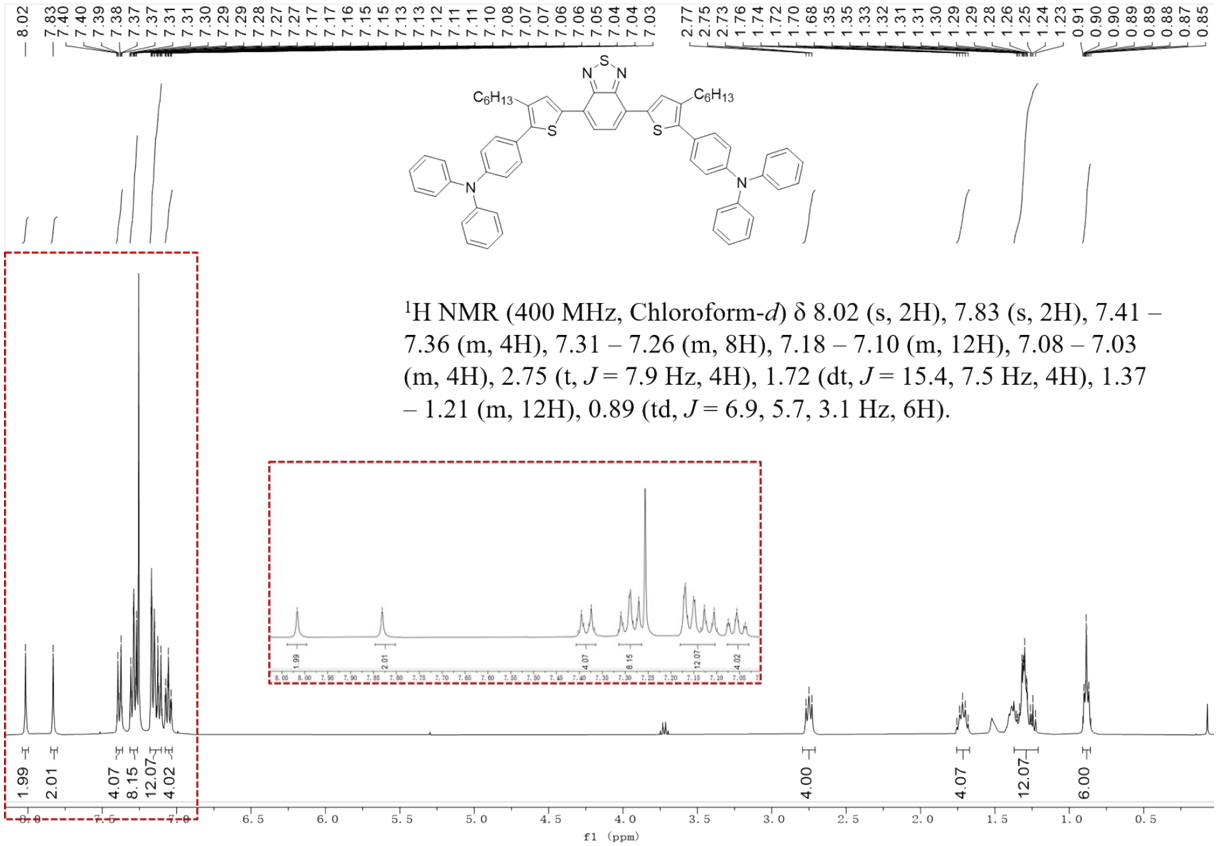

^{1}H NMR (400 MHz, Chloroform-*d*) δ 8.02 (s, 2H), 7.83 (s, 2H), 7.41 – 7.36 (m, 4H), 7.31 – 7.26 (m, 8H), 7.18 – 7.10 (m, 12H), 7.08 – 7.03 (m, 4H), 2.75 (t, *J* = 7.9 Hz, 4H), 1.72 (dt, *J* = 15.4, 7.5 Hz, 4H), 1.37 – 1.21 (m, 12H), 0.89 (td, *J* = 6.9, 5.7, 3.1 Hz, 6H).

^{1}H NMR spectrum of TPAHT-BT ($CDCl_3$)

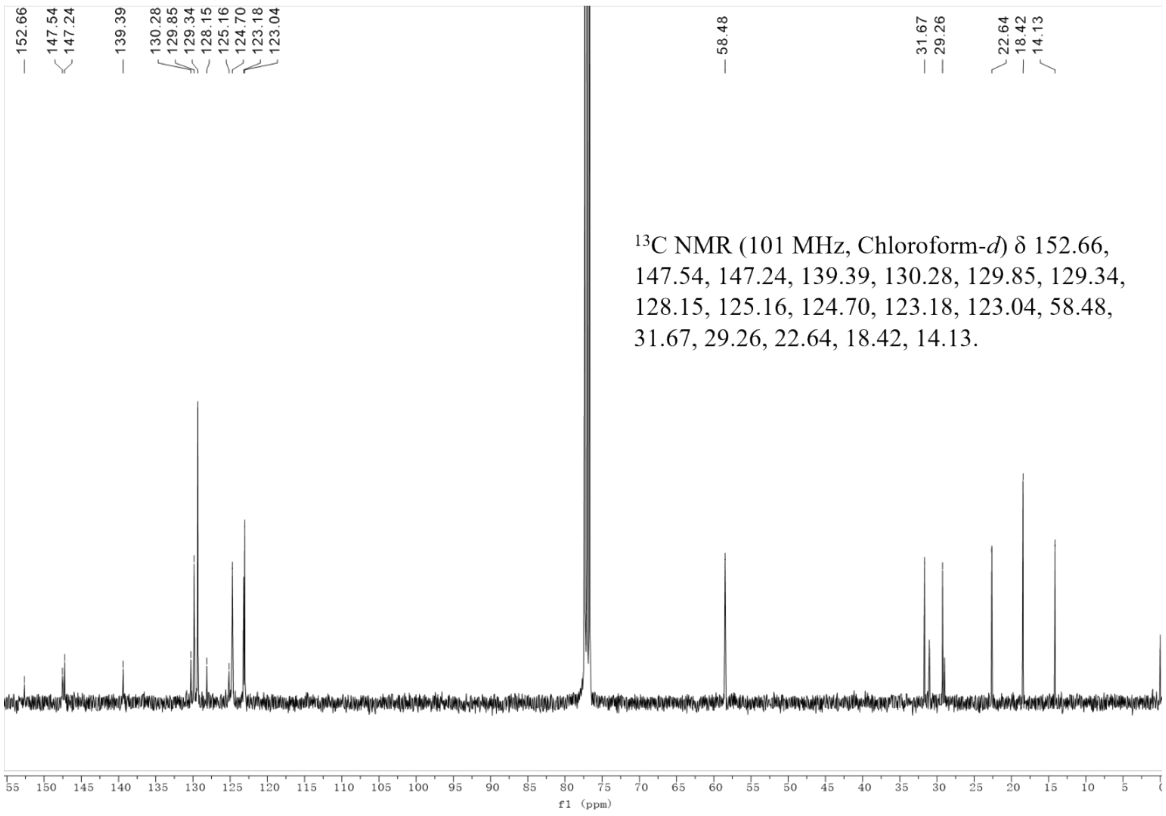

^{13}C NMR (101 MHz, Chloroform-*d*) δ 152.66, 147.54, 147.24, 139.39, 130.28, 129.85, 129.34, 128.15, 125.16, 124.70, 123.18, 123.04, 58.48, 31.67, 29.26, 22.64, 18.42, 14.13.

^{13}C NMR spectrum of TPAHT-BT ($CDCl_3$)

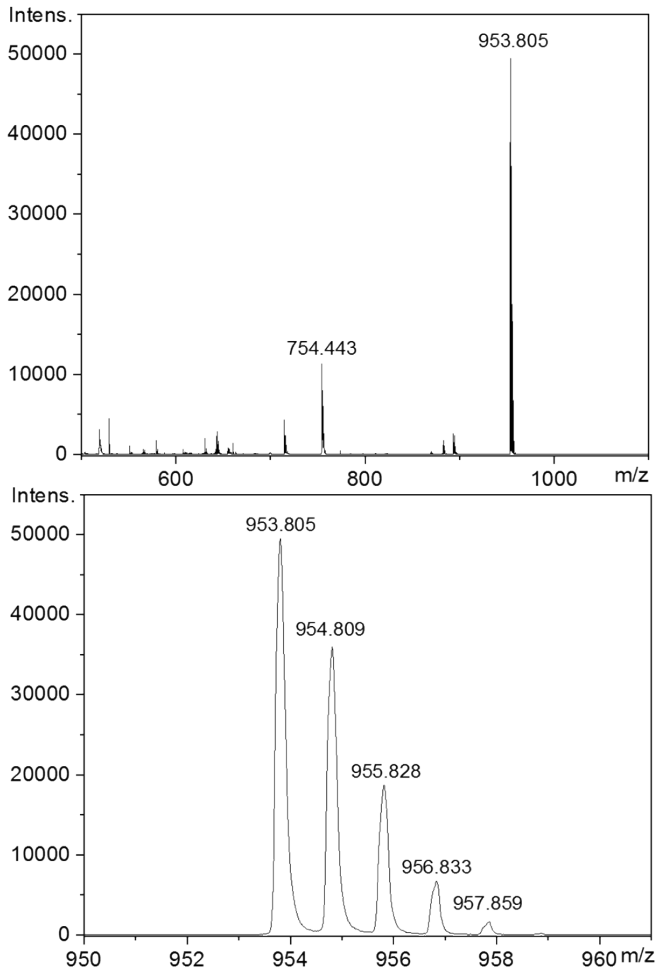

HR-MS spectrum of TPAHT-BT

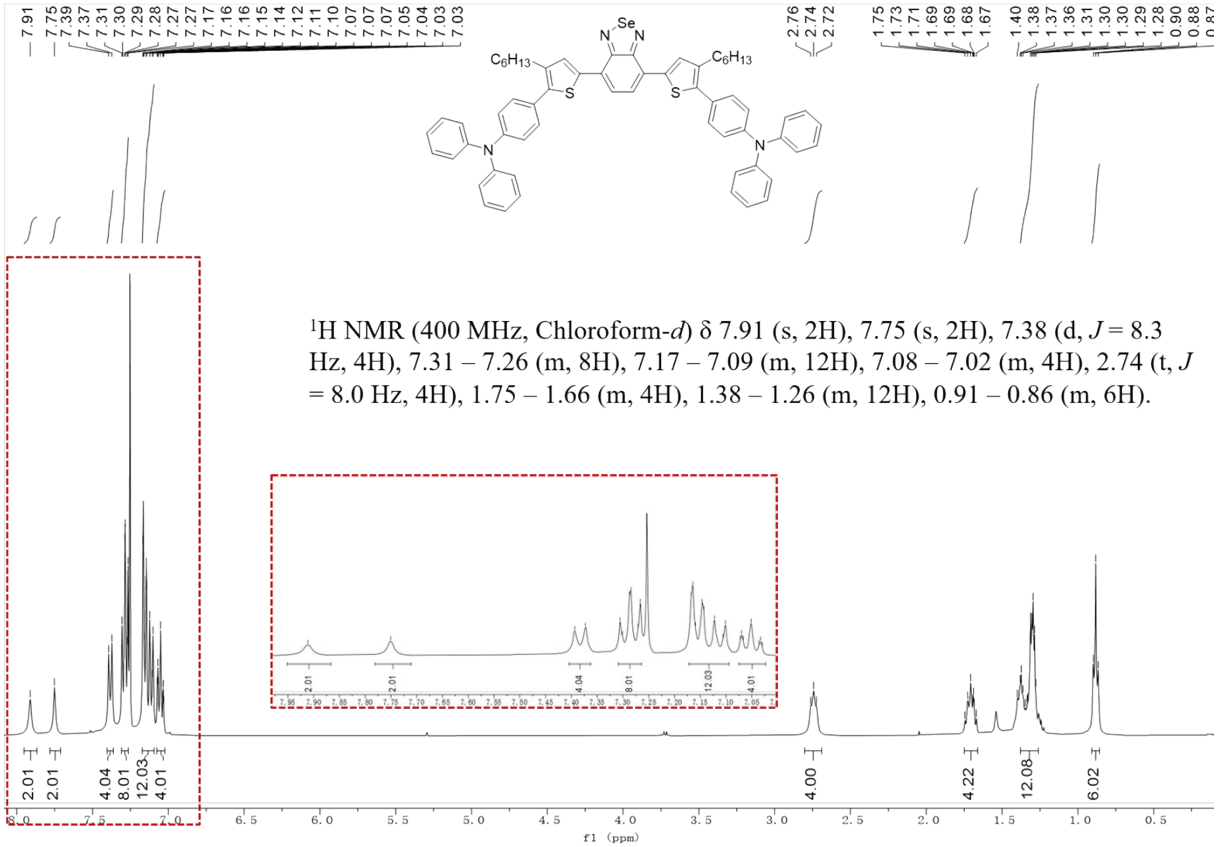

^{1}H NMR (400 MHz, Chloroform-*d*) δ 7.91 (s, 2H), 7.75 (s, 2H), 7.38 (d, *J* = 8.3 Hz, 4H), 7.31 – 7.26 (m, 8H), 7.17 – 7.09 (m, 12H), 7.08 – 7.02 (m, 4H), 2.74 (t, *J* = 8.0 Hz, 4H), 1.75 – 1.66 (m, 4H), 1.38 – 1.26 (m, 12H), 0.91 – 0.86 (m, 6H).

^{1}H NMR spectrum of TPAHT-BSeT ($CDCl_3$)

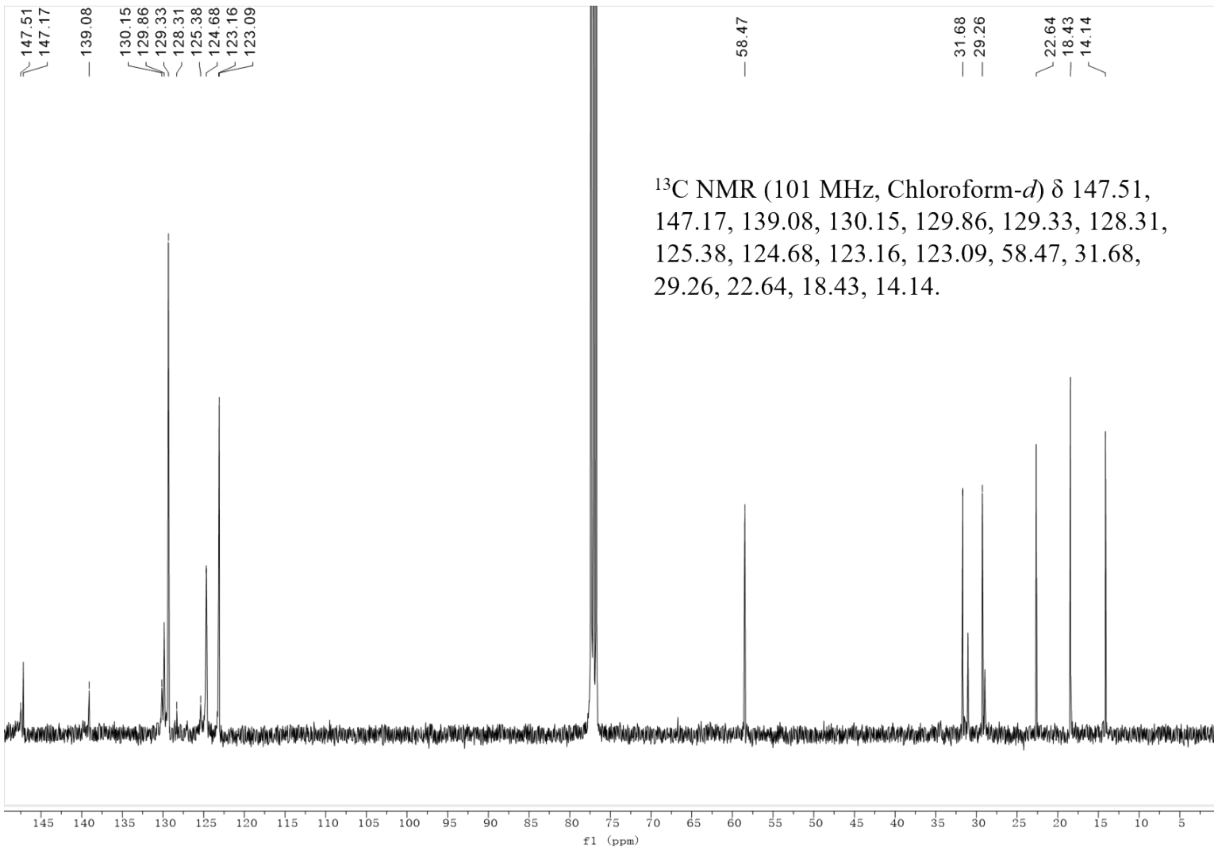

^{13}C NMR (101 MHz, Chloroform-*d*) δ 147.51, 147.17, 139.08, 130.15, 129.86, 129.33, 128.31, 125.38, 124.68, 123.16, 123.09, 58.47, 31.68, 29.26, 22.64, 18.43, 14.14.

^{13}C NMR spectrum of TPAHT-BSeT ($CDCl_3$)

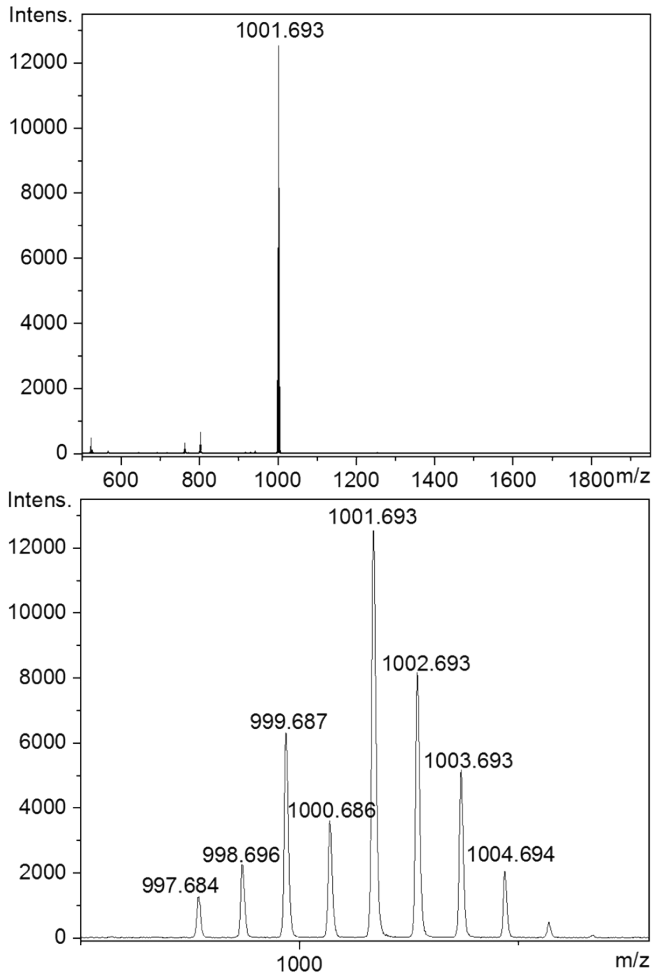

HR-MS spectrum of TPAHT-BSeT

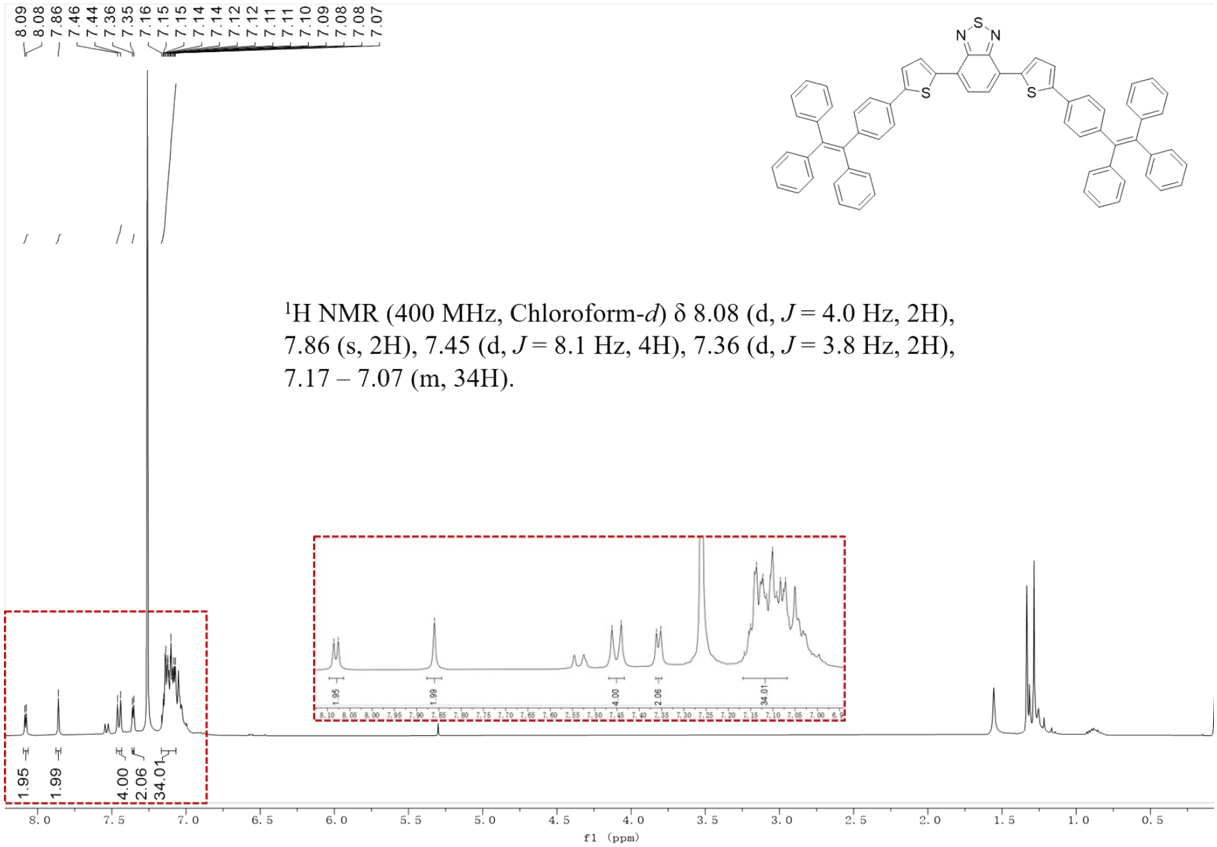

^{1}H NMR spectrum of TPET-BT ($CDCl_3$)

N.D. (Due to the limited solubility of TPET-BT in these deuterium reagent including $CDCl_3$, DMSO-d_6, benze-d_6 and toluene-d_8, the ^{13}C NMR spectrum of TPET-BT was not determined)

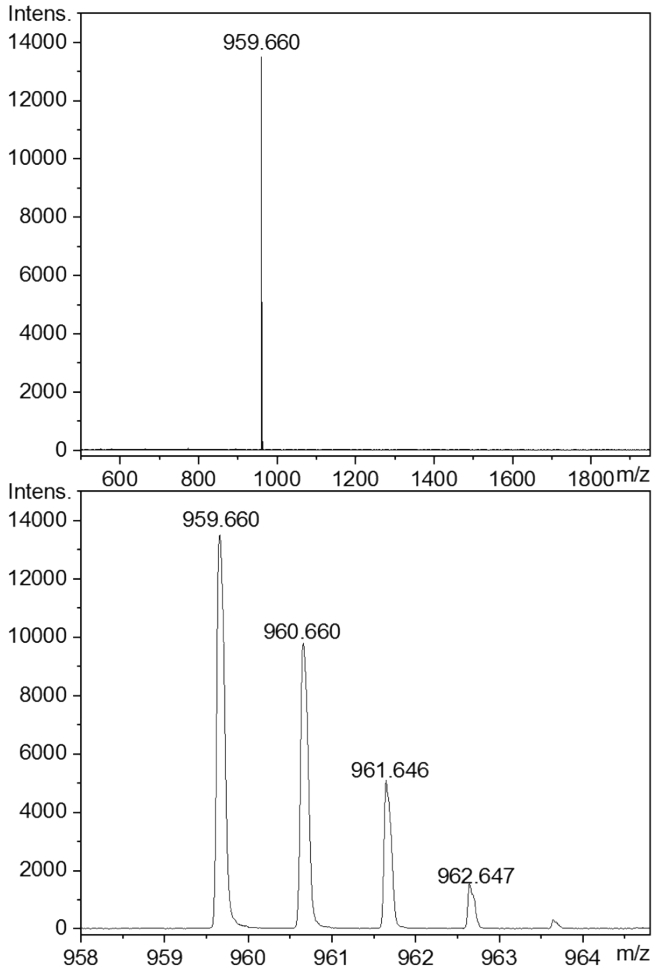

HR-MS spectrum of TPET-BT

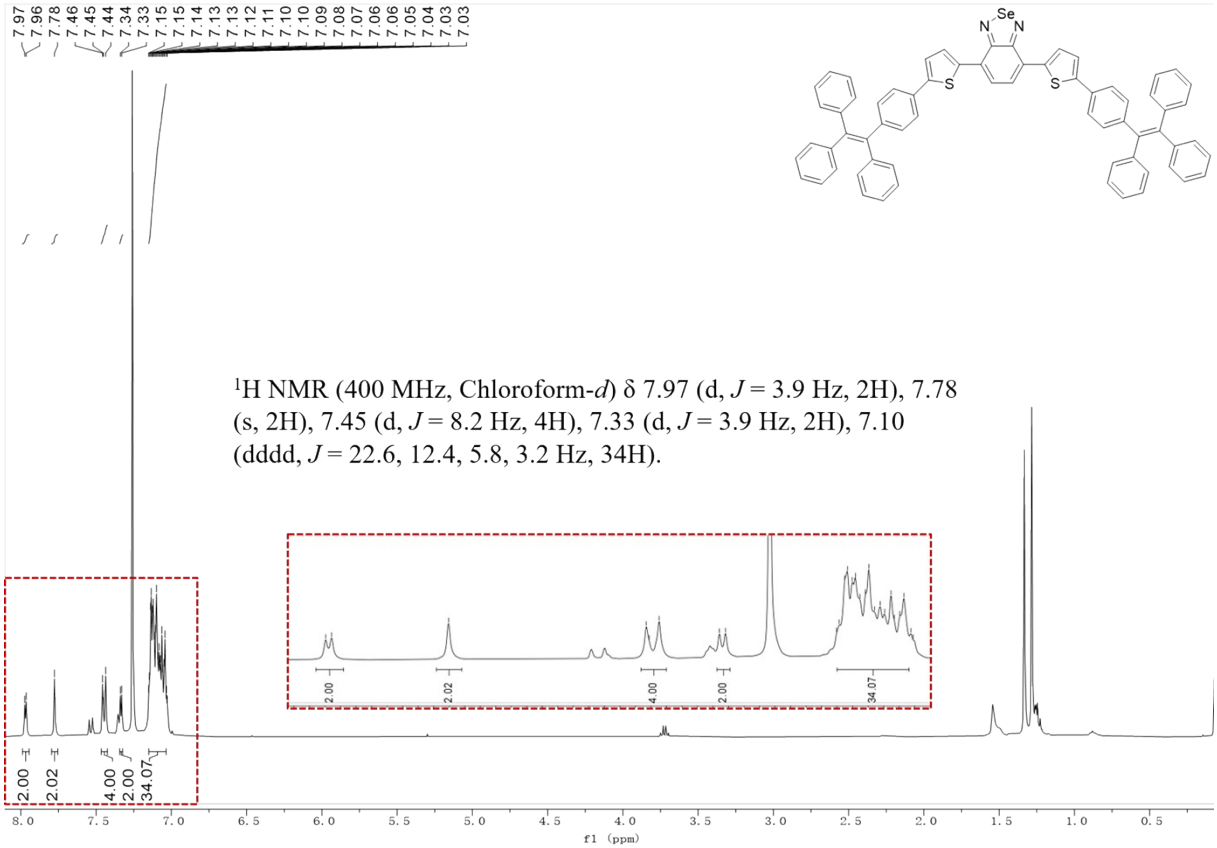

[1]H NMR spectrum of TPET-BSeT ($CDCl_3$)

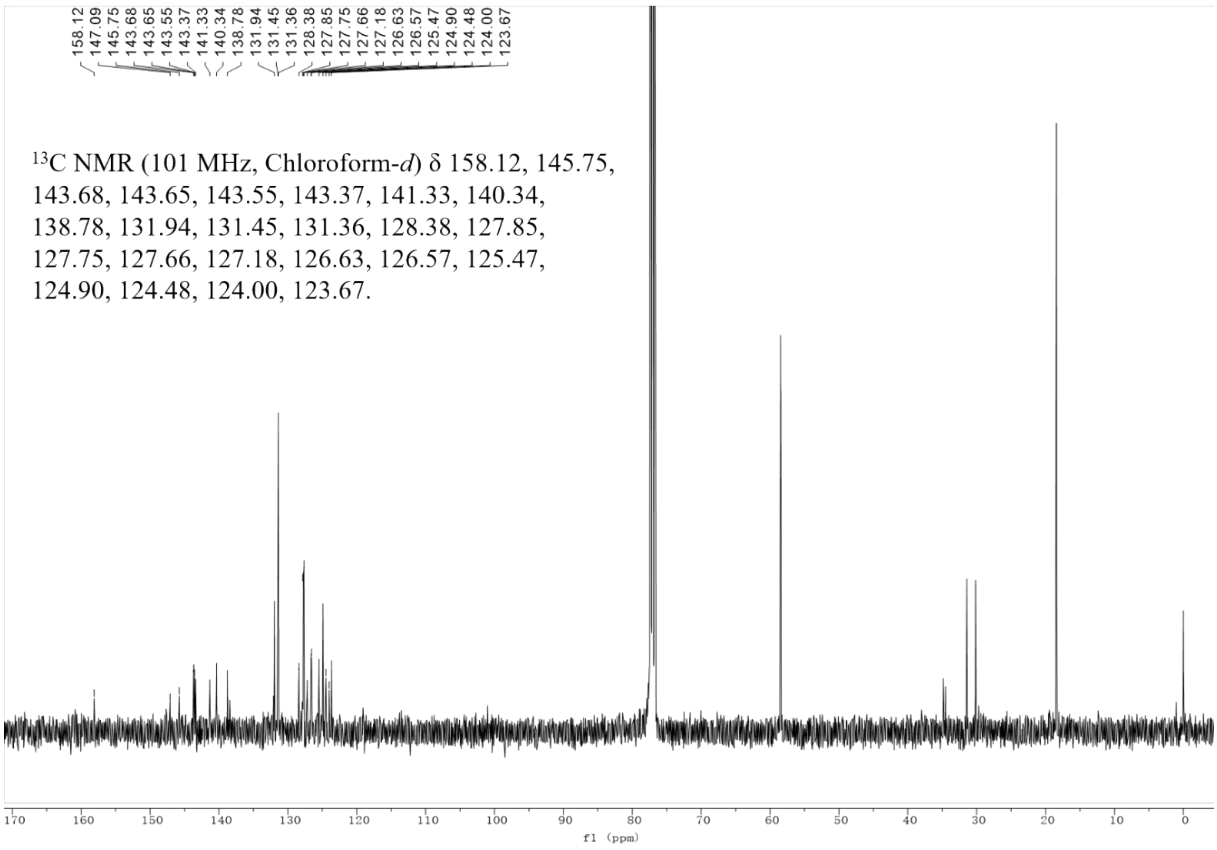

[13]C NMR spectrum of TPET-BSeT ($CDCl_3$)

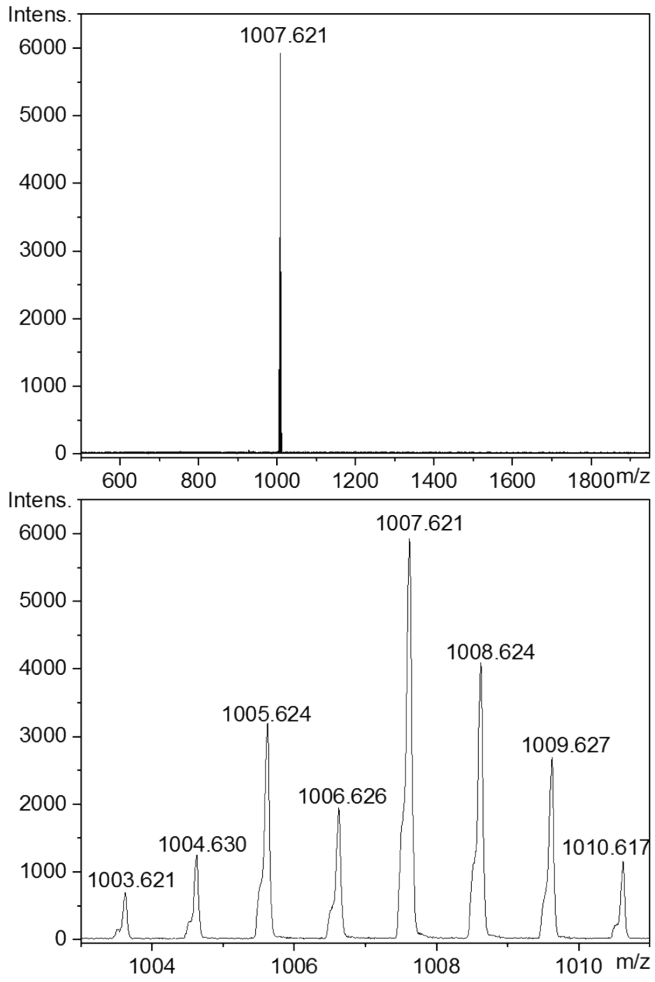

HR-MS spectrum of TPET-BSeT

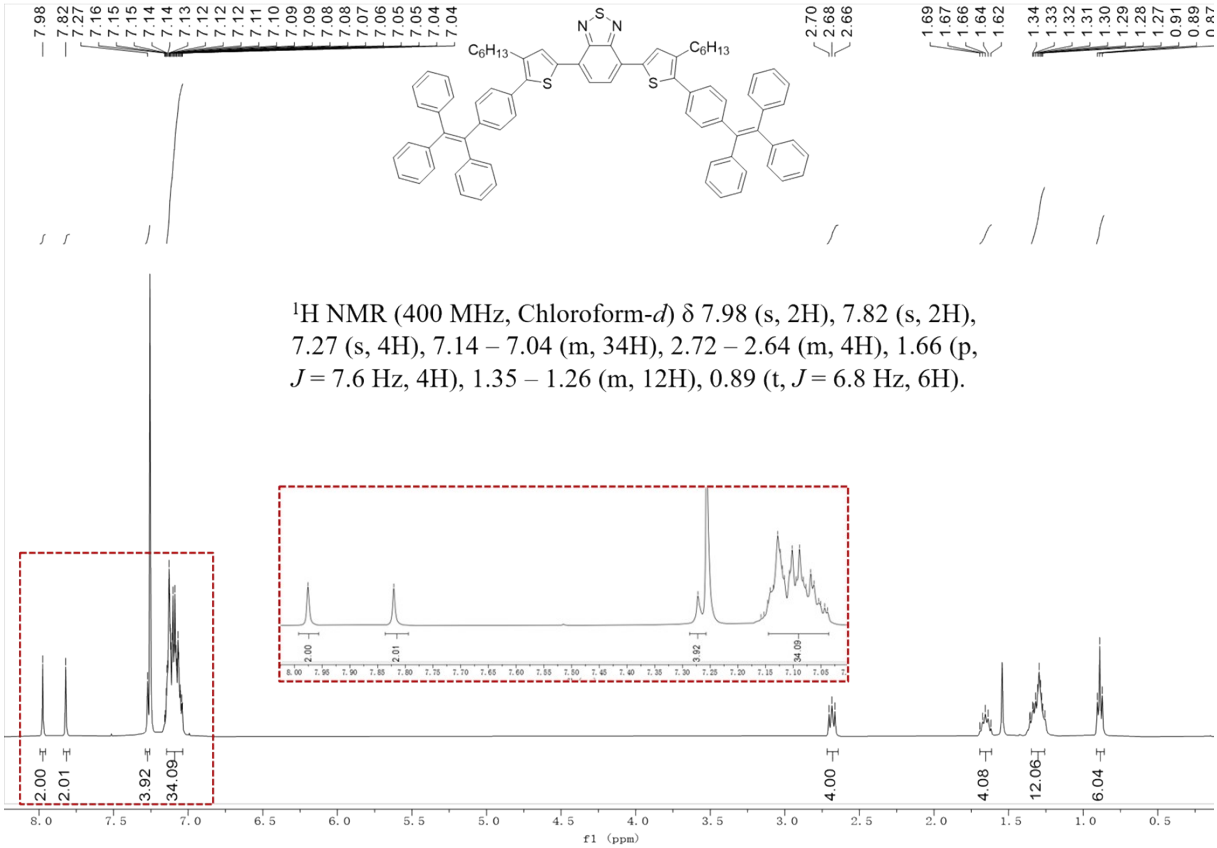

^{1}H NMR (400 MHz, Chloroform-*d*) δ 7.98 (s, 2H), 7.82 (s, 2H), 7.27 (s, 4H), 7.14 – 7.04 (m, 34H), 2.72 – 2.64 (m, 4H), 1.66 (p, *J* = 7.6 Hz, 4H), 1.35 – 1.26 (m, 12H), 0.89 (t, *J* = 6.8 Hz, 6H).

^{1}H NMR spectrum of TPEHT-BT ($CDCl_3$)

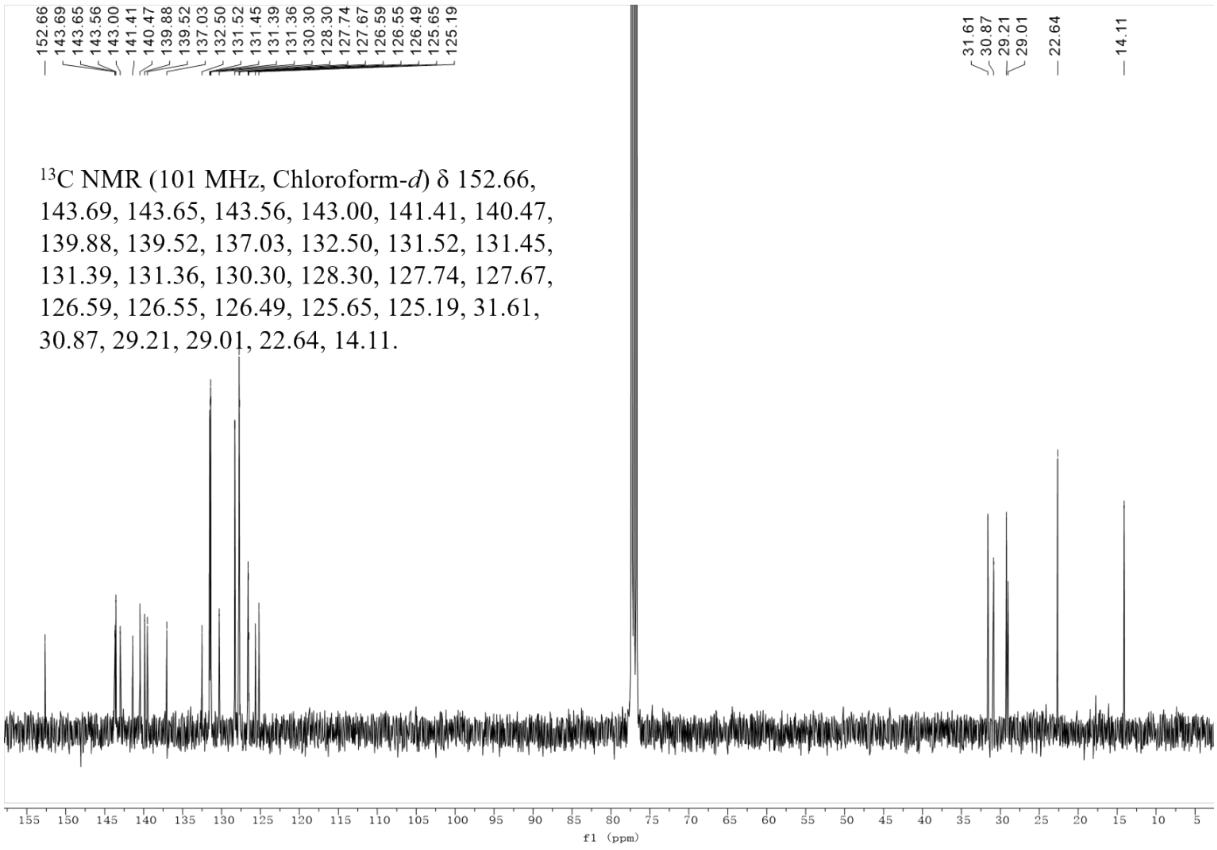

^{13}C NMR (101 MHz, Chloroform-*d*) δ 152.66, 143.69, 143.65, 143.56, 143.00, 141.41, 140.47, 139.88, 139.52, 137.03, 132.50, 131.52, 131.45, 131.39, 131.36, 130.30, 128.30, 127.74, 127.67, 126.59, 126.55, 126.49, 125.65, 125.19, 31.61, 30.87, 29.21, 29.01, 22.64, 14.11.

^{13}C NMR spectrum of TPEHT-BT ($CDCl_3$)

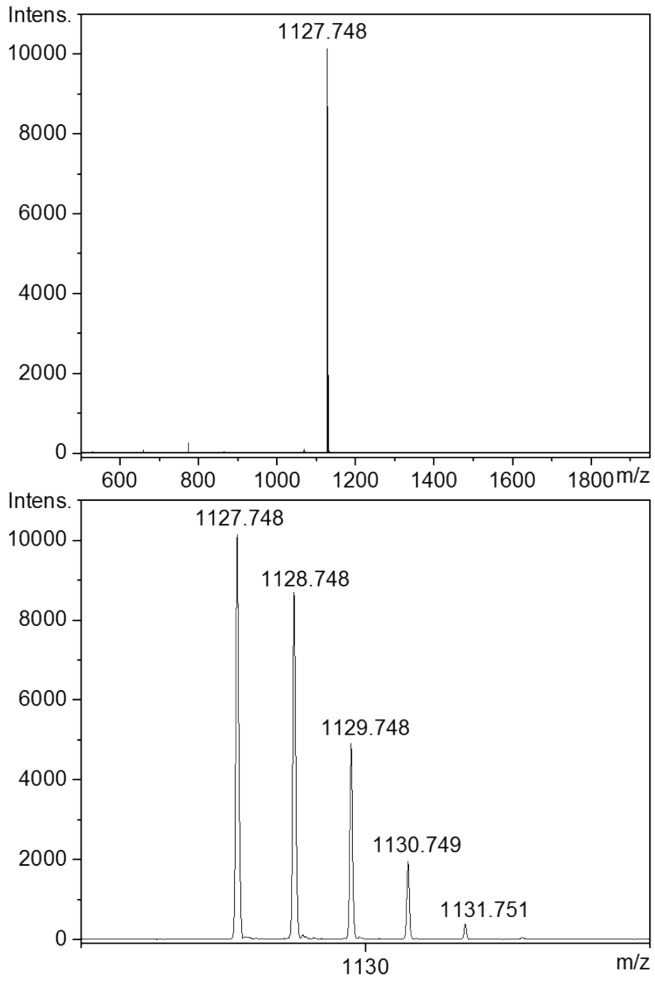

HR-MS spectrum of TPEHT-BT

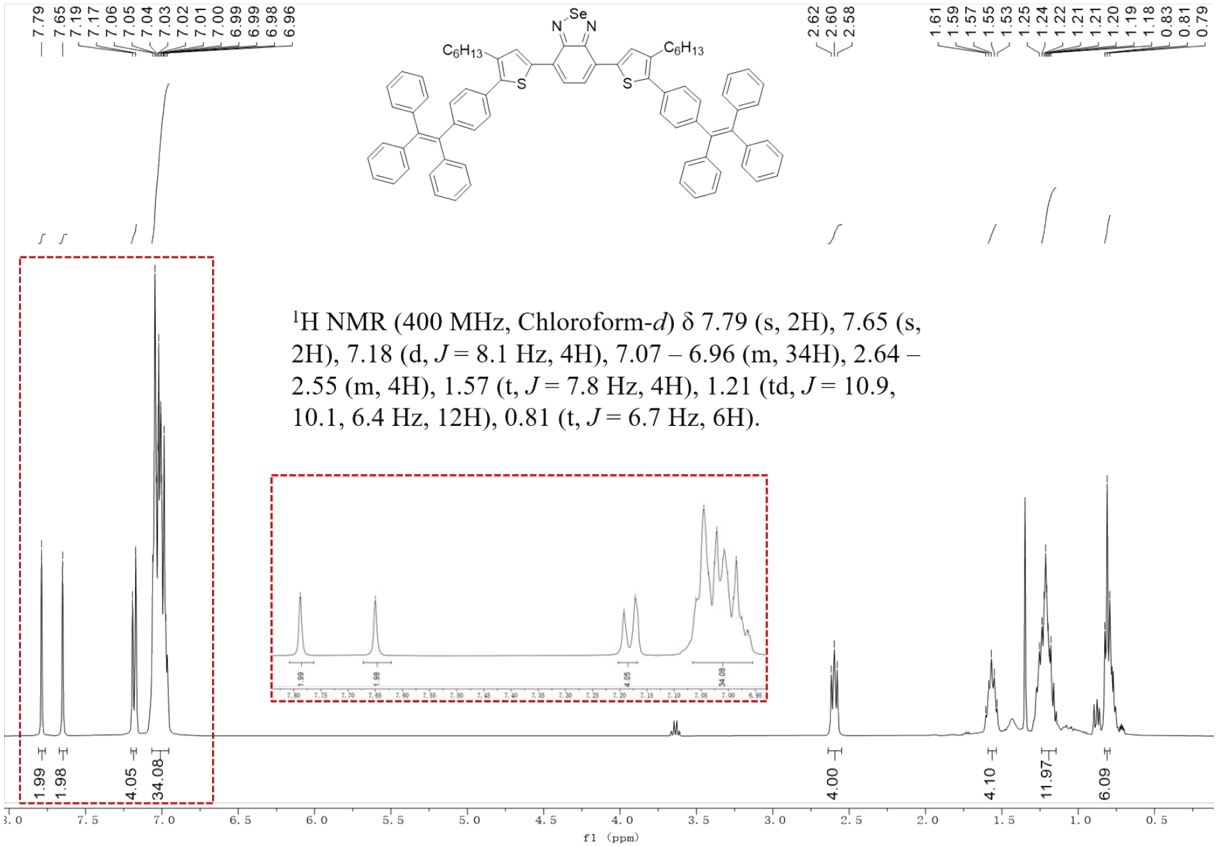

^{1}H NMR spectrum of TPEHT-BSeT ($CDCl_3$)

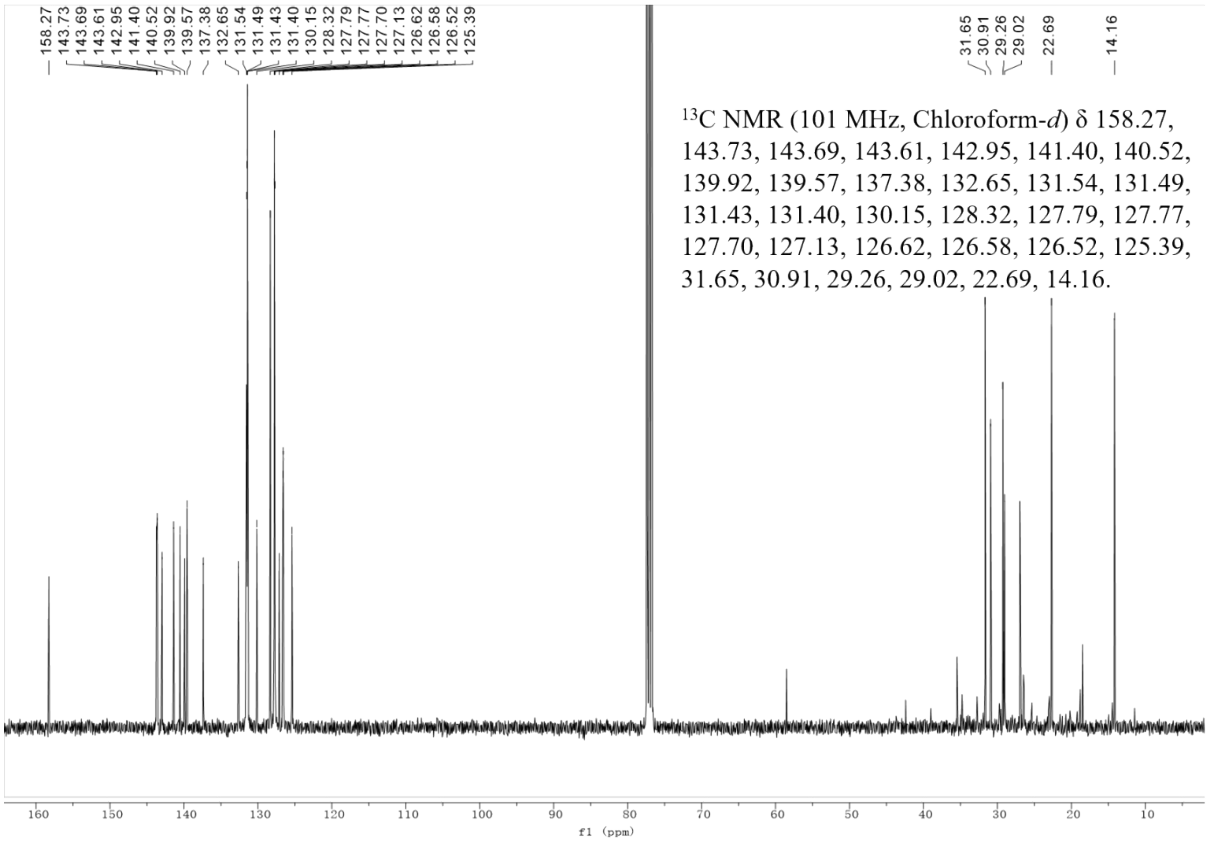

^{13}C NMR spectrum of TPEHT-BSeT ($CDCl_3$)

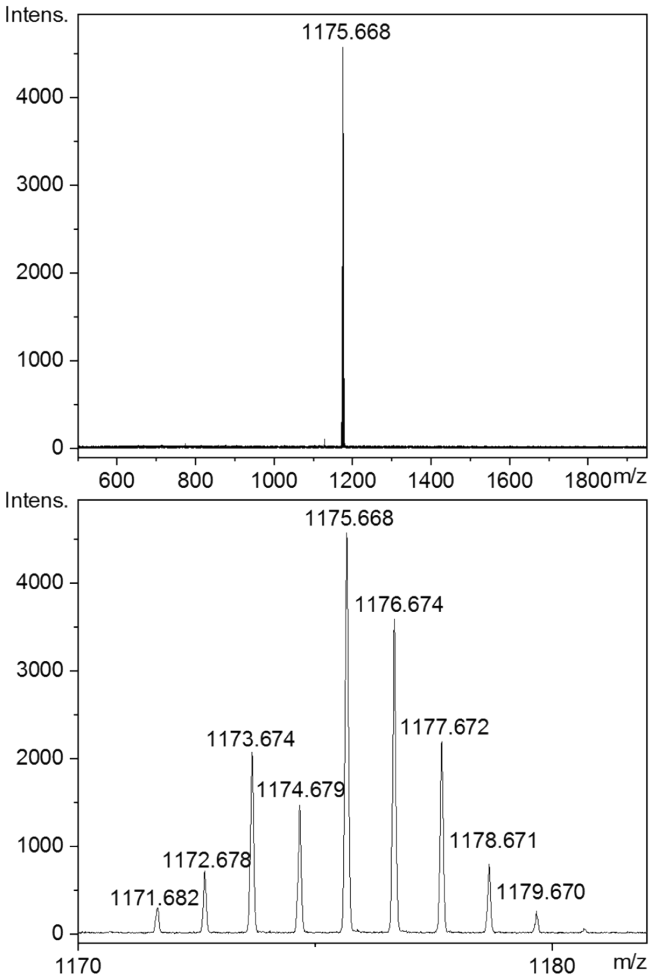

HR-MS spectrum of TPEHT-BSeT

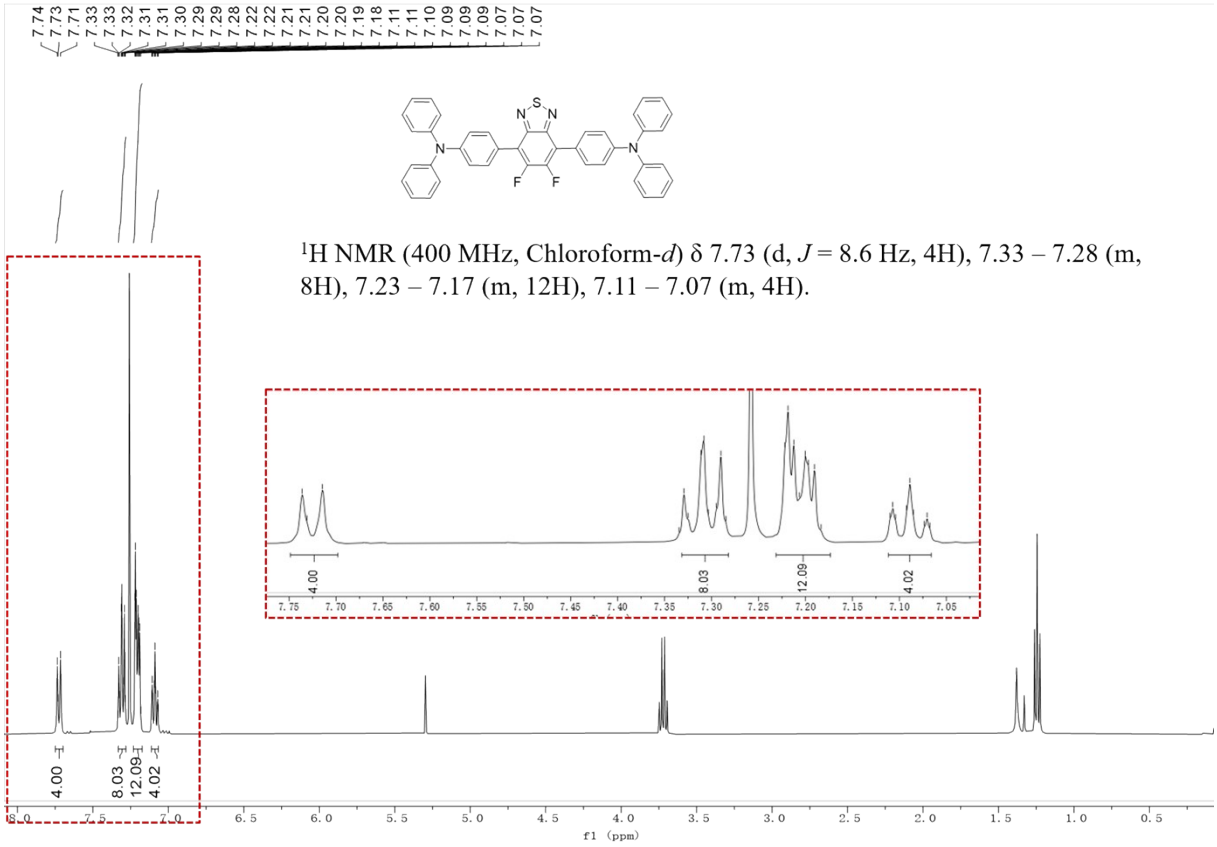

^{1}H NMR (400 MHz, Chloroform-*d*) δ 7.73 (d, *J* = 8.6 Hz, 4H), 7.33 – 7.28 (m, 8H), 7.23 – 7.17 (m, 12H), 7.11 – 7.07 (m, 4H).

^{1}H NMR spectrum of TPA-FBT ($CDCl_3$)

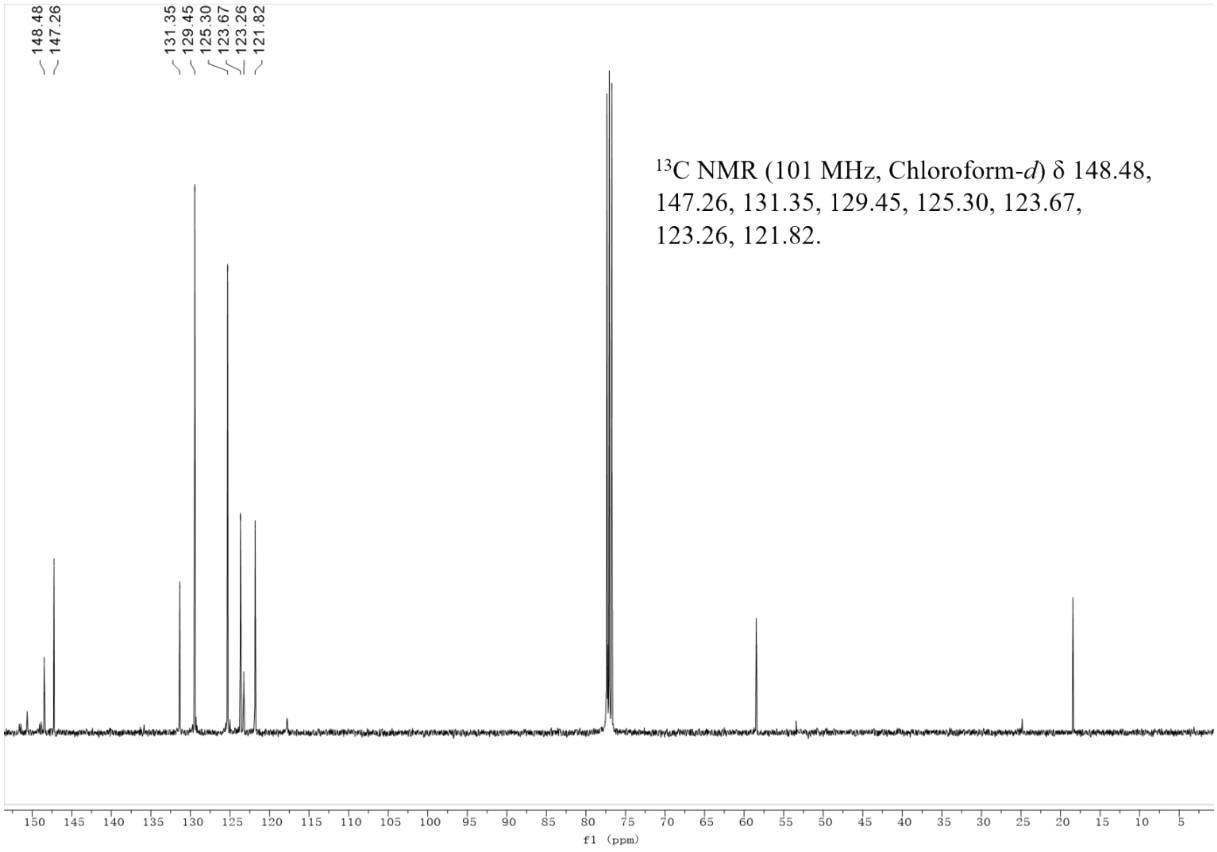

^{13}C NMR (101 MHz, Chloroform-*d*) δ 148.48, 147.26, 131.35, 129.45, 125.30, 123.67, 123.26, 121.82.

^{13}C NMR spectrum of TPA-FBT ($CDCl_3$)

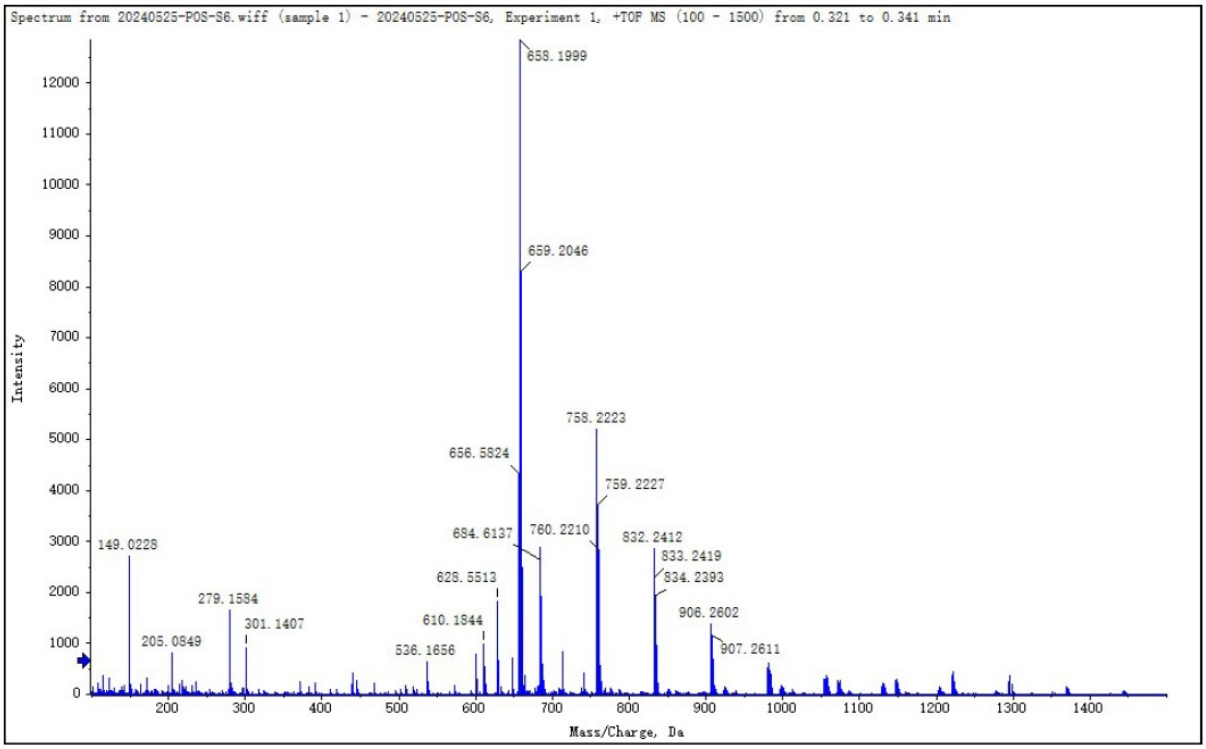

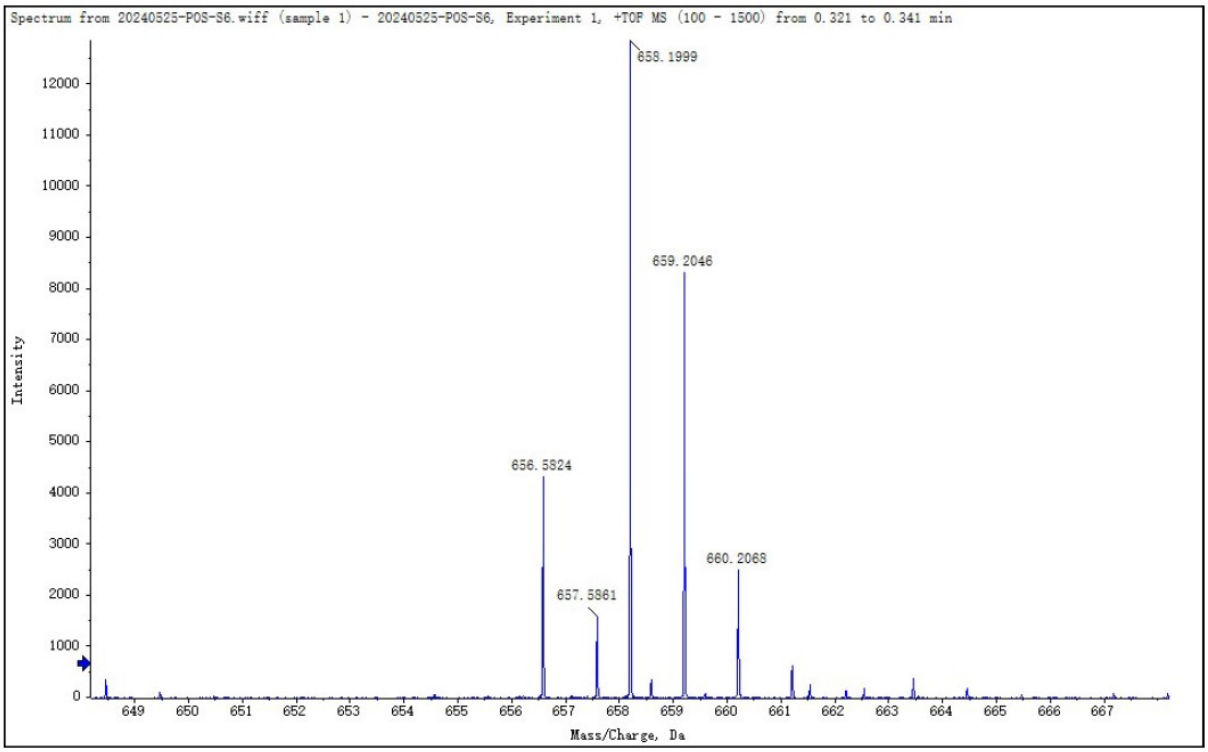

HR-MS spectrum of TPA-FBT

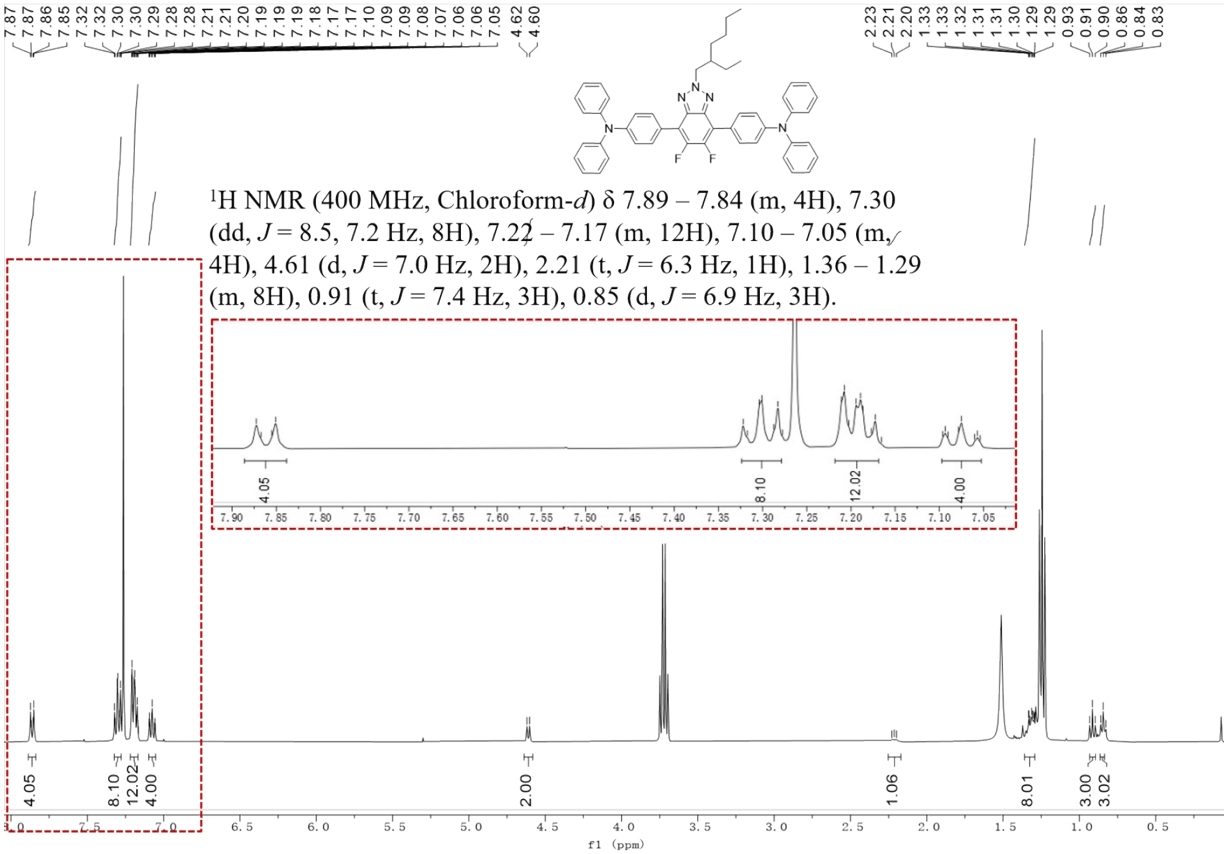

[1]H NMR spectrum of TPA-FBTr ($CDCl_3$)

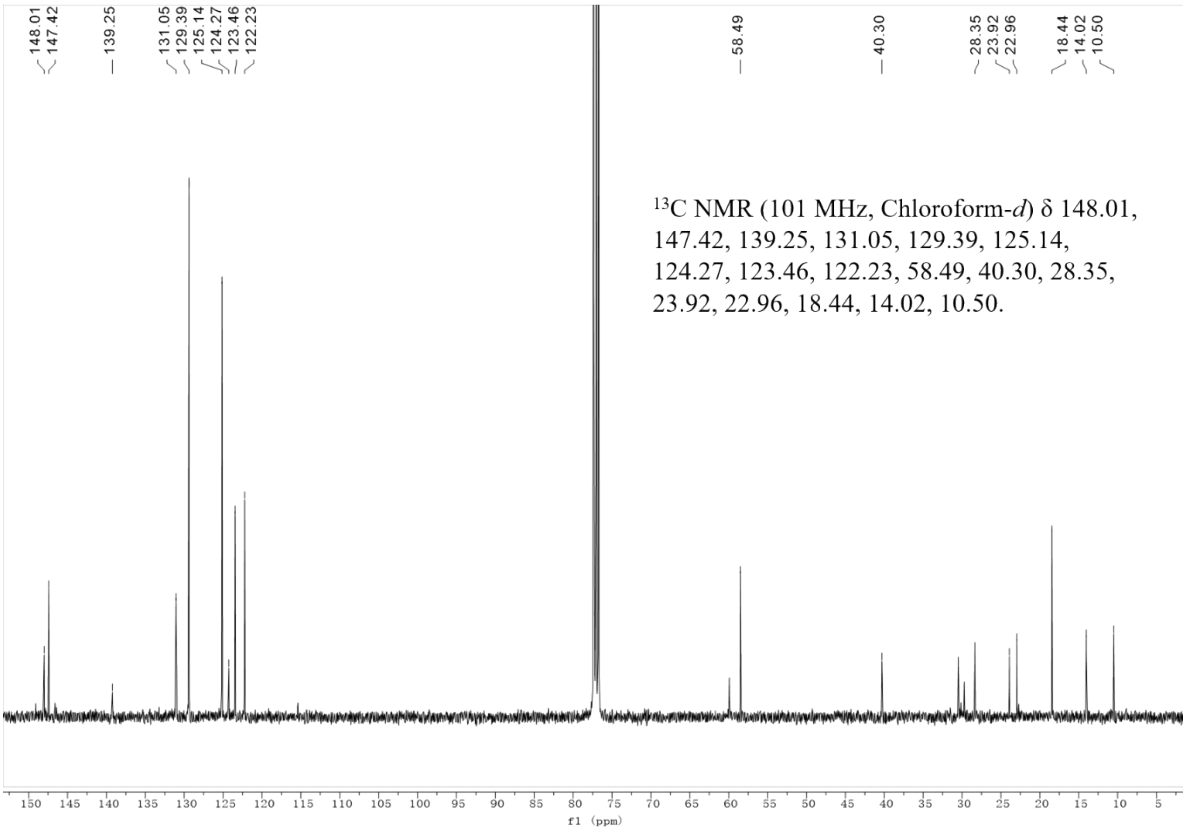

[13]C NMR spectrum of TPA-FBTr ($CDCl_3$)

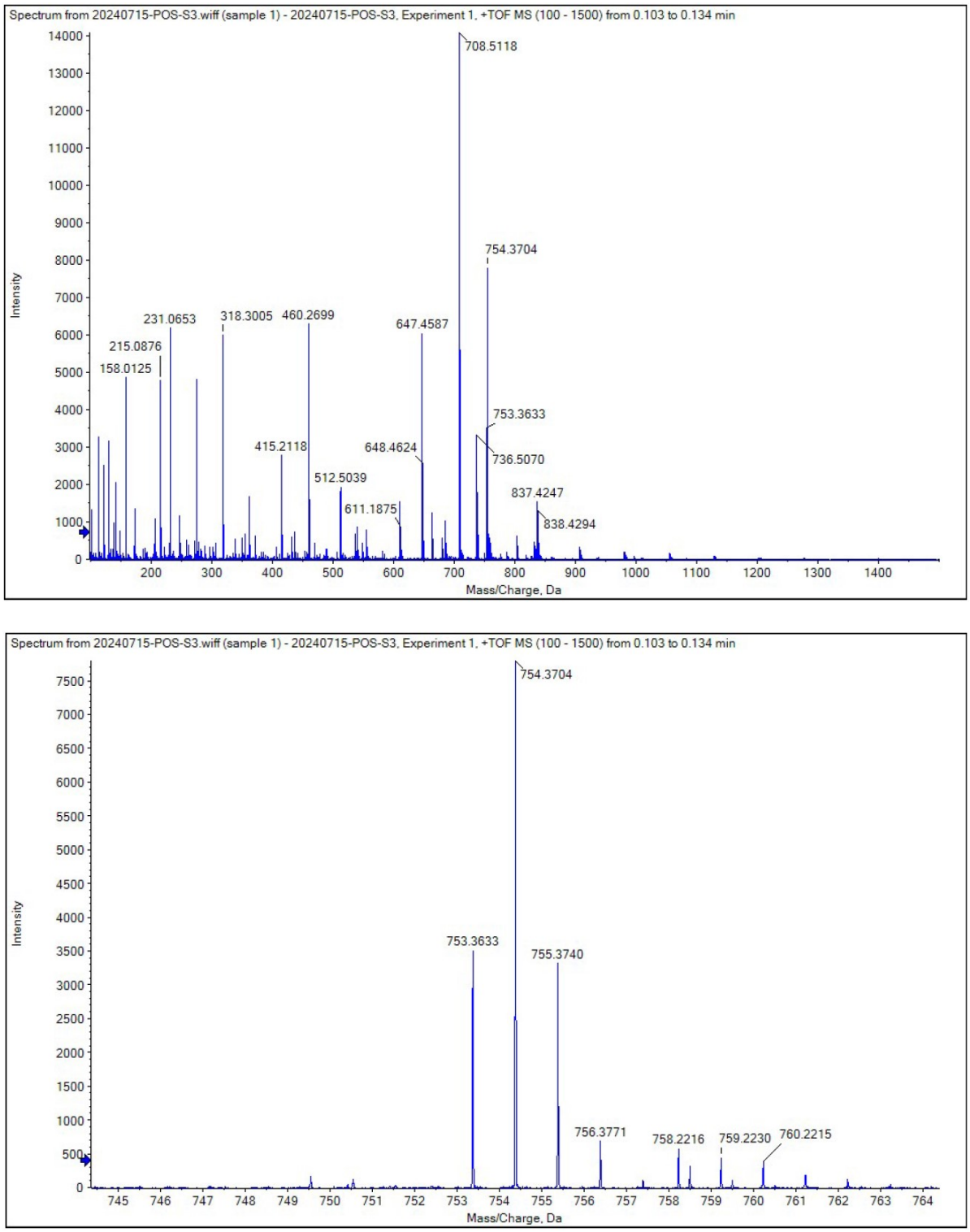

HR-MS spectrum of TPA-FBTr

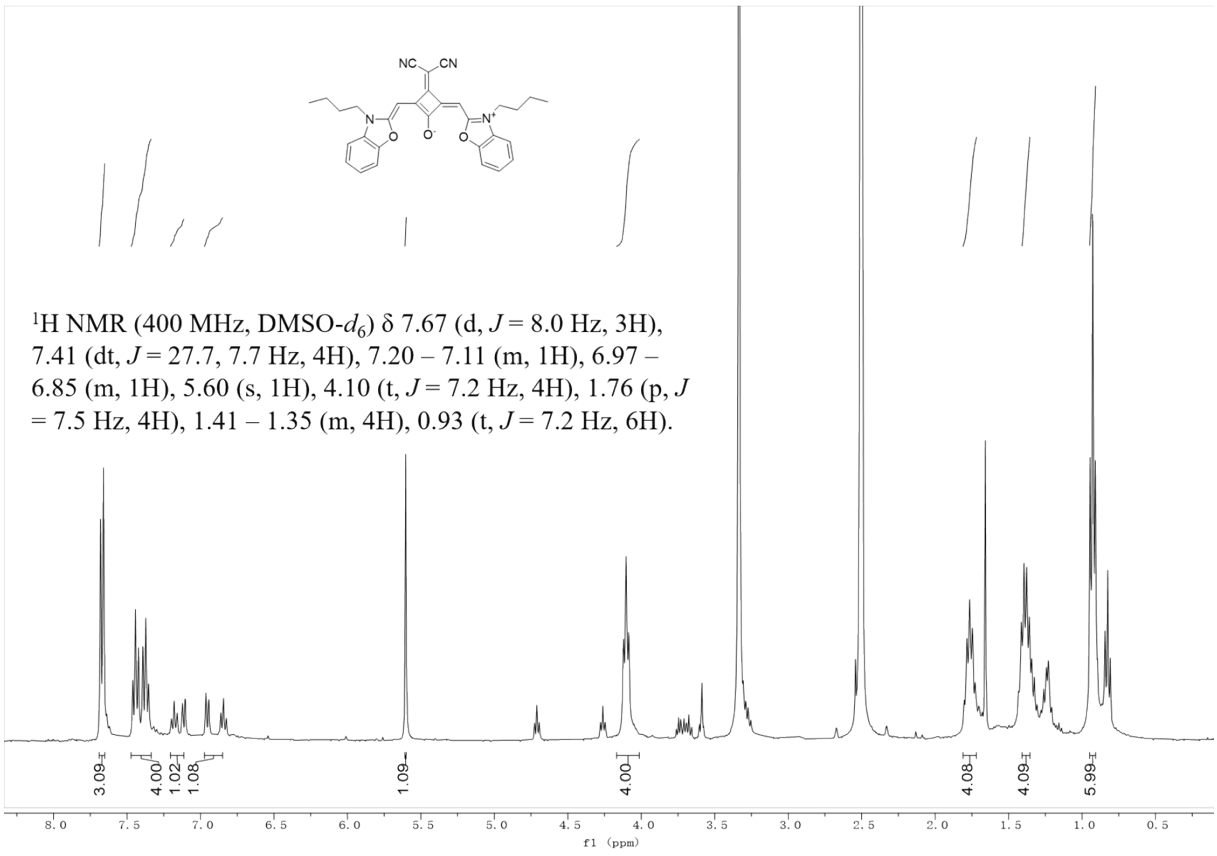

^{1}H NMR (400 MHz, DMSO-d_6) δ 7.67 (d, J = 8.0 Hz, 3H), 7.41 (dt, J = 27.7, 7.7 Hz, 4H), 7.20 – 7.11 (m, 1H), 6.97 – 6.85 (m, 1H), 5.60 (s, 1H), 4.10 (t, J = 7.2 Hz, 4H), 1.76 (p, J = 7.5 Hz, 4H), 1.41 – 1.35 (m, 4H), 0.93 (t, J = 7.2 Hz, 6H).

^{1}H NMR spectrum of SQ650 (DMSO-d_6)

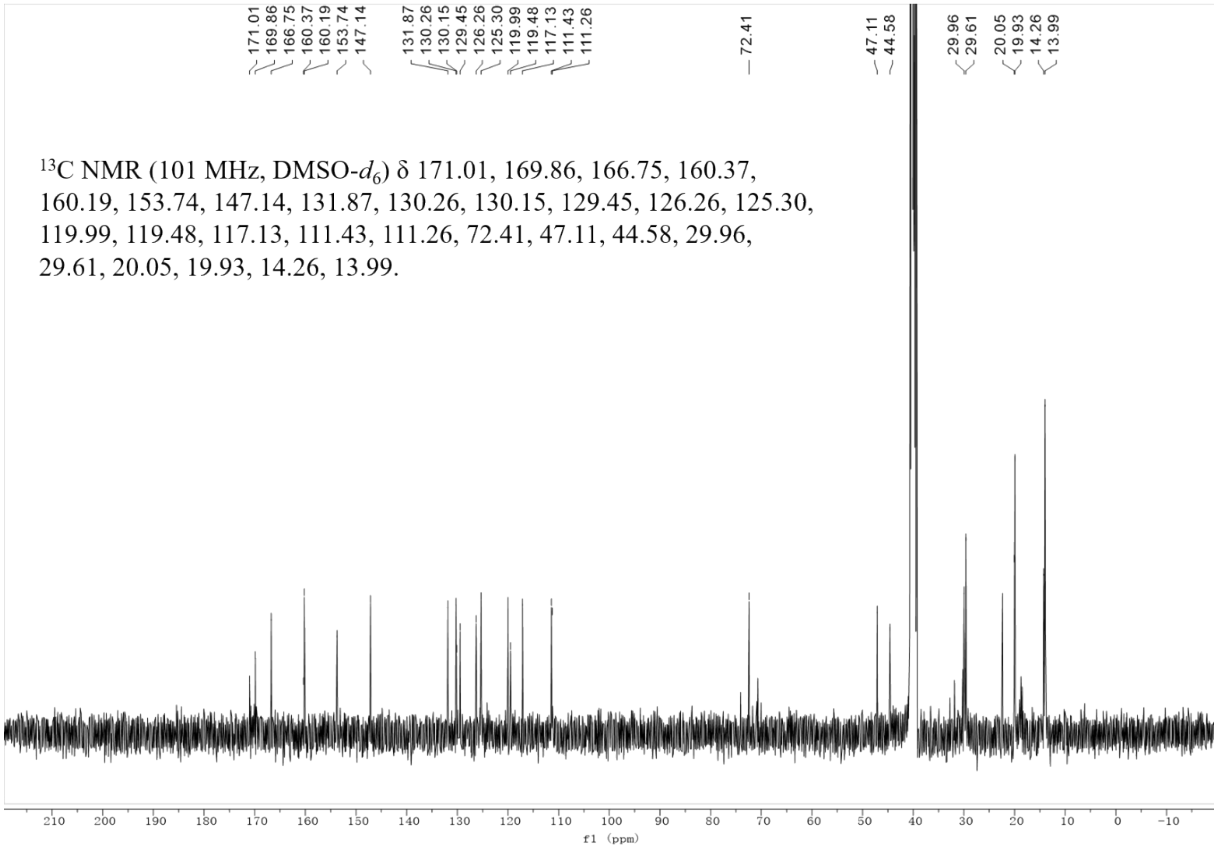

^{13}C NMR (101 MHz, DMSO-d_6) δ 171.01, 169.86, 166.75, 160.37, 160.19, 153.74, 147.14, 131.87, 130.26, 130.15, 129.45, 126.26, 125.30, 119.99, 119.48, 117.13, 111.43, 111.26, 72.41, 47.11, 44.58, 29.96, 29.61, 20.05, 19.93, 14.26, 13.99.

^{13}C NMR spectrum of SQ650 (DMSO-d_6)

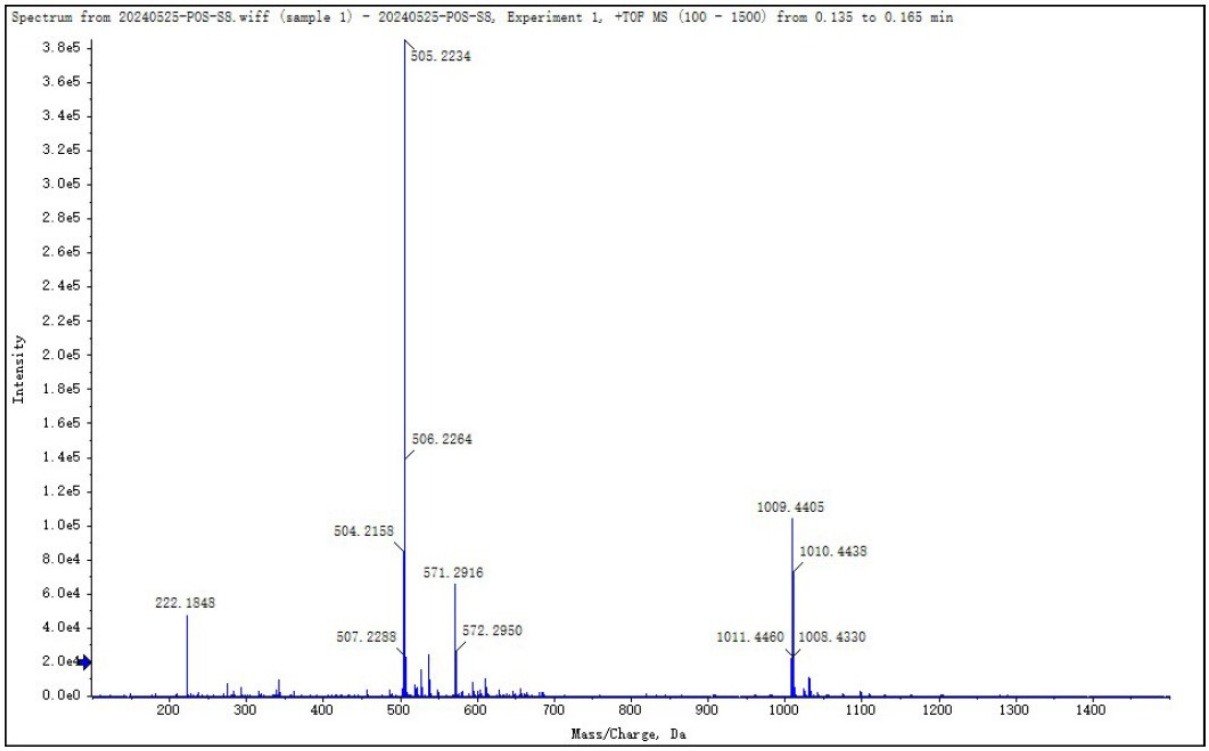

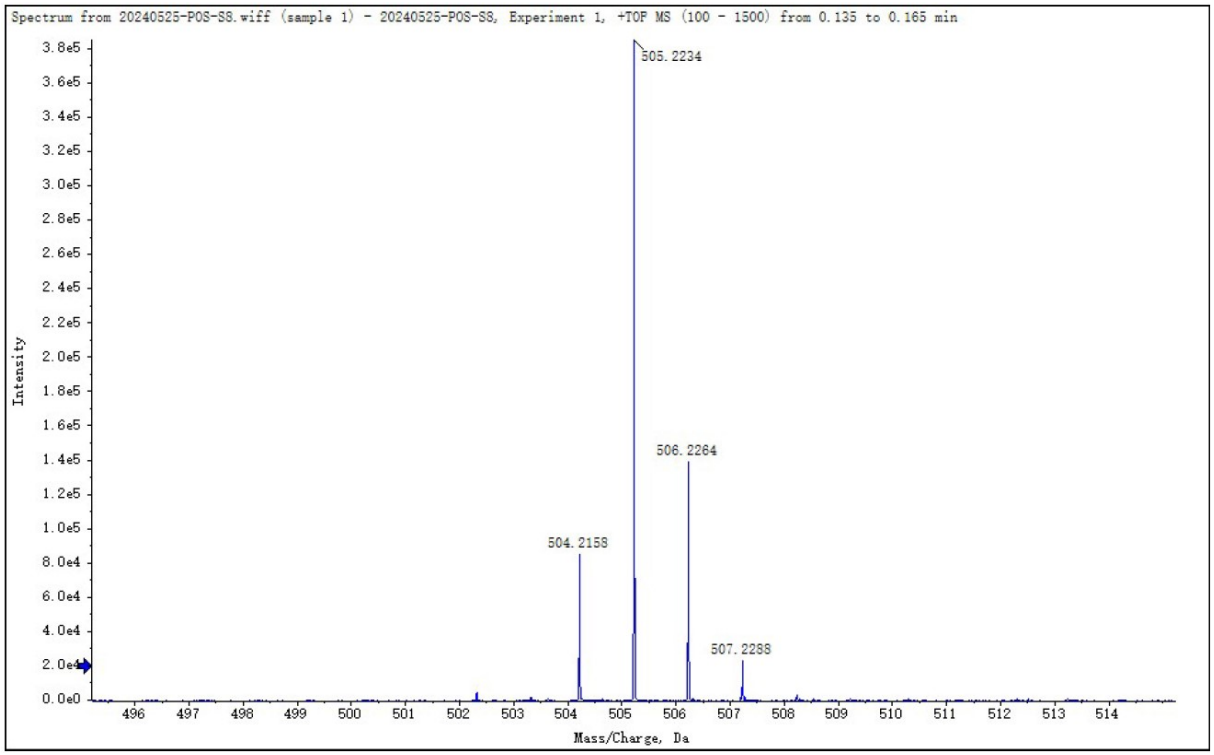

HR-MS spectrum of SQ650

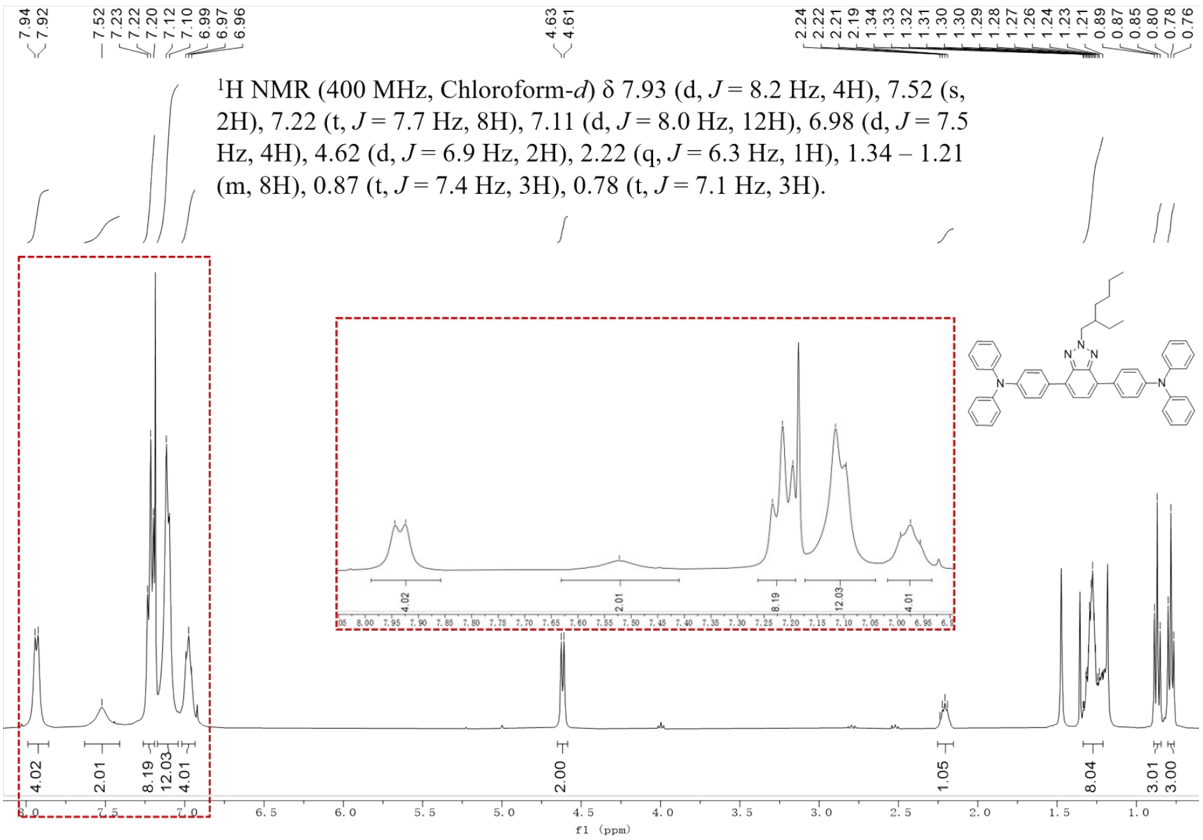

^{1}H NMR spectrum of TPA-BTsr ($CDCl_3$)

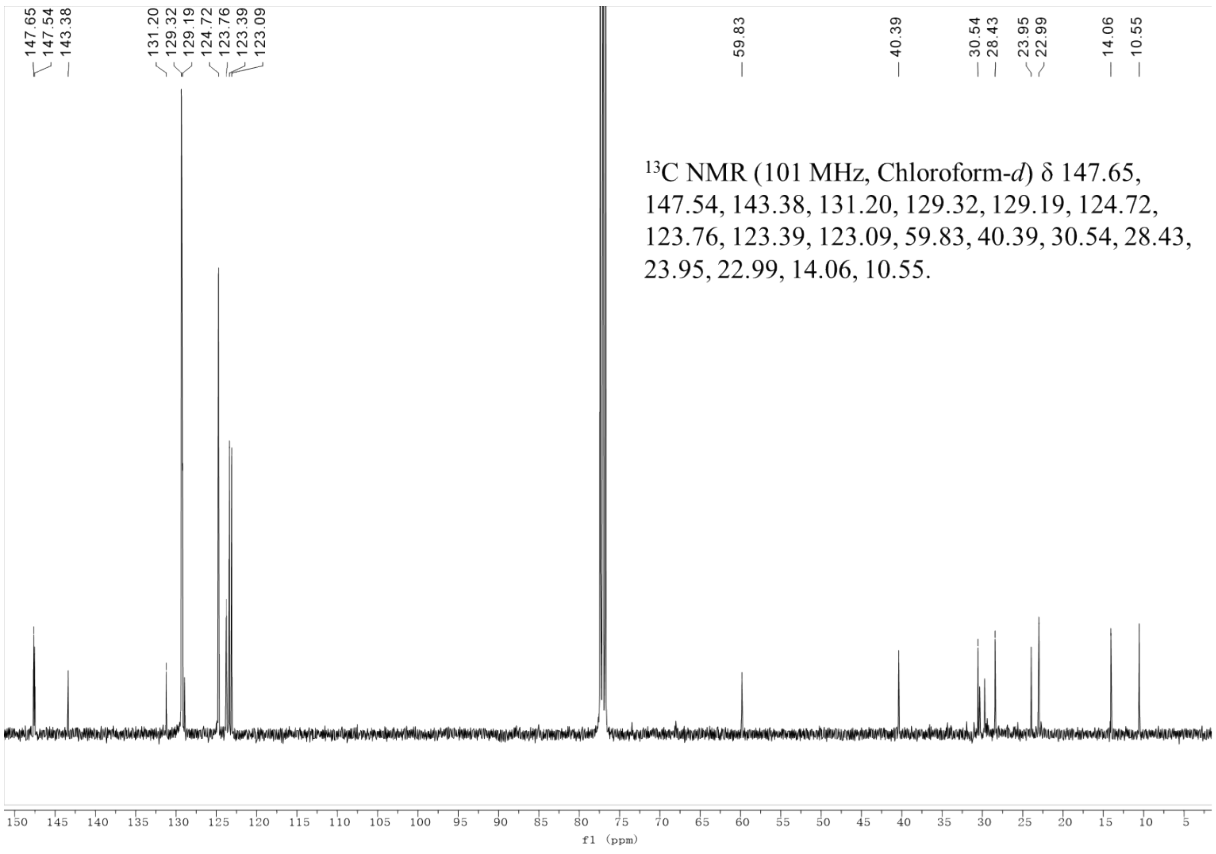

^{13}C NMR spectrum of TPA-BTsr ($CDCl_3$)

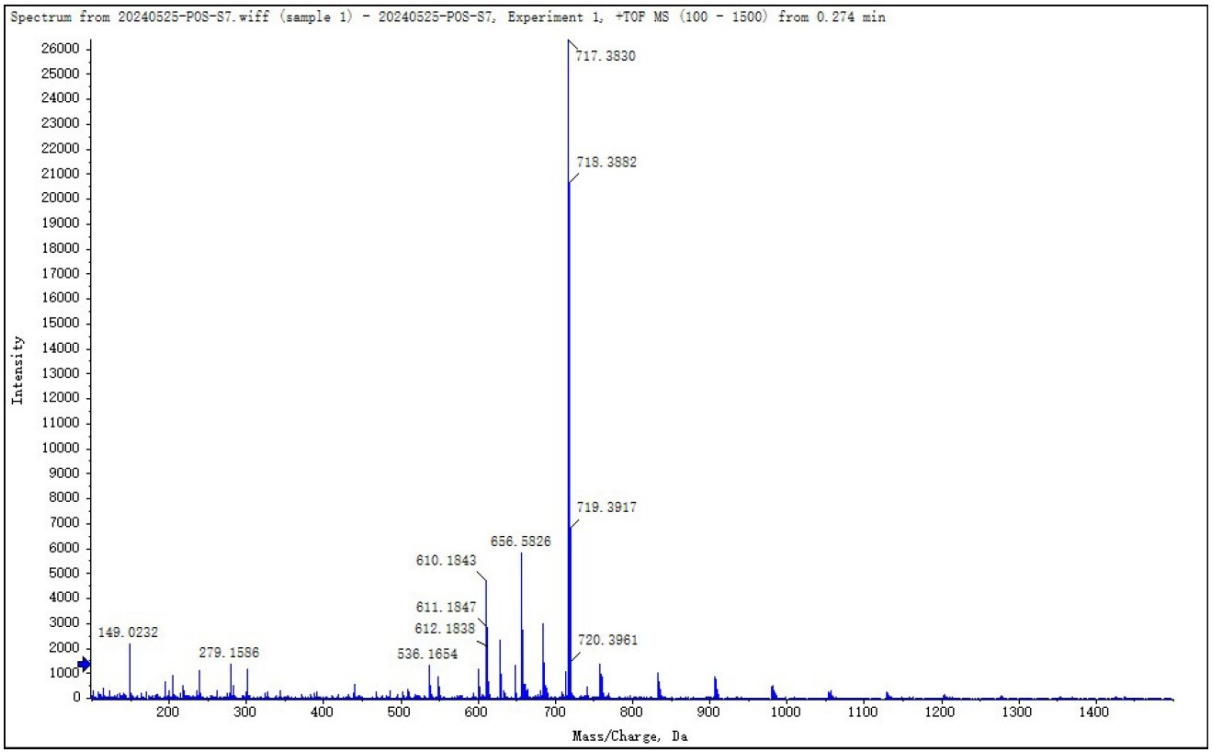

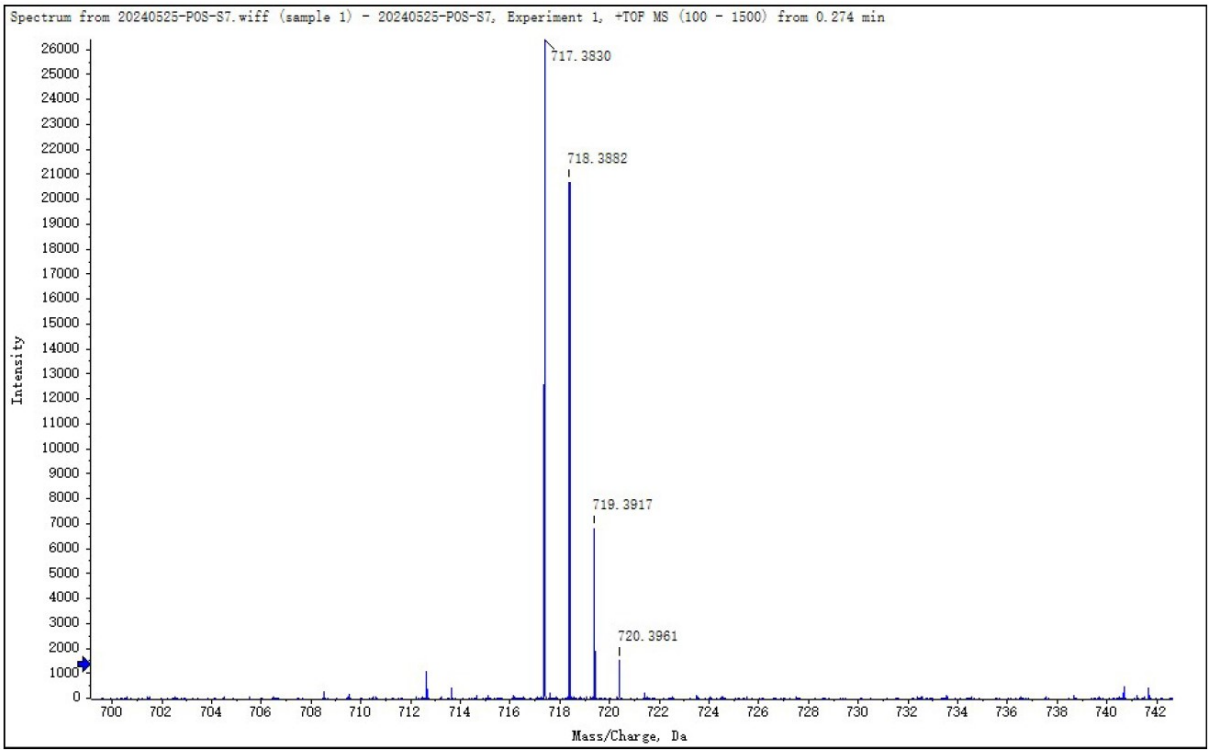

HR-MS spectrum of TPA-BTsr

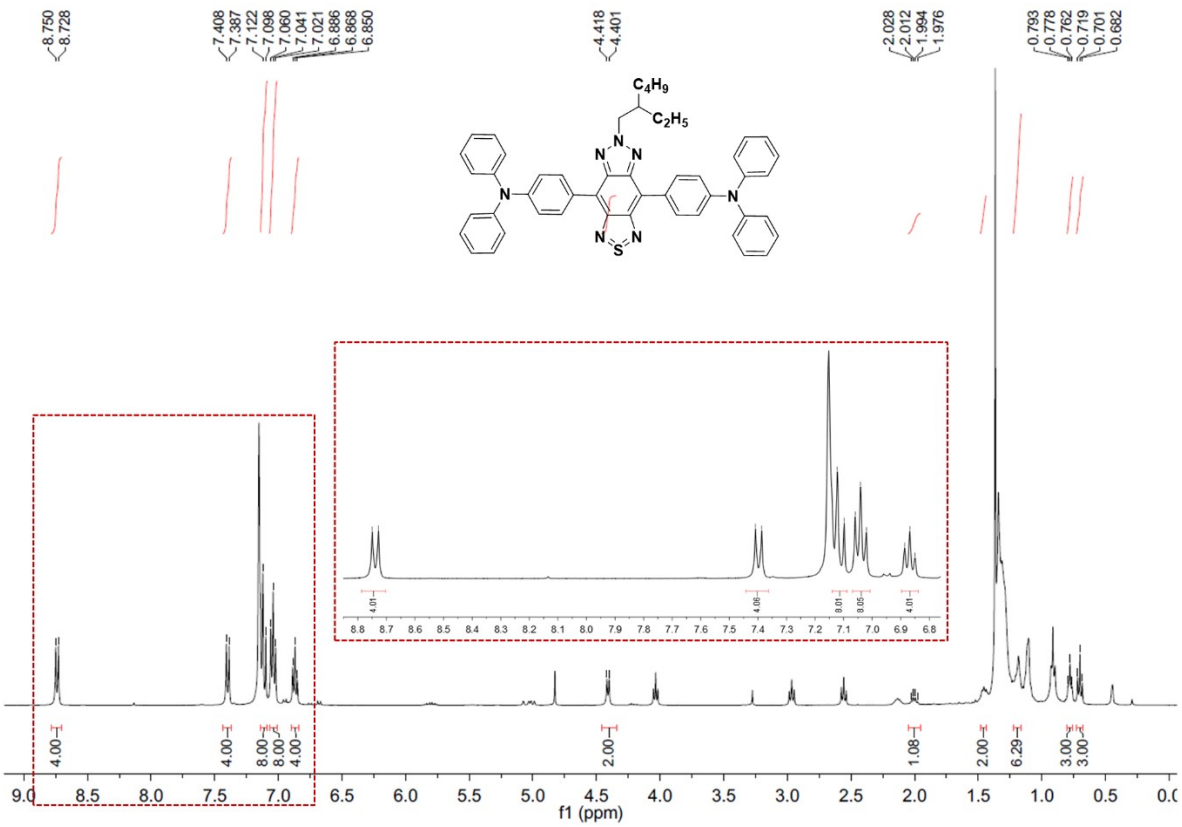

^{1}H NMR spectrum of TPA-TBZ (C_6D_6)

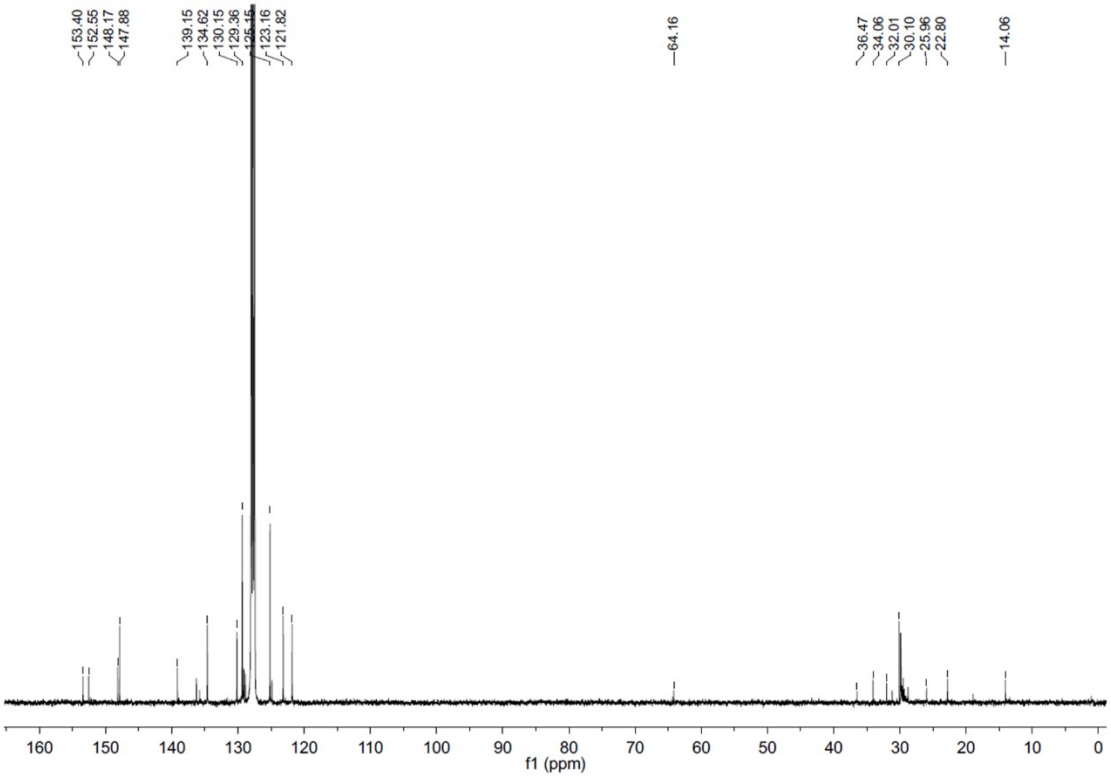

^{13}C NMR spectrum of TPA-TBZ (C_6D_6)

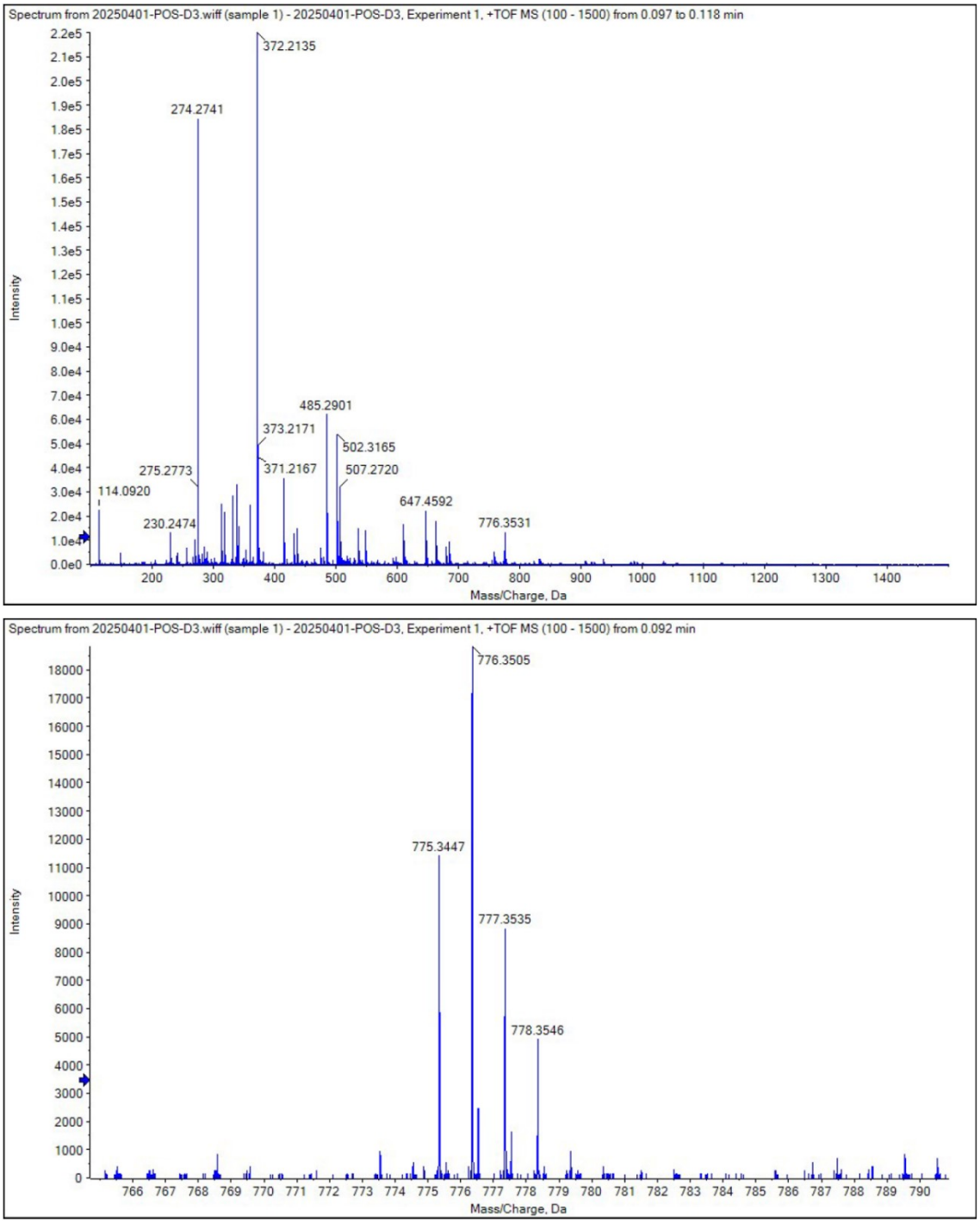

HR-MS spectrum of TPA-TBZ

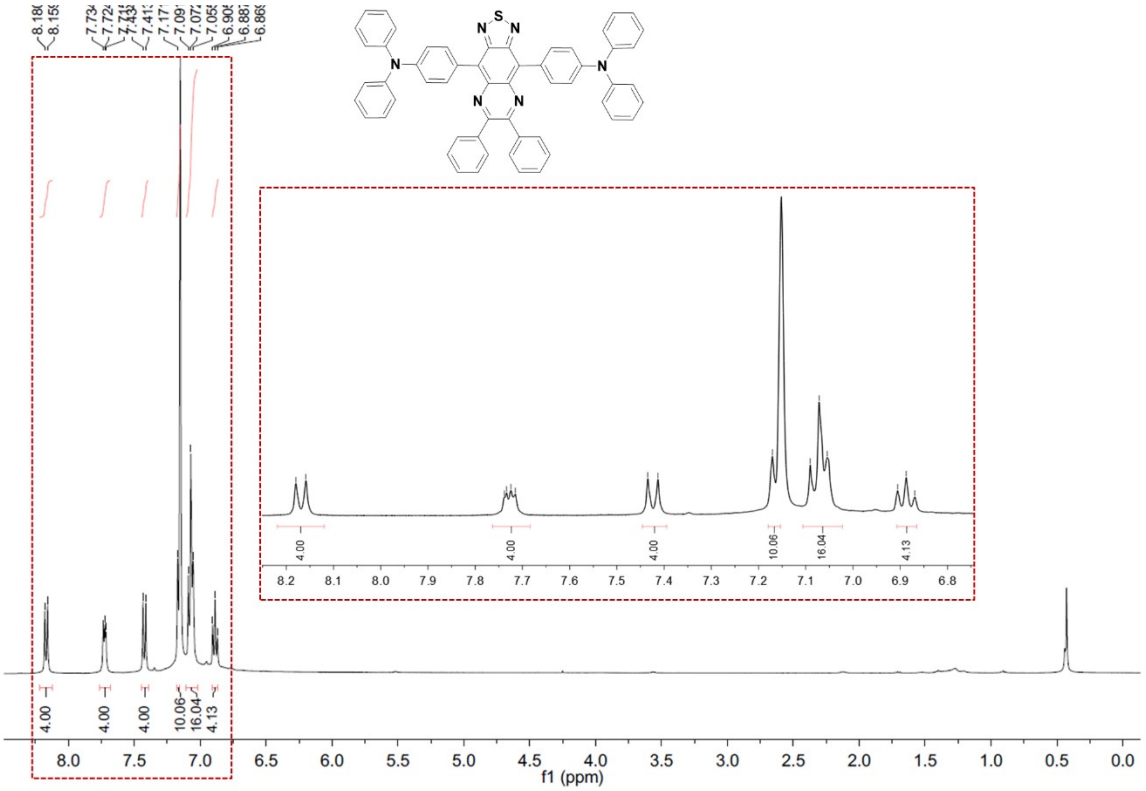

^{1}H NMR spectrum of TPA-QX (C_6D_6)

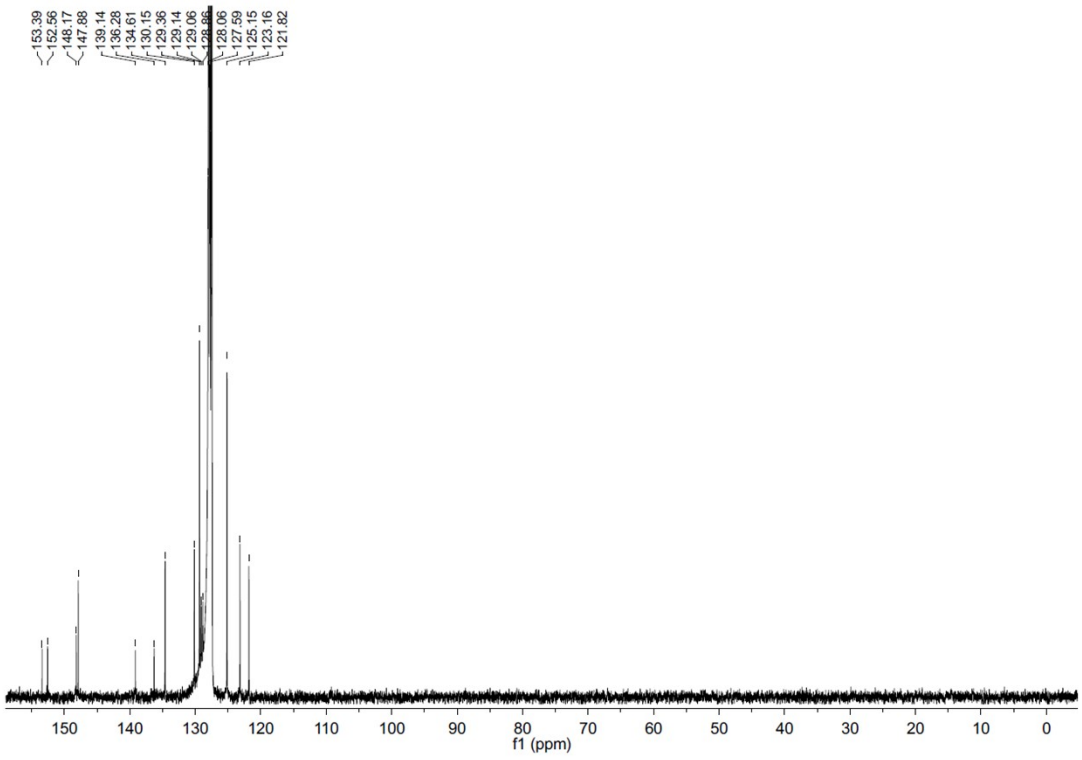

^{13}C NMR spectrum of TPA-QX (C_6D_6)

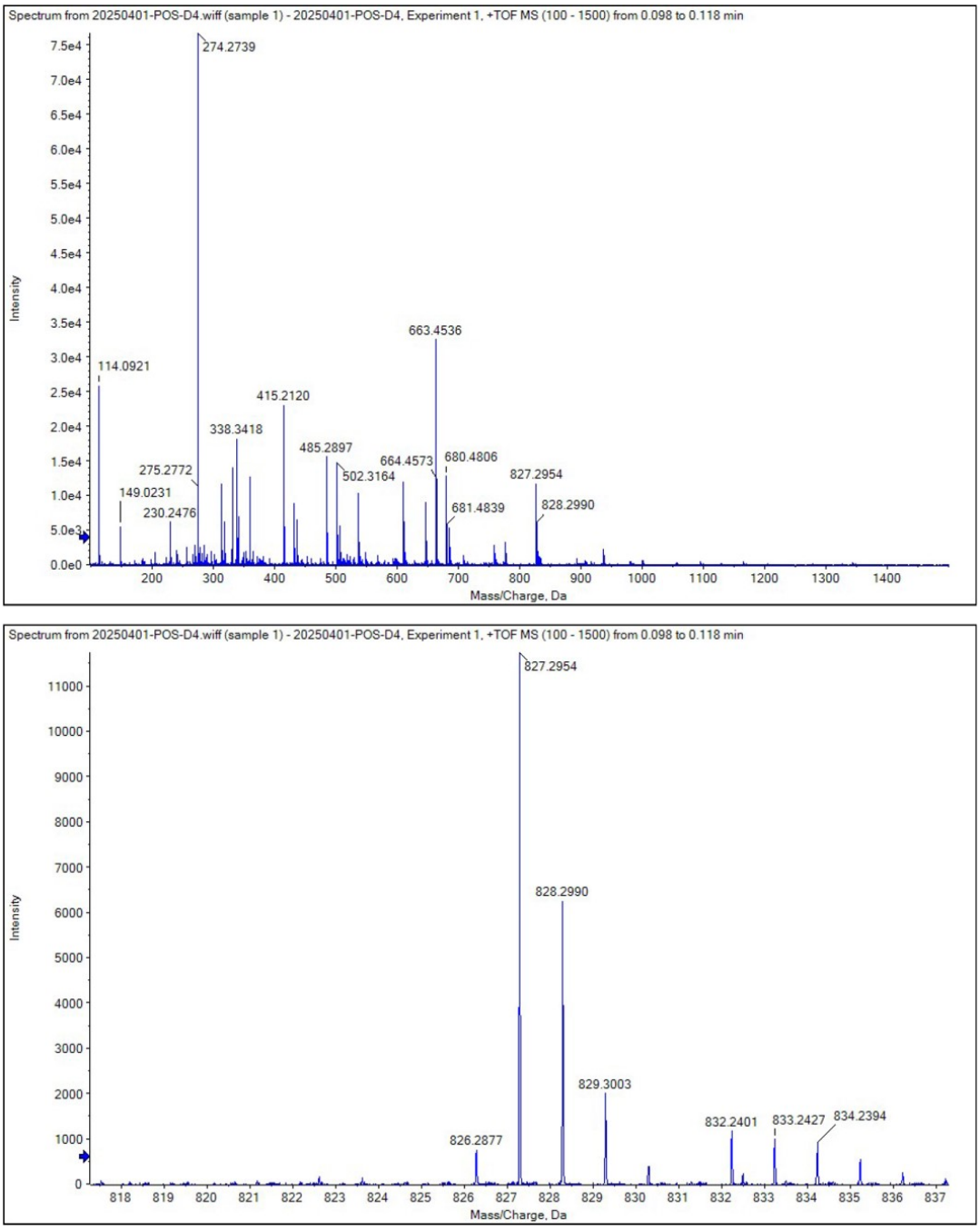

HR-MS spectrum of TPA-QX

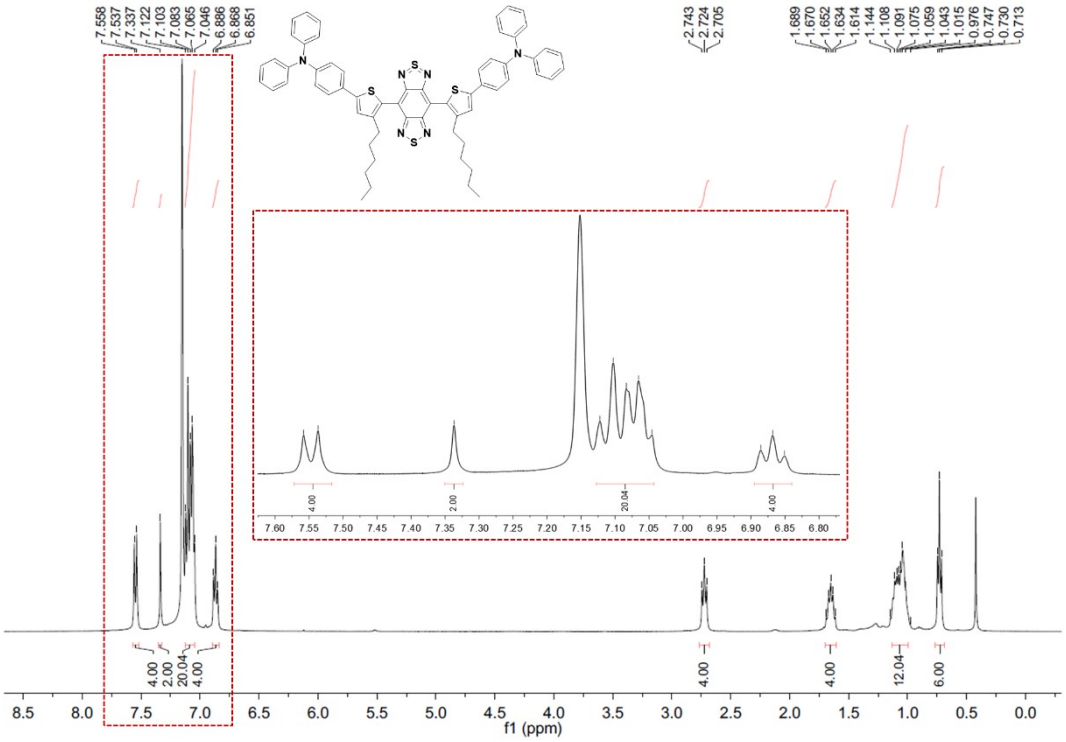

^{1}H NMR spectrum of TPAHT-BBT (C_6D_6)

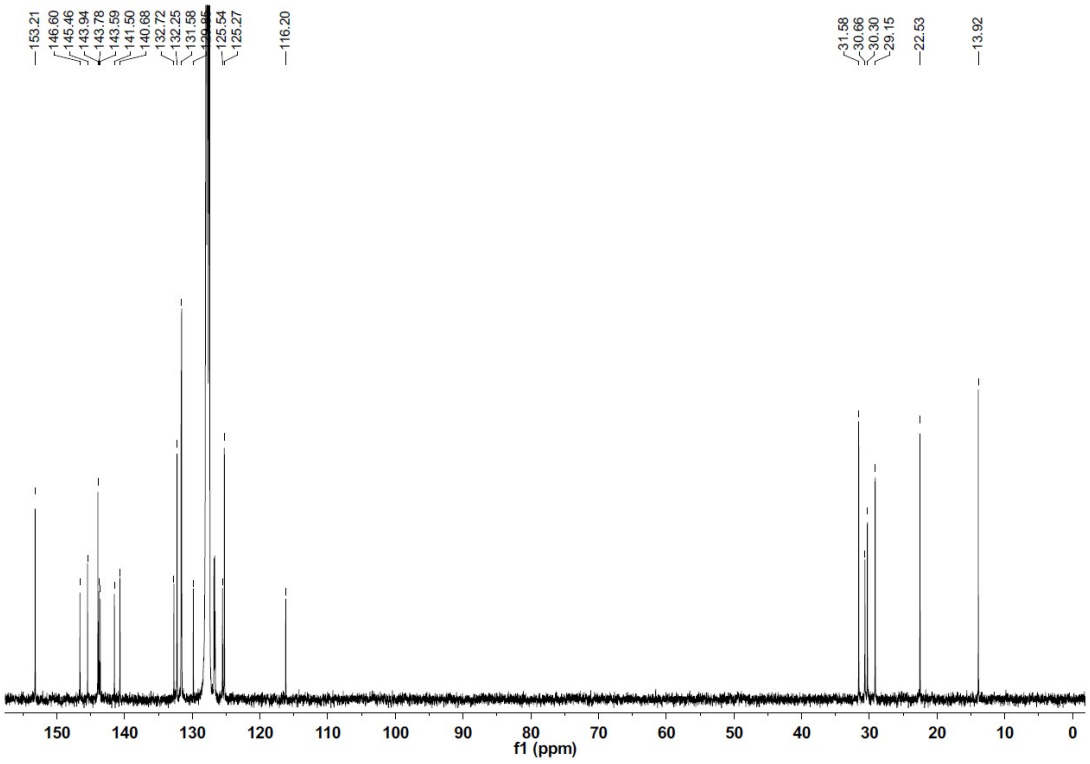

^{13}C NMR spectrum of TPAHT-BBT (C_6D_6)

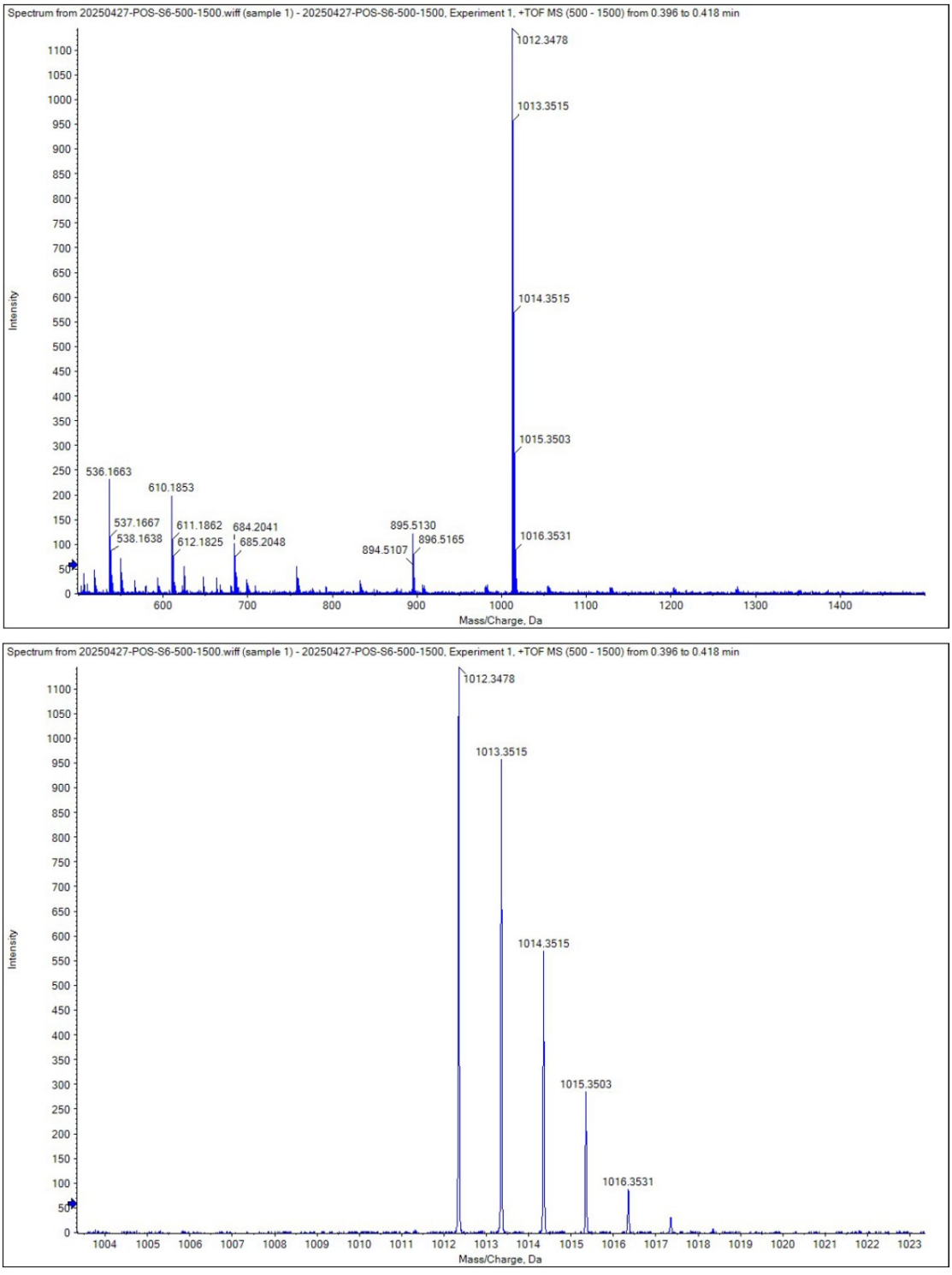

HR-MS spectrum of TPAHT-BBT

Reference

[1] X. Zhou, L. Zhao, K. Zhang, C. Yang, S. Li, X. Kang, G. Li, Q. Wang, H. Ji, M. Wu, J. Liu, Y. Qin, L. Wu, *Chem. Sci.* 2022, *14*, 113-120.

[2] K. Zhang, X. Zhou, S. Li, L. Zhao, W. Hu, A. Cai, Y. Zeng, Q. Wang, M. Wu, G. Li, J. Liu, H. Ji, Y. Qin, L. Wu, *Adv. Mater.* **2023**, *35*, e2305472.

[3] Z. Feng, Y. Li, S. Chen, J. Li, T. Wu, Y, Ying, J. Zheng, Y. Zhang, J. Zhang, X. Fang, X. Yu, D. Zhang, B. Z. Tang, J. Qian, *Nat. Commun.* **2023**, *14*, 5017.

[4] U. Mayerhö ffer, K. Deing, K. Gruß, H. Braunschweig, K. Meerholz, F. Würthner, *Angew. Chem. Int. Ed.* **2009**, *48*, 8776-8779.

[5] Y. Yang, S. Wang, L. Lu, Q. Zhang, P. Yu, Y. Fan, F. Zhang, *Angew. Chem. Int. Ed.* **2020**, *59*, 18380-18385.

[6] K.Rurack and M. Spieles, *Anal. Chem.* **2011**, *83*, 1232-1242.

[7] R. M. Uppu, W. A. Pryor, *Anal. Biochem.* **1996**, *236*, 242-249.

[8] Gaussian 09, Revision A.02, M. J. Frisch, G. W. Trucks, H. B. Schlegel, G. E. Scuseria, M. A. Robb, J. R. Cheeseman, G. Scalmani, V. Barone, G. A. Petersson, H. Nakatsuji, X. Li, M. Caricato, A. Marenich, J. Bloino, B. G. Janesko, R. Gomperts, B. Mennucci, H. P. Hratchian, J. V. Ortiz, A. F. Izmaylov, J. L. Sonnenberg, D. Williams-Young, F. Ding, F. Lipparini, F. Egidi, J. Goings, B. Peng, A. Petrone, T. Henderson, D. Ranasinghe, V. G. Zakrzewski, J. Gao, N. Rega, G. Zheng, W. Liang, M. Hada, M. Ehara, K. Toyota, R. Fukuda, J. Hasegawa, M. Ishida, T. Nakajima, Y. Honda, O. Kitao, H. Nakai, T. Vreven, K. Throssell, J. A. Montgomery, Jr., J. E. Peralta, F. Ogliaro, M. Bearpark, J. J. Heyd, E. Brothers, K. N. Kudin, V. N. Staroverov, T. Keith, R. Kobayashi, J. Normand, K. Raghavachari, A. Rendell, J. C. Burant, S. S. Iyengar, J. Tomasi, M. Cossi, J. M. Millam, M. Klene, C. Adamo, R. Cammi, J. W. Ochterski, R. L. Martin, K. Morokuma, O. Farkas, J. B. Foresman, and D. J. Fox, Gaussian, Inc., Wallingford CT, 2016.

[9] T. Lu, F. Chen, *J. Comput. Chem.* **2012**, *33*, 580-592.

[10] T. Lu, F. Chen, *J. Mol. Graph. Model.* **2012**, *38*, 314-323.